

~~58208~~
59083

**HYDROLOGIC BUDGET ANALYSIS AND NUMERICAL SIMULATIONS
OF GROUNDWATER FLOW IN LOS ALAMOS CANYON
NEAR LOS ALAMOS, NEW MEXICO**

By

ROBERT NORMAN GRAY

B.A. Geology, Indiana University, 1975

THESIS (Volume 1)

Submitted in Partial Fulfillment of
the Requirements for the Degree of

**MASTER OF SCIENCE
EARTH AND PLANETARY SCIENCES**

The University of New Mexico

Albuquerque, New Mexico

MAY, 1997



7190

**HYDROLOGIC BUDGET ANALYSIS AND NUMERICAL SIMULATIONS
OF GROUNDWATER FLOW IN LOS ALAMOS CANYON
NEAR LOS ALAMOS, NEW MEXICO**

by

Robert Norman Gray

B.A. Geology, Indiana University, 1975

THESIS

Submitted in Partial Fulfillment of the
Requirements for the Degree of

**Master of Science
Earth and Planetary Sciences**

The University of New Mexico
Albuquerque, New Mexico

May, 1997

©1997, ROBERT N. GRAY

DEDICATION

This thesis is dedicated to my family; my children, Amanda and Abigail, who tolerated many grumpy days and extended absences, and missed out on lots of quality time with Dad while I was pursuing this degree. They helped keep me going with their love and support. But most of all, it is dedicated to my wife, best friend, and life-long partner, Susan. Without her love, support, unflagging confidence and continuous encouragement, the completion of this study and the accomplishment of concluding the long and arduous efforts to attain this degree would not have been possible.

ACKNOWLEDGEMENTS

The author expresses appreciation to the following individuals for their assistance during this study; to Steve McLin of the ESH-18 Hydrology group for providing alluvial water level data; to David Schaul of ESH-18 and to Phil Teeters of the U.S.G.S. Water Resources Division for providing streamflow discharge data; to Bruce Gallaher of ESH-18 for suggesting several pertinent publications and for reviewing the annual water budget calculations; to Greg Stone of the ESH-17 Meteorology group for information on evapotranspiration determination and site instrumentation; to Dana Kuiper of the U.S. Department of Agriculture Natural Resources Conservation Service for providing access to precipitation and SNOTEL data from the Quemazon site; to Mike Gillespie of the U.S. Department of Agriculture Natural Resources Conservation Service's Snow Survey office for details on the Quemazon site instrumentation and insight into its data interpretation; and to David Sneesby of the FSS-8 Facilities and Infrastructure group for providing information regarding Los Alamos Reservoir.

Above all, the utmost gratitude is owed to Pat Longmire of CST-7 who contributed immeasurably to this project, by first securing the funding, and then providing guidance plus direction toward innumerable Laboratory documents and studies which provided the core of the literature research for this study and the basis for a comprehensive understanding of the hydrogeologic regime in the Los Alamos area. His support, encouragement, extraordinary knowledge and insights were invaluable contributions to this project.

The funding for this project was provided through Los Alamos National Laboratory's Environmental Restoration Project as part of the site characterization activities for Operable Unit 1098 and Los Alamos Canyon.

**HYDROLOGIC BUDGET ANALYSIS AND NUMERICAL SIMULATIONS
OF GROUNDWATER FLOW IN LOS ALAMOS CANYON
NEAR LOS ALAMOS, NEW MEXICO**

by

Robert Norman Gray

ABSTRACT OF THESIS

Submitted in Partial Fulfillment of the
Requirements for the Degree of
Master of Science
Earth and Planetary Sciences

The University of New Mexico
Albuquerque, New Mexico

May, 1997

**HYDROLOGIC BUDGET ANALYSIS AND NUMERICAL SIMULATIONS
OF GROUNDWATER FLOW IN LOS ALAMOS CANYON
NEAR LOS ALAMOS, NEW MEXICO**

By

ROBERT NORMAN GRAY

B.A. Geology, Indiana University, 1975

M.S., Earth and Planetary Sciences, University of New Mexico, 1997

ABSTRACT

A hydrologic budget analysis for the Los Alamos Canyon watershed was prepared including annual budgets for the 1993, 1994, and 1995 water years and detailed budget calculations for the upper basin and middle/upper canyon areas covering nine separate stress periods from 7/10/94 to 11/2/95 corresponding to varying alluvial aquifer behaviors. Data sources included daily measurements of precipitation and snowpack depths, streamflow discharge, and latent heat energy flux from which evapotranspiration rates were determined. Average annual precipitation rates over the watershed varied from ~23 to ~31 inches during the analyzed periods. The annual evapotranspiration component was determined to represent between ~71% and ~84% of the total budget. Annual infiltration rates were calculated as residuals to the basic hydrologic mass balance equation and ranged from ~4 to ~7 inches/year, representing between ~14% and ~26% of the total water budget on an annual basis.

A groundwater flow model of the alluvial system was constructed using Visual MODFLOW[®] which implements the U.S. Geological Survey's three-dimensional finite-difference groundwater flow code. Both steady-state and transient simulations were run. MODFLOW's drain package was used to simulate infiltration seepage from the system,

while the hydrologic budget analysis results constrained the recharge and evapotranspiration stresses. The steady-state model was calibrated to well data by varying the drain conductances. The ZONEBUDGET and MODPATH codes were also utilized, and results showed that infiltration seepage dominated the loss components of the modeled system's water budget, representing ~69% of the total losses, compared to ~28% for evapotranspiration and ~3% for downgradient flow, which was characterized with an average advective velocity of 727 feet/year. Results also quantified enhanced infiltration seepage within the Guaje Mountain fault zone. An error analysis generally corroborated the model results, and a sensitivity analysis was conducted which showed that the model was most sensitive to errors in recharge and evapotranspiration.

TABLE OF CONTENTS

	Page
INTRODUCTION.....	1
Background.....	1
Purpose and Scope.....	2
Study Area Description.....	4
Location and Physical Setting.....	4
Climate.....	8
Vegetation.....	8
Regional Geology.....	9
Local Geology.....	10
Hydrology.....	17
Previous Investigations.....	23
HYDROLOGIC BUDGET ANALYSIS.....	27
Conceptual Model.....	27
Data Sources.....	27
Annual Water Budget.....	32
Detailed Water Budget.....	41
Streamflow Data Analysis.....	58
Hydrologic Budget Analysis Results.....	66
GROUNDWATER FLOW SIMULATIONS.....	71
Purpose.....	71
Computer Code.....	72
Conceptual Model.....	73
Model Design.....	75
Hydrologic Parameters, Assumptions, and Data Sources.....	78
Steady-State Simulation.....	86
Calibration Procedure.....	86
ZONEBUDGET Analysis.....	90
Particle Tracking Analysis.....	97
Modeling for Transient Simulation Initial Conditions-Part 1.....	101
Transient Simulations.....	103
Purpose.....	103
Modeling for Transient Simulation Initial Conditions-Part 2.....	103

TABLE OF CONTENTS (continued)

	Page
GROUNDWATER FLOW SIMULATIONS (continued)	
Transient Simulations (continued)	
Transient Time Periods and Stresses.....	104
Transient Simulation Results.....	106
LAO-B.....	116
LAO-C.....	116
LAO-0.3.....	117
LAO-0.6.....	118
LAO-0.8.....	118
LAO-0.91.....	119
LAO-3.....	119
LAO-4.....	121
LAO-6.....	121
Transient Error Analysis.....	122
Transient ZONEBUDGET Analysis.....	139
Sensitivity Analysis.....	171
SUMMARY AND CONCLUSIONS.....	184
Overview.....	184
Hydrologic Budget Analysis Summary.....	185
Groundwater Flow Simulations Summary.....	187
Model Limitations and Deficiencies.....	189
Recommendations for Future Work.....	191
Major Conclusions.....	194
REFERENCES.....	196
APPENDICES.....	203
Appendix A: TA-6 Station Daily ET & Precipitation 10/1/92-11/2/95.....	204
Appendix B: TA-53 Station Daily Precipitation 10/1/92-11/2/95.....	236
Appendix C: TA-74 Station Daily Precipitation 10/1/92-11/2/95.....	246
Appendix D: North Community Station Daily Precipitation 10/1/92-11/2/95.....	256
Appendix E: Quemazon Station Daily Precipitation 10/1/93-9/30/95.....	266

TABLE OF CONTENTS (continued)

	Page
APPENDICES (continued)	
Appendix F: Quemazon Station Daily Precipitation and Snowpack Data 10/1/93-9/30/95.....	275
Appendix G: Streamflow Discharge Data 10/1/94-9/30/95.....	292
Appendix H: Detailed Water Budget Calculations.....	301
Appendix I: Measured Alluvial Water Levels 1994-1996.....	311
Appendix J: LAO-C Daily Water Level Data (7/10/94-10/28/94).....	320
Appendix K: LAO-3 Daily Water Level Data (7/10/94-11/2/95).....	324
Appendix L: LAO-4 Daily Water Level Data (7/10/94-11/2/95).....	334
Appendix M: LAO-6 Daily Water Level Data (7/10/94-10/28/94).....	344
Appendix N: Model ALUV1196 Cell Top-Bottom Data and Model Correlation Adjustments.....	348
Appendix O: Model ALUV1196 (Steady-State) Calibration Data.....	352
Appendix P: Model ALUV1196 MODPATH Results.....	363
Appendix Q: Model AL1296T0 (Transient-Initial Heads) Calibration Data.....	366
Appendix R: LAO-B Transient Model Calculated Head vs Time Results..	374
Appendix S: LAO-C Transient Model Calculated Head vs Time Results..	383
Appendix T: LAO-0.3 Transient Model Calculated Head vs Time Results	387
Appendix U: LAO-0.6 Transient Model Calculated Head vs Time Results	396
Appendix V: LAO-0.8 Transient Model Calculated Head vs Time Results	405
Appendix W: LAO-0.91 Transient Model Calculated Head vs Time Results.....	414
Appendix X: LAO-3 Transient Model Calculated Head vs Time Results...	423
Appendix Y: LAO-4 Transient Model Calculated Head vs Time Results...	432
Appendix Z: LAO-6 Transient Model Calculated Head vs Time Results...	441
Appendix AA: Transient Alluvial Models: Period End Results Analysis.....	445
Appendix BB: Model ALUV1196 (Steady-State) Sensitivity Results.....	451
Appendix CC: Model AL1296T6 (Transient-Period 6) Sensitivity Results..	467

LIST OF FIGURES

	Page
Figure 1: Regional Location.....	5
Figure 2: Detailed Location.....	6
Figure 3: Topography.....	7
Figure 4: Regional Physiographic Features.....	11
Figure 5: Stratigraphic Diagram.....	12
Figure 6: Block Diagram.....	12
Figure 7: Bedrock Geology.....	13
Figure 8: Locations of Major Faults.....	16
Figure 9: Monitor Well Locations.....	19
Figure 10: Los Alamos Canyon Alluvial Head Profiles.....	21
Figure 11: Precipitation and Streamflow Measurement Stations.....	28
Figure 12: Los Alamos Canyon Watershed Precipitation Data-Monthly Comparison.....	33
Figure 13: Los Alamos Canyon Annual Water Budget Elevation vs Precipitation Regressions.....	34
Figure 14: ET and Precipitation (TA-6).....	35
Figure 15: Los Alamos Canyon Watershed Annual Water Budget.....	37
Figure 16: LAO-3 Alluvial Aquifer Heads and Daily Precipitation (TA-6 Station) 7/10/94-11/2/95.....	43
Figure 17: Quemazon Station 1994 Total Precipitation and Net Non-frozen Yield Comparison.....	45
Figure 18: Quemazon Station 1994 Total Precipitation and Net Non-frozen Yield Comparison.....	46
Figure 19: Quemazon Station Total Precipitation and Net Non-frozen Yield by Stress Period.....	48
Figure 20: TA-6 Maximum and Minimum Temperatures for Stress Period 5 (12/8/94-2/12/95).....	52
Figure 21: Los Alamos Canyon Detailed Water Budget Elevation vs Precipitation Regressions-Periods 1,2,3.....	54
Figure 22: Los Alamos Canyon Detailed Water Budget Elevation vs Precipitation Regressions-Periods 4,5,6.....	55

LIST OF FIGURES (continued)

	Page
Figure 23: Los Alamos Canyon Detailed Water Budget Elevation vs Precipitation Regressions- Periods 7,8,9.....	56
Figure 24: Los Alamos Canyon Combined Streamflow Discharge (10/1/94-9/30/95).....	61
Figure 25: Los Alamos Canyon Seepage Run (5/3/95) Calculated Infiltration.....	65
Figure 26: LAO-3 Alluvial Aquifer Heads with Upper Gage Mean Daily Discharge and Quemazon Station Net Non-frozen Precipitation.....	67
Figure 27: Los Alamos Canyon Alluvial Aquifer Location Map.....	76
Figure 28: Los Alamos Canyon Alluvial Aquifer MODFLOW Cell Configuration.....	77
Figure 29: Alluvial Aquifer Model Surface Grid.....	79
Figure 30: Alluvial Aquifer Model Bottom Grid.....	80
Figure 31: Los Alamos Canyon Alluvial Aquifer Model Cell Configuration Cross-section View.....	81
Figure 32: Model ALUV1196 (Steady-State) Observed vs Calculated Saturated Thickness.....	89
Figure 33: Model ALUV1196 (Steady-State) Zonebudget Results.....	92
Figure 34: Model ALUV1196 (Steady-State) Total Study Area Zonebudget Results.....	94
Figure 35: Model ALUV1196 (Steady-State) Zonebudget Results- Calculated Average Saturated Thicknesses.....	96
Figure 36: Los Alamos Canyon Alluvial Aquifer MODPATH Particle Tracking Results.....	99
Figure 37: MODPATH Velocities and Flowpath Gradients- Model ALUV1196 (Steady-State).....	100
Figure 38: Model AL1296T0 (Steady-State Results).....	102
Figure 39: Model AL1296T0 (Transient Results).....	105
Figure 40: LAO-B Alluvial Aquifer Measured and Modeled Water Levels 7/10/94-11/2/95.....	107
Figure 41: LAO-C Alluvial Aquifer Measured and Modeled Water Levels 7/10/94-10/28/94.....	108

LIST OF FIGURES (continued)

	Page
Figure 42: LAO-0.3 Alluvial Aquifer Measured and Modeled Water Levels 7/10/94-11/2/95.....	109
Figure 43: LAO-0.6 Alluvial Aquifer Measured and Modeled Water Levels 7/10/94-11/2/95.....	110
Figure 44: LAO-0.8 Alluvial Aquifer Measured and Modeled Water Levels 7/10/94-11/2/95.....	111
Figure 45: LAO-0.91 Alluvial Aquifer Measured and Modeled Water Levels 7/10/94-11/2/95.....	112
Figure 46: LAO-3 Alluvial Aquifer Measured and Modeled Water Levels 7/10/94-11/2/95.....	113
Figure 47: LAO-4 Alluvial Aquifer Measured and Modeled Water Levels 7/10/94-11/2/95.....	114
Figure 48: LAO-6 Alluvial Aquifer Measured and Modeled Water Levels 7/10/94-10/28/94.....	115
Figure 49: Model AL1296T1 (Transient) Observed vs Calculated Saturated Thickness at 10/14/94 (End Period 1).....	124
Figure 50: Model AL1296T2 (Transient) Observed vs Calculated Saturated Thickness at 10/18/94 (End Period 2).....	125
Figure 51: Model AL1296T3 (Transient) Observed vs Calculated Saturated Thickness at 11/11/94 (End Period 3).....	126
Figure 52: Model AL1296T4 (Transient) Observed vs Calculated Saturated Thickness at 12/8/94 (End Period 4).....	127
Figure 53: Model AL1296T5 (Transient) Observed vs Calculated Saturated Thickness at 2/13/95 (End Period 5).....	128
Figure 54: Model AL1296T6 (Transient) Observed vs Calculated Saturated Thickness at 7/1/95 (End Period 6).....	129
Figure 55: Model AL1296T7 (Transient) Observed vs Calculated Saturated Thickness at 8/4/95 (End Period 7).....	130
Figure 56: Model AL1296T8 (Transient) Observed vs Calculated Saturated Thickness at 9/12/95 (End Period 8).....	131
Figure 57: Model AL1296T9 (Transient) Observed vs Calculated Saturated Thickness at 11/2/95 (End Period 9).....	132
Figure 58: Total Mean Calculated Head Errors.....	138

LIST OF FIGURES (continued)

	Page
Figure 59: Model AL1296T1 (Transient-Period 1) Zonebudget Results.....	149
Figure 60: Model AL1296T2 (Transient-Period 2) Zonebudget Results.....	150
Figure 61: Model AL1296T3 (Transient-Period 3) Zonebudget Results.....	151
Figure 62: Model AL1296T4 (Transient-Period 4) Zonebudget Results.....	152
Figure 63: Model AL1296T5 (Transient-Period 5) Zonebudget Results.....	153
Figure 64: Model AL1296T6 (Transient-Period 6) Zonebudget Results.....	154
Figure 65: Model AL1296T7 (Transient-Period 7) Zonebudget Results.....	155
Figure 66: Model AL1296T8 (Transient-Period 8) Zonebudget Results.....	156
Figure 67: Model AL1296T9 (Transient-Period 9) Zonebudget Results.....	157
Figure 68: Transient Models Zone #1 Zonebudget Results- Variation Over Time (Model Columns 1-47).....	162
Figure 69: Transient Models Zone #2 Zonebudget Results- Variation Over Time (Model Columns 48-69).....	163
Figure 70: Transient Models Zone #3 Zonebudget Results- Variation Over Time (Model Columns 70-75).....	164
Figure 71: Transient Models Zone #4 Zonebudget Results- Variation Over Time (Model Columns 76-78).....	165
Figure 72: Transient Models Zone #5 Zonebudget Results- Variation Over Time (Model Columns 79-100).....	166
Figure 73: Transient Models Zone #6 Zonebudget Results- Variation Over Time (Model Columns 101-125).....	167
Figure 74: Transient Models Zone #7 Zonebudget Results- Variation Over Time (Model Columns 126-160).....	168
Figure 75: Transient Models Zones 1-7 Zonebudget Results- Variation Over Time (Model Columns 1-160).....	170
Figure 76: Model ALUV1196 (Steady-State) Sensitivity Results- Head Change with Varying Hydraulic Conductivity.....	173
Figure 77: Model ALUV1196 (Steady-State) Sensitivity Results- Head Change with Varying Recharge.....	174
Figure 78: Model ALUV1196 (Steady-State) Sensitivity Results- Head Change with Varying Evapotranspiration.....	175
Figure 79: Model ALUV1196 (Steady-State) Sensitivity Results- Head Change with Varying ET Extinction Depth.....	176

LIST OF FIGURES (continued)

	Page
Figure 80: Model ALUV1196 (Steady-State) Sensitivity Results-Mean Absolute Head Change Variation by Hydrologic Parameter.....	180
Figure 81: Model AL1296T6 (Transient) Sensitivity Results-Mean Absolute Head Change Variation by Hydrologic Parameter.....	181

LIST OF TABLES

	Page
Table 1: TA-6 ET vs Precipitation.....	36
Table 2: Los Alamos Canyon Watershed Annual Water Budget.....	38
Table 3: Los Alamos Canyon Detailed Water Budget Stress Periods.....	49
Table 4: Los Alamos Canyon Detailed Water Budget Calculations Summary.....	59
Table 5: Los Alamos Canyon Detailed Water Budget Results Summary.....	60
Table 6: Los Alamos Canyon Channel Loss Calculations (5/3/95).....	63
Table 7: Alluvial Model Hydrologic Data Sources.....	85
Table 8: Steady-State Model ALUV1196 Zonebudget Results.....	91
Table 9: Average Drain Losses and Calculated Average Saturated Thicknesses.....	95
Table 10: Transient Models Mean Calculated Head Errors Summary.....	134
Table 11: Maximum Observed Head Losses.....	135
Table 12: Transient Model AL1296T1 Zonebudget Results (End Period 1).....	140
Table 13: Transient Model AL1296T2 Zonebudget Results (End Period 2).....	141
Table 14: Transient Model AL1296T3 Zonebudget Results (End Period 3).....	142
Table 15: Transient Model AL1296T4 Zonebudget Results (End Period 4).....	143
Table 16: Transient Model AL1296T5 Zonebudget Results (End Period 5).....	144
Table 17: Transient Model AL1296T6 Zonebudget Results (End Period 6).....	145
Table 18: Transient Model AL1296T7 Zonebudget Results (End Period 7).....	146
Table 19: Transient Model AL1296T8 Zonebudget Results (End Period 8).....	147
Table 20: Transient Model AL1296T9 Zonebudget Results (End Period 9).....	148
Table 21: Sensitivity Results Summary.....	179

INTRODUCTION

Background

Understanding the hydrologic systems and processes in Los Alamos Canyon is important because of the complexity and highly dynamic nature of the hydrogeologic regime encompassed by the canyon. It is also significant because much of the canyon lies within the boundaries of Los Alamos National Laboratory (LANL) and it has been impacted by several contaminants associated with the research activities of nearby LANL facilities. These impacts include both surface water and groundwater contamination by a variety of radionuclides.

For example, maximum measured radionuclide activities in surface water in Los Alamos Canyon during 1993 were 0.040 picoCuries per liter (pCi/L) for ^{239}Pu , 0.017 pCi/L for ^{238}Pu , 2.9 pCi/L for ^{137}Cs and 1,100 pCi/L for ^3H (tritium) (Environmental Protection Group, 1995). Alluvial groundwater also showed elevated radionuclide concentrations, with maximum measured activities of 0.356 pCi/L for ^{238}Pu , 1.584 pCi/L for $^{239,240}\text{Pu}$, 3.0 pCi/L for ^{137}Cs , 0.019 pCi/L for ^{241}Am , 1,300 pCi/L for ^3H , 367.7 pCi/L for ^{90}Sr and total (non-isotopic, non-filtered) uranium at 50.4 $\mu\text{g/L}$ (Environmental Protection Group, 1995). Elevated tritium activities in Los Alamos Canyon are primarily residual levels resulting from the extensive release of tritium from a primary cooling system leak at the Omega West Reactor (OWR) site which is located on the canyon floor near the Guaje Mountain fault zone. This leak released a maximum of 70 gallons per day of cooling water into the groundwater system with typical tritium concentrations of 1.6×10^7 to 2.0×10^7 pCi/L over a time period likely extending from at least 1967 (when tritium activities in the alluvial groundwater were measured at 4.1×10^4 pCi/L) until the reactor was shut down in 1993 (Los Alamos National Laboratory, 1995).

Neither the surface water or alluvial groundwater are currently utilized for water supply purposes. However, the ultimate fate of the alluvial groundwater and consequent

pathways of contaminant migration are subjects of concern for LANL which, along with the community of Los Alamos, derives its water supply from the underlying regional aquifer.

Though past sampling of wells penetrating the regional aquifer have typically shown it to be free of the radiochemical contaminants affecting the surface waters and shallow groundwater, more recent results suggest that some of these contaminants may indeed impact the water quality of the regional aquifer. For example, analysis of a groundwater sample taken in 1994 from Test Well 3 which penetrates the regional aquifer at a depth of approximately 750 feet and is located at the confluence of Los Alamos Canyon and DP Canyon within the study area indicated a ^{90}Sr activity of 35.1 pCi/L, a level which is below the Department of Energy's Derived Concentration Guide for ^{90}Sr in drinking water systems of 40 pCi/L, but which is significantly higher than the U.S. Environmental Protection Agency's Maximum Contaminant Level for ^{90}Sr in drinking water systems of 8 pCi/L (Purtyman, 1995; Environmental Assessments and Resource Evaluations Group, 1996).

This suggests that an apparent hydrologic connection between the shallow groundwater in Los Alamos Canyon and the regional aquifer could indeed have an adverse impact on the region's water supply, and that these concerns are not unfounded. These are also concerns for neighboring property owners whose groundwater quality may be affected by the contaminants' movement. The primary pathways for contaminant migration are along the groundwater flow paths. Thus, information on the flow dynamics of the groundwater system is necessary to address these concerns.

Purpose and Scope

This study was thus undertaken to achieve a greater level of understanding of the hydrologic behavior of the near surface (alluvial) perched aquifer and its dynamic relations to associated hydrologic systems within the Los Alamos Canyon drainage. In order to

quantify hydrologic parameters such as recharge, evapotranspiration (ET), surface runoff and surface infiltration rates, a hydrologic budget analysis of the Los Alamos Canyon watershed was prepared. This analysis included the determination of annual water budgets for the 1993, 1994, and 1995 water years (October 1-September 30) as well as detailed budget calculations for nine separate stress periods between July 10, 1994 and November 2, 1995 which were defined on the basis of varying alluvial aquifer behavior as determined from available well hydrograph data.

The detailed water budget results were used to constrain input parameters for steady-state and transient three-dimensional groundwater flow simulations of the alluvial aquifer system which were performed using the United States Geological Survey's (USGS) MODFLOW finite-difference groundwater flow model (McDonald and Harbaugh, 1988) and Visual MODFLOW® software (Waterloo Hydrogeologic Software, 1996). The steady-state model was calibrated to water level data from seven alluvial observation wells during the peak snowmelt runoff period in the spring of 1995. Varying recharge and ET rates determined from the water budget were applied to transient models representing each of the nine stress periods and comparisons to observed water levels in nine alluvial observation wells were made. An error analysis was performed on all of the transient models and sensitivity analyses were performed on the steady-state model and one transient model.

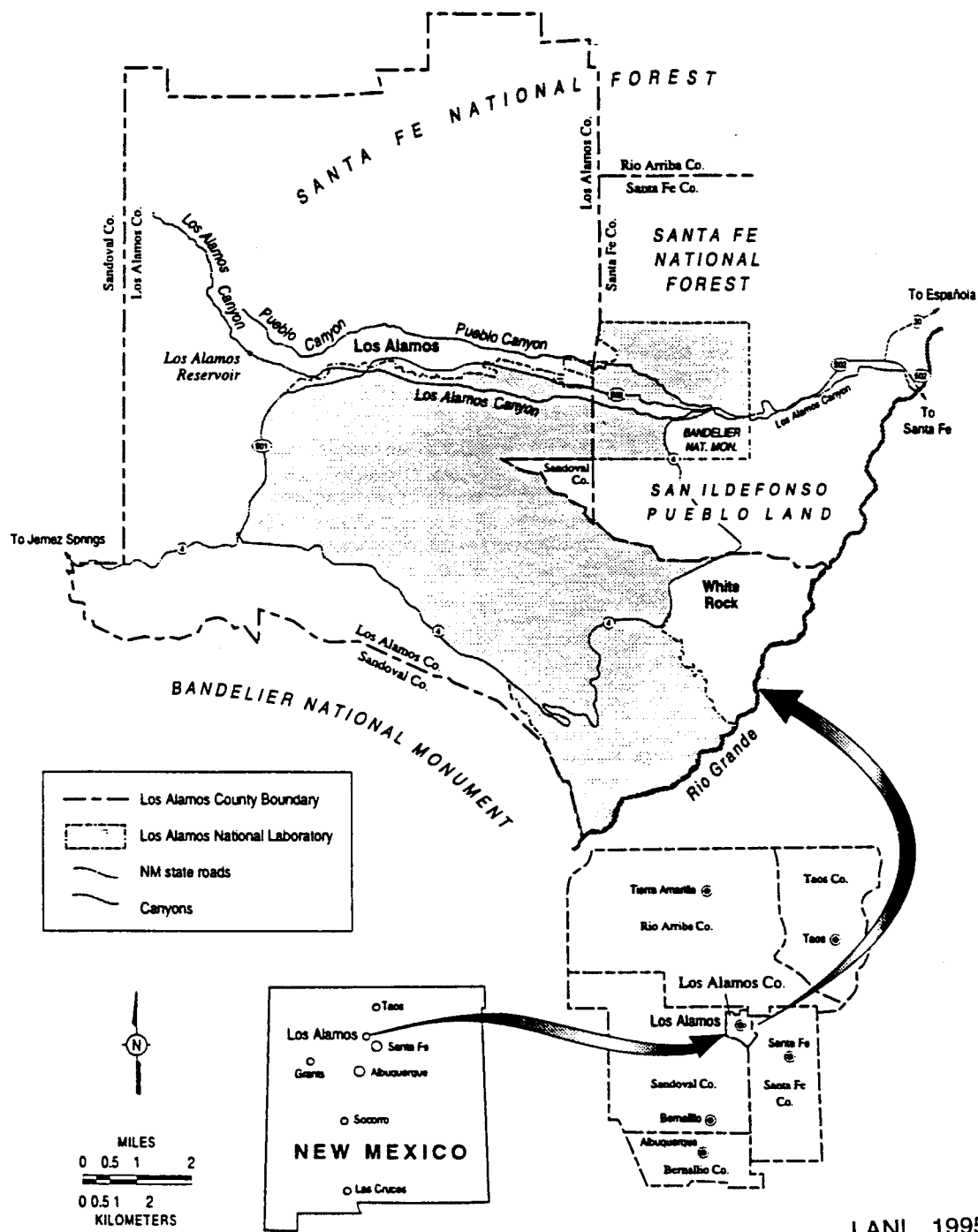
The USGS ZONEBUDGET water budgeting code for user-defined zones (Harbaugh, 1990) was utilized in conjunction with the flow models to quantify recharge, ET, and infiltration seepage volumes under steady-state conditions, and varying recharge, ET, infiltration seepage and storage volumes under transient conditions for the nine separate stress periods and for nine separate zones within the alluvial aquifer system. The USGS MODPATH particle tracking code (Pollock, 1989) was also used with the steady-state flow model to quantify varying gradients and flow velocities within the alluvial aquifer system.

Study Area Description

Location and Physical Setting

Los Alamos Canyon is located within the Pajarito Plateau geomorphic province of north-central New Mexico, a gently dipping platform dissected with numerous deep and steep walled canyons, on the eastern flank of the Jemez Mountains and on the west side of the Rio Grande valley. Its orientation is nearly west to east and it runs just south of the community of Los Alamos, lying largely within the boundaries of LANL (Figure 1). The Los Alamos Canyon watershed extends approximately four miles west of the LANL boundary into the adjacent Santa Fe National Forest and extends east of the LANL boundary into Bandelier National Monument (outlier) and San Ildefonso Pueblo lands, including portions of Los Alamos, Sandoval, and Santa Fe Counties (Figures 1 and 2). Its headwaters form in the Sierra de Los Valles of the Jemez Mountains and it drains intermittent runoff to the Rio Grande. A significant topographic gradient exists in the Los Alamos Canyon watershed with elevations ranging from 10,441 feet atop Pajarito Mountain near the western boundary of the watershed to about 6,300 feet at its confluence with Pueblo Canyon near State Road 4 (Figure 3). Below this confluence, the lower Los Alamos Canyon drainage carries the runoff from several other major canyons including Pueblo Canyon, Guaje Canyon, Rendija Canyon, Bayo Canyon and Barrancas Canyon. Since the focus of this study is limited to Los Alamos Canyon, the downstream limit evaluated has been restricted to the point where it crosses State Road 4, immediately above the confluence with Pueblo Canyon, rather than include the contributions of the significantly larger area drained by the other canyons. The study area as shown in Figures 2 and 3 comprises an area of approximately 10.13 square miles, encompassing the upper basin and upper to middle canyon areas while excluding lower Los Alamos Canyon.

The channel length within the study area is about 12.3 miles and the canyon is deeply incised throughout this length, its depth ranging from about 600 feet in the upper basin to about 300 to 400 feet in the upper and middle canyon reaches. The channel



LANL, 1995

Figure 1: Regional Location

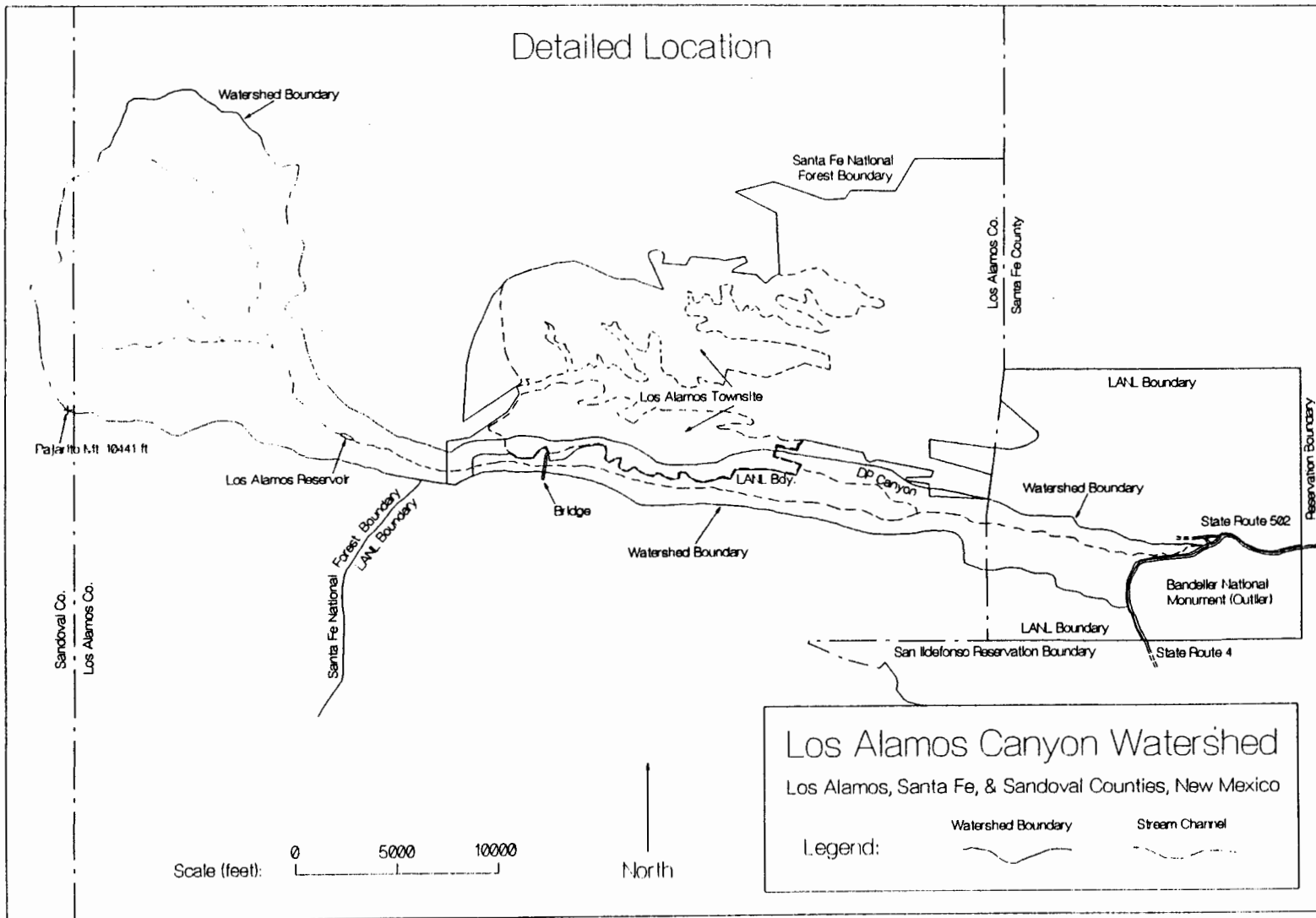


Figure 2

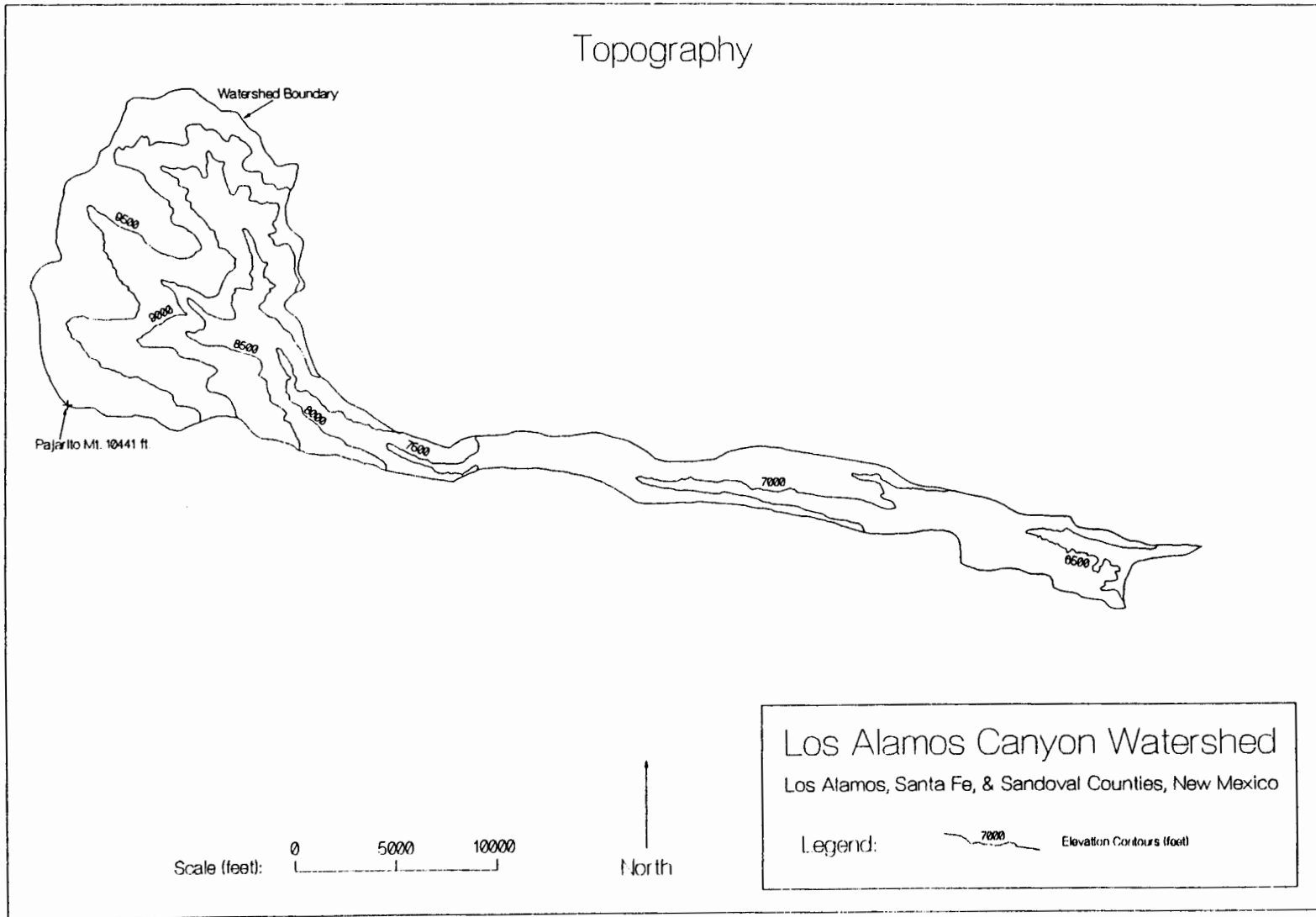


Figure 3

7

gradient ranges from ~20% in the upper basin to ~2% in the middle canyon. The canyon is generally narrow, with a floor ranging from about 100 feet or less in width in the upper basin to about 250 feet in width throughout most of the upper and middle canyon reaches. In the lower 2 miles of the study area, the floor widens to about 600 to 1,000 feet.

Steep slopes are typical of the canyon walls, on the order of 60% to 80% throughout most of the main drainage. The portions of the watershed that extend onto the adjacent mesa tops have slopes on the order of 1 to 2%. In the uppermost portion of the watershed, slopes on the order of 30 to 40% are typical.

Climate

The Los Alamos area has a semi-arid, temperate, mountain climate. Normal monthly precipitation ranges from less than one inch in the winter months to nearly 4 inches in August. Normal monthly snowfall depths are on the order of 5-12 inches in the winter months, generally between November and March (Bowen, 1990). Average annual snowfall totals ~50 inches. Mean annual precipitation totals 19.3 inches in the vicinity of LANL, but varies significantly with elevation, with lower amounts toward the Rio Grande valley to the east and higher amounts toward the Sierra de Los Valles highlands to the west. Summer rainfall provides ~75% of the total annual precipitation (Los Alamos National Laboratory, 1990). The precipitation pattern in the Los Alamos area is characteristic of a semi-arid climate in that variations from year to year are large, with annual precipitation amounts ranging from 6.80 to 30.34 inches between 1910 and 1989. The rainfall pattern during the summer months is monsoonal, with 40% of the annual precipitation falling in July and August (Bowen, 1990).

Vegetation

The Los Alamos Canyon watershed supports a diverse collection of vegetation species, with five major vegetation community types present within its ~4,100 foot

elevation range. These are the piñon-juniper, ponderosa pine, mixed conifer, spruce-fir, and subalpine grassland communities (U.S. Department of Energy, 1979).

The piñon-juniper community primarily occurs on the bordering mesa tops and the canyon slopes from the base of the watershed study area up to about 6,900 feet elevation. The ponderosa pine community generally exists at elevations between about 6,900 and 7,500 feet, but there is extensive commingling of these communities in the transitional elevations. For example, the upper and middle canyon areas of the watershed which comprise the lower portion of the study area are typically characterized by mixed ponderosa pine and piñon-juniper species. The mixed conifer community lies between about 7,500 and 9,500 feet in elevation and overlaps the ponderosa pine community in the canyon bottom and on the north slope, but primarily occurs on high mesas extending into the upper mountain slopes of the Sierra de Los Valles. The subalpine grassland community is mixed with the spruce-fir community from about 9,500 feet in elevation extending to the top of the watershed at about 10,400 feet (U.S. Department of Energy, 1979). Aspen is also prevalent in many parts of the upper basin portion of the watershed.

Regional Geology

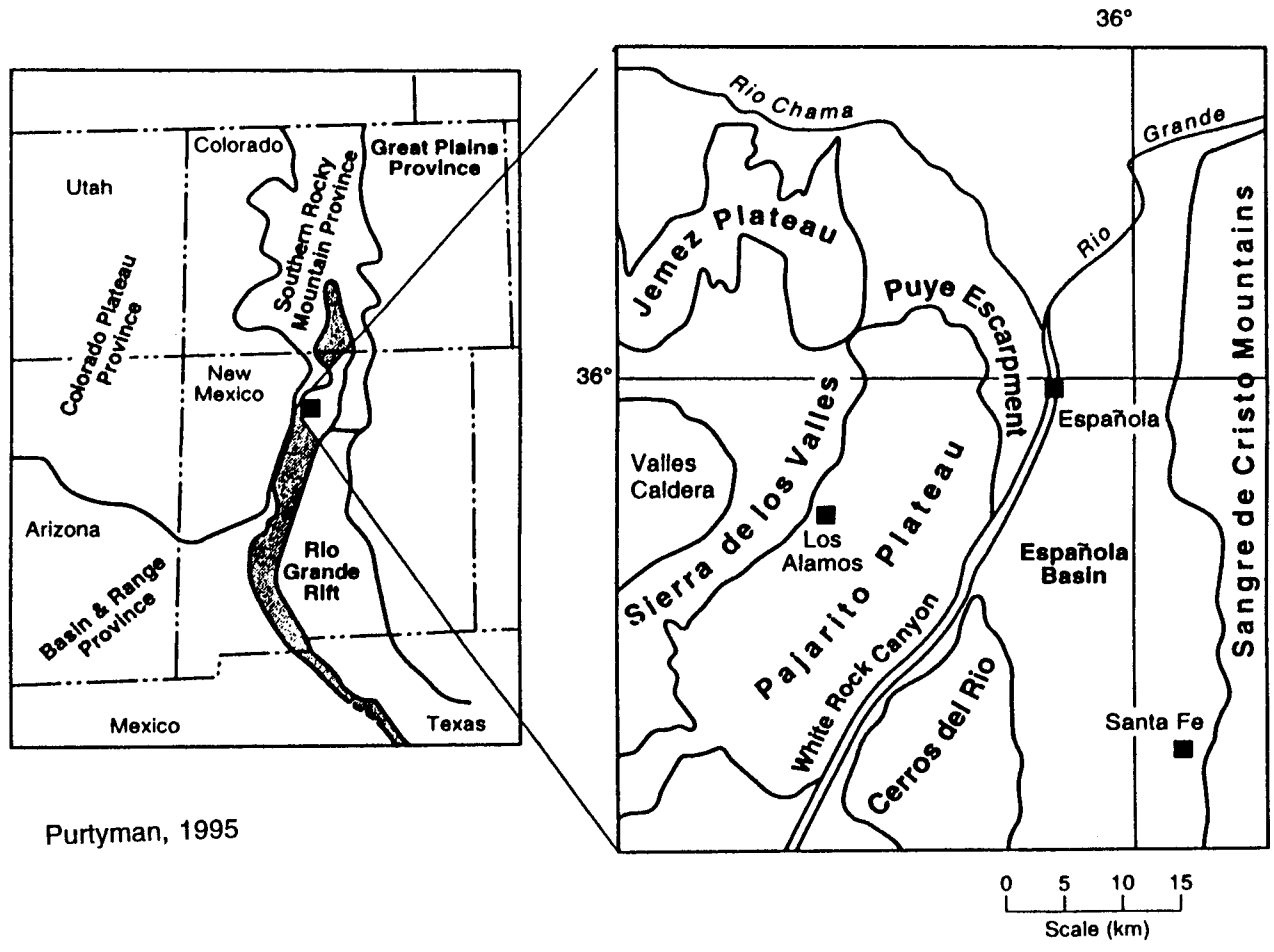
The rocks of the Jemez volcanic field (JVF) range in age from about 16.5 (± 1.4) Ma to as recent as 0.13 Ma, comprising a total volume of approximately 480 mi³ of mafic to silicic volcanic materials (Gardner et al., 1986). The formation of the JVF was related to its proximity to the Rio Grande Rift, a series of fault bounded grabens which follow a zone of crustal weakness due to extensional deformation that extends from central Colorado over 600 miles into northern Mexico (Baldrige and Olsen, 1989). The JVF occurs at the intersection of this rift zone with the Jemez lineament, a northeast trending alignment of volcanic fields (Aldrich, 1986). Thus, the extensive volcanic activity which formed the JVF was facilitated by the crustal thinning and attendant structural adjustments and crustal weakness associated with extension (Aldrich, 1986).

The Pajarito Plateau is bounded on the east by the Rio Grande and White Rock Canyon in the central and southern parts, and by the Puye escarpment to the northeast and north (Figure 4). It is bounded on the west by the Sierra de los Valles and the Pajarito fault zone (Figure 5). The Pajarito fault zone is a series of discontinuous displacements with both east and west downdrops generally trending N-S, which forms the western margin of the Velarde graben, a currently active central subbasin of the Española basin section of the Rio Grande Rift (Golombek, 1983). The overall downdrop to the east exhibits a total displacement of about 650 to 2,000 feet, 300 feet of which has occurred in the last 1.1 million years (Golombek, 1983). The southern edge of the plateau abuts sediments of the Santa Fe Group which fill the Albuquerque-Belen basin to the south and the Española basin east of the plateau and east and north of the Puye escarpment (Smith et al., 1970).

The JVF volcanics are underlain by and interbedded with the Miocene to early Pliocene Santa Fe Group (18 to 4.5 Ma), which consists of gravels, sandstones and mudstones deposited on alluvial fans that extended into the downdropped rift basins from adjacent highlands (Baldrige and Olsen, 1989). The stratigraphic relationships of the JVF volcanics are quite complex with temporal overlaps among the major stratigraphic groups (Gardner et al., 1986). The major geologic units from oldest to youngest are: the Keres Group (> 13 Ma to ~6 Ma) which forms the highlands in the southern Jemez Mountains; the Polvadera Group (~10 to ~3 Ma) which forms the highlands in the northern Jemez Mountains; and the Tewa Group (3.6 to 0.13 Ma) which forms the broad, gently dipping plateau adjacent to the parent calderas (Gardner et al., 1986). Rock types range from alkaline to silicic including alkaline basalt, andesite, dacite and rhyolite (Gardner et al., 1986).

Local Geology

The Pajarito Plateau is capped by the Bandelier Tuff of Pleistocene age, the predominant, rhyolitic unit of the Tewa Group (Figures 5, 6, 7). It ranges from ~1,000



Purtyman, 1995

Figure 4 - Regional Physiographic Features

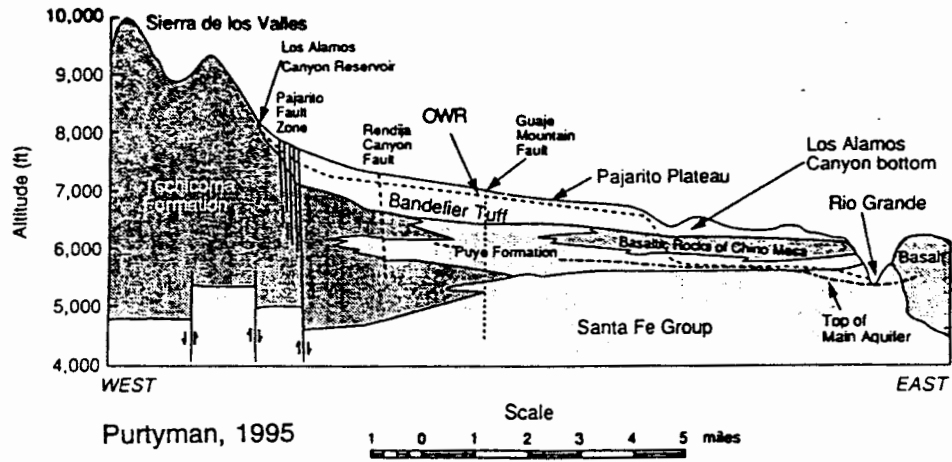


Figure 5 - Stratigraphic Diagram

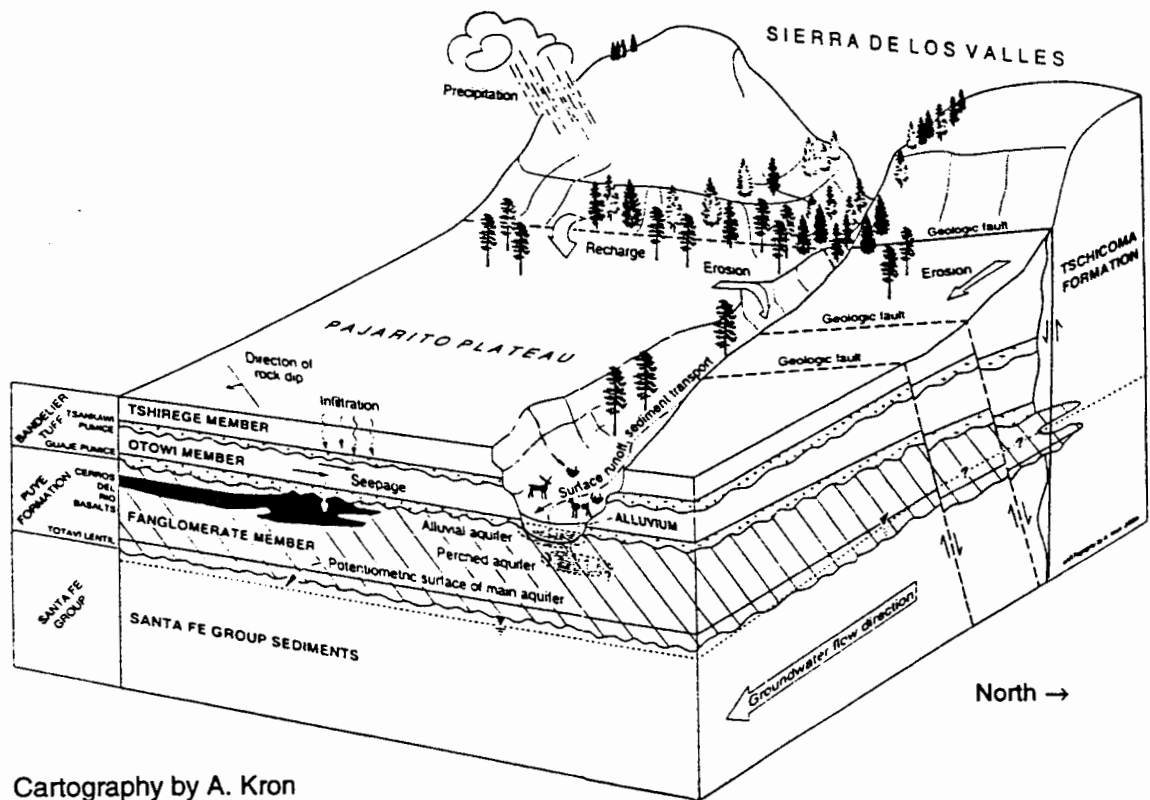
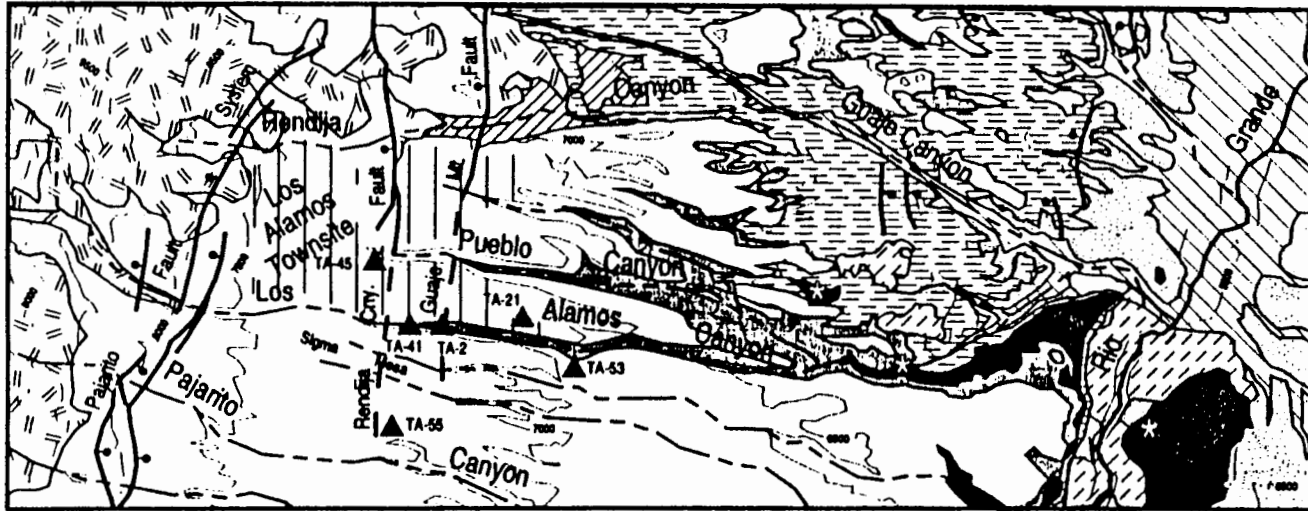


Figure 6 - Block Diagram



Modified from Smith et al., 1970

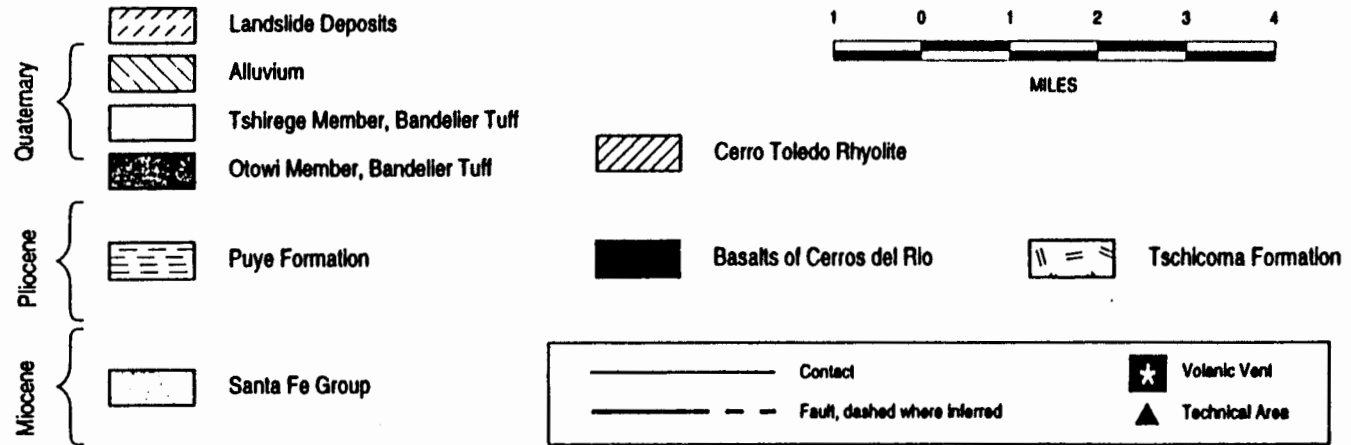


Figure 7 - Bedrock Geology

feet thick in the western part of the plateau, thinning eastward to ~260 feet thick above the Rio Grande (Stoker et al., 1991). This unit consists of two thick, superposed ash flow sheets overlying ash-fall units (Gardner et al., 1986; Purtyman, 1995).

The upper Tshirege Member of the Bandelier Tuff (Figures 6, 7) formed from the eruption of the Valles Caldera (~1.12 Ma) and consists of multiple flow units of crystal rich ash flow tuff (ignimbrite) displaying variable degrees of welding (Gardner et al., 1986; Spell et al., 1990; Broxton et al., 1995a). Within the project area it is moderately to highly welded and ~260 to ~320 feet thick, forming the nearly vertical walls of Los Alamos Canyon (Los Alamos National Laboratory, 1993).

The Tsankawi Pumice unit (Figure 6) is discontinuous and where present, occurs at the base of the Tshirege Member (Bailey et al., 1969; Broxton et al., 1995a). The unit is 0 to ~30 feet thick and consists of three to five air fall tuffs interbedded with epiclastic sands and gravels derived from the Tschicoma Formation of the Polvadera Group and with the cobbles and boulders of the Cerro Toledo Rhyolite (Purtyman, 1995; Los Alamos National Laboratory, 1993). Its age range is about 1.5 to 1.2 Ma (Gardner et al., 1986).

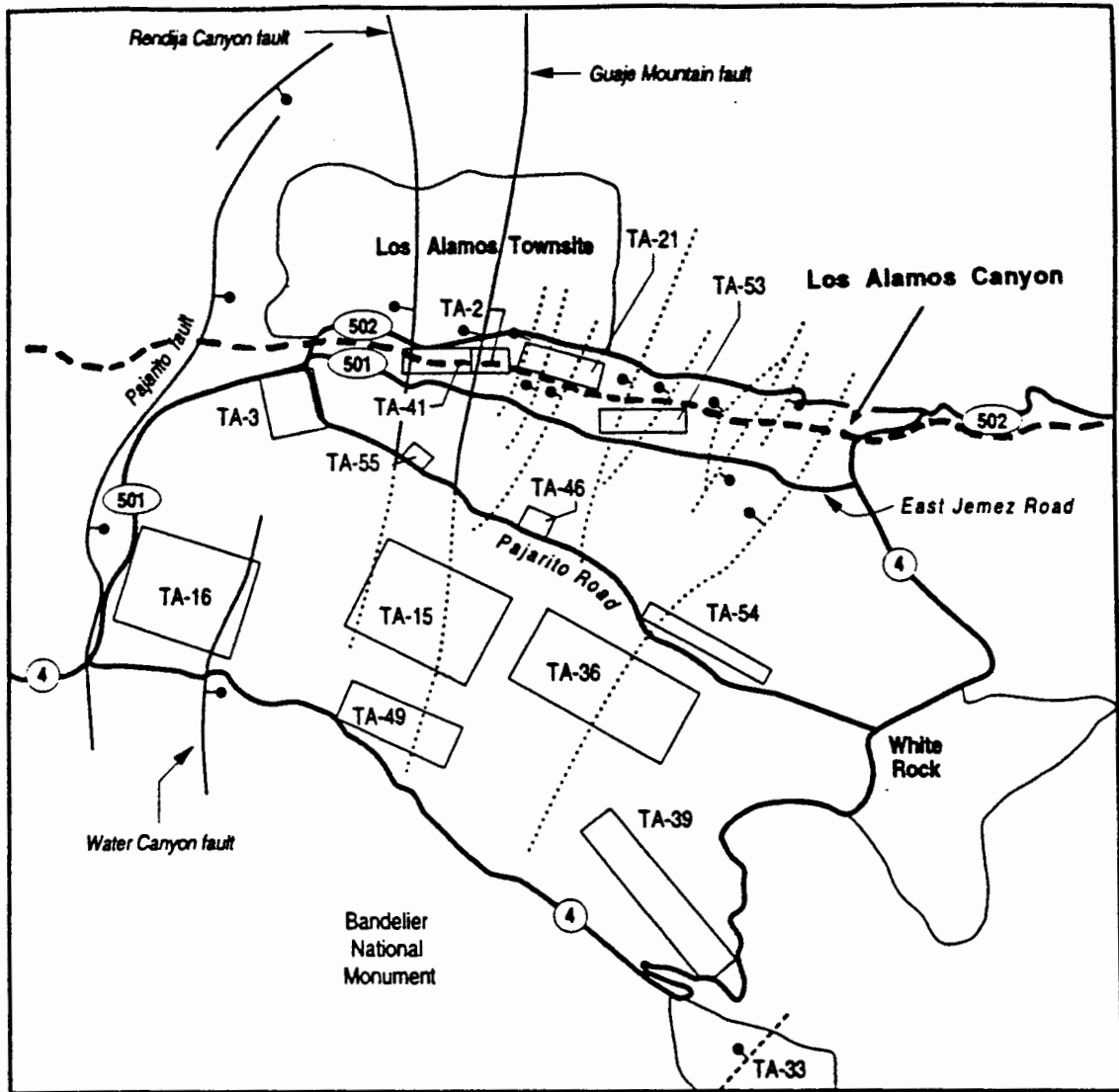
The underlying Otowi Member of the Bandelier Tuff (Figures 6, 7) formed from the eruption of the Toledo Caldera (1.45 Ma) and consists of multiple flow units of non-welded, highly porous and poorly indurated ignimbrite (Gardner et al., 1986; Spell et al., 1990). Within the project area it is ~290 to ~310 feet thick, primarily occurring in the subsurface beneath the canyon floor (Los Alamos National Laboratory, 1993).

The Guaje Pumice bed (Figure 6) occurs at the base of the Bandelier Tuff, unconformably overlying older rocks, and consists of an ash-fall unit containing lump-pumice fragments up to 2 inches in length (Purtyman, 1995). This unit is ~20 to ~28 feet thick in the project area based on drilling data from intermediate observation wells LADP-3 and LAOI(a)-1.1 located in the middle canyon area of Los Alamos Canyon and LADP-4 located in DP Canyon, a tributary to Los Alamos Canyon (Figure 2) (Broxton, et al., 1995b; Los Alamos National Laboratory Environmental Restoration Program, 1994a).

The Guaje Pumice bed is underlain by the Puye Formation (1.45 to 7 Ma) (Figures 5, 6, 7), which consists of alluvial fan deposits of conglomerates, lahars, tuffs and volcanoclastic gravels, mostly derived from and interbedded with the Polvadera Group and locally containing interbedded basalt flows of Cerros del Rio as well as dacitic to andesitic flows of the Tschicoma Formation (Gardner et al., 1986). The Puye Formation is 627 feet thick where encountered in supply well Otowi-4 located in the middle reach of Los Alamos Canyon (Purtyman, 1995). Locally, this unit includes the underlying Totavi Lentil, a poorly consolidated channel-fill deposit up to ~50 feet thick, including cobbles and boulders of quartzite, granite, gneiss, and schist reflecting a source area distant from the Jemez Mountains (Purtyman, 1995; Los Alamos National Laboratory, 1993). This unit possibly represents channel gravels of the ancestral Rio Grande (Los Alamos National Laboratory, 1993). The Puye Formation is underlain by the Santa Fe Group at a depth of 810 feet beneath Los Alamos Canyon in supply well O-4 (Purtyman, 1995).

Intermittent stream flow in the canyons has deposited alluvium ranging from about 3 to 76 feet in thickness throughout the LANL area (Purtyman, 1995). In Los Alamos Canyon, the alluvium consists of sand, gravel, pebbles, cobbles, and boulders derived from the Tschicoma Formation in the upper basin area of the watershed, and clay, silt, sand, gravel, and cobbles derived from the Bandelier Tuff in the upper and middle canyon areas. It ranges from less than 10 feet thick to a maximum observed thickness of at least 27 feet in the upper canyon area based on drilling data (Purtyman, 1995; Los Alamos National Laboratory Environmental Restoration Program, 1994b).

Several segments of the Pajarito fault system are present within the study area (Figures 5, 6, 7, 8) and generally trend north-south. The main Pajarito fault zone crosses the upper canyon approximately 2,000 feet west of the LANL boundary. This system is characterized by a number of associated normal faults that are downdropped to the east, forming a series of prominent fault scarps at the boundary between the Pajarito Plateau and the adjacent Sierra de Los Valles highlands. These scarps are most prominent south of the



Sources: Dransfield and Gardner 1985, 6612;
Gardner and House 1987, 6632

F 3-14 / LA&P WP / 110295

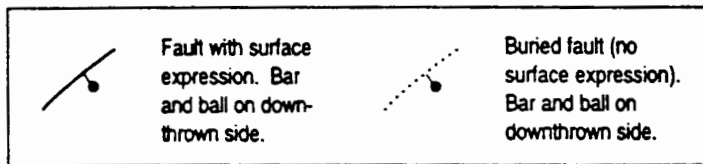


Figure 8 - Locations of Major Faults

study area, but decrease in size northward towards Los Alamos Canyon where the fault system is more poorly defined (Gardner and House, 1987; Gardner, et al., 1990). Other associated segments of the Pajarito fault zone which cross the study area are the Rendija Canyon and Guaje Mountain segments (Figures 5, 7, 8). The Guaje Mountain segment is associated with a ~650 foot wide zone of abundant fracturing observed in the canyon walls (Vaniman and Wohletz, 1990). The Rendija Canyon segment is associated with two such adjacent zones of similar width (Vaniman and Wohletz, 1990). Where exposed north of Los Alamos Canyon, these faults are expressed as zones of gouge and breccia generally 100 to 150 feet wide with visible offsets of stratigraphic horizons. Both fault segments are dominantly normal-oblique faults with downdropped west sides (Los Alamos National Laboratory, 1993). The Guaje Mountain segment has exhibited movement as recently as 4,000 to 6,000 years ago (Gardner et al., 1990).

Hydrology

All surface water drainage and groundwater discharge from the Parajito Plateau that doesn't evaporate eventually reaches the Rio Grande, which flows adjacent to the mouth of Los Alamos Canyon at Otowi about 3 miles east of the LANL boundary and about 4 miles east of the study area (Purtyman, 1995; Puye Quadrangle, USGS 7½ minute series topographic map, rev. 1993). Surface water within LANL occurs primarily as intermittent streams. Springs on the flanks of the Jemez Mountains supply base flow to some of the canyons, including Los Alamos Canyon, and storm runoff and snowmelt periodically swell the stream flows, but the amounts are insufficient to maintain perennial flow except in upper Los Alamos Canyon and in lower Pajarito and Ancho Canyons (Purtyman, 1995).

Perennial streamflow only occurs in the upper basin portion of the Los Alamos Canyon watershed above Los Alamos Reservoir (Figure 2). Below the reservoir dam, streamflow is intermittent and primarily occurs during spring snowmelt and during periods

of heavy rainfall generally occurring in the summer and fall. Several seeps have been observed to provide minimal flow levels to portions of the stream in the upper and middle canyon areas during intervening dry periods (personal communication, David Shaull, ESH-18). This baseflow is due to discharging groundwater which is likely derived from prior recharge in the upper basin of the watershed. For most of the canyon however, during dry periods and when winter precipitation is maintained in a frozen state as snowpack, the streambed dries up completely.

Flow from spring snowmelt only occasionally extends to the confluence with the Rio Grande. Between 1975 and 1986, snowmelt runoff reached the Rio Grande during only 5 of those years for a total of 205 days, averaging 41 days per year but only 4.7% of the days in the total 12-year period (Los Alamos National Laboratory, 1995).

Los Alamos Reservoir has a surface area of approximately 2.5 acres and has a maximum depth of approximately 25 to 30 feet, holding an estimated water volume of approximately 41 acre-feet (Purtyman et al., 1987). The reservoir provided part of the LANL water supply through the late 1950's, but since then the only water usage has been approximately 5 million gallons/year for irrigating the high school football field during the summer months. (personal communication, David Sneesby, LANL Utilities and Infrastructure group).

The alluvium deposited in the canyon bottom is substantially more permeable than the underlying tuff. Based on the results from slug tests conducted on nine alluvial observation wells in the canyon (Figure 9; refer to Table 7), the saturated hydraulic conductivity (K_{sat}) of the alluvium ranges from 3.8×10^{-5} ft/s to 7.9×10^{-4} ft/s with a mean value of 3.2×10^{-4} ft/s (9.6×10^{-3} cm/s) (Gallaher, 1995). The K_{sat} for the Otowi Member ranges from 3.6×10^{-7} ft/s to 2.6×10^{-4} ft/s with a mean value of 2.1×10^{-5} ft/s (6.3×10^{-4} cm/s) based on laboratory permeameter test results for 25 core samples from a number of locations within LANL (Rogers and Gallaher, 1995). It is also possible that water-rock reactions (hydrolysis of glass) have altered the underlying tuff to clay minerals (smectite

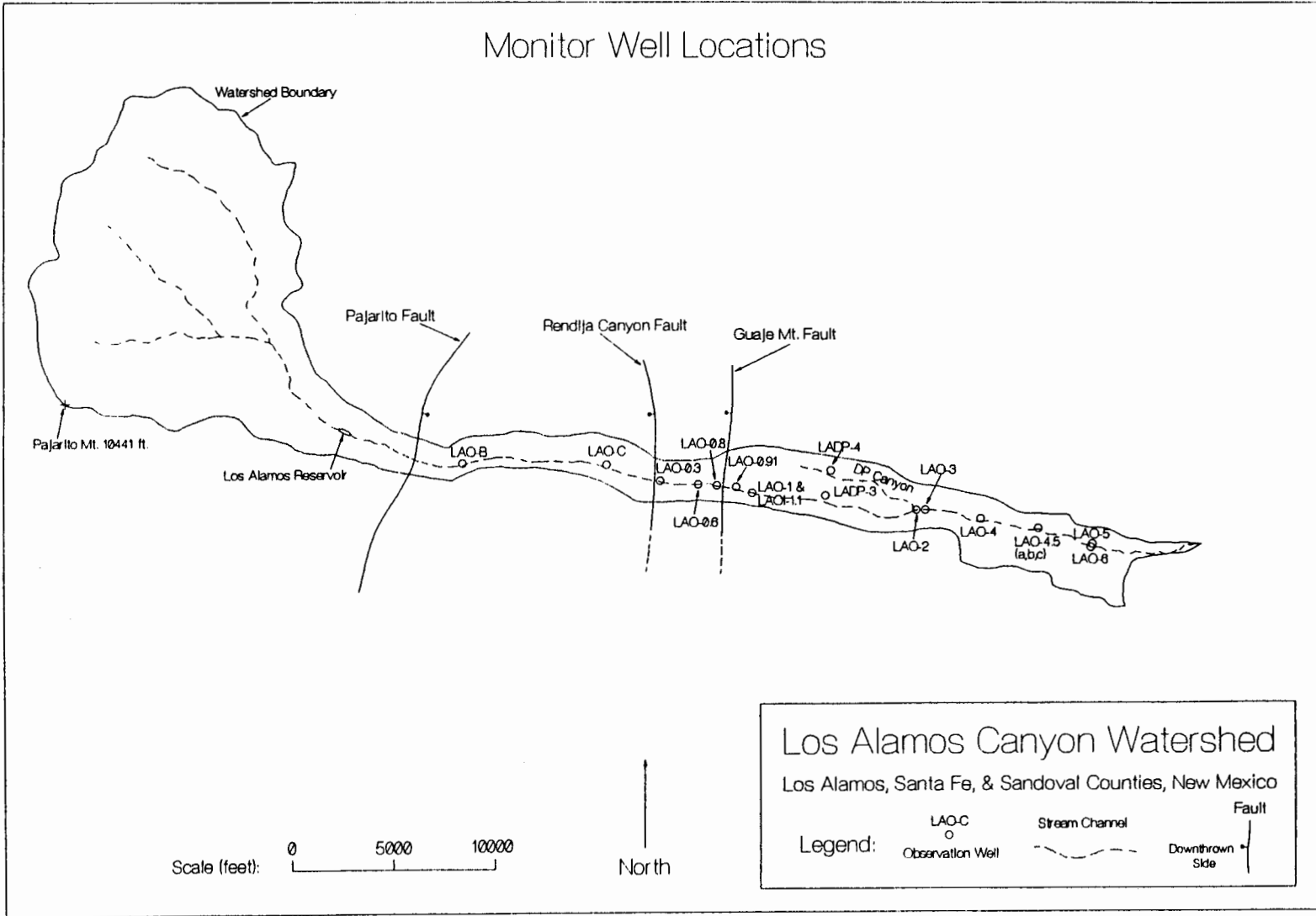


Figure 9

and kaolinite) at the base of the alluvium, forming material with lower hydraulic conductivity, and thus a perching layer (Longmire et al, 1996). These factors have resulted in the development of a variably saturated, perched aquifer in the alluvium with a highly dynamic behavior.

Whereas alluvial well water levels in the upper canyon area are fairly stable, presumably due to recharge from baseflow, in the middle canyon area infiltration of surface water creates a variably saturated zone in the alluvial deposits with the highest saturation levels occurring during spring snowmelt and during the summer monsoon season when active streamflow occurs. During dry periods, the alluvium dries out completely in about the lower third of the study area (from wells LAO-1 to LAO-6, see Figure 9). Saturation levels have been observed by the author to fluctuate by up to over eight feet with highly dynamic responses to precipitation events or to drying out conditions occurring during a time period of a few days.

This bi-modal behavior of alluvial saturation level variation is illustrated in Figure 10 which shows varying aquifer head profiles developed from observed water levels in several alluvial observation wells on three different dates in 1995; the first during the winter frozen period, the second during the peak spring snowmelt runoff period, and the third during the fall dry period. As can be seen, the water levels upgradient from well LAO-0.8 are relatively consistent while the levels fluctuate more dramatically down-gradient from this well. In LAO-0.8, the water level remains anomalously low. This well is located very near (within) the Guaje Mountain fault zone. It thus appears that while the upper canyon area has somewhat constant saturation levels likely due to consistent recharge from baseflow, this source of recharge is apparently absent in the middle canyon area, presumably lost to enhanced infiltration seepage from the alluvium into fractures associated with the fault zone, thus resulting in the consistently low water levels observed in well LAO-0.8. Downgradient from this point, saturation of the alluvium appears to be more dependent on intermittent streamflow infiltration for recharge, thus explaining the

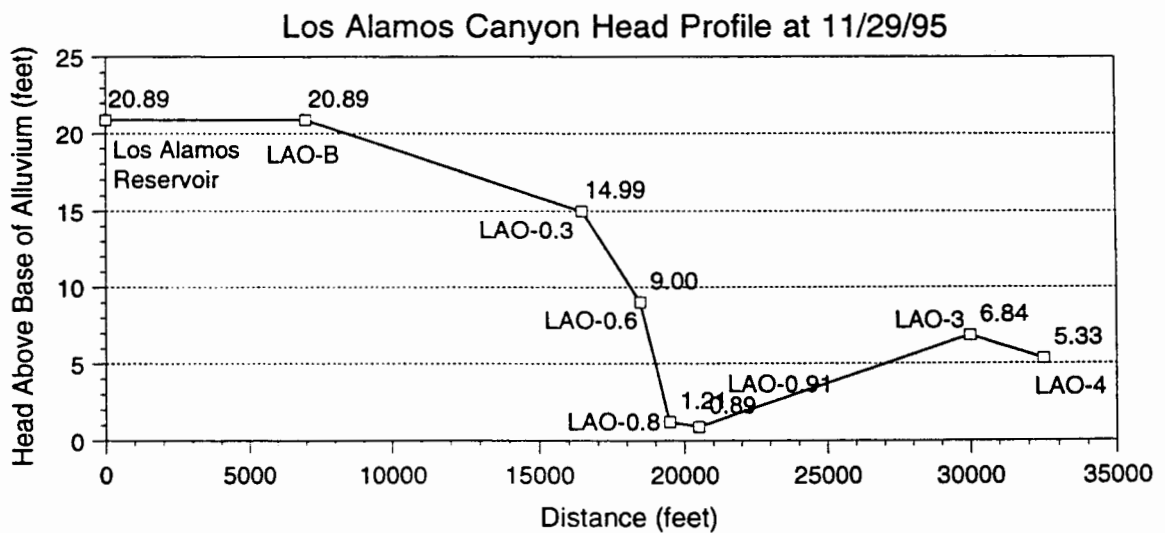
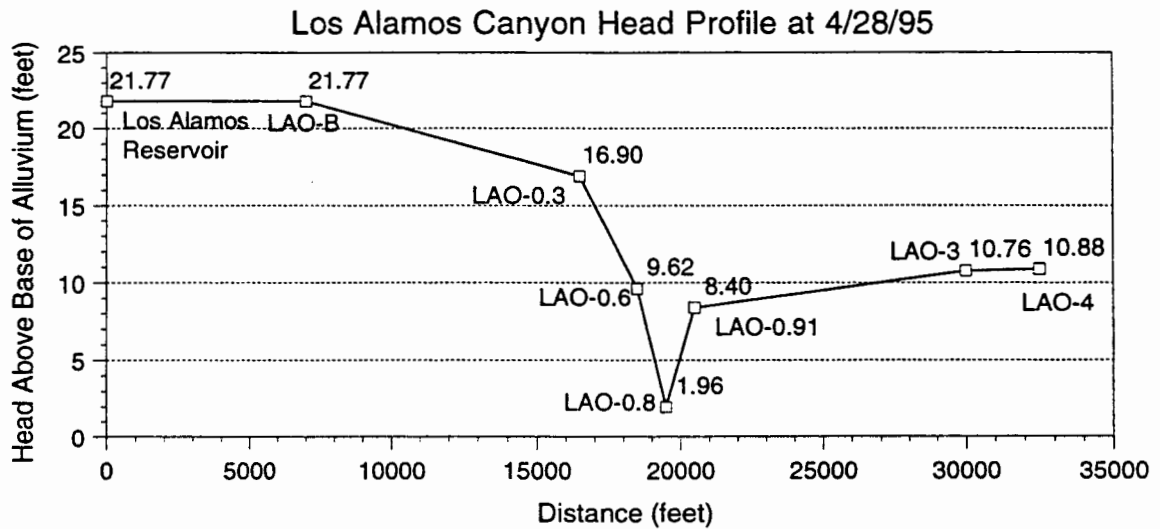
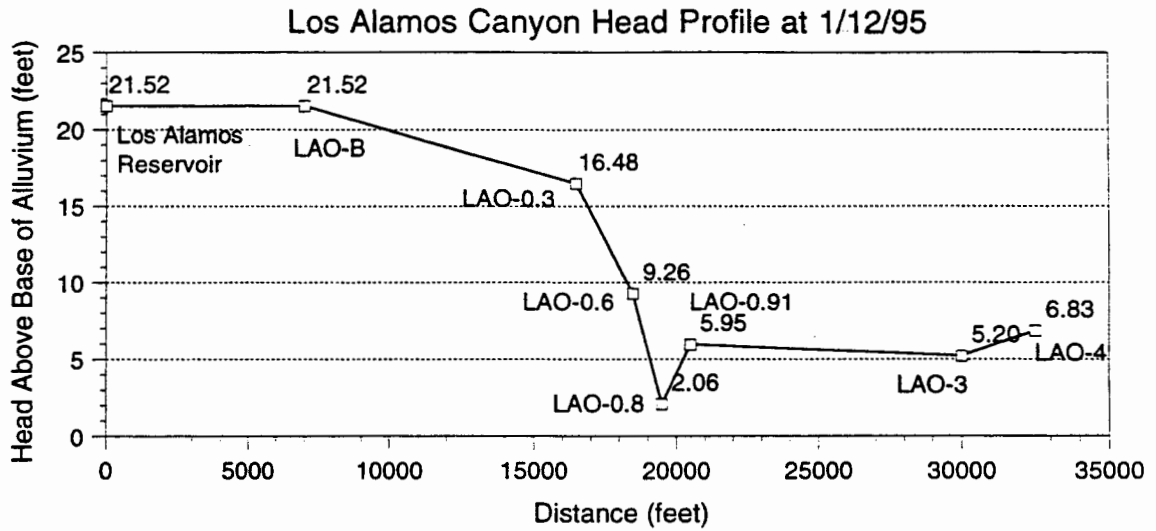


Figure 10: Los Alamos Canyon Alluvial Head Profiles

more dynamic nature of the water level fluctuations observed in the middle canyon area.

Beneath the alluvial aquifer, the Bandelier Tuff (Otowi Member) is unsaturated. The Otowi Member has an average porosity of 47% throughout the LANL area (Rogers and Gallaher, 1995). Data from observation well LADP-3, drilled in the middle reach of Los Alamos Canyon in 1993, indicate an average gravimetric moisture content of 16% for the unsaturated Otowi Member extending to a depth of 325 feet (Broxton et al., 1995b). Unsaturated hydraulic conductivity for the Bandelier Tuff varies with moisture content and typically has values two to five orders of magnitude lower than that for saturated tuff, ranging from 1.0×10^{-7} to 1.1×10^{-10} ft/s (3.1×10^{-6} to 3.3×10^{-9} cm/s) for non-welded tuff (Stoker et al., 1991).

An intermediate depth perched saturated zone occurs in the Guaje Pumice bed at the base of the Bandelier Tuff, intercepted at a depth of 294 feet in observation well LAOI-1.1 and at 325 feet depth in observation well LADP-3 (see Figure 9). The zone of saturation is about 5 to 22 feet or more thick based on the well data and likely extends into the underlying Puye Formation (Los Alamos National Laboratory, 1995). The extent of this aquifer is poorly defined, but the scarce data suggest that the perched aquifer probably does not extend beneath the mesas (Purtyman, 1975, 1995). Chemical data suggest a direct connection between the alluvial aquifer and the intermediate perched aquifer (Broxton et al., 1995b; Longmire et al., 1996). The perched aquifers in the alluvium and Guaje Pumice bed are minor in volume and localized in extent and are not utilized for water supply.

The water supply for both LANL and the community of Los Alamos is produced from the regional aquifer which occurs within the sediments of the Santa Fe Group about 750 feet beneath the canyon floor in the middle canyon area and extends into the lower part of the Puye Formation in the central and western portions of the plateau (Purtyman, 1995). The regional aquifer is separated from the intermediate depth perched aquifer in the Guaje Pumice Bed by approximately 590 feet of unsaturated Puye Formation (Broxton et

al., 1995b; Los Alamos National Laboratory, 1992).

Until recently, it was assumed there was little, if any, hydrologic connection between the regional aquifer and the alluvial aquifer (Purtyman, 1995). However, tritium measurements in groundwater samples collected from regional aquifer supply wells located in lower Los Alamos Canyon and observation wells in Pueblo Canyon indicate the presence of young water with ages less than 30 years (Goff and Adams, 1993; Blake et al, 1995). Also, the previously mentioned recent detection of ^{90}Sr in Test Well 3 in the middle canyon area indicates that some hydrologic connection is suggested, although the mechanism and extent of recharge are unknown.

Previous Investigations

Historically, the focus of hydrological studies in the Los Alamos area has emphasized characterization of the regional aquifer in the Santa Fe Group (Theis, 1950; Theis and Conover, 1962; Griggs, 1964; Cushman, 1965; Purtyman, 1977, 1984; Goff and Sayer, 1980; Stoker et al., 1993).

A few studies have examined the perched alluvial aquifers occurring in the canyon bottoms including an extensive monitoring study of the alluvial groundwater in Mortandad Canyon, located about 4,000 feet south of Los Alamos Canyon (Abrahams et al., 1962; Purtyman, 1974; Purtyman et al., 1983; Stoker et al., 1991; Longmire et al, 1996). Tracer studies using tritium and chloride in Mortandad Canyon have shown that the velocity of groundwater flow ranges from about 60 feet/day in the upper reach to about 7 feet/day in the lower reach of the canyon (Purtyman, 1974). In Los Alamos Canyon, the average groundwater flow velocity in the alluvium has been estimated at ~3 feet/day (Los Alamos National Laboratory, 1992; Gallaher, 1995).

A few studies have addressed the unsaturated zone beneath the alluvium in the canyon bottoms. Stoker et al. (1991) analyzed tritium distributions from core samples in Mortandad Canyon and concluded that LANL effluents have migrated downward at least

200 feet vertically beneath the canyon bottom. Another recent study determined moisture retention characteristics for a large number of core samples of the Bandelier Tuff and related units from laboratory tests, but concluded that flow velocities derived from these data did not adequately account for apparent travel times suggested by geochemical data (Rogers and Gallaher, 1995). A comparison of the decay curve for tritium extrapolated from the activity observed in the Guaje Pumice Bed in intermediate observation well LADP-3 to annually measured tritium activities in the alluvium suggests a minimum downward flow velocity of about 15 feet/year (Broxton et al., 1995b).

The intermediate depth perched aquifers occurring between the alluvial and Santa Fe Group aquifers have received only sporadic and brief attention (Weir et al., 1963; Abrahams and Purtyman, 1966; Purtyman, 1975). In Los Alamos Canyon, a perched aquifer identified as occurring in the Puye Formation was encountered at a depth of 253 feet in supply well Otowi-4 drilled in 1989, but was not reported in test well TW-3 located 300 feet to the east, suggesting a limited extent for this aquifer. However, that test well was drilled in 1947 with a cable tool rig and consequently, a direct comparison of drilling data could be suspect (Stoker et al., 1992). Observation well LADP-3 is located about 4,300 feet west of Otowi-4 and encountered perched water at 325 feet depth, but indicated that the zone of saturation was in the Guaje Pumice bed overlying the Puye Formation (Broxton et al., 1995b). Analysis of major ion chemistry shows a strong similarity between the alluvial and Guaje Pumice bed/Puye Formation groundwaters. Along with the presence of low-level tritium concentrations in the intermediate depth perched aquifer, this suggested a hydrologic connection between the two aquifers. Volumetric mixing calculations comparing the average chloride concentration over a 25 year span in alluvial observation well LAO-1 (located 3700 feet upgradient from LADP-3) to the chloride concentration in the perched aquifer in the Guaje Pumice bed measured in LADP-3 suggested that up to 70% of the groundwater in the Guaje Pumice bed originated from the alluvial groundwater (Broxton et al., 1995b).

Only a few previous workers have addressed water budget computations in any kind of detail in the Los Alamos area. Most of this work has been focused in Mortandad Canyon, which has received the greater part of treated waste effluent discharges from LANL (Purtyman, 1975). Purtyman (1967) made extensive water budget calculations for three separate reaches of the canyon for the period from July, 1963 to July, 1965. Koenig and McLin (1992) used a lumped parameter analytical model based on a water balance equation to estimate seepage from the alluvial aquifer into the underlying tuff.

Nyhan (1989) used the CREAMS model (Knisel, 1980) with daily precipitation, mean monthly temperature and mean monthly solar radiation data along with moisture probe data to study water balance relationships at the Area P landfill site located about 11,000 feet south of upper Los Alamos Canyon.

Very little previous work has been done to quantify a comprehensive water budget for the Los Alamos Canyon area. Some bits and pieces of this type of information have been developed, however. Investigations of streamflow runoff in Los Alamos Canyon and other nearby drainages have been made by the U.S. Geological Survey (1961, 1962) and by LANL in conjunction with the USGS (Wilcox, et al., 1996; Shaull et al., 1996a, 1996b). McLin (1992) simulated floodplain hydrology in Los Alamos Canyon using the U.S. Army Corps of Engineers HEC-1 Flood Hydrograph Package and HEC-2 Water-Surface Profile codes. Nyhan et al. (1989) used statistical correlations of LANL area precipitation data to predict 10-year and 100-year monthly precipitation amounts. Climatology has also been addressed in a general fashion for the LANL area (Bowen, 1990). Evapotranspiration rates determined from latent heat flux data were analyzed over a 10 month period in 1992 for the Technical Area-59 site (Pope, 1993). However, a comprehensive hydrologic budget analysis for any part of the Los Alamos Canyon area incorporating all of these data types has not been previously attempted.

Only a few numerical groundwater flow modeling studies within the Los Alamos area have been previously made. Saturated flow modeling of the regional aquifer using

MODFLOW (McDonald and Harbaugh, 1988) was conducted by McAda and Wasiolek (1988), McAda (1990), and Frenzel (1995), who produced steady-state and transient models with the purpose of investigating the effects of supply well pumping. The only previous numerical flow modeling of a saturated alluvial aquifer in a canyon bottom in the LANL area was by Stone (1995) in which MODFLOW was used to create a one-dimensional steady-state model representing the alluvial aquifer in Mortandad Canyon. The use of a streamflow routing package with this model generated continuous streamflow, which was determined to represent a quantification of infiltration seepage from the alluvium into the underlying tuff since continuous streamflow seldom actually occurs in Mortandad Canyon. Geddis (1992) constructed a two-dimensional unsaturated flow model for a portion of Mortandad Canyon using the finite-element UNSAT2 code (Davis and Neuman, 1983). Birdsell et al. (1995) conducted numerical modeling of unsaturated flow in two dimensions beneath a mesa top at Material Disposal Area G located on Mesita del Buey (about 7,000 feet south of Los Alamos Canyon) using the finite-element FEHMN code (Zyvoloski et al., 1995).

HYDROLOGIC BUDGET ANALYSIS

Conceptual Model

The conceptual model that was employed to evaluate the water budget is the basic hydrologic mass balance equation (mod. after Viessman, Jr., et al., 1989):

$$P - R - I - ET = \Delta S \quad (1)$$

where P = precipitation, R = runoff, I = infiltration, ET = evapotranspiration, and ΔS = change in storage. Since there are no data specific to the study area available for assessing variations in soil moisture content, for this evaluation it was assumed that $\Delta S = 0$. The impact of this assumption is felt to be minimal for the annual budget calculations presuming that seasonal variations are balanced out on an annual cycle. The assumption is a probable source of error in the detailed budget calculations, however, inasmuch as shorter time periods were analyzed and were defined on the basis of generally alternating wetting and drying conditions. Since data were available to assess the P , R , and ET parameters, I was thus determined as the residual from equation 1; i.e.:

$$I = P - R - ET. \quad (2)$$

Data Sources

The water budget calculations utilized data obtained from several sources. Meteorological data were collected by the LANL meteorology group (ESH-17) and the United States Department of Agriculture Bureau of Natural Resources Conservation (USDABNRC). Streamflow data were collected by the USGS and the LANL environmental surveillance group (ESH-18). Data from 5 precipitation measurement stations and 3 streamflow gages were utilized in the budget calculations (Figure 11). The

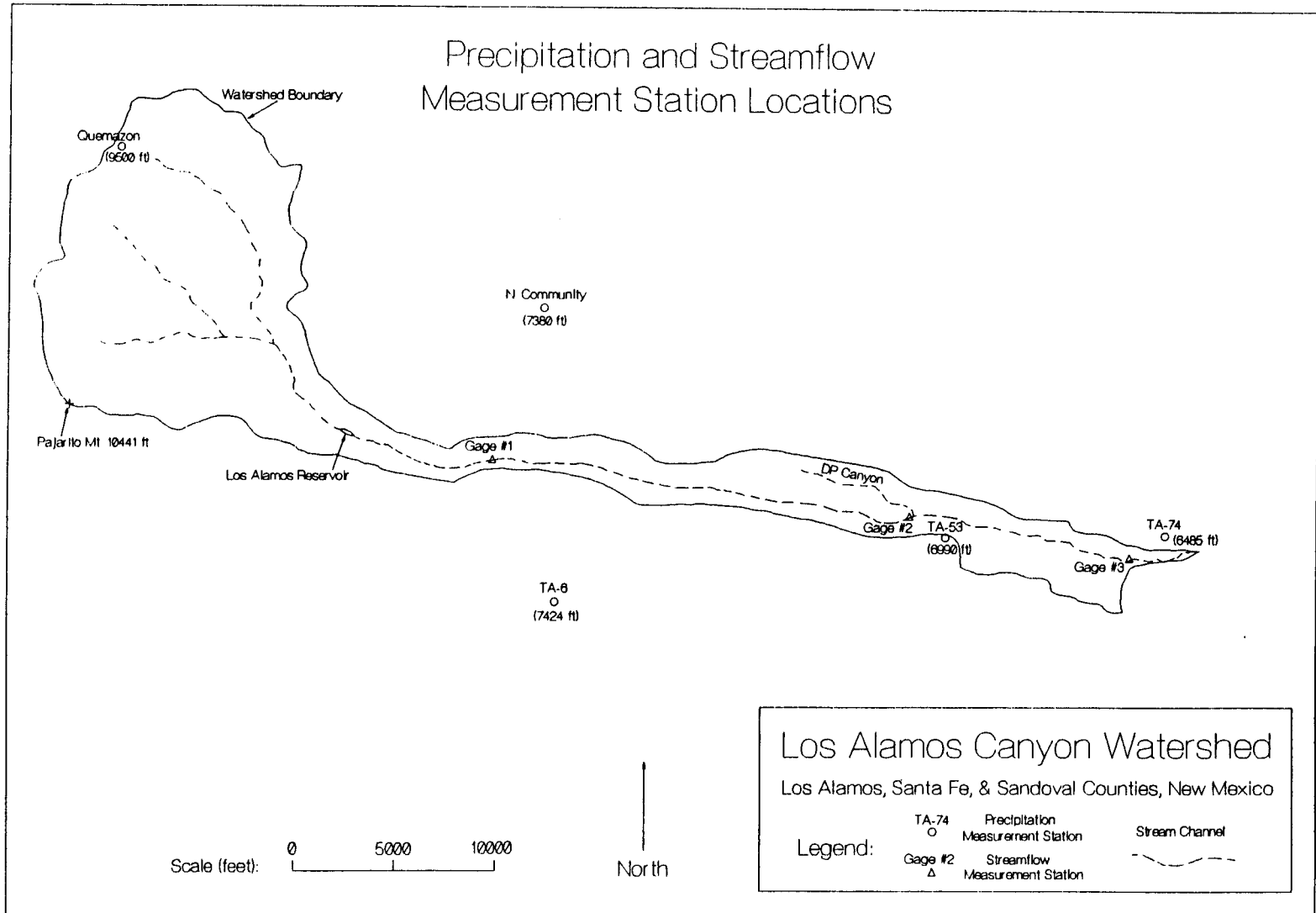


Figure 11

TA-6, TA-53, TA-74, and North Community stations are operated by the LANL meteorology group while the Quemazon station is operated by the USDABNRC. Daily precipitation totals for the LANL stations were obtained by downloading the data from the ESH-17 World Wide Web home page (<http://weather.lanl.gov/cgi-bin/datarequest.pl>). Precipitation measurements at the LANL stations are made with tipping bucket gages that are heated and protected by wind screens. Their accuracy is estimated at $\pm 10\%$ (personal communication, Greg Stone, ESH-17). Tabulations of these data for the 1993, 1994, and 1995 water years and 10/1/95 to 11/2/95 period are included as Appendices A through D.

Daily precipitation and snowpack data for the Quemazon station precipitation gage and "SNOTEL" (snow telemetry) site were downloaded from the USDABNRC Portland, Oregon office ftp site (<ftp.wntc.nrcs.usda.gov>). Daily precipitation totals are measured with a calibrated pressure transducer in a 12-inch diameter rain gage with alter shield. Snowpack measurements are made with a 10-foot diameter hypalon rubber snow pillow filled with an anti-freeze fluid that is displaced by overlying snowpack weight into a manometer equipped with a calibrated pressure transducer. Accuracy is estimated at $\pm 10\%$ based on comparison to periodic ground truth field measurements (personal communication, Mike Gillespie, USDABNRC Snow Survey Office, Lakewood, Colorado). The Quemazon precipitation data for the 1993, 1994, and 1995 water years provided the precipitation totals for the annual water budget and a tabulation of these data is included in Appendix E. A tabulation of the precipitation and snowpack (water equivalent) data for the 1994 and 1995 water years and 10/1/95 to 11/2/95 period with calculations of daily net non-frozen precipitation yield is included in Appendix F. These data were utilized in the detailed water budget calculations. An analysis of major precipitation events indicated that the Quemazon station data were lagging the LANL data by one day (i.e. reported as occurring one day later). The data were thus adjusted by moving all daily totals back one day, and the included tabulations reflect this adjustment. Since the obtained data set extended only through 9/30/95, daily precipitation totals for the

10/1/95 to 11/2/95 period at the Quemazon site were estimated by multiplying the North Community station data for this period by the average proportion between the two stations during the comparable 10/18/94 to 11/10/94 dry period (assuming no snowpack).

At the TA-6 station, data are also collected on latent heat energy flux. These data are obtained through application of the eddy correlation method which is a standard method employed in micrometeorology (Stull, 1988; Priestly, 1959). Vertical fluctuations in wind velocity and absolute humidity are measured and a covariance is performed on the two signals at an amplitude of 2 Hz. The resulting data are reported in units of mega-Joules per square meter ($J/m^2 = ML^2/T^2L^2 = M/T^2$ units). ET amounts are determined by dividing the latent heat energy flux by the latent heat of vaporization (in units of $J/m^3 = ML^2/T^2L^3 = M/T^2L$ units), yielding units of length. A conversion factor was determined to transform the latent heat energy data to units of mm of ET by the following procedure:

The latent heat of vaporization for water at 21° C = 1049 Btu/lb and the density of water at this temperature is 62.3 lb/ft³ (Viessman, Jr. et al., 1989, p. 762). Since 1 Btu = 1055 J (Young, 1992), and 1 ft³ = 0.0283 m³, thus:

$$\left(\frac{1049 \text{ Btu}}{\text{lb.}}\right)\left(\frac{62.3 \text{ lb.}}{\text{ft}^3}\right)\left(\frac{1 \text{ ft}^3}{0.0283 \text{ m}^3}\right)\left(\frac{1055 \text{ J}}{\text{Btu}}\right) = \frac{2.436 \times 10^9 \text{ J}}{\text{m}^3} \quad (3)$$

and:

$$\frac{1 \text{ MJ}}{\text{m}^2} \Rightarrow \frac{\left(\frac{10^6 \text{ J}}{\text{m}^2}\right)}{\left(\frac{2.436 \times 10^9 \text{ J}}{\text{m}^3}\right)} = 4.1 \times 10^{-4} \text{ m} \left(\frac{1000 \text{ mm}}{\text{m}}\right) = 0.41 \text{ mm ET.} \quad (4)$$

Equation 4 was used to transform the latent heat energy data to units of mm of ET, which were then converted to inches to conform with the precipitation data. Testing of the wind velocity meter by the LANL meteorology group indicated that the propeller was not fast enough to accurately sense all the fluctuations and that the instrument was underestimating moisture flux by ~10%, so the ET amounts determined from equation 2 were increased by this amount. The ET calculations are included with the TA-6 precipitation summary in Appendix A. The wind velocity and hygrometer instrumentation is located on a tower at a height of 12 meters above ground level. The site is in a narrow east-west meadow on Two-mile Mesa at a surface elevation of 7,424 feet above sea level. Vegetation covers about 80% of the surface, characterized by short grasses and low shrubs. Ponderosa pines of 12 meter height are present within 100 meters of the tower to the south and within 150 meters to the north (Los Alamos National Laboratory, 1996). The accuracy of this method of measuring latent heat energy flux and evapotranspiration is not quantified and extrapolation of these single point data throughout the entire watershed area may entail a significant, though unknown level of error.

Streamflow discharge is measured by a Parshall flume (Gage #1), a sharp-crested weir (Gage #2), and a broad-crested weir (Gage #3), calibrated to stage levels recorded by pressure transducers (see Figure 11). Measurement accuracy is $\pm 3\%$ for the Parshall flume (personal communication, David Shaul, ESH-18) and generally $\pm 5\%$ for the weirs (Winter, 1981). Gage #3 was operated by the USGS prior to the 1995 water year and has since been operated by ESH-18. Gages #1 and #2 are also operated by ESH-18 and were installed just shortly before the 1995 water year began. Thus previous years' data are only available for Gage #3. These data were utilized in the annual water budget calculations for the entire watershed. Data from all three gages were utilized in the detailed water budget calculations and allowed a distinction between the upper basin and upper/middle canyon areas. Mean daily discharge rates for the 1995 water year are included in Appendix G and were converted to daily total discharge volumes to facilitate the water budget calculations.

Annual Water Budget

Annual water budget calculations were made for the 1993, 1994, and 1995 water years. Prior to this period, calibration problems with the latent heat flux instrumentation rendered that data unreliable (personal communication, Greg Stone, ESH-17).

The initial requirement for the water budget calculations is the determination of precipitation volumes for the watershed. The watershed boundary was determined by drawing a line along the topographic divide on the U.S.G.S. Los Alamos quadrangle 1:100,000 scale topographic map. The watershed boundary and topographic contours at 500 foot intervals were then digitized with an ACECAD® model A-1212 digitizer using FastCAD® software (Evolution Computing, 1992).

To determine the most appropriate method for regionalizing the discrete point precipitation data, a comparison of monthly precipitation totals from all five utilized measurement stations was made (Figure 12). Though the pattern of variation was not totally consistent, it is clear that there is a fairly strong correlation between precipitation amounts and elevation. Regression analyses were thus performed on the annual precipitation amounts for each station plotted by station elevation to extrapolate the precipitation data to intervening elevations not represented by the limited data available (Figure 13). High r^2 values for each plot indicate a high degree of certainty for predicting precipitation amounts based on varying elevations. Extrapolated annual precipitation depths were then determined for the midpoint values between the elevation contours shown in Figure 3 except for the highest topographic interval. Elevations greater than the 9,500 feet elevation of the uppermost measurement station were assigned the same precipitation depth as was measured at that station. The areas between the elevation contours were determined with the FastCAD® software used to digitize the elevation data.

The ET data were compiled from the TA-6 station data and compared to the precipitation data from that site (Figure 14). As can be seen, the relation between ET and precipitation varies considerably on a seasonal basis. ET amounts vary fairly regularly on

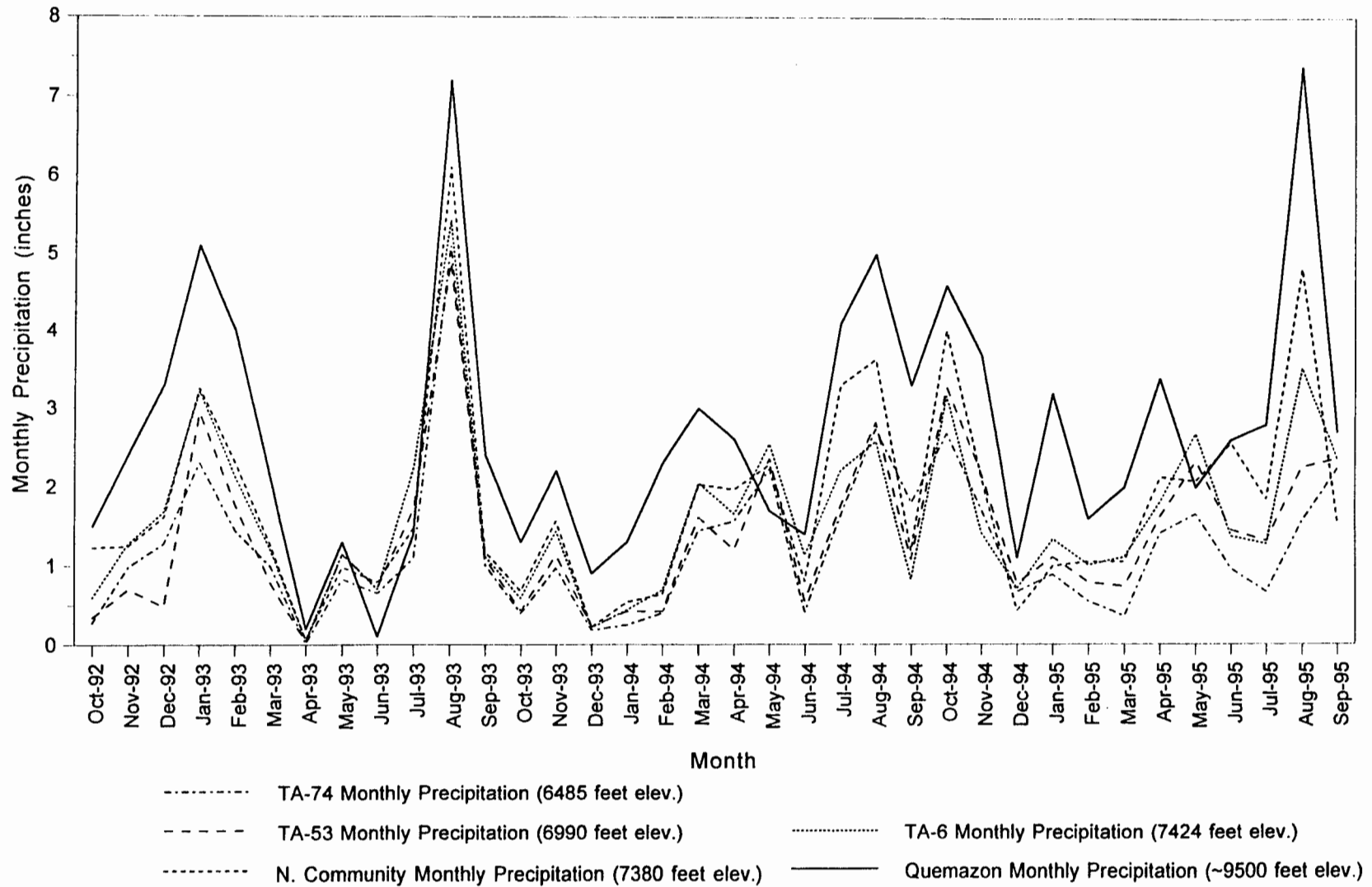


Figure 12: Los Alamos Canyon Watershed Precipitation Data--Monthly Comparison

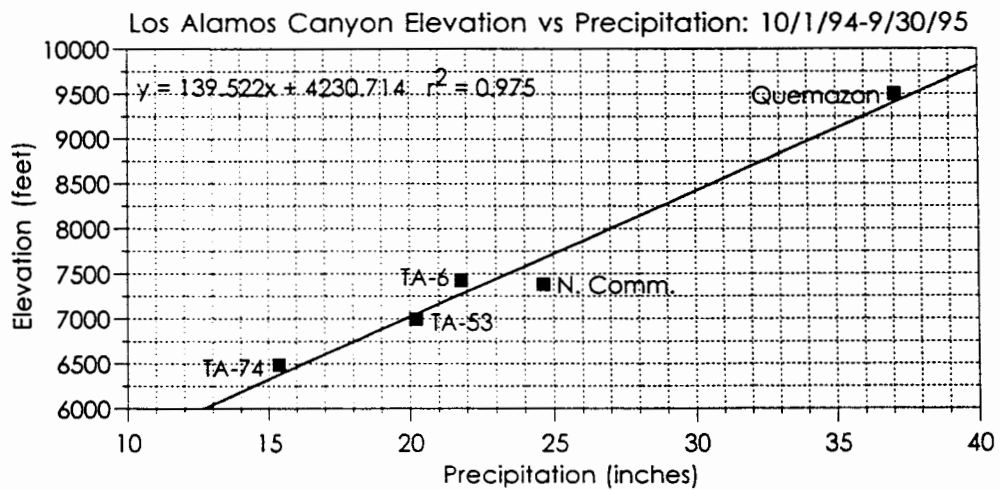
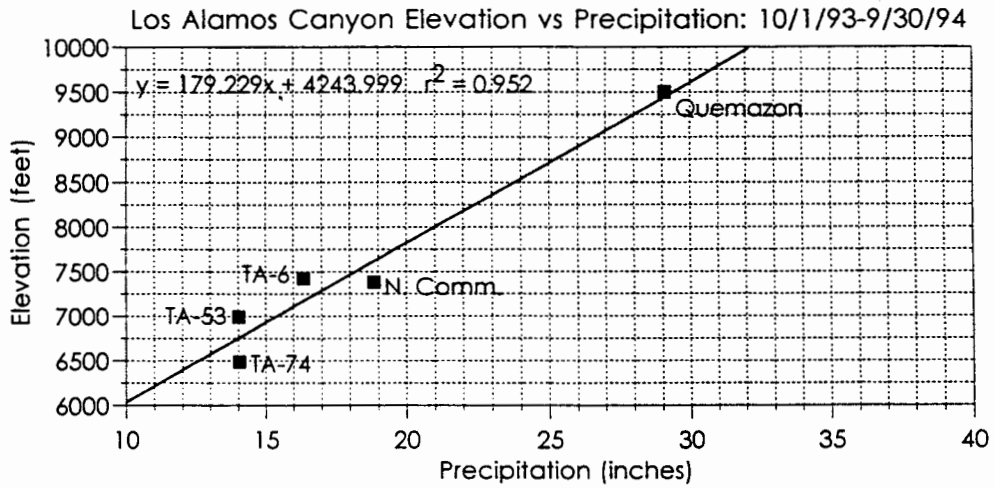
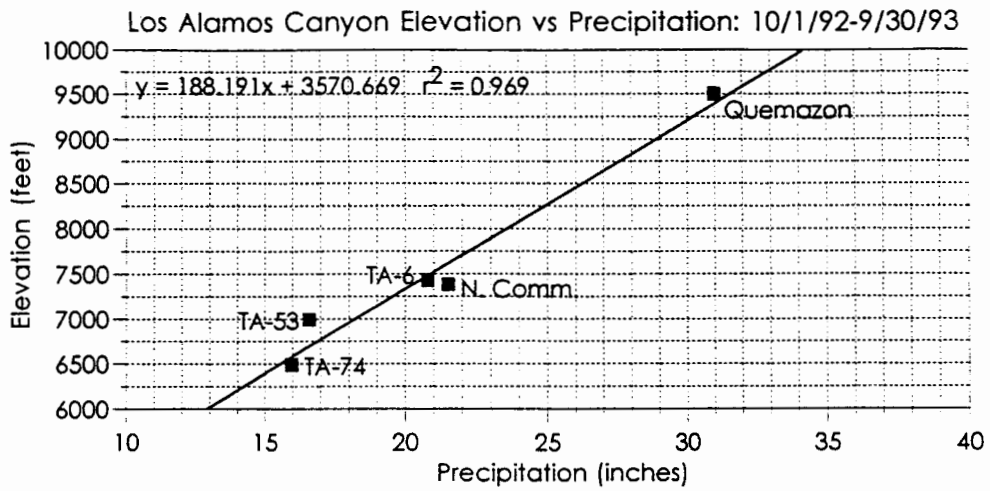


Figure 13: Los Alamos Canyon Annual Water Budget Elevation vs Precipitation Regressions

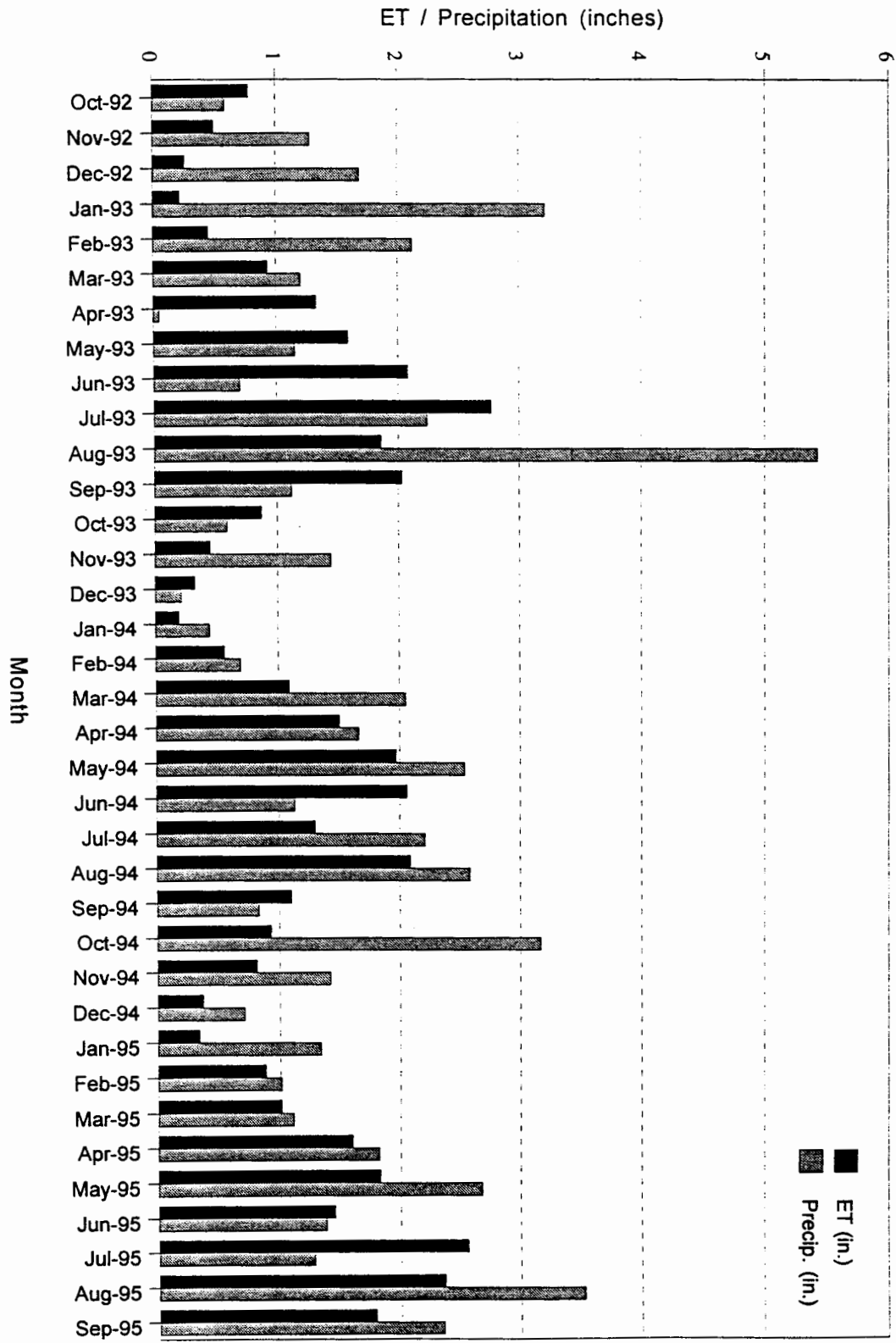


Figure 14: ET and Precipitation (TA-6)

an annual cycle, resulting in a roughly sinusoidal pattern, but precipitation variation is more erratic. ET/precipitation ratio percentages were determined on a monthly and annual basis. These data are shown in Table 1.

Table 1: TA-6 ET vs Precipitation

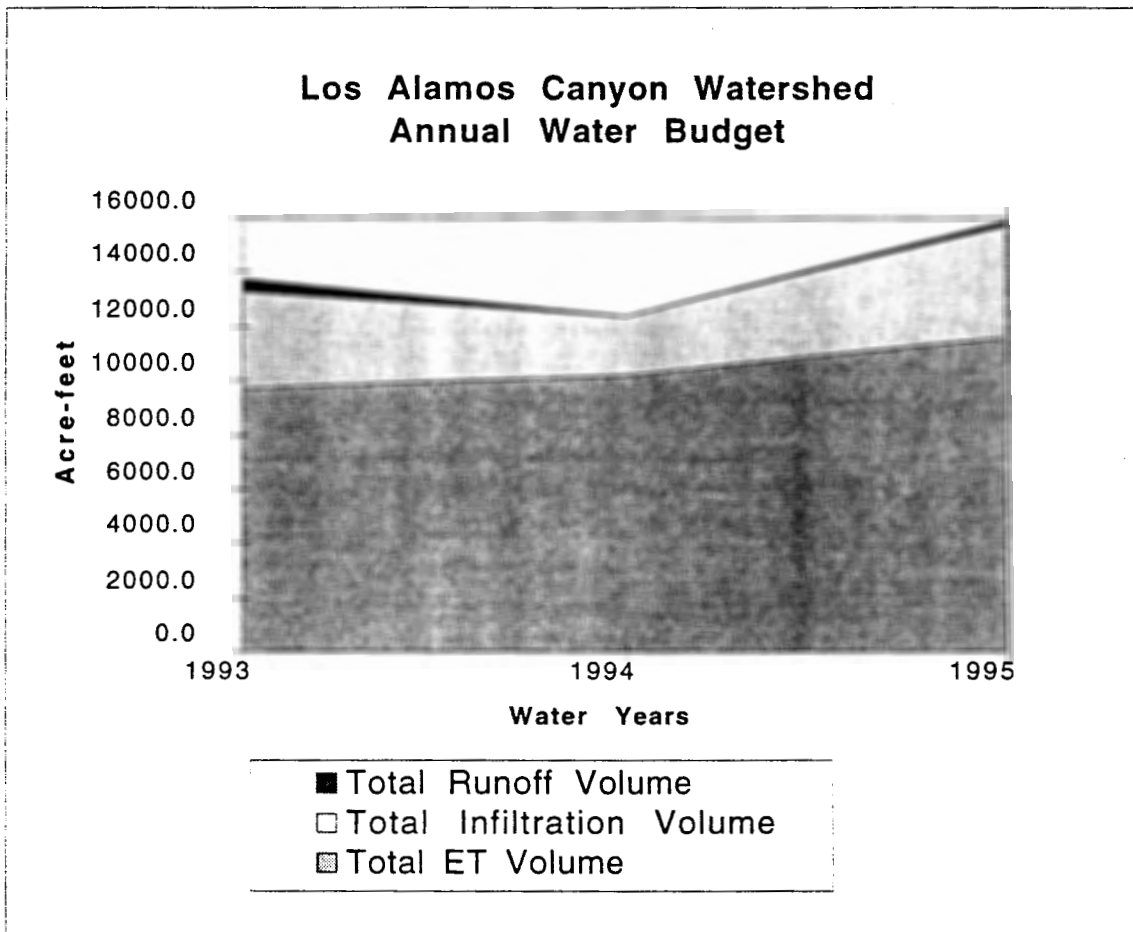
Month	ET (in.)	Precip. (in.)	ET % of Precip.	Month	ET (in.)	Precip. (in.)	ET % of Precip.	Month	ET (in.)	Precip. (in.)	ET % of Precip.
Oct-92	0.78	0.59	132.7	Oct-93	0.87	0.59	147.9	Oct-94	0.93	3.17	29.4
Nov-92	0.50	1.28	39.1	Nov-93	0.45	1.44	31.6	Nov-94	0.81	1.42	57.2
Dec-92	0.26	1.69	15.4	Dec-93	0.32	0.21	150.9	Dec-94	0.37	0.71	51.7
Jan-93	0.22	3.22	6.8	Jan-94	0.19	0.44	42.8	Jan-95	0.34	1.34	25.2
Feb-93	0.45	2.12	21.1	Feb-94	0.56	0.69	81.7	Feb-95	0.88	1.01	87.0
Mar-93	0.93	1.20	77.7	Mar-94	1.09	2.05	53.1	Mar-95	1.01	1.11	90.9
Apr-93	1.33	0.05	2656.2	Apr-94	1.50	1.66	90.4	Apr-95	1.60	1.82	87.7
May-93	1.59	1.15	138.5	May-94	1.97	2.54	77.4	May-95	1.83	2.68	68.4
Jun-93	2.08	0.70	296.7	Jun-94	2.06	1.13	182.7	Jun-95	1.45	1.38	104.8
Jul-93	2.77	2.24	123.7	Jul-94	1.30	2.21	59.0	Jul-95	2.56	1.28	200.2
Aug-93	1.86	5.43	34.2	Aug-94	2.09	2.58	80.8	Aug-95	2.37	3.53	67.1
Sep-93	2.03	1.12	180.9	Sep-94	1.10	0.83	133.1	Sep-95	1.79	2.36	75.8
Totals:	14.80	20.79	71.17	Totals:	13.51	16.37	82.54	Totals:	15.93	21.81	73.06

Though the ratios also varied considerably from month to month, the annual average ratios determined by water year are much less irregular. These annual percentages were then utilized to estimate ET for the entire watershed from the extrapolated precipitation data. Lacking additional data to show otherwise, the ET proportions were thus assumed to be constant throughout all elevations of the watershed. This presumption is another probable source of error in the water budget calculations.

The water budget was calculated in a spreadsheet using Microsoft Excel®. The extrapolated precipitation depths for each subarea were multiplied by the ET/precipitation fractions to determine ET amounts per subarea, from which remaining excess precipitation depths were determined. Excess precipitation volumes were then calculated by multiplying these depths by the measured areas between elevation contours, and the volumes were summed by water year. Annual streamflow discharge data from the lower measurement gage were compiled from USGS and LANL records and converted to total annual discharge volumes. The annual discharge volumes were then subtracted from the annual

excess precipitation volumes to determine calculated annual infiltration volumes. The annual volumetric rates were then converted to units of length by dividing by the total measured watershed area. The spreadsheet calculations and water balance summaries are provided in Table 2. These data are also displayed graphically in Figure 15.

Figure 15



Mean annual precipitation estimates for the LANL area range from 17.8 inches (1911-1988; Bowen, 1990) to 19.3 inches (Los Alamos National Laboratory, 1990). Mean annual precipitation at the TA-6 station over the evaluated period was 19.7 inches while the annual totals ranged from 16.37 to 21.81 inches. Thus, though the analyzed time

Table 2: Los Alamos Canyon Watershed Annual Water Budget

1993 Water Year (10/1/92-9/30/93):									
Elevation (ft.)		Avg.	Area (ft ²)	Extrapolated Precip. (in.)	ET/Precip fraction	ET (in.)	Excess Precip. (in.)	Excess Precip. (ft.)	Excess Precip. Volume (ft ³)
From	To								
6300	6500	6400	6619154	15.0	0.7117	10.7	4.3	0.36	2385378
6500	7000	6750	39591346	16.8	0.7117	12.0	4.8	0.40	15979859
7000	7500	7250	42441134	19.5	0.7117	13.9	5.6	0.47	19883141
7500	8000	7750	12713578	22.1	0.7117	15.7	6.4	0.53	6750306
8000	8500	8250	23578636	25.0	0.7117	17.8	7.2	0.60	14161918
8500	9000	8750	39283348	27.5	0.7117	19.6	7.9	0.66	25954017
9000	9500	9250	52578984	30.1	0.7117	21.4	8.7	0.72	38022624
9500	>9500		65579616	31.0	0.7117	22.1	8.9	0.74	48842059
Total:			282385796						Total Excess Precipitation Volume (ft ³): 171979301
									Total Lower Station Streamflow Discharge* (ft ³): 18601920
									Calculated Total Infiltration Volume (ft ³): 153377381
1993 Water Year Summary:		ft ³	acre-ft	inches	% of total precip.				
Total Precipitation Volume:		596528966	13694.4	25.35					* Streamflow discharge from USGS Water-Data Report NM-93-1, <i>Water Resources Data-New Mexico-Water Year 1993</i> , p. 134.
Total ET Volume:		424549665	9746.3	18.04	71.17				
Total Runoff Volume:		18601920	427.0	0.79	3.12				
Total Infiltration Volume:		153377381	3521.1	6.52	25.71				
Balance:		0.00	0.0	0.00	100.00				

Table 2 (continued): Los Alamos Canyon Watershed Annual Water Budget

1994 Water Year (10/1/93-9/30/94):									
Elevation (ft.)		Avg.	Area (ft ²)	Extrapolated Precip. (in.)	ET/Precip fraction	ET (in.)	Excess Precip. (in.)	Excess Precip. (ft.)	Excess Precip. Volume (ft ³)
From	To								
6300	6500	6400	6619154	12.0	0.8254	9.9	2.1	0.17	1155704
6500	7000	6750	39591346	14.0	0.8254	11.6	2.4	0.20	8064757
7000	7500	7250	42441134	16.7	0.8254	13.8	2.9	0.24	10312559
7500	8000	7750	12713578	19.5	0.8254	16.1	3.4	0.28	3607160
8000	8500	8250	23578636	22.3	0.8254	18.4	3.9	0.32	7650442
8500	9000	8750	39283348	25.2	0.8254	20.8	4.4	0.37	14403632
9000	9500	9250	52578984	28.0	0.8254	23.1	4.9	0.41	21420678
9500	>9500		65579616	29.1	0.8254	24.0	5.1	0.42	27766737
Total:			282385796						Total Excess Precipitation Volume (ft ³): 94381670
									Total Lower Station Streamflow Discharge** (ft ³): 133920
									Calculated Total Infiltration Volume (ft ³): 94247750
1994 Water Year Summary:		ft ³	acre-ft	inches	% of total precip.				
Total Precipitation Volume:		540559394	12409.5	22.97					** Streamflow discharge from USGS Water-Data Report NM-94-1, <i>Water Resources Data-New Mexico-Water Year 1994</i> , p. 133.
Total ET Volume:		446177724	10242.8	18.96	82.54				
Total Runoff Volume:		133920	3.1	0.01	0.02				
Total Infiltration Volume:		94247750	2163.6	4.01	17.44				
Balance:		0.00	0.0	0.00	100.00				

Table 2 (continued): Los Alamos Canyon Watershed Annual Water Budget

1995 Water Year (10/1/94-9/30/95):									
Elevation (ft.)		Avg.	Area (ft ²)	Extrapolated Precip. (in.)	ET/Precip fraction	ET (in.)	Excess Precip. (in.)	Excess Precip. (ft.)	Excess Precip. Volume (ft ³)
From	To								
6300	6500	6400	6619154	15.4	0.7306	11.3	4.1	0.35	2288440
6500	7000	6750	39591346	18.0	0.7306	13.2	4.8	0.40	15998863
7000	7500	7250	42441134	21.5	0.7306	15.7	5.8	0.48	20485274
7500	8000	7750	12713578	25.1	0.7306	18.3	6.8	0.56	7164038
8000	8500	8250	23578636	28.7	0.7306	21.0	7.7	0.64	15192069
8500	9000	8750	39283348	32.3	0.7306	23.6	8.7	0.73	28485731
9000	9500	9250	52578984	36.0	0.7306	26.3	9.7	0.81	42494335
9500	>9500		65579616	37.1	0.7306	27.1	10.0	0.83	54620934
Total:			282385796				Total Excess Precipitation Volume (ft ³):		186729684
							Total Lower Station Streamflow Discharge*** (ft ³):		14298336
							Calculated Total Infiltration Volume (ft ³):		172431348
1995 Water Year Summary:		ft ³	acre-ft	inches	% of total precip.				
Total Precipitation Volume:		693131713	15912.1	29.45			*** Streamflow discharge from LANL (ESH-18)		
Total ET Volume:		506402030	11625.4	21.52	73.06		records (see Appendix G)		
Total Runoff Volume:		14298336	328.2	0.61	2.06				
Total Infiltration Volume:		172431348	3958.5	7.33	24.88				
Balance:		0.00	0.0	0.00	100.00				

period is limited to only 3 years, and though normal climatic fluctuations will certainly cause greater variations in the proportions determined, the calculated annual water budget results should represent a reasonable approximation of the range of budget component values for an average water year for the Los Alamos Canyon watershed.

Detailed Water Budget

Since recharge and ET rates for more restricted time periods than those determined by the annual water budget calculations were desired for transient groundwater flow simulations, the evaluation period for more detailed budget calculations was divided into separate stress periods based on varying behavior of the alluvial aquifer. Water level elevation data collected by ESH-18 were obtained for the period from 7/10/94 to 11/2/95 for the instrumented alluvial observation well LAO-3. This well is roughly centrally located in the middle canyon area of the watershed (see Figure 9). At the time that the detailed water budget study was conducted, this was the only continuous data set of water levels that the author was able to obtain for the alluvial observation wells in the canyon. Partial data sets were also obtained for wells LAO-C and LAO-6, but these only covered the period from 7/10/94 to 10/28/94, after which their transducers were unfortunately removed by ESH-18 because water sampling efforts had disrupted their calibrations. A continuous data set was later obtained for well LAO-4, but not until after the water budget calculations were completed. The other alluvial observation wells in Los Alamos Canyon have not yet been instrumented, and their water levels have been monitored by tape measurements conducted at sporadic intervals. Thus, the period analyzed for the detailed water budget calculations was defined by the LAO-3 data set.

Well instrumentation consists of a Model LTM 3000 Well Sentinel (In-Situ, Inc., 1992) data recorder connected to a pressure transducer hung in the well bottom and calibrated to register water levels by elevation above sea level, recorded at 15-minute intervals. The utilized data set was condensed to single daily water levels recorded at 6:00

A.M. A hydrograph of daily head fluctuations was produced from these data by subtracting the elevation of the bottom of the alluvium (determined from the well's drill log and surveyed surface elevation) from the water level elevations, producing values for hydraulic head above the base of the alluvium which were then plotted against time (Figure 16). The hydrograph was plotted along with a precipitation hyetograph from the TA-6 station data to evaluate the correlation between precipitation and head fluctuation (thus also infiltration recharge) behavior. Periods where the hydrograph shows recession are indicative of periods with low to zero infiltration recharge, and periods showing rising heads indicate active infiltration recharge. Periods of relatively constant head indicate a more or less steady-state situation.

As can be seen, from July through December of 1994, the hydrograph is responsive to precipitation events, especially to the major events which occurred from 10/14/94 to 10/18/94 and 11/11/94 to 11/12/94. From December, 1994 through mid-February, 1995, the hydrograph is in recession despite continued occasional precipitation because the winter precipitation is largely stored as snowpack. In mid-February, the snowmelt began, accompanied by significant infiltration recharge and a steady-state situation was soon reached in which head values were relatively consistent at about 10.5 to 11 feet, which continued through the end of June. After this, a generally dry period ensued, followed by additional recharge from August rainstorms, after which a final recession occurred that marked the beginning of drought conditions that persisted through mid-1996.

Based on the hydrograph behavior, the 480-day period was divided into 9 separate stress periods representing relatively uniform infiltration or drying behaviors, or as in the case of period 2, a significant precipitation event (see Figure 16). The data from each precipitation gage and the ET data from the TA-6 site were then summed for each stress period (see Appendices A, B, C, and D). The streamflow discharge totals for each flow measurement gage were also summed by stress period (see Appendix G).

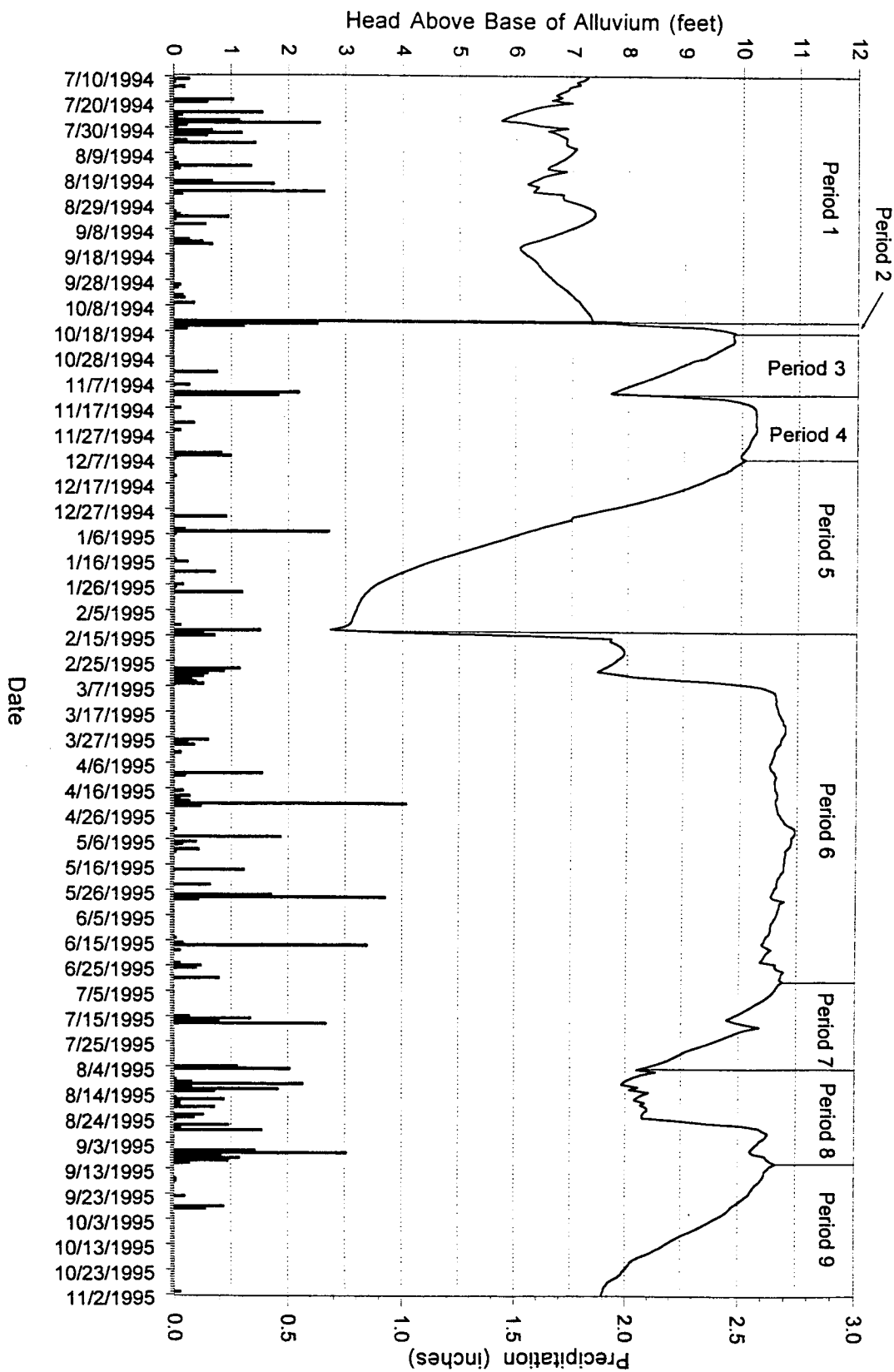
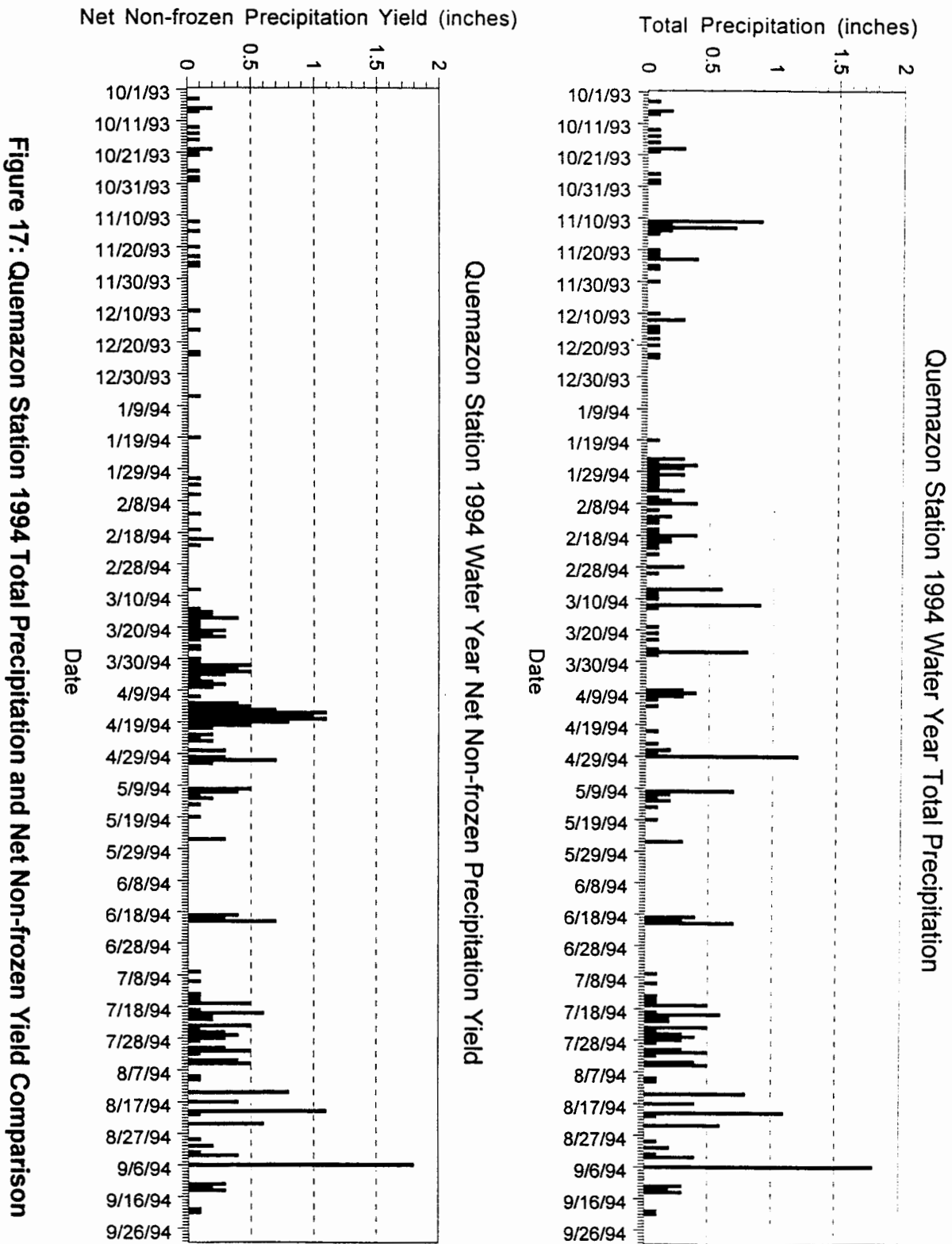


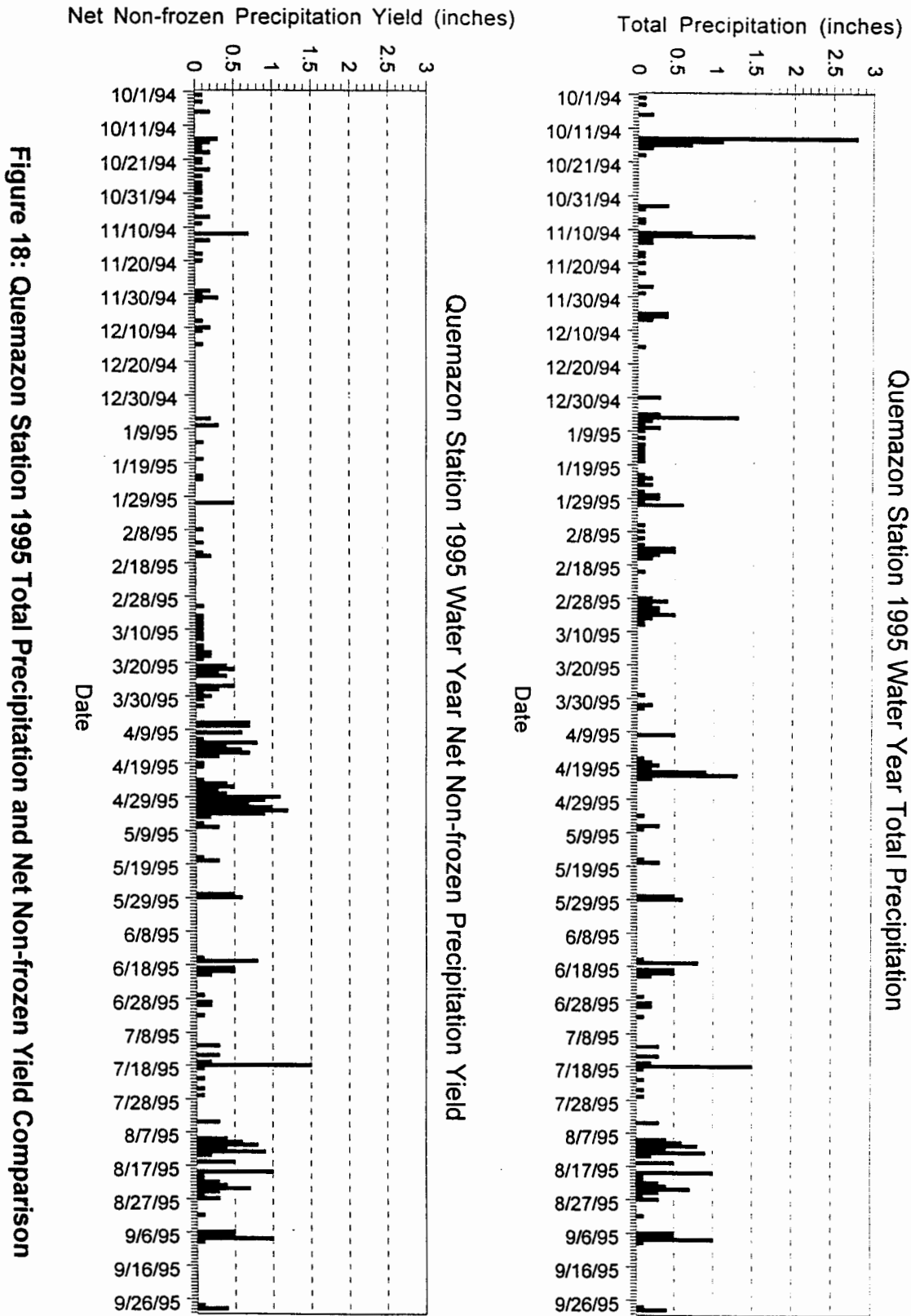
Figure 16: LAO-3 Alluvial Aquifer Heads and Daily Precipitation (TA-6 Station) 7/10/94 to 11/2/95

For the Quemazon station, a distinction is made between recorded total precipitation and the net non-frozen precipitation yield as determined from the SNOTEL data. These calculations are shown in Appendix F. The procedure for determining the daily net non-frozen yield entailed converting the reported annual cumulative precipitation totals to daily precipitation totals by subtracting the preceding day's cumulative total from each daily cumulative total. Daily net change in precipitation stored as snowpack was determined similarly by subtracting the preceding day's value from each daily reported total water equivalent snowpack depth. Daily net yields were determined by subtracting the daily snowpack net changes from the daily precipitation totals.

This procedure revealed inherent inaccuracies in the data involving a lack of perfect correlation between the reported daily precipitation and snowpack values. On several days during both years analyzed, the daily snowpack net change exceeded the reported total precipitation, resulting in the calculation of negative values for net yield. The most likely cause for this discrepancy is that the precipitation gage is less efficient at accurately measuring snowfall precipitation than the snow pillow (personal communication, Mike Gillespie, USDABNRC Snow Survey Office, Lakewood, Colorado). The limited size of the precipitation gage orifice makes it more susceptible to wind effects, which are more pronounced with snowflakes than raindrops, and occasional instrument icing may be another problem. The large diameter of the snow pillow is thus felt to give a more accurate reading of actual snowfall precipitation. Therefore, on days when a positive net change in snowpack depth exceeded the recorded daily precipitation, the precipitation totals were adjusted to match the snow pillow measurements, eliminating the calculated negative yields. These adjustments resulted in an increase in annual precipitation totals of approximately 11-12% over the data recorded by the precipitation gage (see Appendix F).

A comparison of the daily precipitation and net non-frozen precipitation yield totals is shown in Figures 17 and 18. Figure 17 shows that during the 1994 water year, most of the precipitation from November, 1993 through February, 1994 was stored as snowpack,





with only occasional minor releases from melting occurring during this period. The major snowmelt release occurred from mid-March through early May. Figure 18 shows a similar pattern for the 1995 water year, but with snowpack storage effects occurring somewhat earlier, beginning with a major precipitation event on 10/14/94 when 2.8 inches of precipitation was recorded during a single 24 hour period, mostly as snow.

The daily net yield values were summed by stress period as was done with the other stations' precipitation data. The relation between total precipitation and net yield by stress period is shown in Figure 19. This graph reveals that whereas the two parameters were equivalent during periods 1, 7, 8, and 9, precipitation was stored as snowpack in periods 2, 4, and 5, with some minor releases by melting or non-frozen precipitation occurrence. Low precipitation accompanied by minor melting caused net yield to exceed precipitation slightly in period 3. The major release was in period 6 during which most of the snowmelt occurred. These net yield values per stress period were utilized in the detailed water budget calculations for the Quemazon data.

The precipitation (or net yield) totals determined for each stress period at each measurement station are shown in Table 3. For the stations where snowpack data are not available, an adjustment was made between the main winter period (period 5) and main snowmelt period (period 6) by transferring 50% of the period 5 precipitation to period 6. Though snowpack storage at the Quemazon site also occurred in periods 2 and 4, the record of alluvial aquifer head responses to precipitation during these periods (see Figure 16) indicates that most precipitation was not stored as snowpack at the lower elevations of the other stations in periods 2 and 4. However, the major recession which occurred in period 5 suggests that significant snowpack storage did occur then at all elevations above well LAO-3. Examination of daily maximum and minimum temperatures at the TA-6 site during period 5 shows that most daily maximum temperatures were slightly to substantially above freezing, while the overall average temperature during the period was approximately at freezing (Figure 20), thus supporting the assumption of a nominal

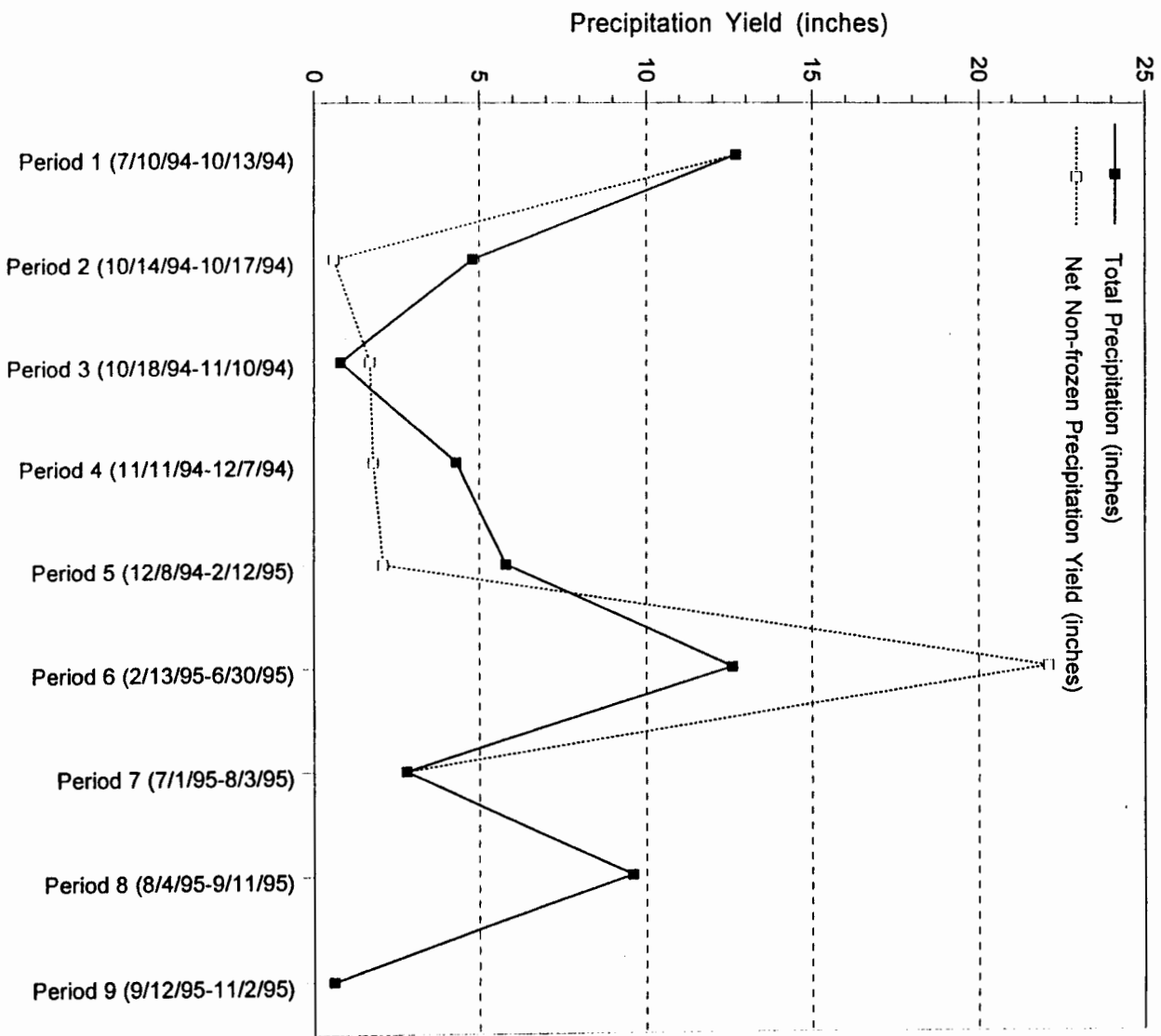


Figure 19: Quemazon Station Total Precipitation and Net Non-Frozen Yield by Stress Period

Table 3: Los Alamos Canyon Watershed Detailed Water Budget Stress Periods

TA-6 Station:								
Period No.	Stress Periods:		No. of days	Conditions	Total Precip.	Adjusted *	Measured ET	Calculated
	From	To			(inches)	Precip. (inches)	(inches)	ET proportion of adjusted precip.
1	7/10/94	10/14/94	96	summer/fall rainstorms	5.78	5.78	4.44	0.77
2	10/14/94	10/18/94	4	heavy rain/snow + melting	2.97	2.97	0.16	0.06
3	10/18/94	11/11/94	24	dry	0.26	0.26	0.78	3.01
4	11/11/94	12/8/94	27	moderate snow/rain + melting	1.63	1.63	0.53	0.33
5	12/8/94	2/13/95	67	frozen + minor melting	1.61	0.81	0.97	1.20
6	2/13/95	7/1/95	138	snow melt + spring rains	7.97	8.78	6.44	0.73
7	7/1/95	8/4/95	34	relatively dry	1.28	1.28	2.70	2.11
8	8/4/95	9/12/95	39	summer rainstorms	5.46	5.46	3.01	0.55
9	9/12/95	11/2/95	51	dry	0.46	0.46	1.80	3.92
		Totals:	480		27.42	27.42	20.84	0.76
Quemazon Station:						Net non-frozen		
Period No.	Stress Periods:		No. of days	Conditions	Total Precip.	Precip. Yield **	ET proportion of	Estimated ET
	From	To			(inches)	(inches)	adj. precip. ***	(inches)
1	7/10/94	10/14/94	96	summer/fall rainstorms	12.7	12.7	0.77	9.75
2	10/14/94	10/18/94	4	heavy snow + no melting	4.8	0.6	0.06	0.03
3	10/18/94	11/11/94	24	dry	0.8	1.7	3.01	5.12
4	11/11/94	12/8/94	27	moderate snow/rain + melting	4.3	1.8	0.33	0.59
5	12/8/94	2/13/95	67	frozen + minor melting	5.8	2.1	1.20	2.53
6	2/13/95	7/1/95	138	snow melt + spring snow/rain	12.6	22.1	0.73	16.22
7	7/1/95	8/4/95	34	relatively dry	2.8	2.8	2.11	5.91
8	8/4/95	9/12/95	39	summer rainstorms	9.6	9.6	0.55	5.30
9	9/12/95	11/2/95	51	dry	0.6 ****	0.6	3.92	2.18
		Totals:	480		54.0	54.0	0.88	47.6

Table 3 (continued): Los Alamos Canyon Watershed Detailed Water Budget Stress Periods

TA-53 Station:								
Period No.	Stress Periods:		No. of days	Conditions	Total Precip. (inches)	Adjusted * Precip. (inches)	ET proportion of adj. precip. ***	Estimated ET (inches)
	From	To						
1	7/10/94	10/14/94	96	summer/fall rainstorms	5.81	5.81	0.77	4.46
2	10/14/94	10/18/94	4	heavy rain/snow + melting	3.08	3.08	0.06	0.17
3	10/18/94	11/11/94	24	dry	0.25	0.25	3.01	0.75
4	11/11/94	12/8/94	27	moderate snow/rain + melting	2.38	2.38	0.33	0.78
5	12/8/94	2/13/95	67	frozen + minor melting	1.42	0.71	1.20	0.85
6	2/13/95	7/1/95	138	snow melt + spring rains	6.94	7.65	0.73	5.62
7	7/1/95	8/4/95	34	relatively dry	1.32	1.32	2.11	2.78
8	8/4/95	9/12/95	39	summer rainstorms	4.19	4.19	0.55	2.31
9	9/12/95	11/2/95	51	dry	0.47	0.47	3.92	1.84
		Totals:	480		25.86	25.86	0.76	19.57
North Community Station:								
Period No.	Stress Periods:		No. of days	Conditions	Total Precip. (inches)	Adjusted * Precip. (inches)	ET proportion of adj. precip. ***	Estimated ET (inches)
	From	To						
1	7/10/94	10/14/94	96	summer/fall rainstorms	8.16	8.16	0.77	6.27
2	10/14/94	10/18/94	4	heavy rain/snow + melting	3.72	3.72	0.06	0.20
3	10/18/94	11/11/94	24	dry	0.29	0.29	3.01	0.87
4	11/11/94	12/8/94	27	moderate snow/rain + melting	2.19	2.19	0.33	0.72
5	12/8/94	2/13/95	67	frozen + minor melting	1.09	0.55	1.20	0.66
6	2/13/95	7/1/95	138	snow melt + spring rains	8.83	9.38	0.73	6.88
7	7/1/95	8/4/95	34	relatively dry	1.86	1.86	2.11	3.92
8	8/4/95	9/12/95	39	summer rainstorms	5.82	5.82	0.55	3.21
9	9/12/95	11/2/95	51	dry	0.56	0.56	3.92	2.20
		Totals:	480		32.52	32.52	0.77	24.93

Table 3 (continued): Los Alamos Canyon Watershed Detailed Water Budget Stress Periods

TA-74 Station:								
Period No.	Stress Periods:		No. of days	Conditions	Total Precip. (inches)	Adjusted * Precip. (inches)	ET proportion of adj. precip. ***	Estimated ET (inches)
	From	To						
1	7/10/94	10/14/94	96	summer/fall rainstorms	6.17	6.17	0.77	4.74
2	10/14/94	10/18/94	4	heavy rain/snow + melting	2.53	2.53	0.06	0.14
3	10/18/94	11/11/94	24	dry	0.19	0.19	3.01	0.57
4	11/11/94	12/8/94	27	moderate snow/rain + melting	1.90	1.90	0.33	0.62
5	12/8/94	2/13/95	67	frozen + minor melting	1.18	0.59	1.20	0.71
6	2/13/95	7/1/95	138	snow melt + spring rains	4.95	5.54	0.73	4.07
7	7/1/95	8/4/95	34	relatively dry	0.67	0.67	2.11	1.41
8	8/4/95	9/12/95	39	summer rainstorms	3.18	3.18	0.55	1.75
9	9/12/95	11/2/95	51	dry	0.63	0.63	3.92	2.47
		Totals:	480		21.40	21.40	0.77	16.49
* 50% of period 5 precipitation moved to period 6 for snowmelt.								
** Net non-frozen yield based on snowpack data.								
*** Proportions from TA-6 data.								
**** Precipitation data not available for 10/1/95-11/2/95 period.								
(Multiplied N.Comm. data by 2.759 = avg. Quem./N.Comm. proportion from 10/18/94-11/11/94 dry period)								

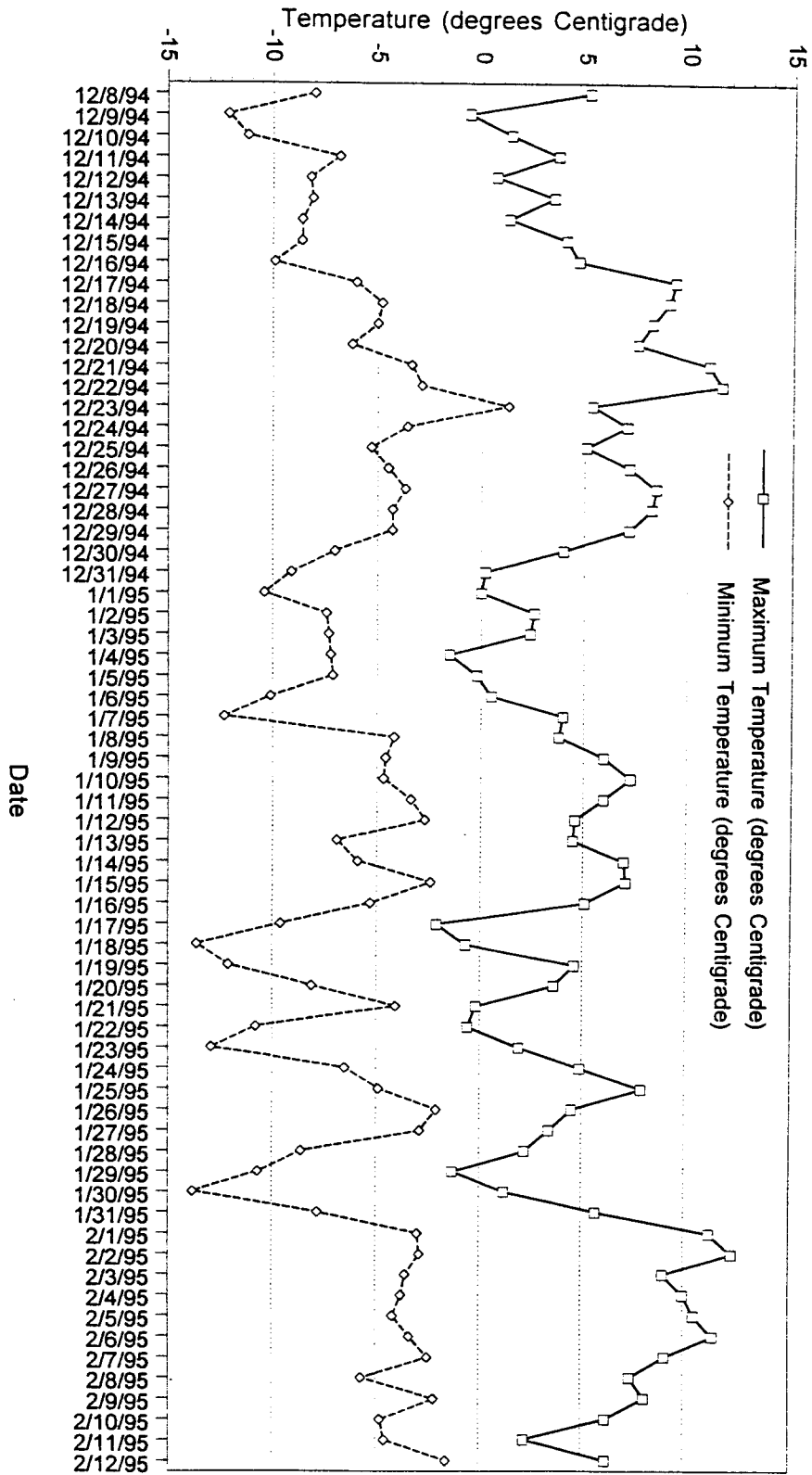


Figure 20: TA-6 Maximum and Minimum Temperatures for Stress Period 5 (12/8/94-2/12/95)

amount of melting for the lower measurement stations during period 5. The Quemazon data show that 63.8% of the period 5 precipitation was stored as snowpack at that site (see Appendix F). Assuming that somewhat greater melting would occur at the lower elevations of the watershed, an arbitrary value of 50% snowpack storage was assumed for the remaining measurement stations during period 5. The adjustment is reflected in the columns labeled as Adjusted Precipitation in Table 3, and these data were utilized in the detailed water budget calculations for the LANL precipitation measurement sites.

Since ET measurements were made only at the TA-6 site, the ET proportion of adjusted precipitation was calculated for each stress period at this site and these proportions were then applied to the other precipitation measurement sites to estimate ET amounts for them. These calculations are also shown in Table 3. As in the annual water budget, the inherent assumption that ET proportions are constant throughout the watershed regardless of elevation is a probable source of error.

As was done for the annual water budget, linear regressions were performed on the adjusted precipitation totals plotted against elevation for each stress period (Figures 21, 22, and 23). The precipitation/elevation relations were not as straightforward in every period as was the case for the annual budget plots since the Quemazon station exhibited lower precipitation yields than the other sites during periods 2 and 4 as a result of snowpack storage at the higher elevation. Also, though the lower stations generally exhibited the previously recognized trend of increased precipitation at higher elevations, there were some exceptions. For example, though having nearly equivalent elevations, the TA-6 and North Community stations exhibited divergent precipitation totals during periods 1, 2, 4, 5, and 7. In period 4, though possessing the second highest elevation, the TA-6 station recorded the lowest precipitation amount and was excluded from the regression analyses. In period 9, the TA-74 station, though representing the lowest elevation, recorded the highest precipitation amount and was also excluded from the regression analysis. The effects of these exclusions on the determination of average

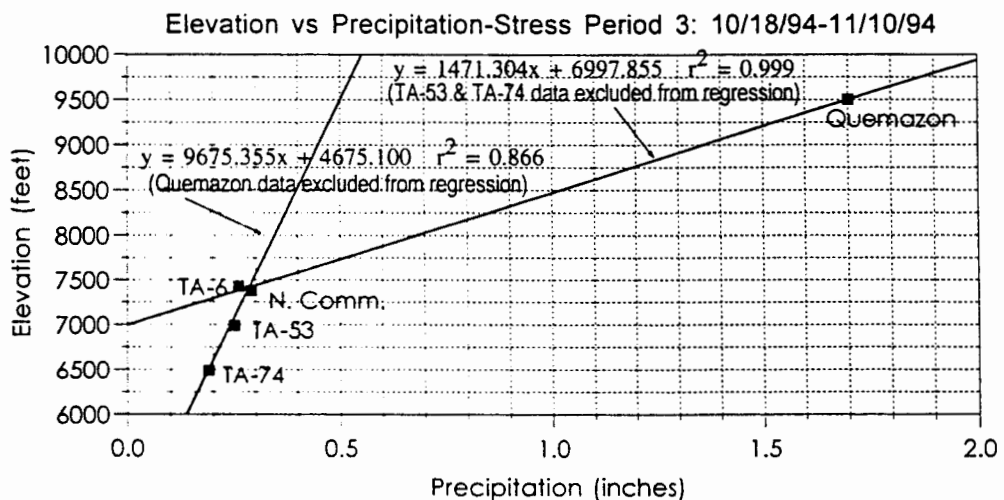
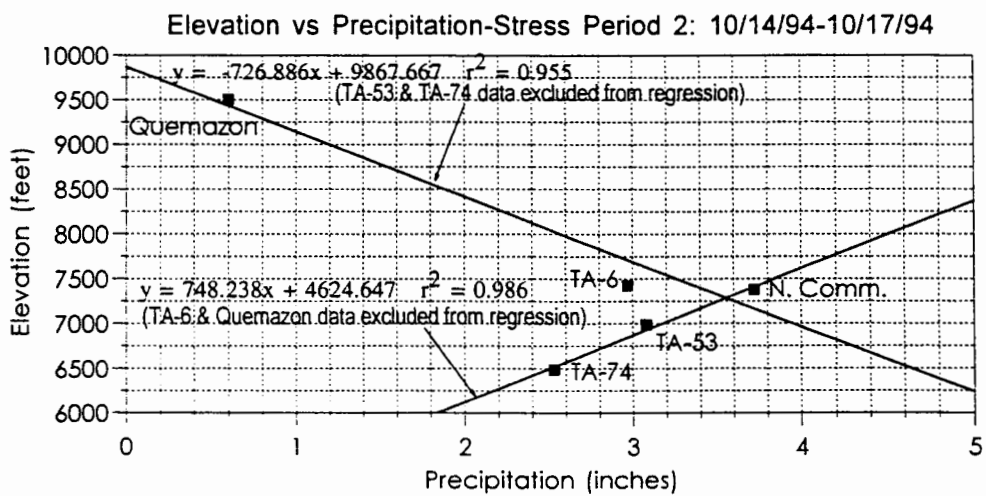
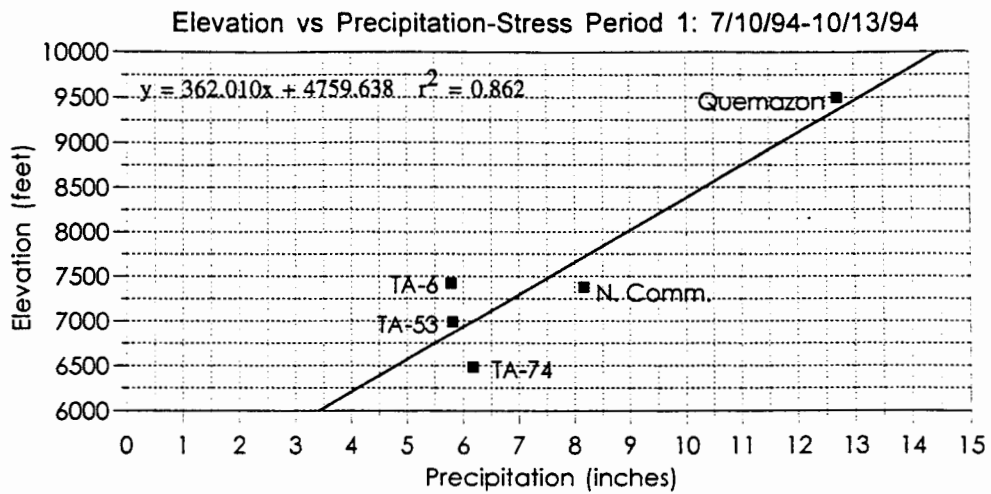


Figure 21: Los Alamos Canyon Detailed Water Budget Elevation vs Precipitation Regressions-Periods 1, 2, 3

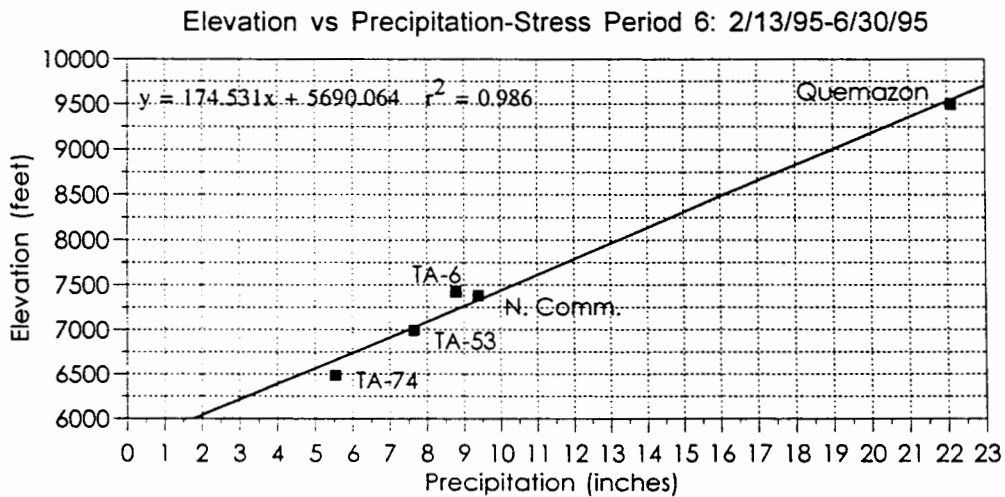
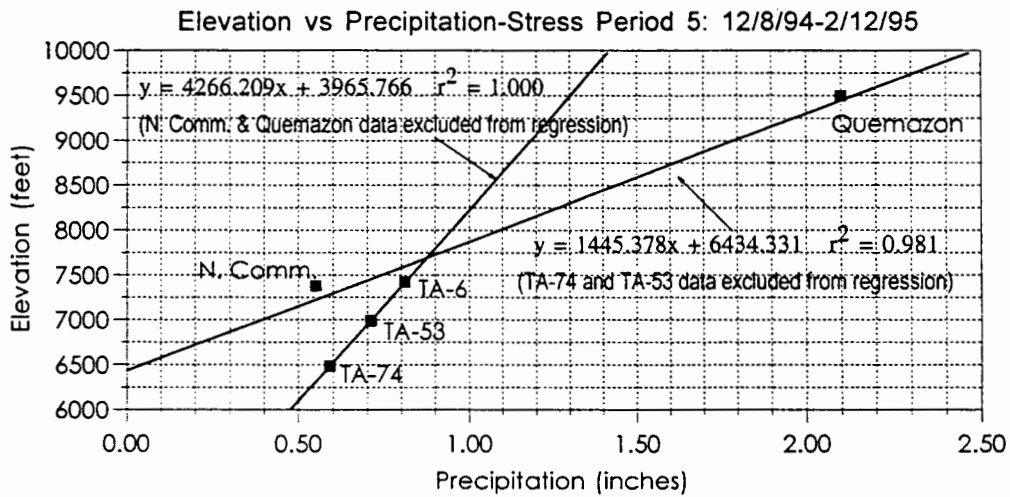
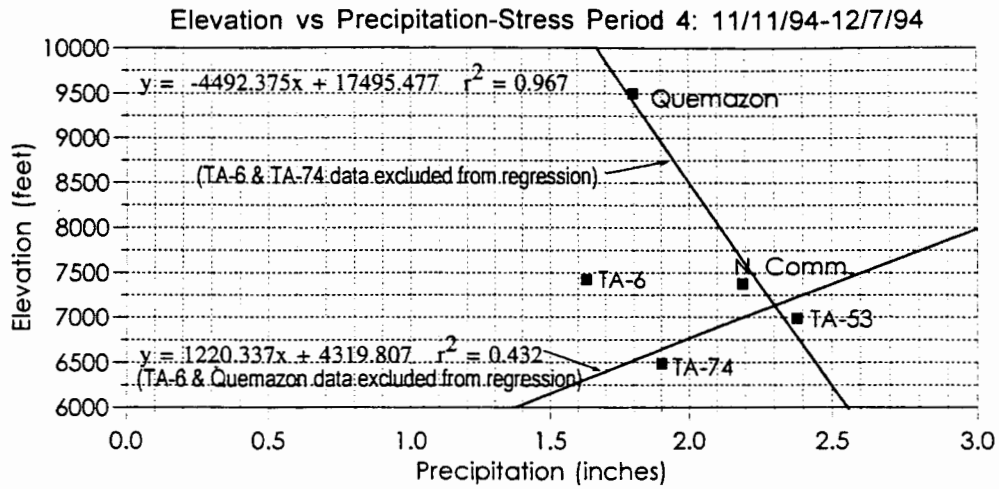


Figure 22: Los Alamos Canyon Detailed Water Budget Elevation vs Precipitation Regressions-Periods 4, 5, 6

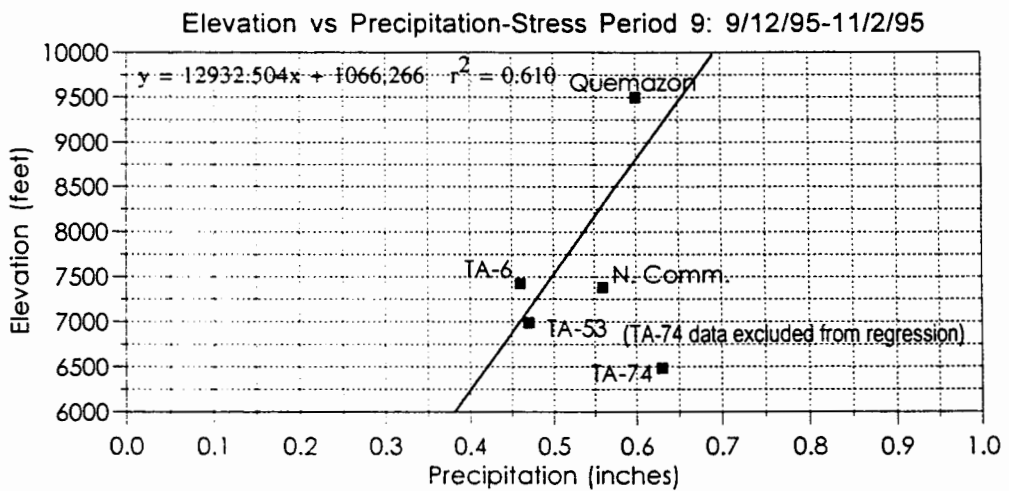
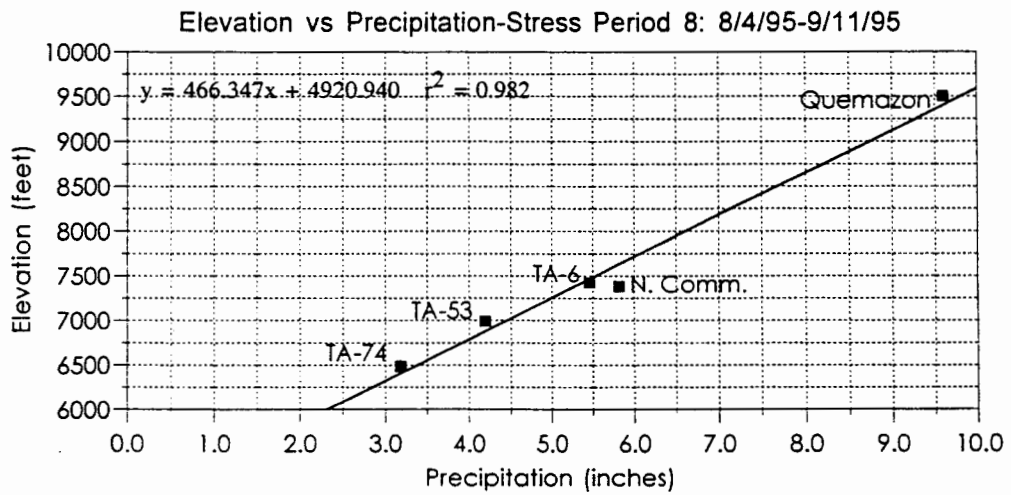
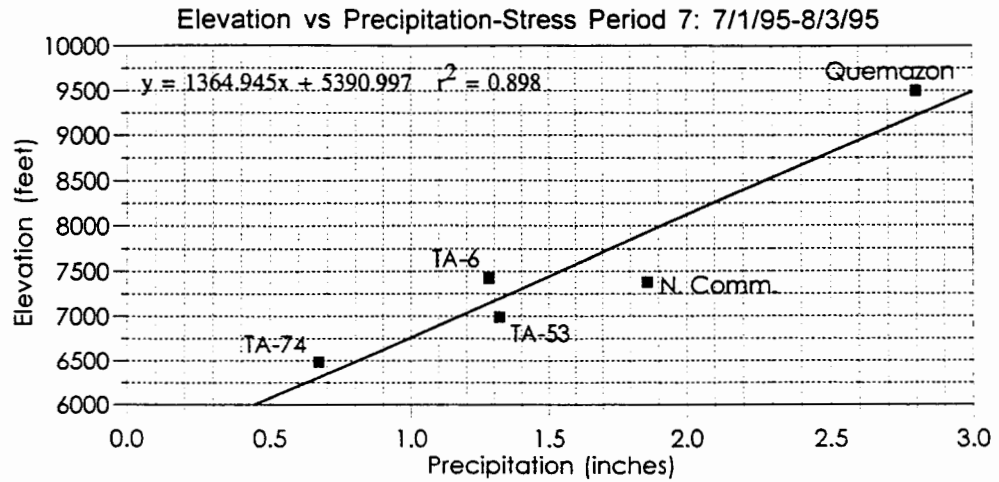


Figure 23: Los Alamos Canyon Detailed Water Budget Elevation vs Precipitation Regressions-Periods 7, 8, 9

precipitation/elevation trends are minimal however, since the affected periods exhibited low precipitation totals at all stations and the discrepancies involved minimal precipitation amounts of much less than one inch.

For the periods when snowpack storage effects caused lower precipitation yields at the Quemazon station, double regressions were performed, thus assuming a linear transition to decreased snowpack storage at the lower sites while maintaining a linear relation between precipitation and elevation for the lower sites. A double regression was also used for periods 3 and 5 as the linearity of the lower stations' data differed substantially from the transition to the Quemazon plot.

The regression plots were then used as before to extrapolate the varying precipitation amounts to intervening average elevations, which when multiplied times the appropriate representative areas yielded total precipitation volumes for each stress period. The calculations were done separately for the upper basin (defined as that part of the watershed higher than the 7,500 feet elevation contour) and middle/upper canyon (lower than the 7,500 feet elevation contour) areas since the upper streamflow gage is located approximately at this division. The ET/precipitation fractions determined from the TA-6 data for each stress period were then applied to the precipitation volumes to calculate estimated ET volumes, which when subtracted from the precipitation volumes yielded excess precipitation volumes by stress period and watershed area.

For the upper basin area, discharge volumes from the upper streamflow gage were subtracted from the excess precipitation volumes and estimated reservoir usage volumes were also subtracted in periods 1, 7, and 8. Since data for the upper streamflow gage were not available for most of period 1, its daily streamflow discharge totals for this period were estimated from the precipitation data by applying the average flow/precipitation ratio for this gage from periods 7-9 which represent a roughly equivalent seasonal interval from the following year (see Table 4). The residual volumes determined represent total upper basin infiltration and were also converted to units of length (inches) by dividing by the

total upper basin area.

For the middle/upper canyon area, the upper streamflow discharge volumes were added to the excess precipitation volumes, and the lower streamflow gage volumes were then subtracted from these totals. The remaining volumes represent total infiltration for the middle/upper canyon area and were also converted to units of length as above.

These calculations are shown in the Los Alamos Canyon Detailed Water Budget Calculations spreadsheet (Appendix H). The detailed water budget calculations are summarized in Table 4, which also shows average daily and annual rates for all evaluated parameters for the entire watershed. The resulting precipitation, ET and calculated net infiltration totals plus daily and annual rates are summarized by stress period and watershed area in Table 5.

Streamflow Data Analysis

The discharge data from all three streamflow measurement stations for the 1995 water year are plotted together in Figure 24. This graph illustrates that relative discharge rates among the three gages exhibited variable behavior over the analyzed period. The upper station recorded greater flow rates than the middle and lower gages mainly during periods of generally low flow. This is apparent during the initiation of spring runoff from late February through late April. After the snowmelt runoff peaked at the upper and middle gages in late April, the greatest flows were recorded at the middle gage through late May while the upper gage then recorded the lowest flows. When the snowmelt runoff tailed off in early June, the upper gage again generally recorded the highest flow rates. This pattern indicates that the stream reach between the upper and middle gages exhibited a gaining behavior during the period when the main bulk of the snowmelt volume was discharged, likely due to the down-gradient migration of snowmelt induced recharge to the alluvium from the upper basin area. During the periods with lower flow levels prior to and following the peak runoff period, the data indicate that this reach exhibited a losing

Table 4: Los Alamos Canyon Watershed Detailed Water Budget Calculations Summary

Upper Basin:										
Period	1	2	3	4	5	6	7	8	9	Totals:
From	7/10/94	10/14/94	10/18/94	11/11/94	12/8/94	2/13/95	7/1/95	8/4/95	9/12/95	7/10/94
To	10/14/94	10/18/94	11/11/94	12/8/94	2/13/95	7/1/95	8/4/95	9/12/95	11/2/95	11/2/95
No. of days	96	4	24	27	67	138	34	39	51	480
Upper Basin precip. vol. (ft ³)	187349940	19380006	22047960	30552750	28687573	308093202	41519582	140144429	9622067	787397509
ET/Precip. Fraction	0.77	0.06	3.01	0.33	1.20	0.73	2.11	0.55	3.92	
Estimated ET Volume (ft ³)	144259454	1162800	66364360	10082407	34425087	224908038	87606318	77079436	37718502	683606403
Est. Reservoir usage (ft ³)	668400						334200	334200		1336800
Excess Volume (ft ³)	42422086	18217205	-44316400	20470342	-5737515	83185165	-46420936	62730793	-28096435	102454306
Upper Station cum. flow (ft ³)	1167785 *	59616	511488	2382048	9504	16118784	237600	834624	120096	21441545
Flow:Precip. Ratio	0.006 **	0.003	0.023	0.078	0.000	0.052	0.006	0.006	0.012	0.027
Calculated Infiltration (ft ³)	41254301	18157589	-44827888	18088294	-5747019	67066381	-46658536	61896169	-28216531	81012761
Calculated Infiltration (in.)	2.56	1.12	-2.78	1.12	-0.36	4.15	-2.89	3.83	-1.75	5.02
* Estimated cumulative flow from flow:precip. ratio. ** Assumed ratio is average ratio from periods 7-9.										
Middle/Upper Canyon:										
Period	1	2	3	4	5	6	7	8	9	Totals:
From	7/10/94	10/14/94	10/18/94	11/11/94	12/8/94	2/13/95	7/1/95	8/4/95	9/12/95	7/10/94
To	10/14/94	10/18/94	11/11/94	12/8/94	2/13/95	7/1/95	8/4/95	9/12/95	11/2/95	11/2/95
No. of days	96	4	24	27	67	138	34	39	51	480
Mid/Upper Canyon precip. vol. (ft ³)	45031868	23039454	1780054	15501108	5182247	53235875	8416102	32260941	3380998	187828649
ET/Precip. Fraction	0.77	0.06	3.01	0.33	1.20	0.73	2.11	0.55	3.92	
Estimated ET Volume (ft ³)	34674539	1382367	5357963	5115366	6218697	38862189	17757975	17743518	13253514	140366127
Upper Station Cum. Flow (ft ³)	1167785	59616	511488	2382048	9504	16118784	237600	834624	120096	21441545
Excess Volume (ft ³)	11525115	21716703	-3066421	12767791	-1026945	30492470	-9104273	15352048	-9752419	68904067
Lower Station cum. flow (ft ³)	0	973728	0	1103328	0	11692512	260064	268704	0	14298336
Flow:Precip. Ratio	0.000	0.042	0.000	0.071	0.000	0.220	0.031	0.008	0.000	0.076
Calculated Infiltration (ft ³)	11525115	20742975	-3066421	11664463	-1026945	18799958	-9364337	15083344	-9752419	54605731
Calculated Infiltration (in.)	1.56	2.81	-0.42	1.58	-0.14	2.54	-1.27	2.04	-1.32	7.39
Total Watershed Summary Results:										
	Total precip. vol. (ft ³)	Total precip. (inches)	Total ET vol. (ft ³)	Total ET (inches)	Infiltration Total (ft ³)	Avg. Infiltration Total (inches)				Lower Station cum. flow (ft ³)
	975226158	41.44	823972530	35.01	135618492	5.76				14298336
	Avg. Precip. (in/day)	Avg. Precip. (in/year)	Avg ET (in/day)	Avg ET (in/year)	ET % of total Precip.	Avg. Infiltration (in/day)	Avg Infiltration (in/yr)	Infiltr. % of total Precip.		Flow % of total Precip.
	0.09	31.51	0.07	26.63	84.49	0.012	4.38	13.91		1.47

Table 5: Los Alamos Canyon Detailed Water Budget Results Summary

Upper Basin:													
Period	From	To	No. of days	Conditions	Precip. (in/period)	Precip. (in/day)	Precip. (in/year)	ET (in/period)	ET (in/day)	ET (in/year)	Net Infiltration (in/period)	Net Infiltration (in/day)	Net Infiltration (in/year)
1	7/10/94	10/14/94	96	summer/fall rainstorms	11.60	0.12	44.12	8.94	0.09	33.97	2.56	0.027	9.72
2	10/14/94	10/18/94	4	heavy rain/snow + melting	1.20	0.30	109.54	0.07	0.02	6.57	1.12	0.281	102.63
3	10/18/94	11/11/94	24	dry	1.37	0.06	20.77	4.11	0.17	62.52	-2.78	-0.116	-42.23
4	11/11/94	12/8/94	27	mod. snow/rain + melting	1.89	0.07	25.58	0.62	0.02	8.44	1.12	0.041	15.15
5	12/8/94	2/13/95	67	frozen + minor melting	1.78	0.03	9.68	2.13	0.03	11.62	-0.36	-0.005	-1.94
6	2/13/95	7/1/95	138	snow melt + spring rains	19.08	0.14	50.47	13.93	0.10	36.85	4.15	0.030	10.99
7	7/1/95	8/4/95	34	relatively dry	2.57	0.08	27.61	5.43	0.16	58.25	-2.89	-0.085	-31.03
8	8/4/95	9/12/95	39	summer rainstorms	8.68	0.22	81.24	4.77	0.12	44.68	3.83	0.098	35.88
9	9/12/95	11/2/95	51	dry	0.60	0.01	4.27	2.34	0.05	16.72	-1.75	-0.034	-12.51
Totals:			480		48.77	0.10	37.09	42.34	0.09	32.20	5.02	0.010	3.82
Middle/Upper Canyon:													
Period	From	To	No. of days	Conditions	Precip. (in/period)	Precip. (in/day)	Precip. (in/year)	ET (in/period)	ET (in/day)	ET (in/year)	Net Infiltration (in/period)	Net Infiltration (in/day)	Net Infiltration (in/year)
1	7/10/94	10/14/94	96	summer/fall rainstorms	6.10	0.06	23.18	4.69	0.05	17.85	1.56	0.016	5.93
2	10/14/94	10/18/94	4	heavy rain/snow + melting	3.12	0.78	284.58	0.19	0.05	17.07	2.81	0.702	256.21
3	10/18/94	11/11/94	24	dry	0.24	0.01	3.66	0.73	0.03	11.03	-0.42	-0.017	-6.31
4	11/11/94	12/8/94	27	mod. snow/rain + melting	2.10	0.08	28.37	0.69	0.03	9.36	1.58	0.058	21.34
5	12/8/94	2/13/95	67	frozen + minor melting	0.70	0.01	3.82	0.84	0.01	4.59	-0.14	-0.002	-0.76
6	2/13/95	7/1/95	138	snow melt + spring rains	7.21	0.05	19.06	5.26	0.04	13.91	2.54	0.018	6.73
7	7/1/95	8/4/95	34	relatively dry	1.14	0.03	12.23	2.40	0.07	25.80	-1.27	-0.037	-13.61
8	8/4/95	9/12/95	39	summer rainstorms	4.37	0.11	40.87	2.40	0.06	22.48	2.04	0.052	19.11
9	9/12/95	11/2/95	51	dry	0.46	0.01	3.28	1.79	0.04	12.84	-1.32	-0.026	-9.45
Totals:			480		25.42	0.05	19.33	19.00	0.04	14.45	7.39	0.015	5.62

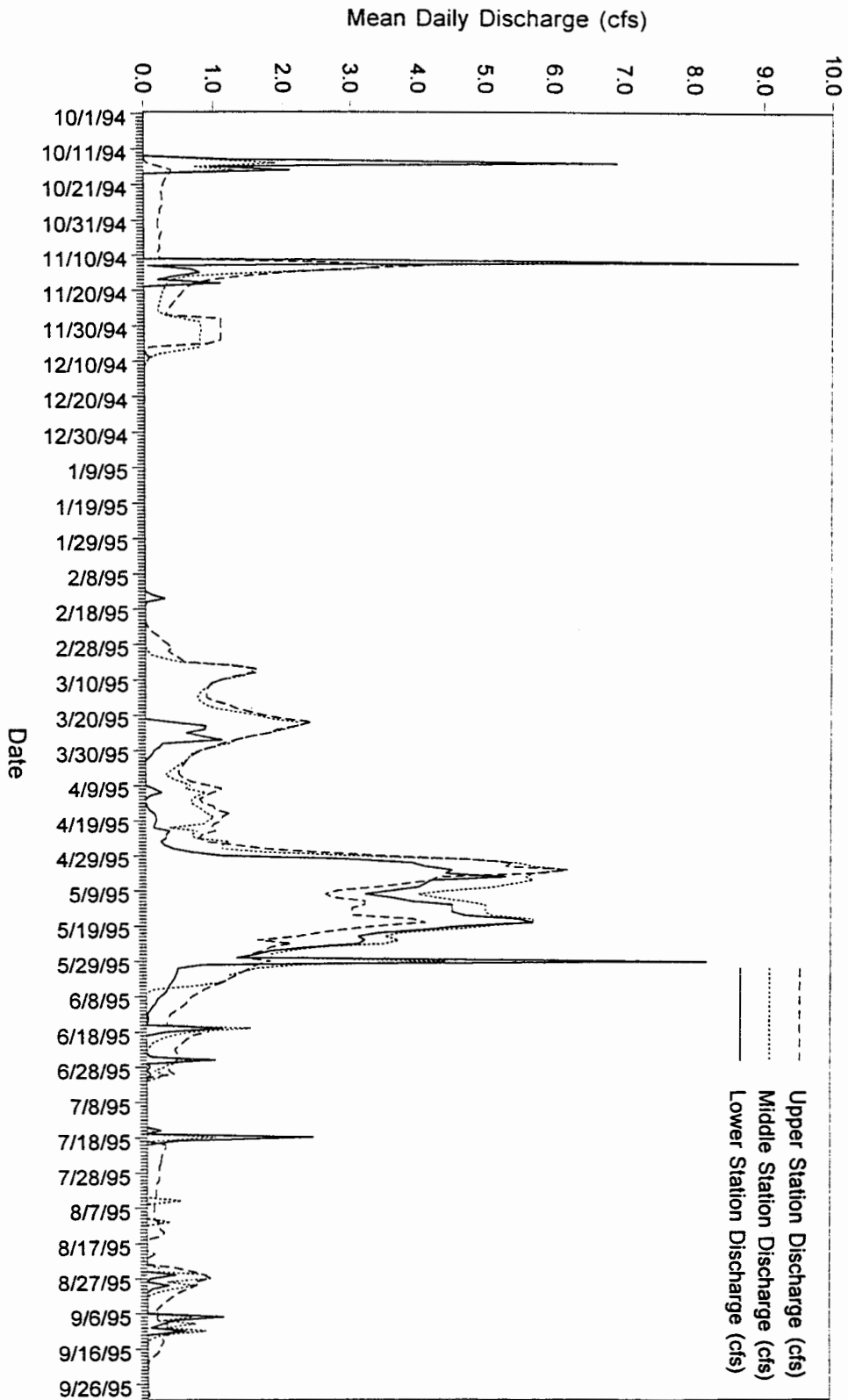


Figure 24: Los Alamos Canyon Combined Streamflow Discharge (10/1/94 to 9/30/95)

behavior. This pattern suggests that the alluvium was nearly fully saturated in at least parts of the upper canyon area for about a month during the peak snowmelt runoff period.

The other notable variation is the occurrence of peak flow rates at the lower gage during several short term periods, i.e. 10/14/94-10/17/94, 11/12/94, 5/29/95, 6/26/95, 7/18/95-7/19/95, and 9/7/95-9/8/95. These periods correspond to major precipitation events (see Figure 16) and this pattern of behavior indicates that streamflow effects from the rapid and short-lived runoff from these events are primarily expressed in the middle canyon area (lower portion of study area). Wilcox et al. (1996) suggest that the cause for the elevated responses to precipitation events in the lower gage data is enhanced runoff from nearby urban development in DP Canyon.

Data were also obtained from a channel loss investigation (seepage run) conducted by USGS and LANL personnel on 5/3/95 during the peak runoff period. Streamflow measurements were taken at 16 sites (including the three permanent flow gages) approximately equally spaced along the stream, of which 15 were located within the study area. The first station was located at the western LANL boundary in the upper canyon area approximately 2,600 feet west of the upper gage, and the station located furthest downstream in the study area was at the lower gage. The station locations were plotted on USGS 7½ minute topographic quadrangles and the intervening stream reach lengths were measured from these maps.

A spreadsheet for the channel loss calculations is shown in Table 6. Reach loss rates were determined by subtracting each succeeding station's flow rate from the preceding station's rate. These results show that negative flow losses occurred over much of the stream between the upper and middle gages, indicating gaining reaches as was interpreted from Figure 24 above. Average stream widths were determined for each reach from the bounding stations' data, which when multiplied times the reach lengths yielded estimates of the active flow streambed areas for each reach. Dividing the flow loss rates (L^3/T) by the streambed areas (L^2) yielded average infiltration rates for each reach in

Table 6: Los Alamos Canyon Channel Loss Calculations (5/3/95)

Station Number From	Station Number To	Reach Length (ft)	Width at "From" (ft)	Avg. Width of Reach (ft)	Active Flow Streambed Area (ft ²)	Flow Rate at "from" (ft ³ /sec)	Reach Loss **** (ft ³ /sec)	Average Infiltration Rate (ft/sec)	Average Infiltration Rate (ft/day)	Avg. Velocity at "from" (ft/sec)	Avg. Velocity of Reach (ft/sec)	Travel Time of Reach (secs)	Reach Loss (ft ³)	Avg. Reach Loss (ft)	
1	2	2600	7.6	5.80	15080	5.57	0.06	3.98E-06	0.34	1.61	1.71	1520.5	91.2	0.01	
2	3	2550	4.0	3.75	9563	5.51	0.27	2.82E-05	2.44	1.81	2.00	1275.0	344.2	0.04	
3	4	2600	3.5	3.55	9230	5.24	-1.09	-1.18E-04	-10.20	2.19	2.38	1094.7	-1193.3	-0.13	
4	5	2100	3.6	3.75	7875	6.33	-0.21	-2.67E-05	-2.30	2.56	2.26	929.2	-195.1	-0.02	
5	6	1650	3.9	4.30	7095	6.54	-0.21	-2.96E-05	-2.56	1.96	2.15	767.4	-161.2	-0.02	
6	7	2050	4.7	4.40	9020	6.75	-0.04	-4.43E-06	-0.38	2.34	2.43	845.4	-33.8	0.00	
7	8	800	4.1	5.25	4200	6.79	-0.17	-4.05E-05	-3.50	2.51	2.38	336.1	-57.1	-0.01	
8	9	2550	6.4	5.70	14535	6.96	0.52	3.58E-05	3.09	2.25	2.22	1148.6	597.3	0.04	
9	10	2800	5.0	6.60	18480	6.44	-0.33	-1.79E-05	-1.54	2.19	2.16	1296.3	-427.8	-0.02	
10	12	3950	8.2	7.20	28440	6.77	0.59	2.07E-05	1.79	2.13	2.34	1688.0	995.9	0.04	
12	**	13	2300	6.2	7.55	17365	6.18	0.33	1.90E-05	1.64	2.55	2.00	1150.0	379.5	0.02
13		14	3400	8.9	7.60	25840	5.85	0.11	4.26E-06	0.37	1.45	1.81	1883.7	207.2	0.01
14		15	2800	6.3	5.85	16380	5.74	0.48	2.93E-05	2.53	2.16	2.13	1317.6	632.5	0.04
15		16	2700	5.4	6.35	17145	5.26	0.50	2.92E-05	2.52	2.09	1.90	1421.1	710.5	0.04
16	***		7.3			4.76				1.71					
Total Length:		34850													
* Upper Gage															
** Middle Gage						108438	= Streambed area between upper and middle gages (ft ²)								
*** Lower Gage						76730	= Streambed area between middle and lower gages (ft ²)								
**** Negative values indicate gaining reaches.															

feet/second which were also converted to daily rates. These results are shown graphically in Figure 25. As can be seen, the gaining rates varied considerably, with the largest rate of 10.2 feet/day occurring between stations 3 and 4. Infiltration rates were less variable, generally between 1.5 and 2.5 feet/day, though two reaches (between stations 1 and 2 and between stations 13 and 14) exhibited low infiltration rates of less than 0.5 feet/day. The greatest infiltration rate was over 3 feet/day between stations 8 and 9. This reach is located just east of TA-2 and south of TA-21. Figure 8 shows three buried faults in this zone plus several other buried faults located further down the canyon (Dransfield and Gardner, 1985; Gardner and House, 1987) which appear to approximately coincide with other reaches that showed significant infiltration rates (between stations 10 and 13 and between stations 14 and 16). Whether these buried faults have any influence on the infiltration behavior of the streambed remains questionable however, lacking more detailed data.

Average velocities were also determined for each station from the field data, which were then utilized to determine average velocities for each reach. Estimated travel times for each reach were determined by dividing the reach lengths (L) by the average velocities (L/T). Total reach loss volumes were then calculated by multiplying the reach loss rates (L^3/T) by the travel times (T) and the average loss depths for each reach were then determined by dividing the loss volumes (L^3) by the streambed areas (L^2). Making the assumption that the measurements were made simultaneously, the instantaneous reach losses were mostly between 0.01 and 0.04 feet while the major gaining reach showed a net gain of 0.13 feet.

The relation between the total annual discharge volumes for the three streamflow gages was also analyzed (see Appendix G). Subtracting the total middle gage volume from the total upper gage volume and dividing by the streambed area as determined from the seepage run data yielded an average net gain of 9.5 feet for the upper reach over the entire 1995 water year. Repeating this procedure for the middle and lower gages showed an average total infiltration loss of 91.4 feet for the lower reach over the entire year.

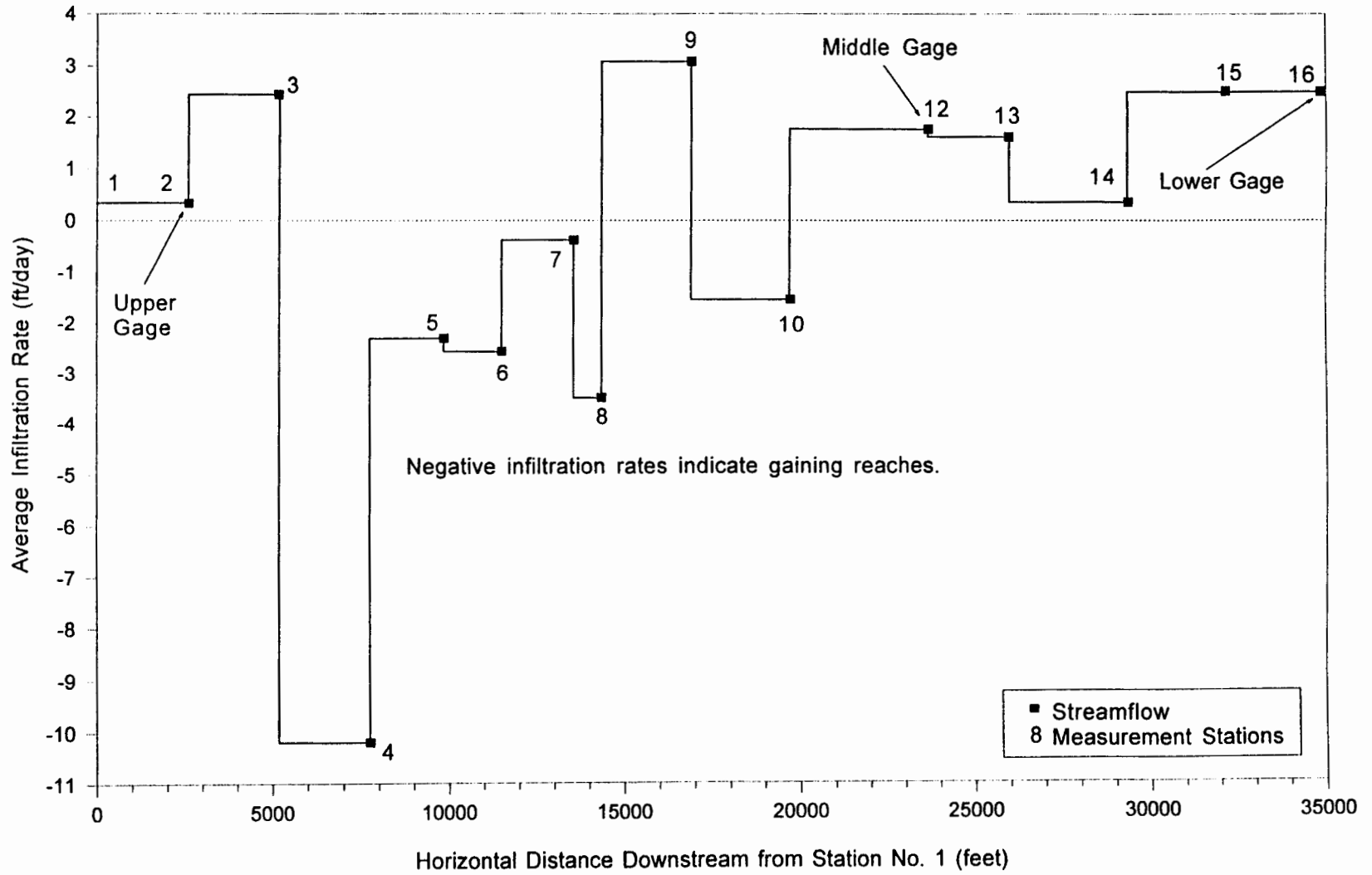


Figure 25: Los Alamos Canyon Seepage Run (5/3/95) Calculated Infiltration

Lastly, the relation between streamflow discharge rates recorded at the upper gage, alluvial aquifer head fluctuations recorded in well LAO-3, and daily net non-frozen precipitation yield amounts from the Quemazon station and SNOTEL site were examined (Figure 26). Discharge data for the upper station prior to 10/1/94 are lacking. Nonetheless, a fairly clear correlation is seen between all three parameters. Flow peaks generally follow precipitation peaks and the pattern of variation in flow rates is strikingly similar to the variation in daily precipitation yields during the active flow periods 10/14/94-12/9/94 and 2/22/95-6/30/95. These periods both represent times when snowmelt releases occurred in the upper basin (see Appendix F). The correlation is not as strong during the active flow period 7/20/95-9/20/95 when runoff was strictly from rainfall. However, these data suggest that it may be possible to roughly reconstruct streamflow discharge patterns in the upper canyon area from net precipitation yield amounts determined from snowpack data for prior years before the upper streamflow gage was installed.

Also, periods of active recharge and steady state saturation conditions in the alluvium can be seen to correspond directly with periods of active streamflow. The obvious conclusion drawn from this relation is that the primary pathway for recharge to the alluvial aquifer in the middle canyon area near well LAO-3 is through streamflow infiltration as opposed to areal recharge.

Hydrologic Budget Analysis Results

In the annual water budgets, average total precipitation for the watershed ranged from about 23.0 inches for 1994 to about 29.5 inches for 1995, with an intermediate value of about 25.4 inches determined for 1993. ET amounts ranged from about 18.0 inches in 1993 to about 21.5 inches in 1995, with the median value of about 19.0 inches occurring in 1994. Runoff amounts were negligible, averaging from 0.01 inches in 1994 to about 0.8 inches in 1993, with about 0.6 inches determined for 1995. The calculated infiltration amounts were between about 4.0 inches in 1994 and about 7.3 inches in 1995, with about

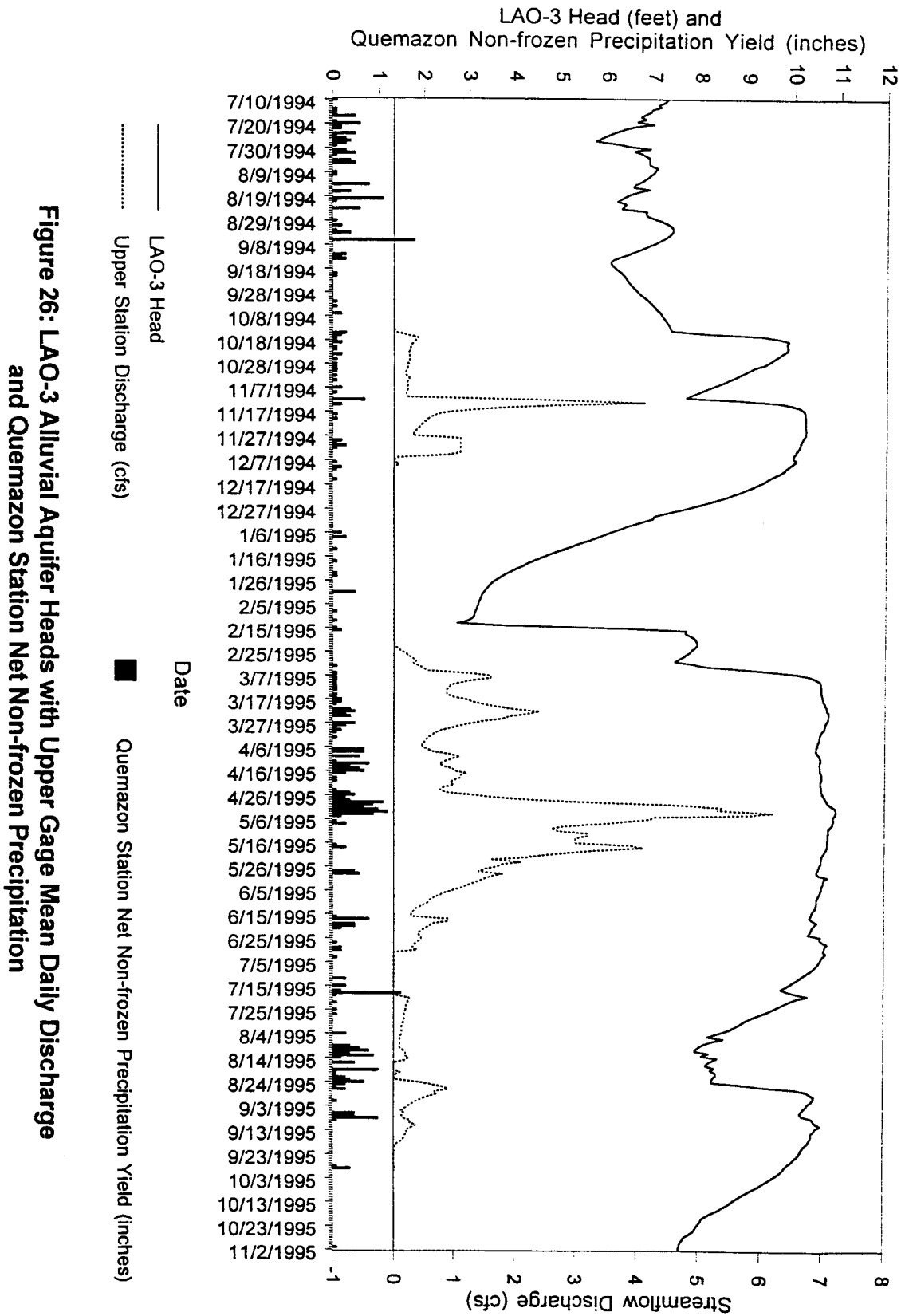


Figure 26: LAO-3 Alluvial Aquifer Heads with Upper Gage Mean Daily Discharge and Quemazon Station Net Non-frozen Precipitation

6.5 inches computed for 1993.

These results show that by far, the major water output pathway for the watershed is through ET, which varied between ~71% and ~83% of total precipitation over the 3-year period analyzed. The next largest pathway for water output is by infiltration, which varied between ~17% and ~26% of total precipitation. Very little water left the watershed as streamflow, as evidenced by the proportionally small runoff volumes measured, ranging from <0.1% to ~3% of the total precipitation volume over the evaluated time period (see Table 2).

The detailed water budget calculations, which essentially covered the last quarter of the 1994 water year, all of the 1995 water year, and extended slightly into the 1996 water year gave similar results, though showing somewhat higher average annual rates for precipitation and ET and lower infiltration than the roughly comparable 1995 annual budget results. These differences are likely attributable to: 1.) the fact that the detailed budget calculations incorporated the snowpack data from the Quemazon site, which were determined to represent more accurate measurements of winter precipitation than the precipitation gage data used in the annual budget calculations; and 2.) the greater complexity (and consequent poorer regression fits) of some of the elevation-precipitation plots used in the detailed budget calculations.

Examination of the calculated net infiltration rates from the detailed budgets shows reasonable patterns of behavior (see Table 5). The effects of ET exceeding precipitation in the dry periods (periods 3, 7, and 9) produced negative infiltration rates ranging from about -0.03 to -0.12 inches/day in the upper basin area and between about -0.02 and -0.04 inches/day in the middle/upper canyon area. The highest infiltration rates occurred in response to the major precipitation event during period 2 (about 0.28 inches/day in the upper basin area and about 0.70 inches/day in the middle/upper canyon area) which totaled nearly 3 inches at the lower precipitation gages and exceeded 4 inches at the Quemazon site over a period of 4 days, the most extreme event that occurred during the analyzed period.

These high calculated infiltration rates are partly the result of the fact that period 2 was limited to this 4 day interval when the water levels in well LAO-3 showed a dramatic response to the effects of increased infiltration (see Figure 11), and it was desired to isolate these rates for the purpose of simulating this type of aquifer response in a numerical groundwater flow model. Otherwise, the infiltration rates outside of the winter period were relatively consistent, ranging from about 0.03 to 0.10 inches/day for the upper basin area and between about 0.02 and 0.06 inches/day in the middle/upper canyon area. During the winter period (period 5), essentially zero infiltration was determined, with rates of about -0.005 inches/day for the upper basin area and about -0.002 inches/day in the middle/upper canyon area.

The average annual precipitation rate for the upper basin area over the entire analyzed period was 37.09 inches/year, nearly double the 19.33 inches/year rate determined for the middle/upper canyon area. ET effects were also more pronounced in the upper basin area, averaging 32.20 inches/year and representing ~87% of total precipitation compared to 14.45 inches/year representing ~75% of total precipitation in the middle/upper canyon area. However, the average calculated annual infiltration rate of 5.62 inches/year for the middle/upper canyon area was ~47% greater than the 3.82 inches/year infiltration rate determined for the upper basin area. Infiltration represented ~10% of total precipitation in the upper basin area but ~29% in the middle/upper canyon area.

For the entire watershed, precipitation averaged 31.51 inches/year over the analyzed period, while ET averaged 26.63 inches/year and the average infiltration rate was 4.38 inches/year. Out of the total precipitation volume determined for the entire watershed over the analyzed period, ET represented ~84%, infiltration represented ~14%, streamflow runoff represented 1.5%, and estimated reservoir usage represented 0.1% of the water budget (see Table 4).

Thus, the detailed water budget calculations yielded somewhat higher overall ET and lower infiltration proportions than were determined in the annual budget calculations.

However the differences are not significant taking into account that a 10% error margin must be considered for all of the precipitation data sources and that the error in determining ET is unquantified. Nevertheless, the results appear reasonable, and it thus seems clear that ET losses comprise the major component of the water budget for the Los Alamos Canyon watershed, while infiltration losses are nearly an order of magnitude less and streamflow runoff losses are almost 2 orders of magnitude less in significance.

GROUNDWATER FLOW SIMULATIONS

Purpose

According to Anderson and Woessner (1992), the first step in a modeling application should be to establish the purpose of the model. This is necessary to determine the type and level of modeling effort needed, as well as deciding if a numerical model is necessary or whether an analytical approach would be adequate to answer the pertinent questions.

The purpose of the modeling efforts undertaken in this study is to evaluate the hydrologic dynamics of the perched alluvial aquifer system in Los Alamos Canyon. Although basic characteristics such as average groundwater flow velocity have been previously addressed in a general fashion (Gallaher, 1995), there have been no prior attempts to characterize with any level of detail the variability and dynamic range of groundwater flow conditions in this alluvial system. And though the hydrologic budget analysis produced estimates of variable recharge rates to the system including the effects of ET, a major remaining question is the nature of the hydrologic connection between the saturated alluvial system and the underlying strata. Specifically, what is the rate of infiltration seepage out of the alluvial system and how does this seepage vary with time and space throughout the canyon? How do these variations relate to the other components of the canyon's water budget including changes in storage in the alluvial system and the amount of water that moves out of the study area via downgradient flow? These questions are important in the context of assessing potential contaminant migration from the alluvial system into deeper hydrologic systems including ultimately, the regional aquifer water supply for the area.

It was decided that because of the highly dynamic nature of the alluvial system and the complexity of its hydrogeologic regime, that analytical solutions to these questions would not only be difficult to formulate, but also that the results would likely be

insufficient to adequately address the scope of the problem with the level of detail desired. It was therefore determined that numerical groundwater flow modeling would be the preferred approach to answering the questions posed regarding the components of the groundwater budget not previously addressed in the preceding hydrologic budget analysis.

Computer Code

The USGS MODFLOW finite-difference groundwater flow model was selected to perform the numerical flow modeling since it has been extensively verified in numerous previous applications and is widely accepted throughout the groundwater industry and academic community. Visual MODFLOW® was used to generate the necessary input files to run the MODFLOW code and provided a variety of techniques to analyze the program's output. Model setup and output visualization is handled via a graphical interface, which facilitated the development of a complex, three-dimensional model configuration for this study, and aided the model calibration process.

The MODFLOW code produces a numerical solution using a finite difference formulation of the following differential equation describing groundwater flow in three dimensions, which is derived by combining a water balance equation with Darcy's law (McDonald and Harbaugh, 1988):

$$\frac{\partial}{\partial x} \left(K_x \frac{\partial h}{\partial x} \right) + \frac{\partial}{\partial y} \left(K_y \frac{\partial h}{\partial y} \right) + \frac{\partial}{\partial z} \left(K_z \frac{\partial h}{\partial z} \right) - W = S_s \frac{\partial h}{\partial t} \quad (5)$$

where K_x , K_y , and K_z are hydraulic conductivity values in the x, y and z directions;

h is the hydraulic head;

W is a volumetric flux for water sources or sinks;

S_s is the specific storage of the porous medium; and

t is time.

For steady-state simulations S_s is set equal to zero. For unconfined aquifer simulations, S_s is assumed to be equivalent to specific yield (S_y).

The finite difference solution technique requires that the model domain be discretized into a grid of rectangular cells for each layer, with uniform aquifer properties assumed within each cell (Wang and Anderson, 1982). MODFLOW utilizes a block-centered grid formulation in which the nodes at which head values are calculated are envisioned as occurring at the centers of each cell (McDonald and Harbaugh, 1988). The finite difference formulation results in a set of equations represented in matrix form which can be solved with a variety of iterative techniques. The solution technique utilized in this study was a bi-conjugate gradient stabilized acceleration routine implemented with Stone incomplete decomposition for preconditioning of the finite difference equations, a proprietary code provided with Visual MODFLOW® (Waterloo Hydrogeologic Software, 1996). The implementation of this code, designated as the WHS solver, was important to the successful application of MODFLOW in this study as none of the USGS solution techniques would converge for the numerically difficult model configuration created to represent the long, thin and narrow alluvial system in three dimensions.

Conceptual Model

The areal boundaries of the alluvial deposits in the canyon were assumed to represent the lateral boundaries of the alluvial aquifer, and the base of the alluvium was assumed to represent the bottom of the zone of saturation. The system is envisioned as a single layer of sediments with varying saturation levels due to water inputs from baseflow recharge at the upgradient boundary and recharge from percolation of precipitation and surface runoff over its upper surface, countered by water outputs to groundwater flow from the downgradient boundary, evapotranspiration of near surface moisture from the upper surface, and infiltration seepage into underlying strata from its lower surface.

The upper end of the modeled system was thus assumed to be defined by a constant head boundary at Los Alamos Reservoir, providing a source for baseflow recharge. The lower end was also assumed as a constant head boundary to stimulate downgradient flow in the system and was set at approximately 10,000 feet beyond the eastern boundary of the study area at State Road 4 to minimize boundary effects in the area of interest. The recharge to and evapotranspiration from the system were constrained by the results of the hydrologic budget analysis. Infiltration seepage from the bottom of the system into the underlying strata was simulated with MODFLOW's drain package.

The drain package represents a head dependent boundary in that MODFLOW calculates discharge from the drain using the difference between a cell's computed head and the assigned drain elevation (McDonald and Harbaugh, 1988):

$$QD_{i,j,k} = CD_{i,j,k} (h_{i,j,k} - d_{i,j,k}) \quad \text{for } h_{i,j,k} > d_{i,j,k} \quad (6)$$

$$QD_{i,j,k} = 0 \quad \text{for } h_{i,j,k} \leq d_{i,j,k} \quad (7)$$

where $QD_{i,j,k}$ is the drain's discharge rate (L^3/T);

$CD_{i,j,k}$ is the drain conductance (L^2/T);

$h_{i,j,k}$ is the cell's computed head (L); and

$d_{i,j,k}$ is the drain's elevation (L).

Though the small stream in the canyon was determined to furnish some recharge contribution to the system, it was decided that MODFLOW's river package would be difficult to implement since the actual physical situation was characterized by highly intermittent and ephemeral streamflow conditions. Also, even though some data were available on stream discharge rates, the river package requires the user to specify stream stage elevations and detailed data of this type suitable for a three-dimensional model were lacking. Furthermore, the determination of areally averaged precipitation and ET rates was

inherent in the hydrologic budget analysis procedure utilized. Therefore, the conceptual model employs areal recharge only, recognizing that this represents a simplification of the real system.

Different recharge and ET rates were applied to the upper and lower portions of the modeled system as determined by the hydrologic budget analysis results, and these rates were assumed to abruptly change at the division between the upper basin and upper/middle canyon areas. This was another simplification of the real system in which variations in precipitation and ET rates are gradational, occurring with changes in elevation.

Model Design

The areal boundaries of the alluvium were estimated by analysis of a 1 inch:1,000 feet scale topographic map of the canyon (FIMAD, 1994). The boundaries were estimated by drawing a line at the topographic break between the steep canyon walls and the comparatively level, low relief topography of the canyon floor. This line was then digitized using FastCAD® along with well locations and other nearby physical features of interest to provide a base map for delineation of the model boundaries (Figure 27). The digitized map was rotated counterclockwise by 6.5 degrees to orient the alluvial system to a west-east configuration with the minimum north-south distance deviation in order to most efficiently fit within the rectangular grid required by MODFLOW. This also served to maximize the alignment of the primary direction of downgradient flow in the system with the x-axis of the model grid.

A grid with rectangular cells of 250 feet length by 100 feet width consisting of 200 columns by 30 rows was overlain on the digitized base map and no-flow boundary conditions were specified for each cell that fell more than 50% outside of the alluvial boundary except for the easternmost 2,000 feet, defined as a linear extension of two rows of active-flow cells representing a continuation of the system beyond the LANL boundary and study area of interest (Figure 28). This defined the areal configuration of the model.

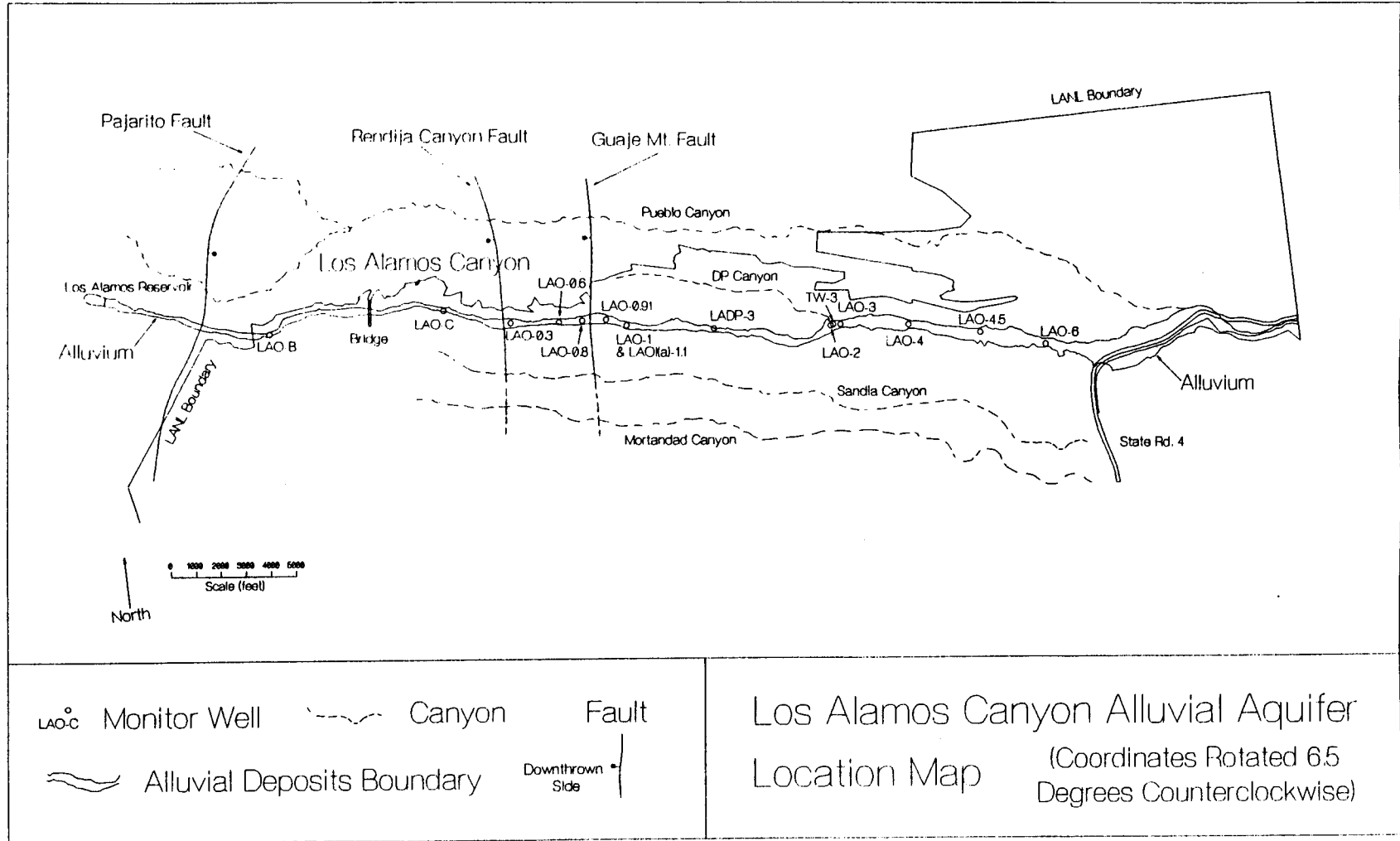


Figure 27

77

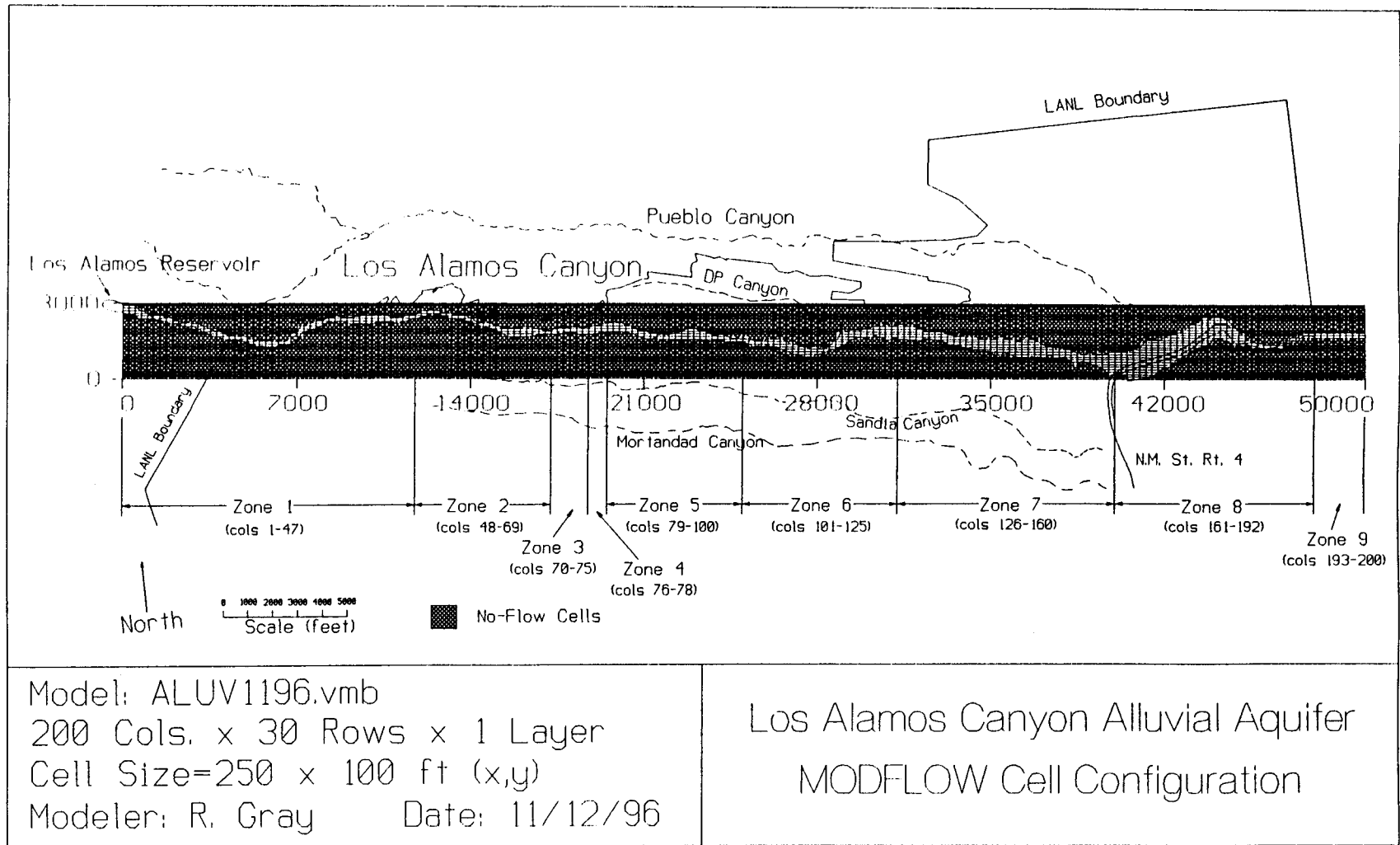


Figure 28

The three-dimensional grid configurations representing the top and bottom of the alluvial system were created using SURFER® (Golden Software, Inc., 1991). The upper surface grid was generated using the surveyed surface elevation data from the sites of most of the alluvial observation wells as well as topographic elevations obtained from the topographic map used to define the alluvial boundaries. The grid was leveled in the y dimension by assigning equivalent x and z coordinates (representing alluvium surface elevations) to the y coordinates representing rows 1 and 30 of the model grid. An ASCII file of these x,y,z coordinates was created which provided the input data for SURFER®. The kriging option was used to generate a three-dimensional grid with the same cell configuration as the MODFLOW grid (Figure 29). A second ASCII file was then created to represent elevations of the bottom of the alluvium by subtracting the alluvium thicknesses determined from the well logs from the surface elevations in the ASCII file used to create the surface grid. SURFER® was again used with the kriging option to create a three-dimensional grid leveled in the y dimension representing the bottom of the alluvial aquifer (Figure 30). These surfaces were then imported into the model grid with Visual MODFLOW® to generate the model's three-dimensional configuration. The model is shown in cross-section view in Figure 31 which also shows the locations of utilized observation wells as well as approximate fault locations.

Drains were then assigned to each active-flow cell in the model except for those with specified head boundary conditions in columns 1 and 200. In order to accurately simulate infiltration seepage from the bottom of the system, each drain elevation was set to exactly match the corresponding cell bottom elevations.

Hydrologic Parameters, Assumptions, and Data Sources

The lateral boundaries of the model are defined by Neumann conditions in that the specified flow rates are set at zero. The boundary conditions in columns 1 and 200 of the model are defined by Dirichlet conditions whereas constant heads are assumed. The

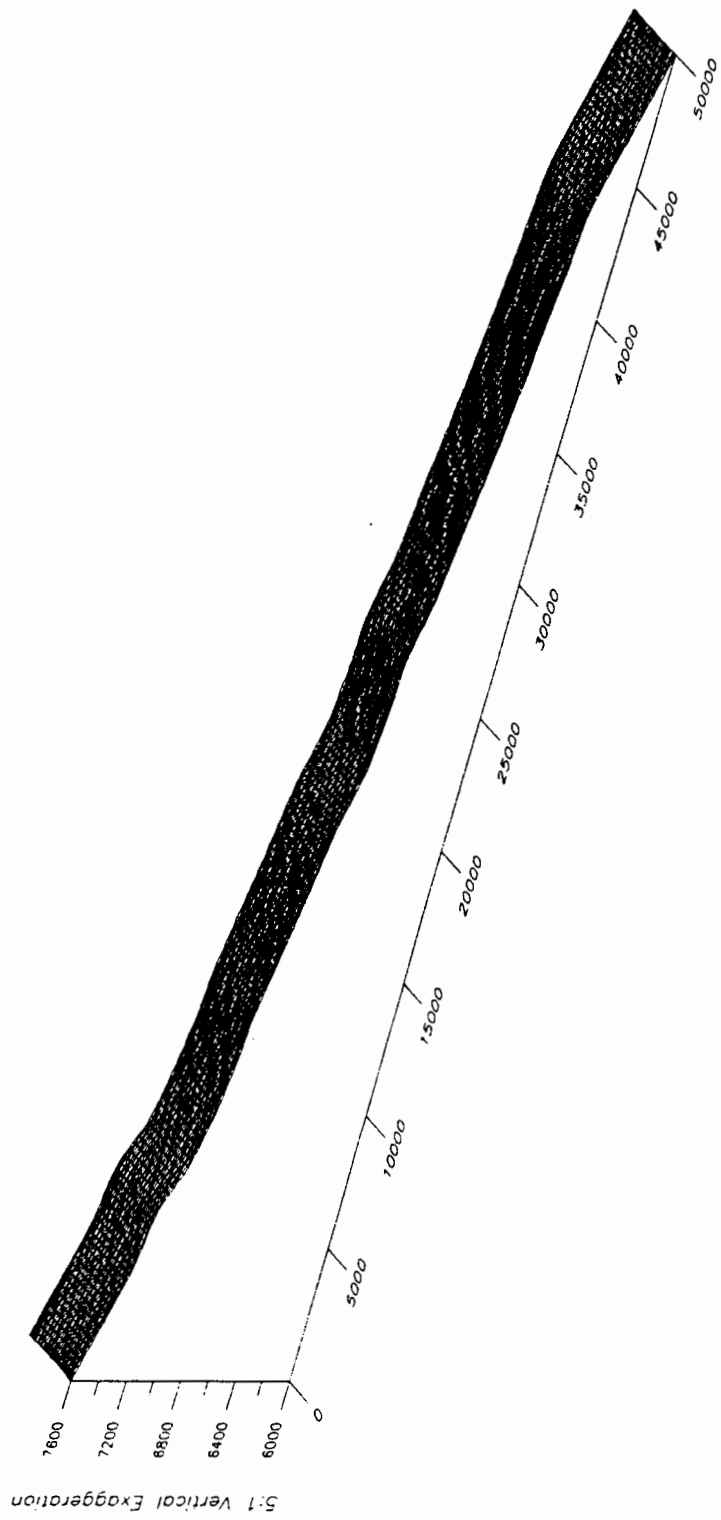


Figure 29: Alluvial Aquifer Model Surface Grid

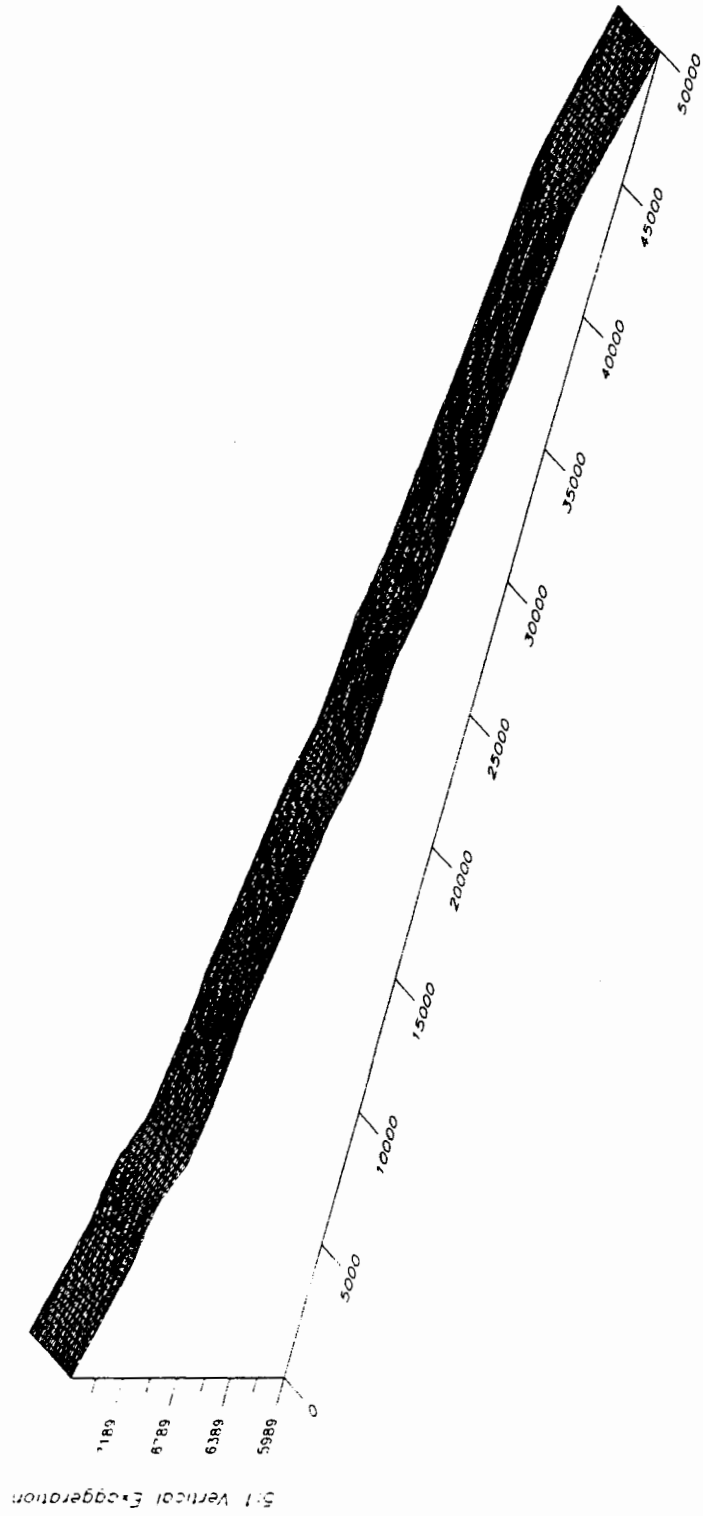
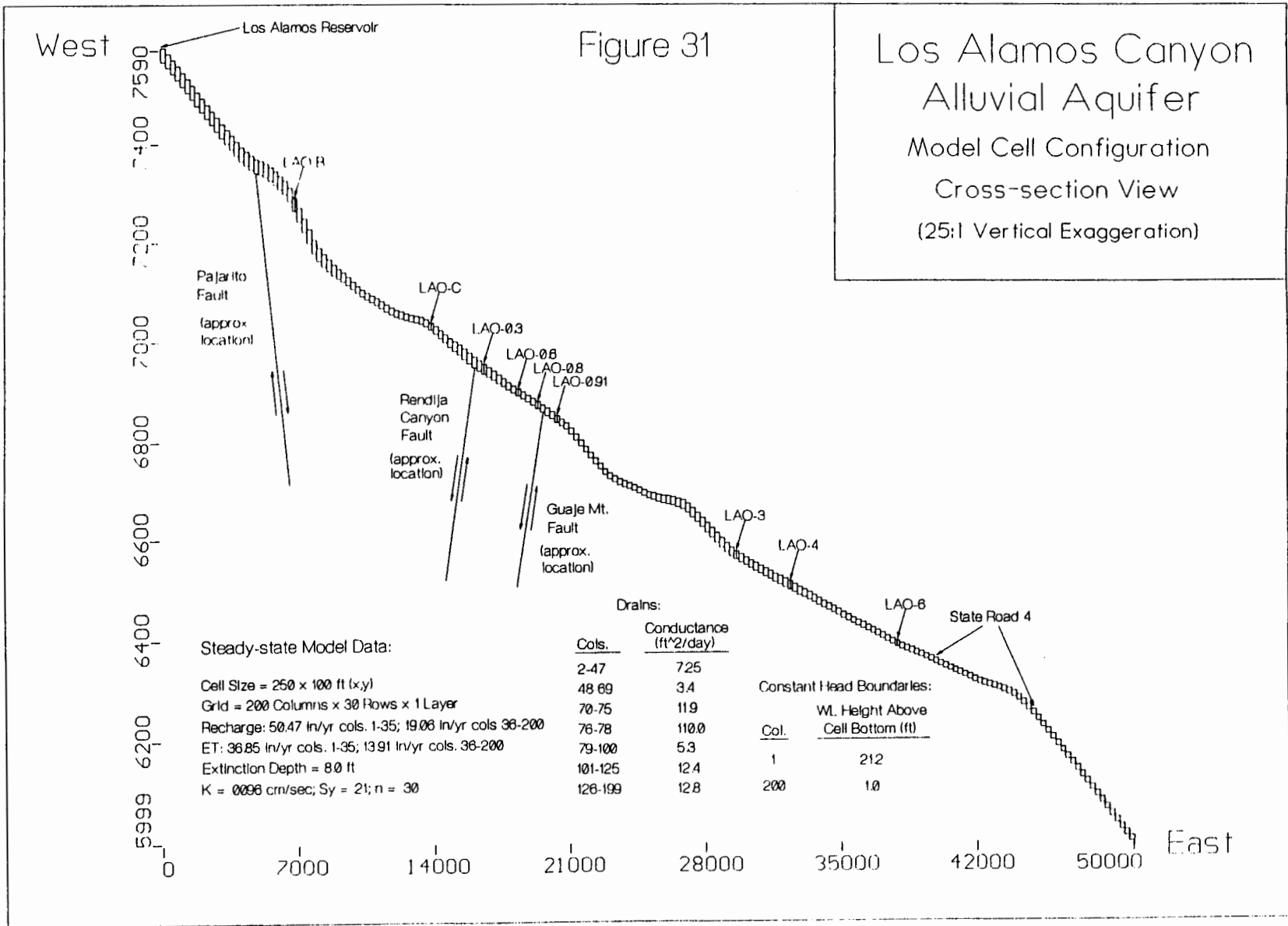


Figure 30: Alluvial Aquifer Model Bottom Grid



based on a study of root lengths at LANL in which average root lengths for piñon, juniper and ponderosa were reported at 3.9 to 5.6 feet (Tierney and Foxx, 1987). However, the lengths determined in this study were often estimated because the excavated roots were frequently broken. Anderson and Woessner (1992, p. 129) state that the extinction depth is normally 6 to 8 feet below the surface unless deep-rooted phreatophytes are present. Taking into account the lack of certainty in the LANL data, the extinction depth was thus conservatively estimated at 8 feet.

Although the alluvial strata are undoubtedly heterogeneous in their structure, this aspect has not been evaluated in any detail. Therefore, the model incorporates the assumptions of a homogeneous and isotropic medium, certainly a major simplification of the actual physical system. The model was thus assigned equivalent hydraulic conductivities in all three dimensions (K_x , K_y , K_z) of 9.6×10^{-3} cm/s based on the mean value of results from slug tests of 9 alluvial observation wells conducted by ESH-18 (Gallaher, 1995).

Site-specific data for specific yield (S_y) were not available, so its value was estimated from literature sources. Anderson and Woessner (1992), per Morris and Johnson (1967) reported a range of S_y values of 0.13-0.25 for coarse gravel, 0.17-0.44 for medium gravel, and 0.02-0.47 for tuff, with mean values of 0.21, 0.24, and 0.21 respectively. Since a major portion of the alluvial material is comprised of medium to coarse gravel derived from the Bandelier Tuff, a value of 0.21 was assigned for the S_y for the entire model.

Site-specific information on porosity (n) was limited, with only one core sample of alluvial material from intermediate observation well LAOI(a)-1.1 yielding a calculated value of 0.277 based on laboratory analysis (Daniel B. Stephens & Associates, Inc., 1995; sample AAB 0143(A)). Domenico and Schwartz (1990) reported a porosity range of 0.24-0.36 for coarse gravel with a mean value of 0.30, plus a range of 0.25-0.38 for fine gravel with a mean value of 0.315. The average value of the core analysis and the mean

reported values for coarse gravel and fine gravel is 0.297. Thus, the model was assigned a porosity value of 0.30. This parameter was not required for the flow calculations performed by MODFLOW as it does not appear in the governing equation (eqn. 5), but it is utilized by MODPATH for calculating particle tracking times.

The model assigned hydrologic parameters and data sources are summarized in Table 7 along with summary statistics for the slug test data. Though the mean and median values for hydraulic conductivity are close, there are high values for the standard error and standard deviation due to the large range encompassing greater than an order of magnitude difference in measured values.

Since the measurements were made from slug tests, they are less reliable than pump test results because the slug exerts a much lower stress on the aquifer and thus determines hydraulic properties within only a small radius of the well bore. Slug tests are also consequently more sensitive to well development variations such as screen and gravel pack/annular material characteristics along with undocumented differences such as variable hole diameters. Indeed, the tested wells were constructed between 1964 and 1989 and their documentation indicates that some of the earlier wells are not gravel packed and were manually screened while others have gravel packs and uniform commercial screens. Given these constraints on the data sources, it was felt that it would be inappropriate to assign variable hydraulic conductivities throughout the model based on the varying test results, and thus the mean value was assumed to represent a constant hydraulic conductivity for the entire model.

The criteria used for calibration of the steady-state simulation and in error analysis of the transient simulations are the water level data collected from several alluvial observation wells located in the canyon (see Figures 9 and 27). Water levels were measured by tape at irregular time intervals in wells LAO-B, LAO-C, LAO-0.3, LAO-0.6, LAO-0.8, LAO-0.91, LAO-1, LAO-2, LAO-4.5, and LAO-6. These data are included in Appendix I. Daily water level data collected by ESH-18 were available for wells LAO-C,

Table 7: Alluvial Model Hydrologic Data Sources

Slug Test Data:		Source: LANL Memo ESH-18/WQ&H-959409, 9/11/95		
Well	Hydraulic Conductivity	Hydraulic Conductivity	Hydraulic Conductivity Summary Statistics	
	(ft/sec)	(cm/sec)	cm/sec	
LAO-C	3.80E-05	0.0012	Mean	0.0096
LAO-1	5.20E-04	0.0158	Standard Error	0.0026
LAO-2	3.30E-04	0.0101	Median	0.0101
LAO-3	4.80E-04	0.0146	Standard Deviation	0.0078
LAO-3a	4.00E-04	0.0122	Sample Variance	0.0001
LAO-4	7.90E-04	0.0241	Kurtosis	-0.4624
LAO-4.5a	7.65E-05	0.0023	Skewness	0.6266
LAO-4.5c	9.10E-05	0.0028	Range	0.0229
LAO-5	1.10E-04	0.0034	Minimum	0.0012
			Maximum	0.0241
Average:	3.15E-04	0.0096 *	Confidence Level(95.0%)	0.0060
* = assigned value for alluvial models; Kx = Ky = Kz				
Assumed Data:		Assigned		
		Model Values	Range	
Specific Yield (Sy):	0.21	0.13-0.25	= range for coarse gravel	
	(mean for coarse gravel & tuff)	0.17-0.44	= range for medium gravel	
		0.02-0.47	= range for tuff	
			Source: Anderson and Woessner, 1992, p. 43; per Morris and Johnson, 1967.	
Porosity (n):	0.30	0.24-0.36	= range for coarse gravel	
	(avg. of means for coarse gravel, fine gravel and core)	0.25-0.38	= range for fine gravel	
		0.277	Source: Domenico & Schwartz, 1990, p. 26.	
			Source: LAOI(a)-1.1 core analysis	
Steady-state Model Meteorological Data:		Source: Detailed water budget; stress period 6 (2/13/95-7/1/95)		
	Recharge (in/yr)	ET (in/yr)	Extinction Depth (ft)	
Cols. 2-35	50.47	36.85	8.00	Source: Anderson and Woessner, 1992, p. 129.
Cols. 36-199	19.06	13.91	8.00	
Boundary Conditions:		Type	Head Elevation (ft)	Saturation Thickness (ft)
Upstream Boundary:	col. 1, row 2	Constant Head	7588.4	21.2 **
	col. 1, row 3	Constant Head	7588.1	21.2 **
	col. 1, row 4	Constant Head	7587.5	21.2 **
Downstream Boundary:	col. 200, row 12	Constant Head	5995.7	1.0 ***
	col. 200, row 13	Constant Head	5995.7	1.0 ***
** Based on average saturation thickness at well LAO-B from 4/28/94 to 7/29/96.				
*** Assumed saturation thickness at 10,000 ft east of model area of interest boundary at St. Rd. 4.				

LAO-3, LAO-4, and LAO-6. However, the instrumented data from wells LAO-C and LAO-6 were limited to the 110-day period from 7/10/94 to 10/28/94 when their transducers were removed because of conflicts with a water sampling program. The data from LAO-3 and LAO-4 cover the 480-day period from 7/10/94 to 11/2/95. These data are included in Appendices J, K, L, and M.

Steady-state Simulation

Calibration Procedure

Using the recharge and ET rates from period 6 when the LAO-3 hydrograph indicated that more or less steady-state conditions existed in the alluvial system, the steady-state model was calibrated to available water level measurements from 7 alluvial wells made on 4/28/95. This date is at about the middle of the period. Water levels were measured by tape in wells LAO-B, LAO-0.3, LAO-0.6, LAO-0.8, and LAO-0.91, and the data for wells LAO-3 and LAO-4 are from their daily record. Observation points for each well were assigned to the appropriate locations in the model with Visual MODFLOW® to allow monitoring of saturation levels in the model and a comparison of these levels with the observed data during the calibration process.

The procedure used to generate the three-dimensional grids for the model's upper and lower surfaces resulted in some minor inaccuracies in the model's surface elevations when compared to the surveyed elevation data for each well. Thus, the water level data were adjusted to compensate for these errors and allow an accurate correlation with the model results. These adjustments are detailed in Appendix N.

The elevations of the top and bottom of the model cells corresponding to the observation well locations were compared to the wells' surveyed surface elevations and the alluvium bottom elevations extrapolated from the well logs. Except for wells LAO-B and LAO-3, there were slight discrepancies between the cell top and bottom deviations from the survey data. Since the alluvial aquifer is an unconfined system and saturation

levels have never been observed to reach the surface beyond the actual streambed, the bottom elevations constrain the water table conditions. Thus, the observed water levels were adjusted by the difference between the extrapolated alluvium bottom elevations and the appropriate cell bottom elevations.

The model correlation calculations and water level adjustments to the 4/28/95 data are given in Appendix N (model designation ALUV1196). Appendices I-M also incorporate the adjustments for all the water level data available for each well.

Since the recharge and ET rates were constrained by the hydrologic budget analysis results, the model was calibrated by varying the simulated infiltration seepage from the bottom of the system through trial and error adjustments of each cell's drain conductance. Seven separate zones were assigned within the model corresponding to the 7 wells to which the model's saturation levels were calibrated. Each zone encompassed a range of model columns with lateral boundaries defined at the columns which most closely bisected the lateral distances between each well. Constant drain conductances were applied within each zone. The zone boundaries and varying drain conductances for each trial model run are detailed in Appendix O which is a record of the calibration process giving calculated mean errors, mean absolute errors, and root mean squared errors for each run based on comparing the model's calculated saturation levels to the observed water levels.

Convergence of the model with the WHS solver was defined at a residual head value of 0.001 feet. The initial conductance configuration applied to the first model run detailed in Appendix O was determined from numerous trials with a separate model of the alluvial system constructed earlier and not discussed in detail here. It was found through the application of many different drain conductance configurations to the earlier modeling efforts that successful convergence of the numerical solution was contingent on having a distribution of drain conductance values that was reasonably close to the eventual calibrated configuration. If the conductance values were varied too much, the model either failed to converge or the program would crash.

The previous model was a linearized representation of the system which facilitated observation of model head distributions in a cross-section view with Visual MODFLOW®. This approach was taken because the long and narrow configuration of the model made meaningful interpretations in plan view difficult, and numerous unsuccessful early modeling attempts prompted the desire to evaluate trial results in a cross-section view. However, Visual MODFLOW® only allows cross-section views for single rows and the narrow and sinuous configuration of the alluvium as configured in the current model yields cross-section views consisting of mostly no-flow cells in any one row.

Through trial and error, a single drain conductance value for the entire linearized model was found that permitted a numerical solution. The procedure for calibrating the model to the alluvial well data was then developed, and gradual variations of the conductance values through repeated trials eventually resulted in a distribution of drain conductances which produced the desired head distribution and allowed convergence. These values were then applied to the current model which was configured to accurately represent the areal distribution of the alluvium, but which then required recalibration to the observed head distribution determined by the well data.

The final calibrated distribution of drain conductance values and well zone boundaries are shown in Appendix O (run 121696d). The conductance values ranged from a low of 3.4 ft²/day in zone 2 (LAO-0.3) to a high of 110.0 ft²/day for zone 4 (LAO-0.8). The high value assigned to zone 4 was necessary to draw the modeled head down to the low level observed in LAO-0.8, supporting the interpretation that significant infiltration seepage into fractures associated with the Guaje Mountain Fault zone occurs there.

Figure 32 shows the observed saturated thicknesses plotted against the calibrated steady-state model calculated saturated thicknesses for each of the 7 wells used in the model calibration. The data points show an exact linear correlation with a slope of one illustrating that a perfect calibration of the steady-state model was achieved based on the available well data.

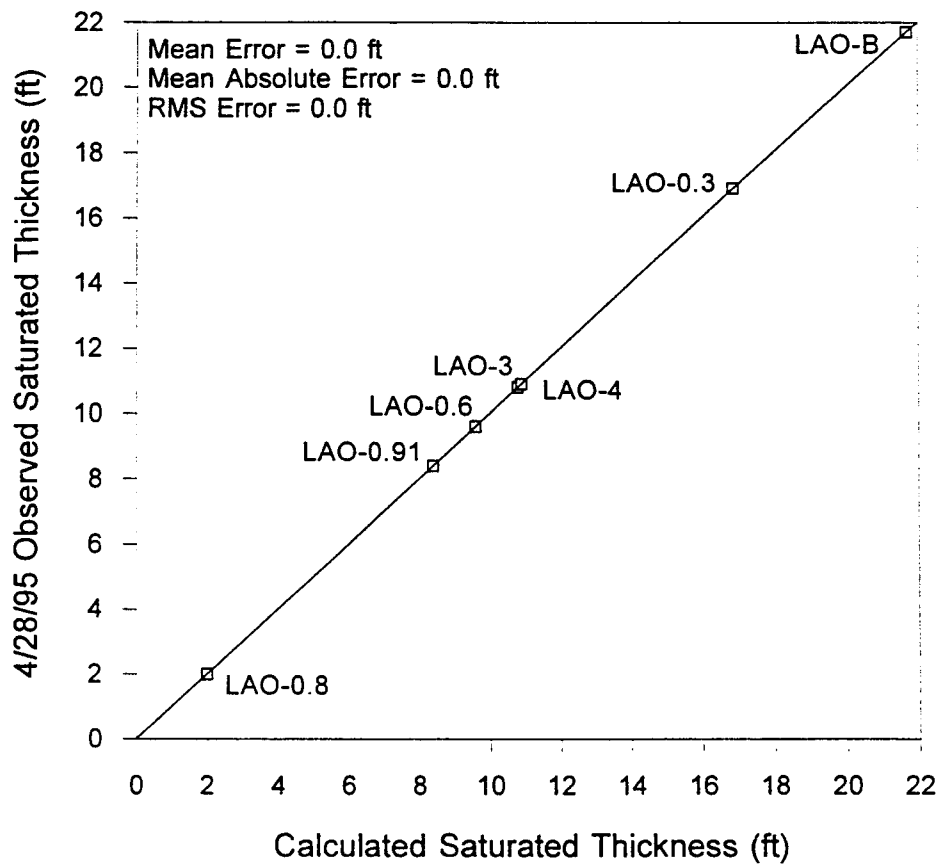


**Figure 32: Model ALUV1196 (Steady-State)
 Observed vs Calculated Saturated Thickness**

ZONEBUDGET Analysis

The USGS ZONEBUDGET (Harbaugh, 1990) code was used to analyze the variability in the different components of water losses from the modeled system. The ZONEBUDGET code allows the user to specify zones in the model within which separate water budget calculations are performed. Nine separate zones were specified (see Figure 28) which corresponded to the well zones in which differing drain conductances were assigned, except for zone 7 representing well LAO-4. Whereas constant drain conductances were specified in columns 126-199 for this zone in the MODFLOW simulation, it was limited to columns 126-160 in the ZONEBUDGET analysis to facilitate water budget calculations confined to the study area of interest west of State Road 4. Columns 161-192 were assigned to zone 8 representing the portion of the model outside of the study area but within the LANL boundary, and columns 193-200 were assigned to zone 9 representing the portion of the model which lies outside of the LANL boundary.

The results of the ZONEBUDGET calculations are given in Table 8 which shows daily volumetric loss rates for infiltration, ET, and downgradient flow within each zone, and the total amounts for the study area west of State Road 4 (zones 1-7). The percentages of the total losses comprised by each component are also given, as well as the average loss rates within each zone in inches/day. The calculated volumetric loss rates and average loss rates are compared graphically in Figure 33.

As can be seen, infiltration losses dominate the system's water budget, with substantial variations among each zone. A relative comparison among the zones is best made with the average loss rates determined by calculating an areally weighted average for each zone as the sizes of the zones varied significantly. As was expected, the greatest infiltration loss occurred in zone 4 which represents well LAO-0.8 and falls within the Guaje Mountain fault zone, exceeding 0.11 inches/day under steady-state conditions. Significant infiltration loss also occurred in zone 1 (nearly 0.08 inches/day), due primarily to the greater saturated thicknesses in the upper canyon area as seen in well LAO-B, since

Table 8: Steady-State Model ALUV1196 Zonebudget Results

		-----Zone Budget Results-----						
Volumetric Losses:		Columns		Infiltration	ET Loss	Downgradient	Constant	Total Loss
Zone #	Area/Wells	From	To	(ft ³ /day)	(ft ³ /day)	(ft ³ /day)	(ft ³ /day)	(ft ³ /day)
1	LA Reservoir to 1100 ft east of Bridge/LAO-B	1	47	18163.0	11852.0	1385.9		31400.9
2	LAO-C, LAO-0.3	48	69	2553.3	1962.5	2635.8		7151.6
3	LAO-0.6	70	75	1897.8	540.7	1829.2		4267.7
4	LAO-0.8	76	78	2654.5	0.0	371.7		3026.2
5	LAO-0.91, LAO-1	79	100	3347.4	2922.2	1391.0		7660.6
6	LAO-2, LAO-3a	101	125	9468.5	720.7	2515.7		12704.9
7	LAO-4, LAO-4.5, LAO-6	126	160	16827.0	4117.9	2132.2		23077.1
	West of St. Rd. 4 Totals:			54911.5	22116.0	2132.2		79159.7
8	St. Rd. 4 to Lab boundary	161	192	19958.0	7955.9	1089.7		29003.6
9	East of Lab boundary	193	200	1166.4	419.8		1026.6	2612.8
Loss Percentages:		Columns		Loss to	Loss to	Downgradient	Const. Head %	Total (%)
Zone #	Area/Wells	From	To	of Total Loss	of Total Loss	of Total Loss	of Total Loss	
1	LA Reservoir to 1100 ft east of Bridge/LAO-B	1	47	57.84	37.74	4.41		100.00
2	LAO-C, LAO-0.3	48	69	35.70	27.44	36.86		100.00
3	LAO-0.6	70	75	44.47	12.67	42.86		100.00
4	LAO-0.8	76	78	87.72	0.00	12.28		100.00
5	LAO-0.91, LAO-1	79	100	43.70	38.15	18.16		100.00
6	LAO-2, LAO-3a	101	125	74.53	5.67	19.80		100.00
7	LAO-4, LAO-4.5, LAO-6	126	160	72.92	17.84	9.24		100.00
	West of St. Rd. 4 Totals:			69.37	27.94	2.69		100.00
8	St. Rd. 4 to Lab boundary	161	192	68.81	27.43	3.76		100.00
9	East of Lab boundary	193	200	44.64	16.07	0.00	39.29	100.00
Average Losses:		Columns		Avg. Loss to	Avg. Loss to	Avg. Loss to	Avg. Loss to	Average
Zone #	Area/Wells	From	To	(inches/day)	(inches/day)	Downgrad. Flow (inches/day)	Constant Head (inches/day)	Total Losses (inches/day)
1	LA Reservoir to 1100 ft east of Bridge/LAO-B	1	47	0.077	0.050	0.006		0.133
2	LAO-C, LAO-0.3	48	69	0.023	0.018	0.024		0.065
3	LAO-0.6	70	75	0.061	0.017	0.059		0.137
4	LAO-0.8	76	78	0.116	0.000	0.016		0.132
5	LAO-0.91, LAO-1	79	100	0.024	0.021	0.010		0.055
6	LAO-2, LAO-3a	101	125	0.044	0.003	0.012		0.059
7	LAO-4, LAO-4.5, LAO-6	126	160	0.043	0.010	0.005		0.059
	West of St. Rd. 4 Totals:			0.048	0.019	0.002		0.069
8	St. Rd. 4 to Lab boundary	161	192	0.039	0.015	0.002		0.056
9	East of Lab boundary	193	200	0.035	0.013	0.000	0.031	0.078
							Cell Length (ft):	250
* Number of cells/zone (utilized in average loss calculations):							Cell Width (ft):	100
#1=113, #2=53, #3=15, #4=11, #5=67, #6=104, #7=189, #8=247, #9=16; 1-7=552.							Cell Area (ft ²):	25000

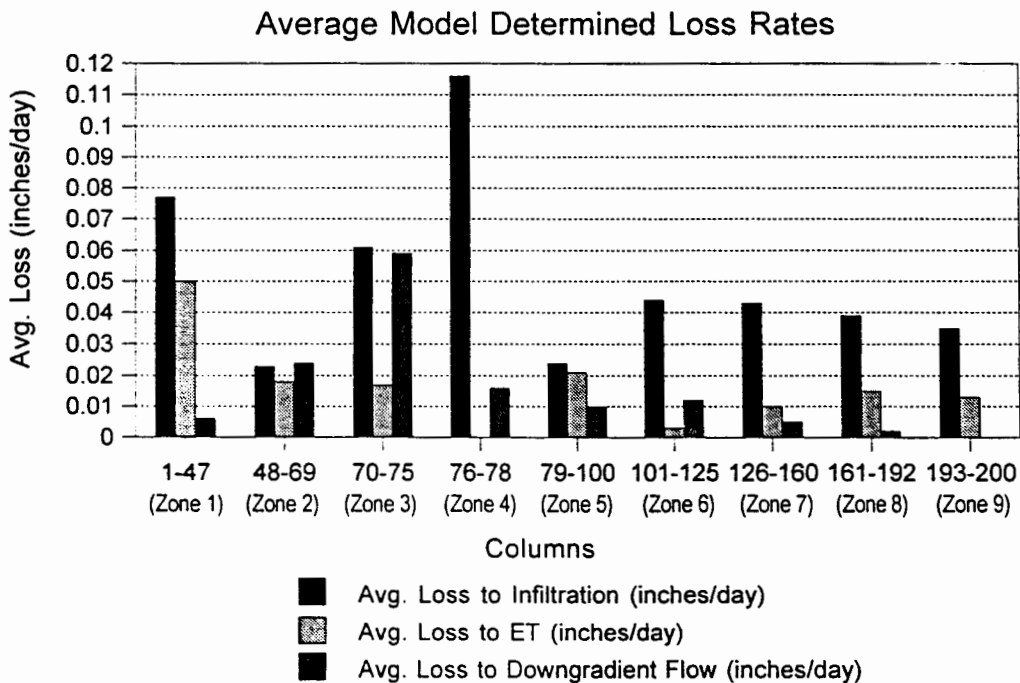
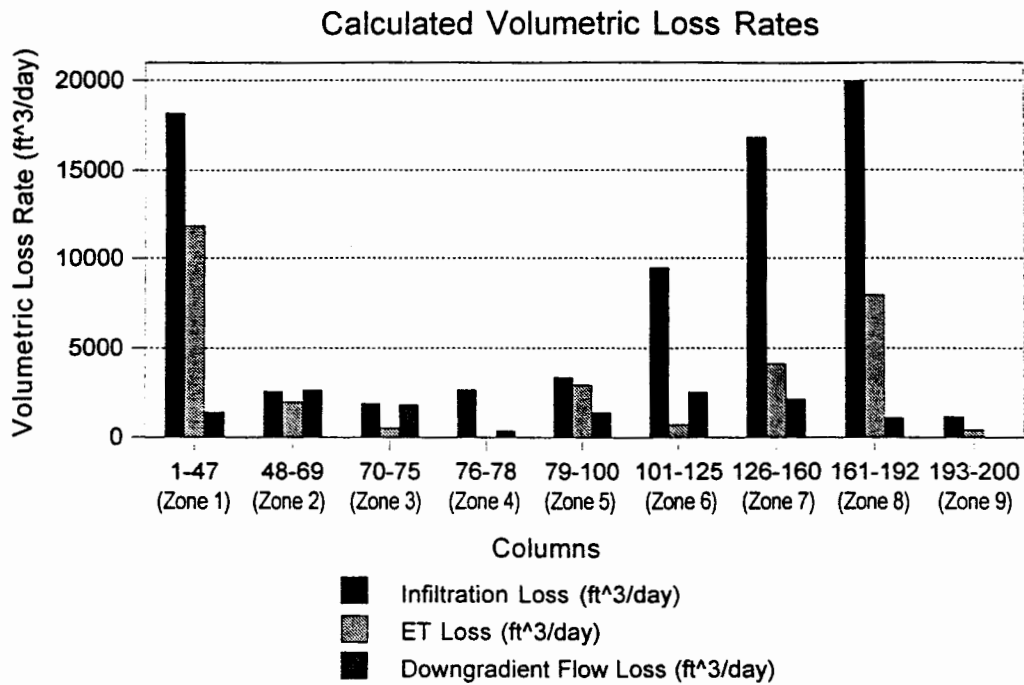


Figure 33: Model ALUV1196 (Steady-State) Zonebudget Results

the calculated drain discharge is proportional to the head difference between the water table and the drain elevation (base of the alluvium). Substantial infiltration also occurred in zone 3 (~0.06 inches/day), likely because of its proximity to the Guaje Mountain fault zone. Infiltration rates were relatively constant at ~0.04 inches/day in the lower portions of the model (zones 6-9), while the lowest rates occurred in zones 2 and 5 (~0.02 inches/day).

The highest evapotranspiration rate occurred in zone 1 (0.05 inches/day) because the water table is closest to the surface there. Elsewhere, ET was fairly consistent at about 0.01 to 0.02 inches/day except in zone 4 where it was zero because the depth of the water table exceeded the extinction depth.

Downgradient flow losses were generally low at about 0.01 to 0.02 inches/day except in zone 3 where it was ~0.06 inches/day, nearly equaling the infiltration rate there. The downgradient loss was generally a minor component except in zone 3 and also in zone 2 where it exceeded both infiltration and ET.

The losses for the total study area are shown in figure 34, both as total volumetric rates and average rates. These charts clearly show the dominance of infiltration in the system's water budget, with volumetric infiltration losses totaling ~55,000 ft³/day for the entire study area, while ET losses totaled ~22,000 ft³/day and downgradient losses totaled only ~2,000 ft³/day, representing approximately 69%, 28% and 3% of the total system losses respectively. The calculated average loss rates were ~0.05 inches/day for infiltration, ~0.02 inches/day for ET, and ~0.002 inches/day for downgradient flow.

Because the calculated drain loss is proportional to the difference between the hydraulic head and the drain elevation (see equation 6), and since the drain elevations were specified at the bottom of the system, it is possible to utilize this relation to evaluate the head configuration of the model on an average basis within each zone rather than just at the calibration points. Average saturated thickness calculations for each zone are shown in Table 9. These data are displayed graphically in Figure 35 which represents an average head profile of the alluvial system under steady-state conditions.

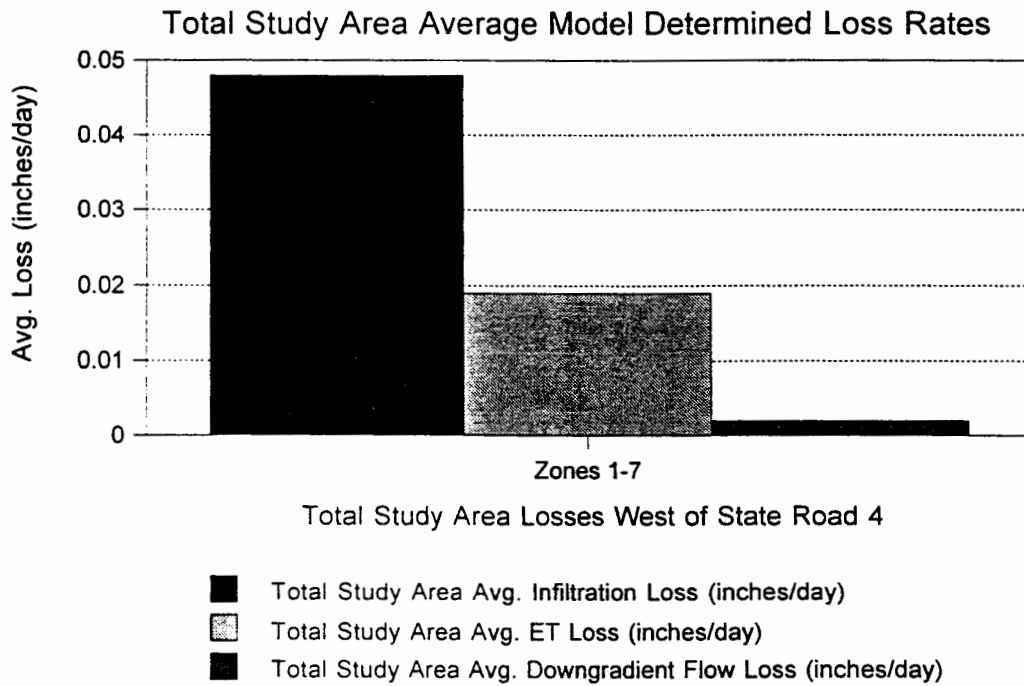
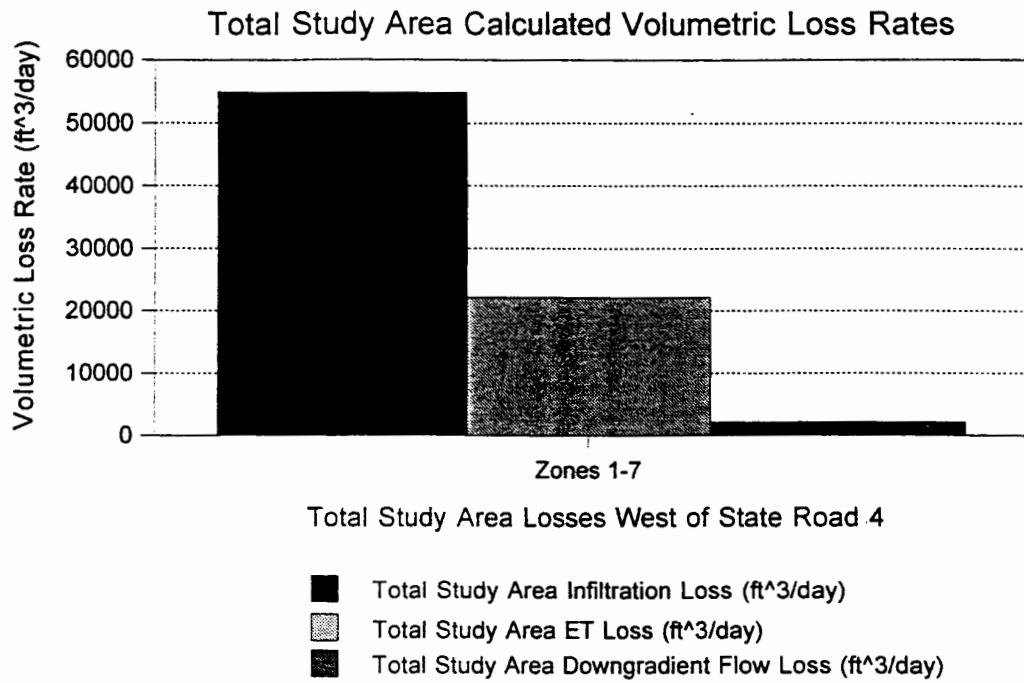


**Figure 34: Model ALUV1196 (Steady-State)
Total Study Area Zonebudget Results**

Table 9: Average Drain Losses and Calculated Average Saturated Thicknesses

Steady-State Model ALUV1196 Data:								
Zone #	Area/Wells	Columns		Ind. Drain Con- ductance (CD)	Infiltration (Drain Loss)	Model Number	Avg. Drain Loss	Avg. Sat. Th.*
		From	To	(ft ² /day)	(ft ³ /day)	of Cells	(QD) per Cell (ft ³ /day)	(h-drain elev.) (ft)
1	LA Reservoir to 1100 ft east of Bridge/LAO-B	1	47	7.25	18163.0	113	160.7	22.17
2	LAO-C, LAO-0.3	48	69	3.40	2553.3	53	48.2	14.17
3	LAO-0.6	70	75	11.90	1897.8	15	126.5	10.63
4	LAO-0.8	76	78	110.00	2654.5	11	241.3	2.19
5	LAO-0.91, LAO-1	79	100	5.30	3347.4	67	50.0	9.43
6	LAO-2, LAO-3a	101	125	12.40	9468.5	104	91.0	7.34
7	LAO-4, LAO-4.5, LAO-6	126	160	12.80	16827.0	189	89.0	6.96
West of St. Rd. 4 Totals/Averages:				11.69	54911.5	552	99.5	8.51
8	St. Rd. 4 to Lab boundary	161	192	12.80	19958.0	247	80.8	6.31
9	East of Lab boundary	193	200	12.80	1166.4	16	72.9	5.70
* Saturated thickness = h-drain elev. with drain elev. at cell bottom.								
(h-drain elev.)=QD/CD per eqn. 69, p. 9-3, McDonald and Harbaugh, 1988:								
QDi,j,k = CDi,j,k (hi,j,k - di,j,k) for hi,j,k > di,j,k.								

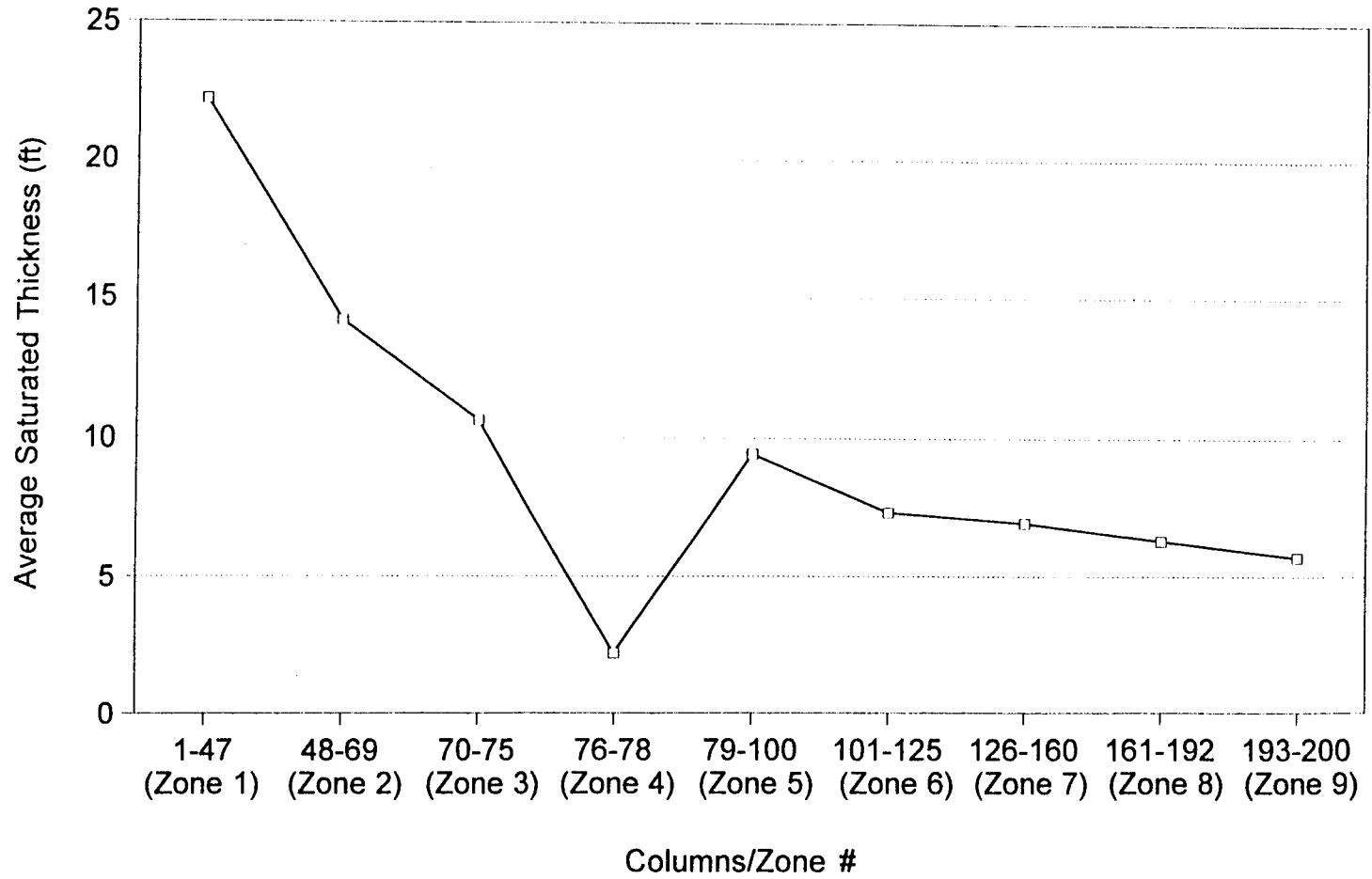


**Figure 35: Model ALUV1196 (Steady-State) Zonebudget Results
Calculated Average Saturated Thicknesses**

A comparison of this profile to Figure 10 shows a high degree of similarity, but with notable exceptions. The prominent head loss at LAO-0.8 (zone 4) is satisfactorily represented, and the saturated thicknesses upgradient from this point and immediately downgradient are in general agreement with the well data. However, the average saturated thicknesses in zones 6 and 7 representing LAO-3 and LAO-4 are only about 7 feet while the well data indicated saturated thicknesses of nearly 11 feet for these wells on the calibration date. This indicates that while the model was calibrated accurately at the well control points, there is significant head variation between these points and especially downgradient of LAO-4, contributing to the lower calculated average saturated thicknesses in zones 6 and 7. This points out a problem area in the model in that while the available well data appear to be adequate to effectively represent the upper portion of the system, there is inadequate data coverage in the lower part, where the widening of the canyon bottom leads to a greater aquifer volume represented by only 2 wells which are located rather close together, leaving the lower part of the model essentially uncontrolled.

Particle Tracking Analysis

The USGS MODPATH (Pollock, 1989) particle tracking code was utilized with the steady-state model to evaluate advective flow characteristics of the alluvial system. MODPATH uses a semi-analytical procedure based on the assumption that each directional velocity component varies linearly within a grid cell in its own coordinate direction. Linear interpolation produces a continuous velocity vector field within each individual cell that satisfies the conservation of mass everywhere within the cell. Three-dimensional pathlines and particle positions at specified points in time are computed based on inter-cell flow rates determined by MODFLOW (Pollock, 1989).

Several particles were assigned at approximately regularly spaced intervals in the model and Visual MODFLOW[®] was used to run the MODPATH code and generate a graphical representation of the resulting pathlines with demarcations at 365-day intervals

(Figure 36). This plan view of the time-marked pathlines shows that the calculated advective travel times throughout the model show a significant degree of variability. Whereas relatively consistent travel times prevail in about the lower third of the model where the canyon widens and flattens out, they vary substantially in the upper reaches of the system where the canyon is more narrow and there are greater elevation differences.

In order to analyze the MODPATH output in more detail, it was exported in a DXF (AutoCAD®) file format which was then imported into FastCAD® for three-dimensional analysis. The x,y,z coordinates for each particle and each 365-day time mark were determined with FastCAD® and input into an Excel® spreadsheet. The angular distances between the time-specified points were calculated by the simple geometric relation:

$$Distance = [(x_2 - x_1)^2 + (y_2 - y_1)^2 + (z_2 - z_1)^2]^{1/2} \quad (8)$$

yielding annual advective travel velocities between each time mark. The pathline gradients between each time mark were similarly determined by standard formula:

$$Gradient = (z_2 - z_1) / [(x_2 - x_1)^2 + (y_2 - y_1)^2]^{1/2}. \quad (9)$$

These calculations are detailed in Appendix P, in which summary statistics for each particle path and the entire model were also calculated. The results of the calculations for each point are plotted against the model's x-dimension in Figure 37 which graphically shows the variation in advective velocity and gradient throughout the alluvial system. Pathline gradients varied between 0.007 and 0.063 with a mean value of 0.025. Advective velocities varied between approximately 294 and 1,522 feet/year with a mean value of about 727 feet/year. The mean values determined with the model compare reasonably well with previous estimates of 0.027 for average gradient and ~900 feet/year for average velocity (Gallaher, 1995).

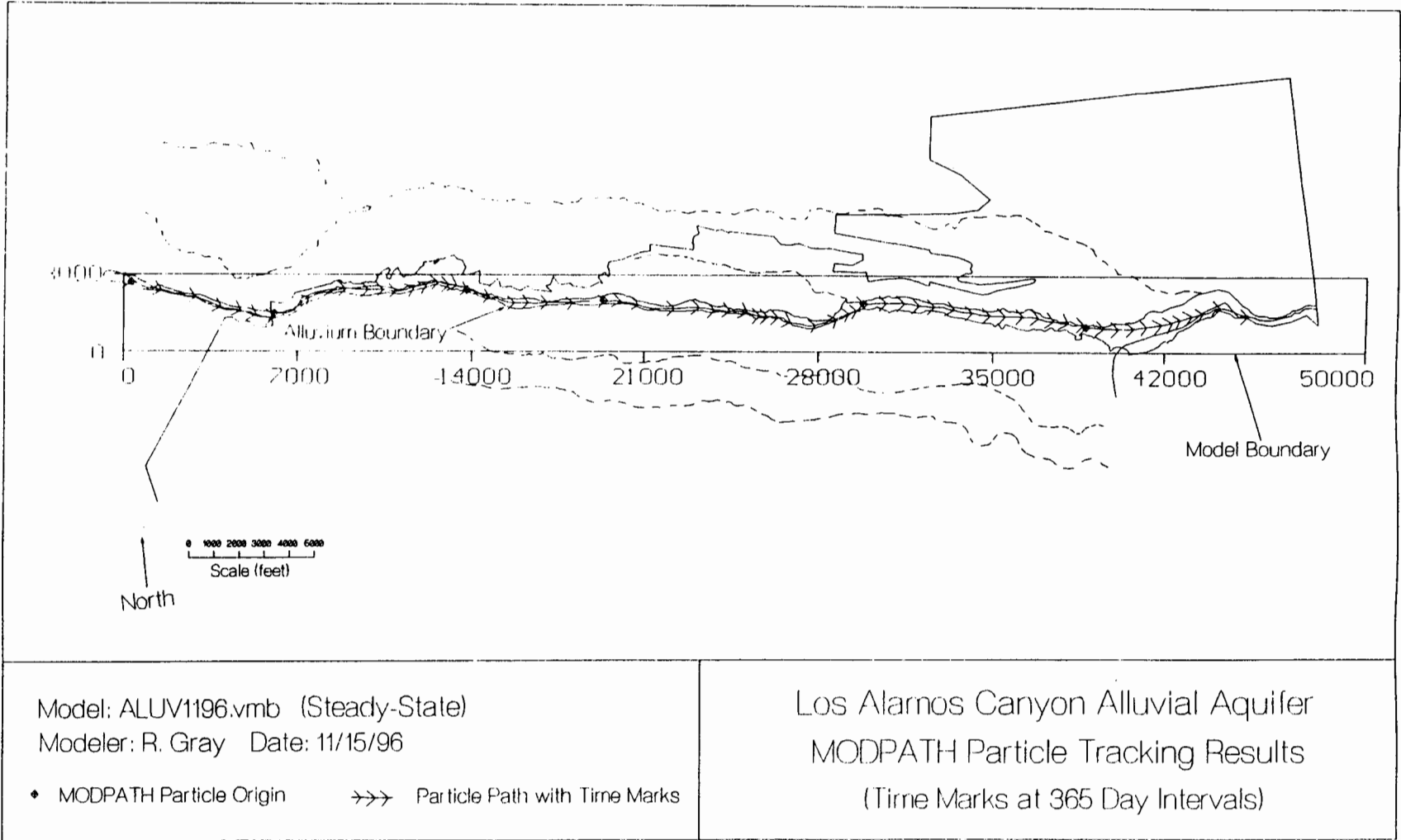


Figure 36

100

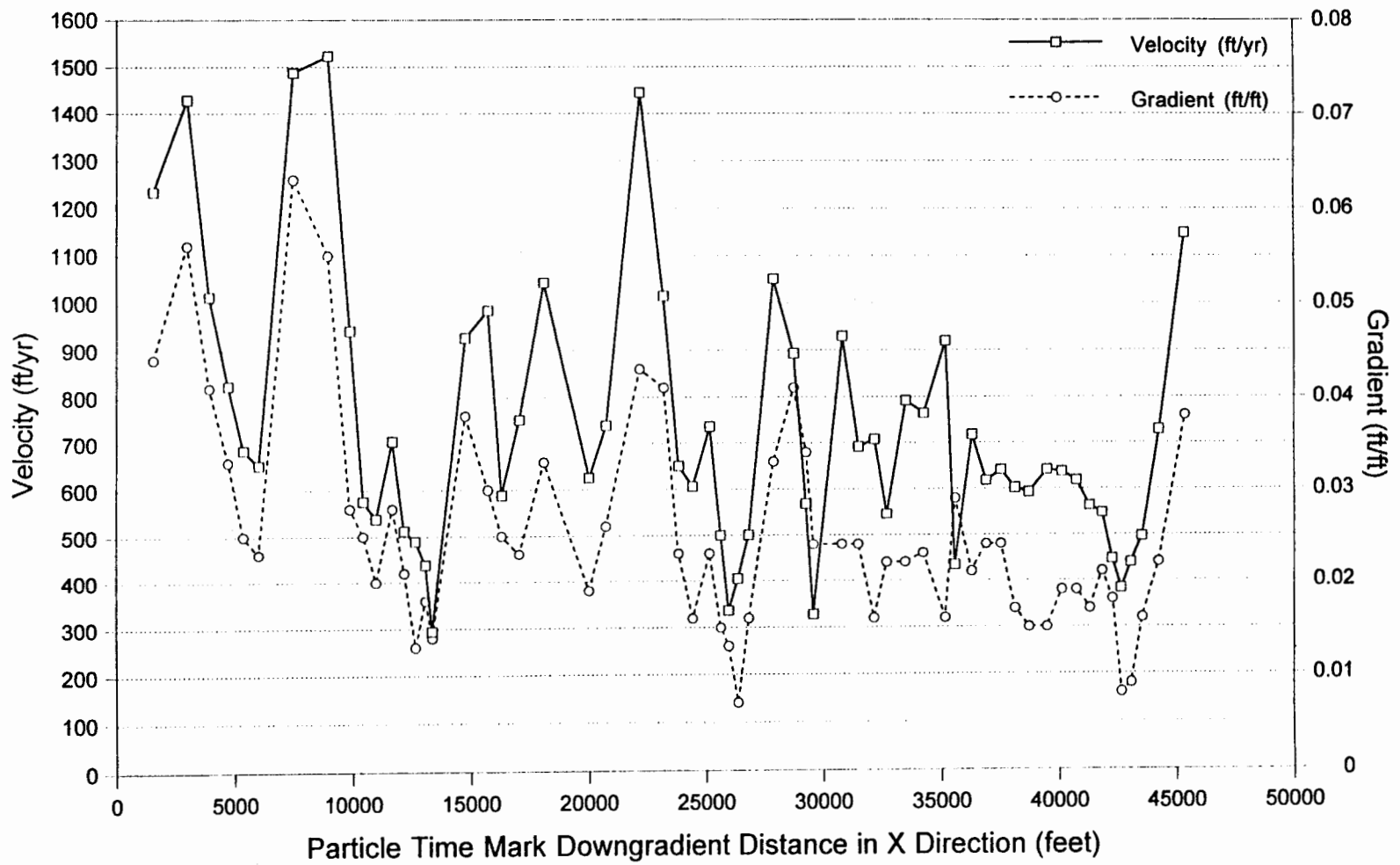


Figure 37: MODPATH Velocities and Flowpath Gradients--Model ALUV1196 (Steady-State)

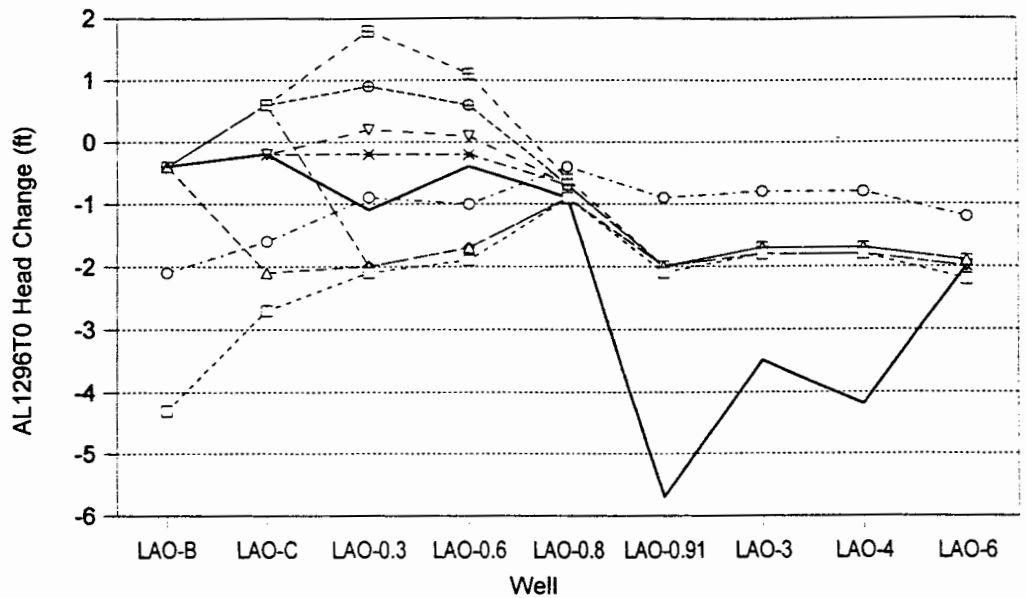
Modeling for Transient Simulation Initial Conditions-Part 1

Transient models require a distribution of specified heads as initial conditions. In MODFLOW this must be in a grid format identical to the flow model. This is typically calculated in a steady-state simulation prior to the transient simulation, representing dynamic average steady-state conditions where the head varies spatially and flows into and out of the system are equivalent (Anderson and Woessner, 1992).

Since the well data record begins at 7/10/94 for the instrumented wells which provided the primary basis for error analysis of the transient modeling, it was desired to use the head distribution at that date as the initial conditions rather than that provided by the steady-state model which was calibrated to water level measurements taken at 4/28/95. The first efforts to create the desired head distribution were a series of steady-state simulations in which varying recharge and ET rates were applied to the calibrated steady-state model in an attempt to produce a head distribution that was reasonably close to the 7/10/94 data. The parameter variations and results of these trial model runs are detailed in Appendix Q (model designation AL1296T0) which documents the attempted calibration process.

The results of these steady-state simulations are compared with the desired head changes from the calibrated steady-state model (ALUV1196) head distribution to that for the 7/10/94 data in Figure 38. As can be seen, only minor head drops of generally less than one foot were required for wells LAO-B, LAO-C, LAO-0.3, LAO-0.6, LAO-0.8, and LAO-6. However more significant head drops of about 4 to 6 feet were necessary in wells LAO-0.91, LAO-3, and LAO-4.

The initial attempt (run 120396a) employed zero recharge with ET rates based on the hydrologic budget analysis results for period 7 in which dry conditions prevailed. This trial run resulted in too much head drop upgradient from LAO-0.8 and not enough drop downgradient from there. All successive trials with varying configurations of recharge and ET rates failed to adequately resemble the 7/10/94 head distribution (runs 120396b,



- Actual Head Change (from steady-state to 7/10/94 obs. ft)
- - - □ - - - AL1296T0 Head Change (Calc. - Initial ft) Run 120396a; Zero recharge for 100 days; ET per 7/1/95-8/3/95 period: 58.25 in/yr cols. 1-35; 25.80 in/yr cols. 36-200 for 100 days.
- - - ○ - - - AL1296T0 Head Change (Calc. - Initial ft) Run 120396b; Recharge: 27.61 in/yr cols. 0-35; 12.23 in/yr cols. 36-200; & ET: 58.25 in/yr cols. 0-35; 25.80 in/yr cols. 36-200 per 7/1/95-8/3/95 period for 100 days.
- - - △ - - - AL1296T0 Head Change (Calc. - Initial ft) Run 120396c; Recharge: 44.12 in/yr cols. 1-35 per 7/10/94-10/13/94 period for 100 days; assumed zero in/yr cols. 36-200; ET: 33.97 in/yr cols. 1-35; 17.85 in/yr cols. 36-200 per 7/10/94-10/13/94 period for 100 days.
- - - ▣ - - - AL1296T0 Head Change (Calc. - Initial ft) Run 121096a; Recharge: 44.12 in/yr cols. 1-75 per 7/10/94-10/13/94 period for 100 days; assumed zero in/yr cols. 76-200; ET: 33.97 in/yr cols. 1-75; 17.85 in/yr cols. 76-200 per 7/10/94-10/13/94 period for 100 days.
- - - ◆ - - - AL1296T0 Head Change (Calc. - Initial ft) Run 121096b; Recharge: 44.12 in/yr cols. 1-60 per 7/10/94-10/13/94 period for 100 days; assumed zero in/yr cols. 61-200; ET: 33.97 in/yr cols. 1-60; 17.85 in/yr cols. 61-200 per 7/10/94-10/13/94 period for 100 days.
- - - ⊕ - - - AL1296T0 Head Change (Calc. - Initial ft) Run 121096c; Recharge: 44.12 in/yr cols. 1-60 per 7/10/94-10/13/94 period for 100 days; 30 in/yr cols. 61-75; assumed zero in/yr cols. 76-200; ET: 33.97 in/yr cols. 1-60; 17.85 in/yr cols. 76-200 per 7/10/94-10/13/94 period for 100 days; 20 in/yr cols. 61-75.
- - - ▽ - - - AL1296T0 Head Change (Calc. - Initial ft) Run 121196a; Rech.: 44 in/yr cols. 1-35; 23 in/yr cols. 36-75; 0 in/yr cols. 76-200. ET: 34 in/yr cols. 1-35; 20 in/yr cols. 36-200.
- - - * - - - AL1296T0 Head Change (Calc. - Initial ft) Run 121196b; Rech.: 44 in/yr cols. 1-35; 23 in/yr cols. 36-61; 19 in/yr cols. 62-75; 0 in/yr cols. 76-200. ET: 34 in/yr cols. 1-35; 20 in/yr cols. 36-200.

Figure 38: Model AL1296T0 (Steady-State Results)

Calculated head changes at varying recharge and ET rates vs actual change from model ALUV1196 steady-state conditions to water levels observed at 7/10/94 (initial conditions for transient models).

120396c, 121096a, 121096b, 121096c, 121196a, and 121196b). It was clear from these trials however, that continued recharge in the upper part of the model was necessary to generate a similar head distribution upgradient from LAO-0.8. Even with zero recharge in the lower part of the model though, the heads would not drop enough. This suggested that recharge was more persistent in the upper part of the system when it was drying out. It also indicated that the calibrated steady-state model did not allow sufficient infiltration seepage from the lower part of the system to allow it to dry out under drought conditions.

Transient Simulations

Purpose

The primary reason for performing the transient simulations was to test the validity of the steady-state model, which is a significantly simplified representation of the real physical system. This was done by applying stresses to the modeled system and comparing the model responses to actual data from the physical system. A reasonable duplication of the physical data by the model under transient conditions would validate the steady-state model's quantification of the loss components of the hydrologic budget for the alluvial aquifer system. Additionally, if the transient modeling is reasonably successful at reproducing observed head fluctuations in the system, a ZONEBUDGET analysis of the transient models will quantify the variations in the hydrologic budget loss components of the system under transient conditions, including the aspect of aquifer storage which is assumed to be constant in a steady-state simulation.

Modeling for Transient Simulation Initial Conditions-Part 2

The recharge and ET values determined from the steady-state trials with model AL1296T0 that yielded the best match with the target head drops were utilized in a continuation of the effort to produce a model approximating the 7/10/94 head distribution. Transient simulations were run for varying time periods to allow the lower portion of the

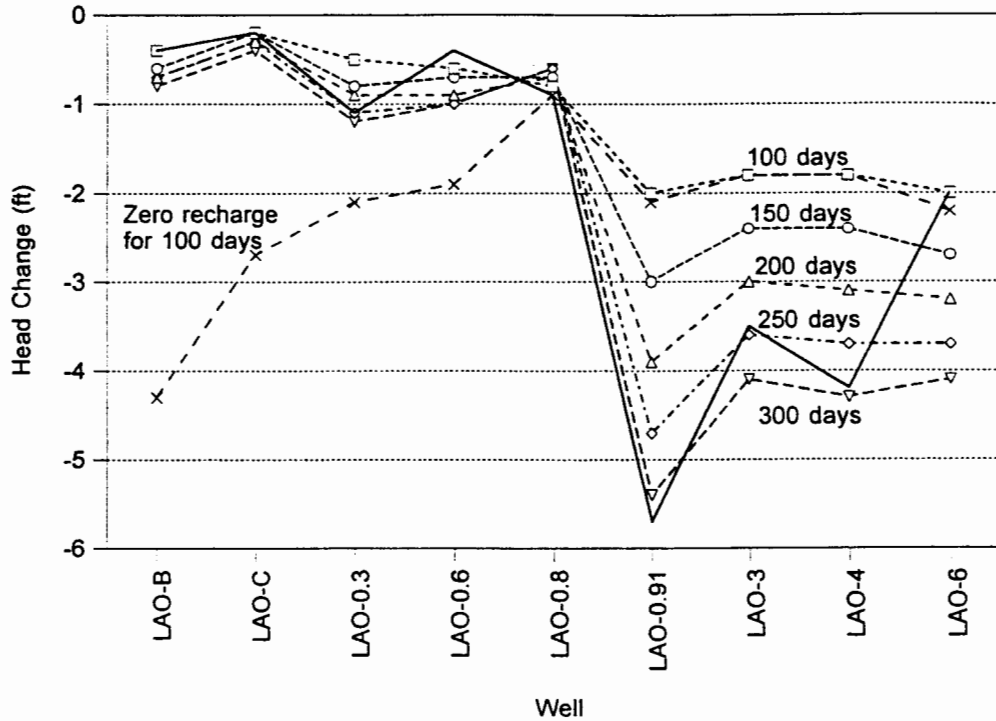
model to further dry out. These trial runs are also documented in Appendix P. The results of these models are shown in Figure 39 which again compares the varying head drop configurations with that desired to match the 7/10/94 head distribution.

The trial simulations were run for 100, 150, 200, 250, and 300 days. The 300-day simulation most closely approximated the desired head drops, but failed to maintain a high enough saturation level in LAO-6. This could be at least partly due to the fact that no data for LAO-6 were available for the 4/28/95 date to which the steady-state model was calibrated, and thus the lower part of the model was largely uncontrolled in the calibration. These trials also suggested a problem with the lower portion of the model in that intuitively, it should not have taken as long as 300 days to drain the system from its steady-state conditions to the head distribution observed at 7/10/94. Thus, as was indicated with the steady-state attempts, the model did not appear to permit sufficient infiltration seepage in the lower part of the system.

It was finally decided that the best way to produce a model with the desired head configuration was to simply recalibrate the steady-state model as was done previously by varying drain conductance values until the model matched the 7/10/94 head distribution. This was done with a separate model however (designated model AL1296T0), which only provided the first initial head distribution for the transient simulations. The transient models employed the same drain conductance configuration as that for the steady-state simulation (ALUV1196) which was determined by calibration to the 4/28/95 well data.

Transient Time Periods and Stresses

As previously described, the 480-day time period for which well data were obtained was divided into 9 separate stress periods based on varying aquifer behaviors as determined from the LAO-3 hydrograph (Figure 16). The varying annual recharge and ET rates determined from the hydrologic budget analysis (see Table 5) were assigned to each of 9 separate transient models designated as AL1296T1-AL1296T9. The head



- Actual Head Change (from steady-state to 7/10/94 obs. ft)
- - x - - AL1296T0 Head Change (Calc. - Initial ft) Run 120396a
Zero recharge; Time = 100 days.
ET: 34.0 in/yr cols. 1-35; 20.0 in/yr cols 36-200.
- - □ - - AL1296T0 Head Change (Calc. - Initial ft) Run 121296a
Recharge: 44.0 in/yr cols 1-35; 23.0 in/yr cols.36-61; 15.0 in/yr
cols. 62-75; 0 in/yr cols. 76-200.
ET: 34.0 in/yr cols. 1-35; 20.0 in/yr cols 36-200. Time = 100 days.
- - ○ - - AL1296T0 Head Change (Calc. - Initial ft) Run 121296b
Recharge & ET as above; Time = 150 days.
- - △ - - AL1296T0 Head Change (Calc. - Initial ft) Run 121296c
Recharge & ET as above; Time = 200 days.
- - ◇ - - AL1296T0 Head Change (Calc. - Initial ft) Run 121296d
Recharge & ET as above; Time = 250 days.
- - ▽ - - AL1296T0 Head Change (Calc. - Initial ft) Run 121296e
Recharge & ET as above; Time = 300 days.

Figure 39: Model AL1296T0 (Transient Results)

Calculated head change at varying run times vs actual change from model ALUV1196 steady-state conditions to water levels observed at 7/10/94 (initial conditions for transient models).

configuration from model AL1296T0 was used for the initial heads for the period 1 simulation, then the final head distribution from that simulation was used as the initial heads for the period 2 simulation, and so on.

The lengths of the separate stress periods varied significantly, from a minimum of 4 days for period 2 to a maximum of 138 days for period 6. MODFLOW distinguishes between stress periods, in which all the model stresses and boundary conditions on the system are constant, and time steps, which are the stress period increments at which head values are calculated. The user specifies the number of time steps desired and a time step multiplier which defines the ratio of the length of each time step to that of the preceding time step. This results in a geometric progression of lengthening head calculation intervals for each stress period. The transient simulations for this study utilized a time step multiplier of 1.2. The number of time steps specified for each stress period varied with the period lengths from a minimum of 10 to a maximum of 30.

Transient Simulation Results

The model calculated heads were determined at the cells representing the locations of each of the nine wells for which water level data were available for comparison. These data are presented in Appendices R, S, T, U, V, W, X, Y, and Z which contain the adjusted water level data (adjusted for model correlation) plus the model calculated heads and corresponding time intervals for the wells LAO-B, LAO-C, LAO-0.3, LAO-0.6, LAO-0.8, LAO-0.91, LAO-3, LAO-4, and LAO-6 respectively. These data are shown graphically in Figures 40-48 as plots of the measured water levels and modeled heads against time for each well.

These graphs give a qualitative comparison of the modeled head variations and measured water level data and indicate reasonably good fits for wells LAO-C, LAO-0.3, LAO-0.6, and LAO-0.8 with deviations of generally less than one foot throughout the entire simulated time. The plots for wells LAO-B, LAO-0.91, LAO-3, and LAO-4 show

LAO-B Water Level Elevation (feet above msl)

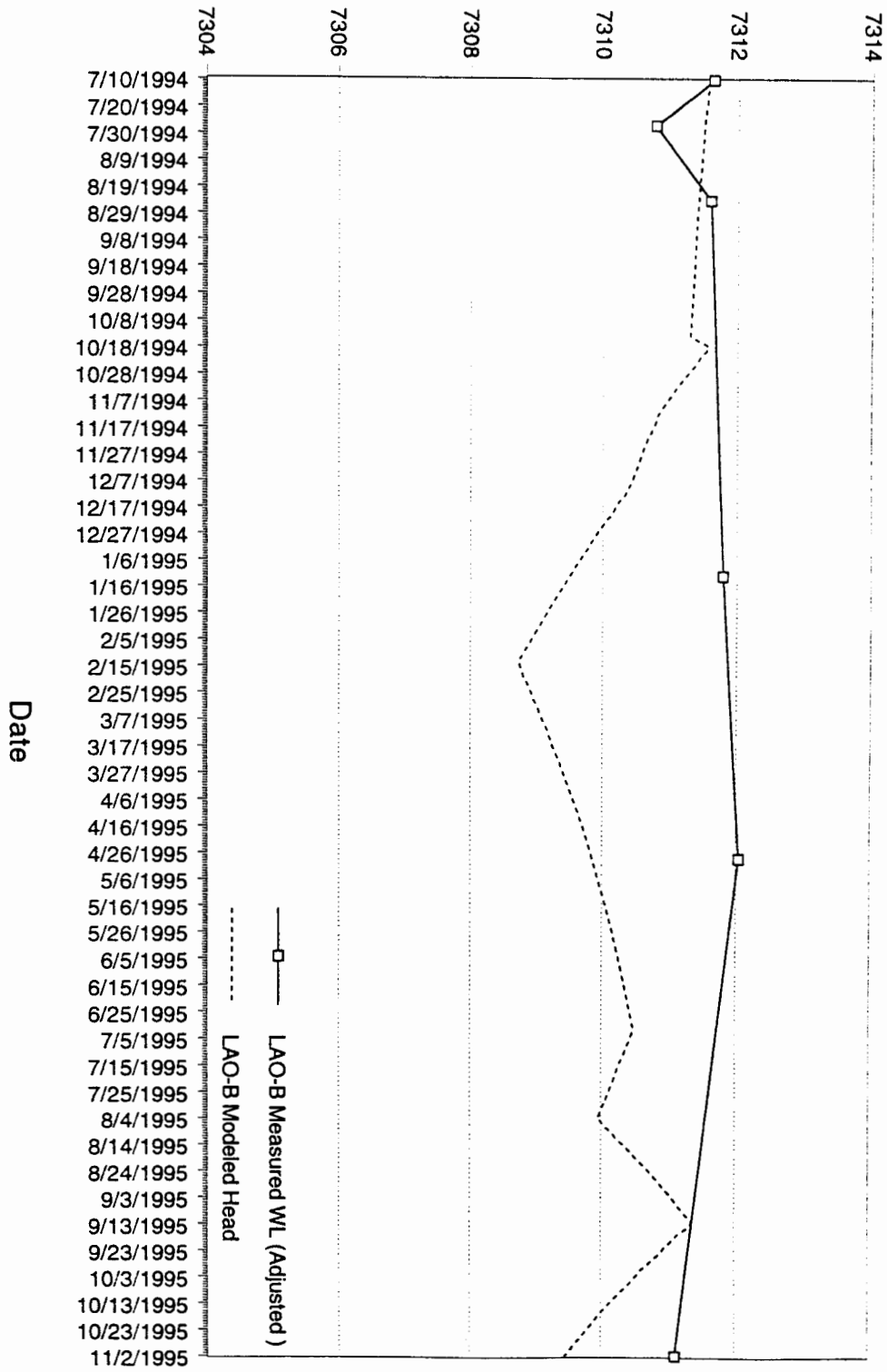


Figure 40: LAO-B Alluvial Aquifer Measured and Modeled Water Levels 7/10/94-11/2/95

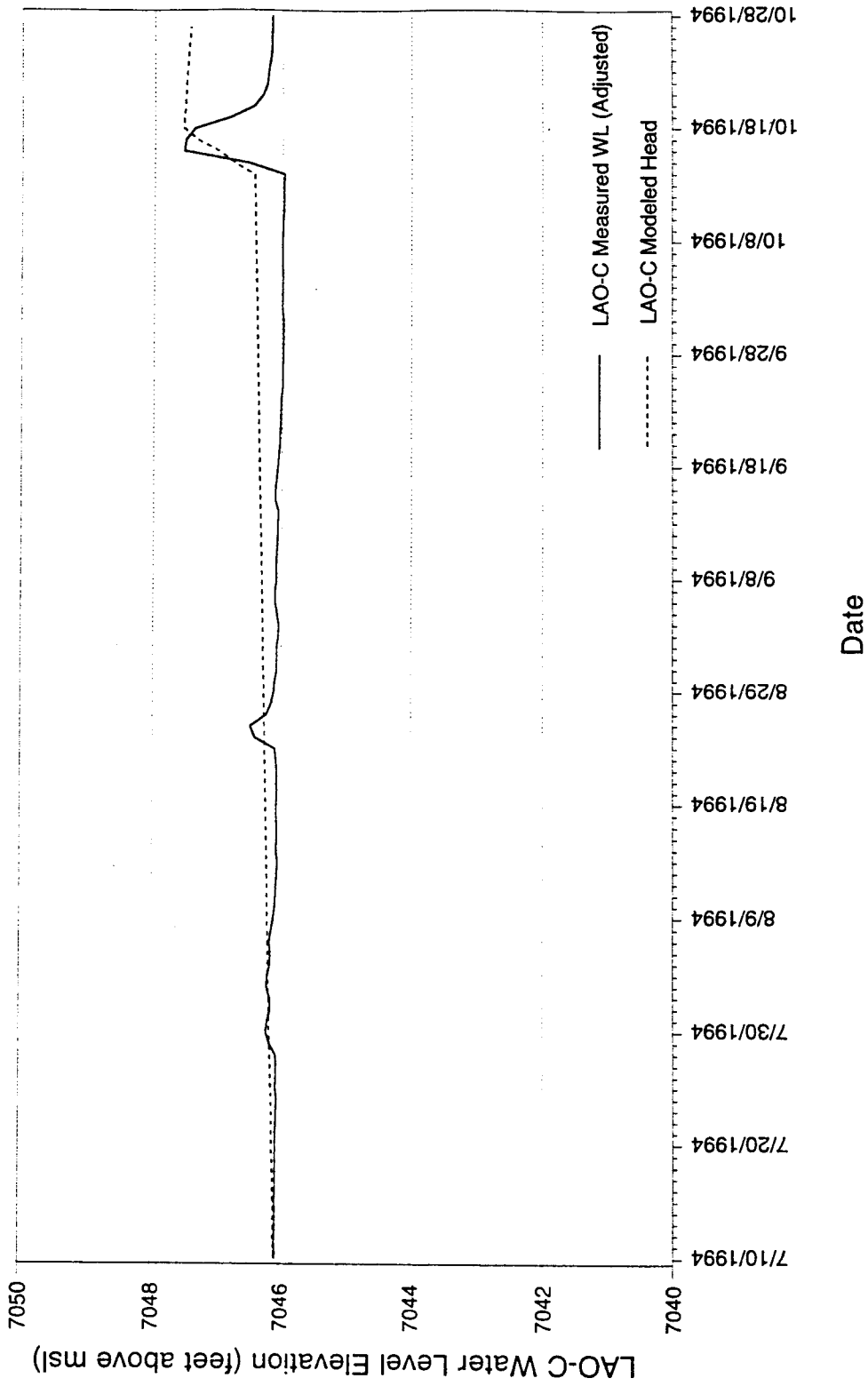


Figure 41: LAO-C Alluvial Aquifer Measured and Modeled Water Levels 7/10/94-10/28/94

LAO-0.3 Water Level Elevation (feet above msl)

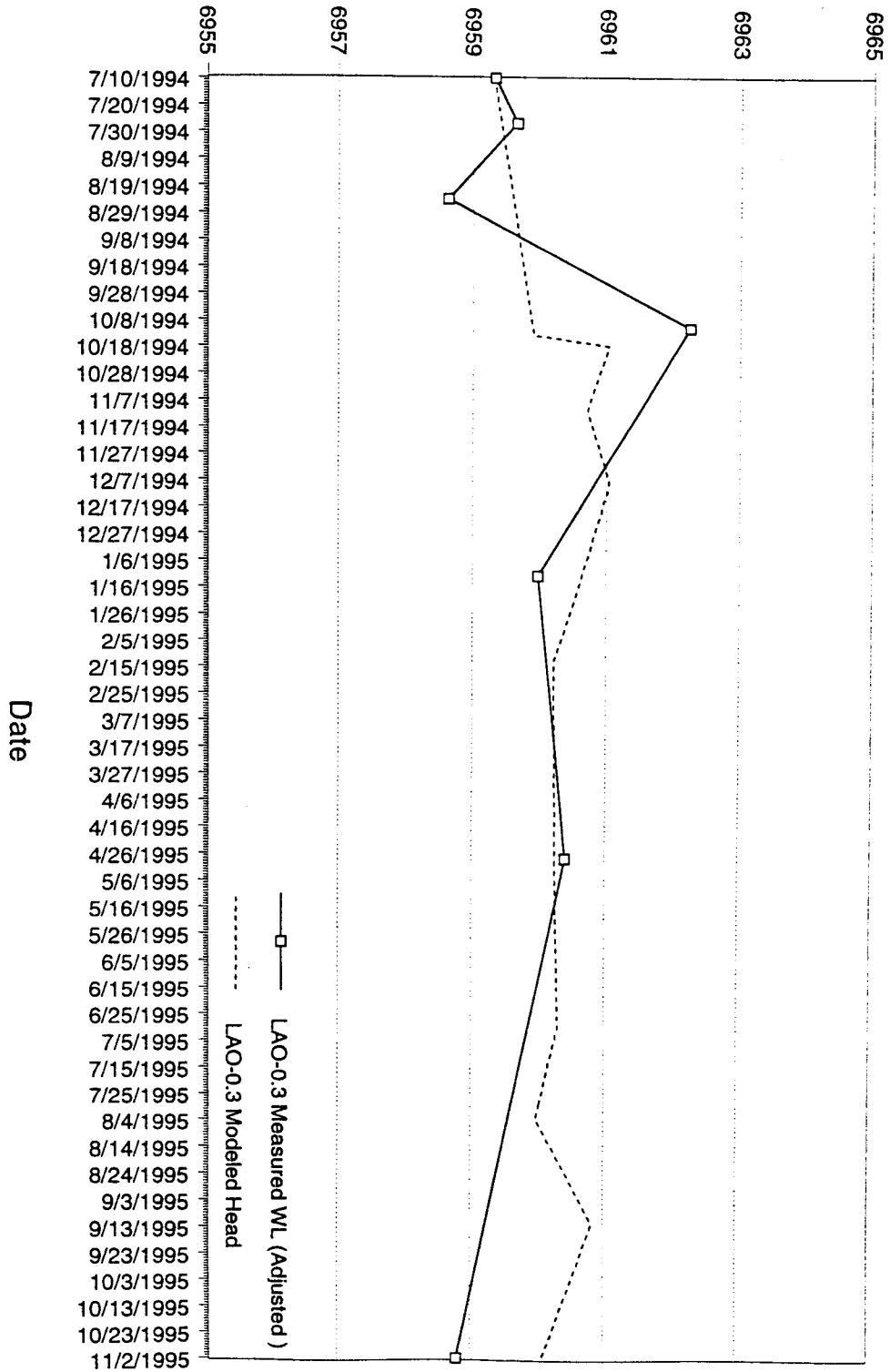


Figure 42: LAO-0.3 Alluvial Aquifer Measured and Modeled Water Levels 7/10/94-11/2/95

LAO-0.6 Water Level Elevation (feet above msl)

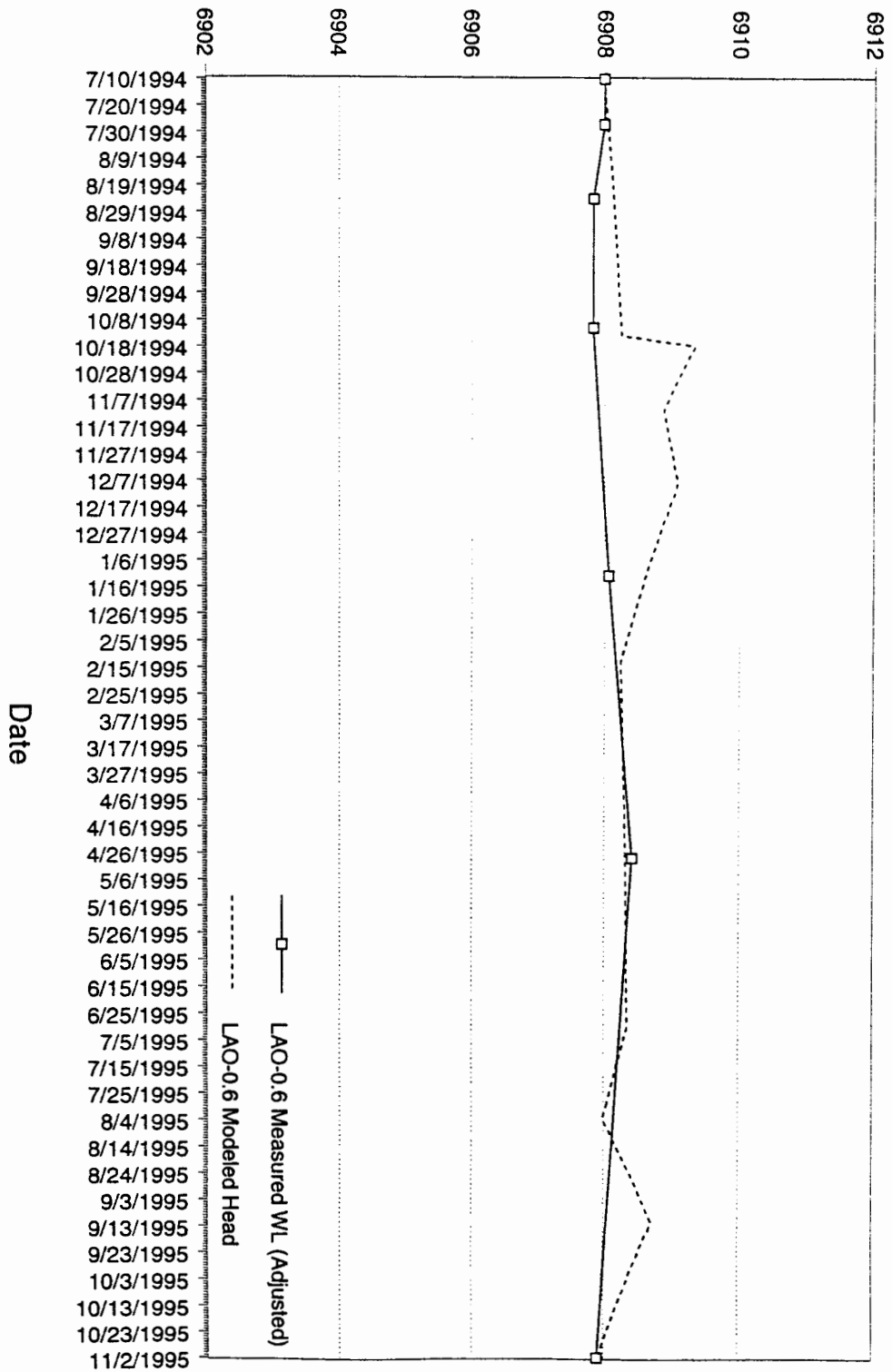
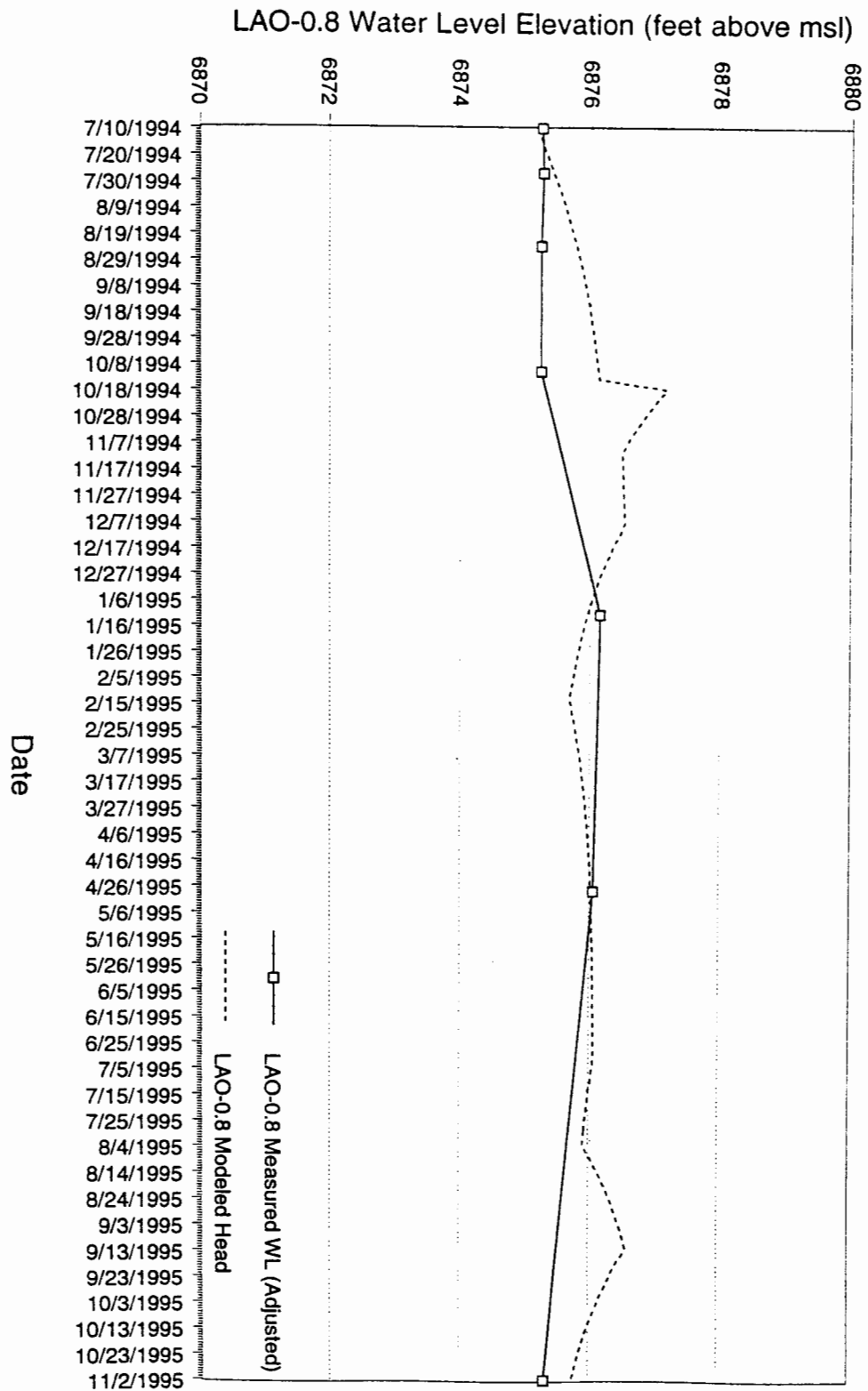


Figure 43: LAO-0.6 Alluvial Aquifer Measured and Modeled Water Levels 7/10/94-11/2/95

Figure 44: LAO-0.8 Alluvial Aquifer Measured and Modeled Water Levels 7/10/94-11/2/95



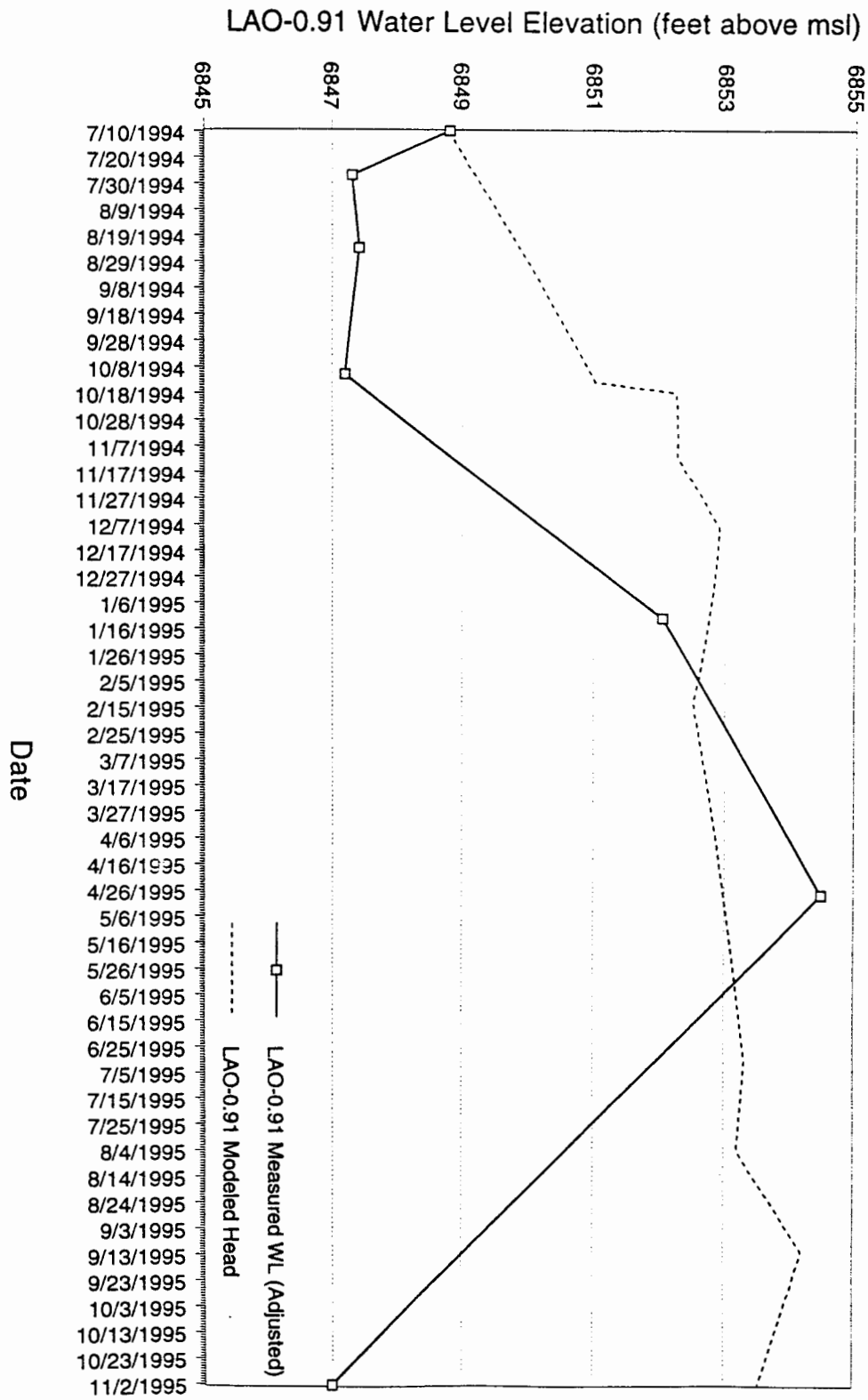


Figure 45: LAO-0.91 Alluvial Aquifer Measured and Modeled Water Levels 7/10/94-11/2/95

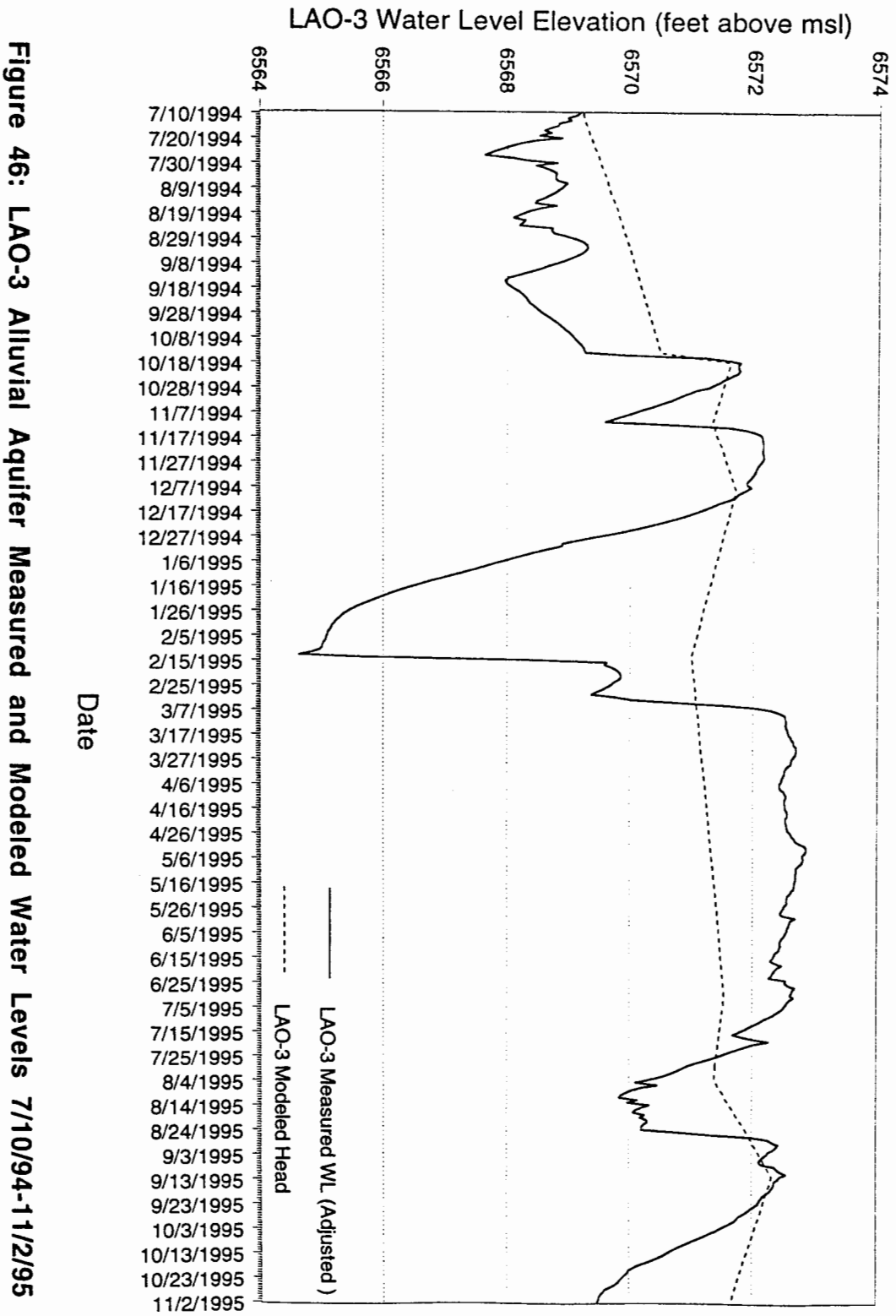


Figure 46: LAO-3 Alluvial Aquifer Measured and Modeled Water Levels 7/10/94-11/2/95

LAO-4 Water Level Elevation (feet above msl)

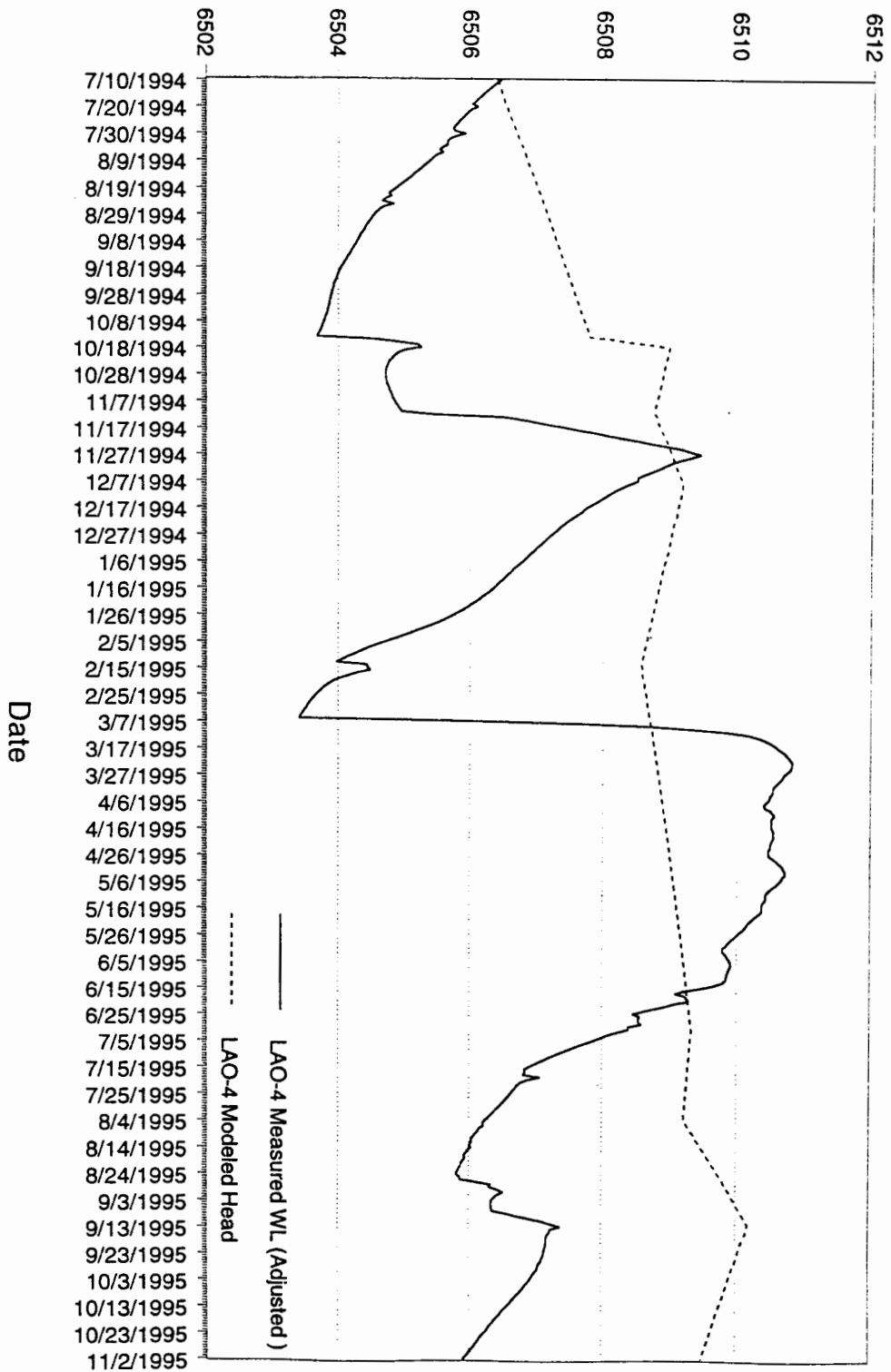


Figure 47: LAO-4 Alluvial Aquifer Measured and Modeled Water Levels 7/10/94-11/2/95

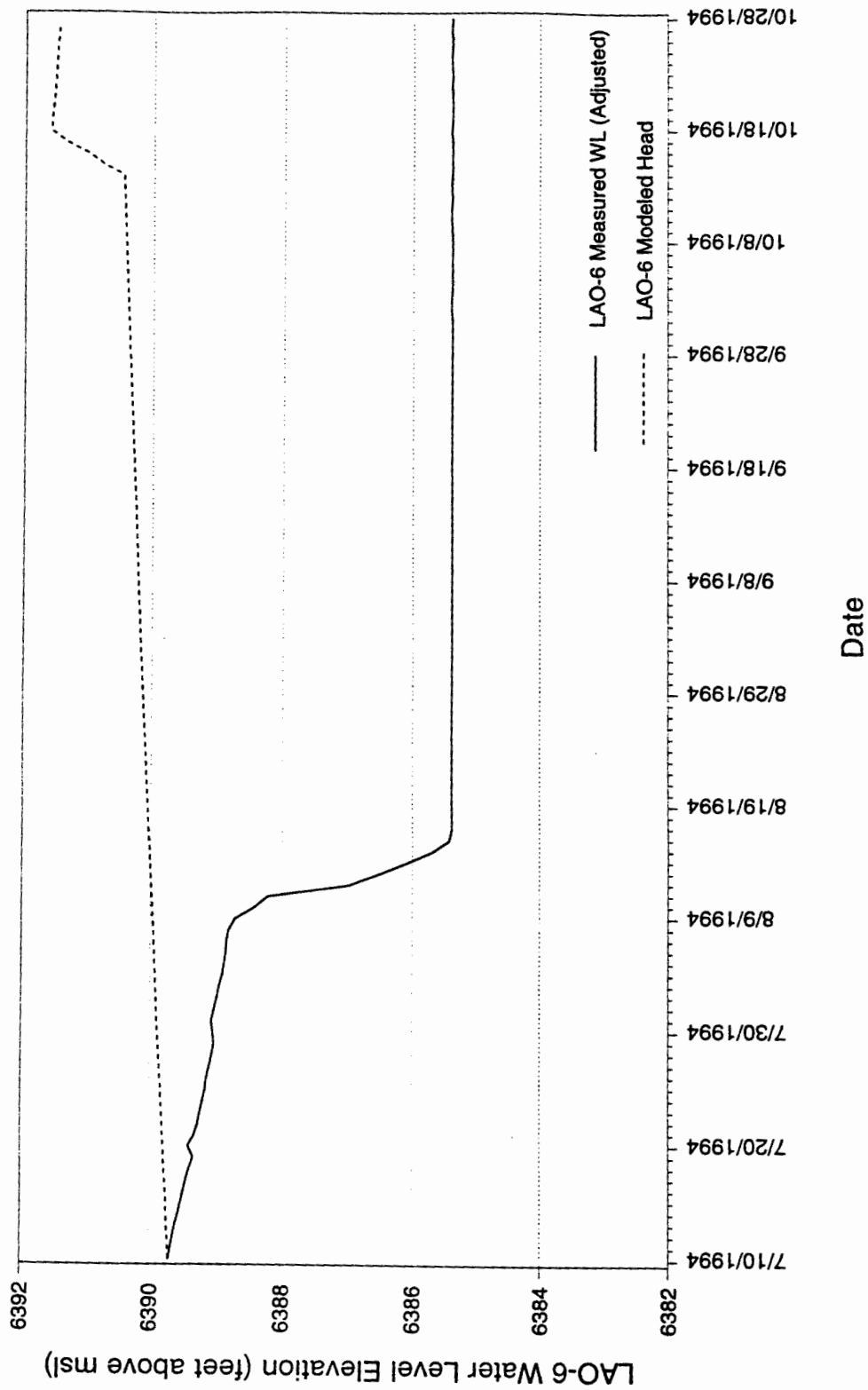


Figure 48: LAO-6 Alluvial Aquifer Measured and Modeled Water Levels 7/10/94-10/28/94

some periods of fairly reasonable correlation between the calculated heads and observed data, but also indicate periods with substantial deviation, while the graph for LAO-6 displays the poorest match. These results are in accord with the previous observations of model problems addressed above in adequately simulating sufficient drainage from the system in the lower portion of the model. A discussion of the comparison of the transient modeling results with the well data for each well follows.

LAO-B

In Figure 40, the observed water level data for well LAO-B consist of only 6 measurements, so there are significant gaps in the record where changes in the water level are undocumented. There is good agreement with the modeled heads at 7/10/94-10/18/94, encompassing periods 1 and 2. At 10/18/94-9/12/95 (periods 3-8) the modeled heads fall below the observed water levels by apparently as much as approximately 3 feet, though the differences on the two dates when water levels were actually measured during this interval are on the order of about 2 feet. At the beginning of period 9, the modeled head appears to coincide with the measured water level plot, but this is only extrapolated from the measurements taken at 4/28/95 and 11/15/95 (assumed level for the end of period 9). The measured data indicate a greater degree of stability in water levels for this well than the model simulated, suggesting that either infiltration seepage in this zone of the model is too high, or that the recharge rate is underestimated. Since previous interpretations suggest that baseflow recharge is a significant source in the upper canyon area, it is felt that the latter case is most likely.

LAO-C

In Figure 41, the well record for LAO-C is limited to the 110 day period from 7/10/94 to 10/28/94, encompassing periods 1 and 2 and a small portion of period 3, so model results were only evaluated for this time interval. As is seen, the modeled heads

show very good agreement with the well data through most of the analyzed period, including the steep water level rise during the 10/14/94-10/18/94 period which was a response to the significant precipitation event that occurred then, and which defined the limits for period 2. However, the short data set for period 3 shows a deficiency in the modeled head responses in that the model was unable to simulate the abrupt recession which immediately followed the short recharge event.

This is thought to be at least partly due to the determination of most of the stress periods as intervals which are too long, resulting in too much averaging of the recharge and ET stresses, and thus inhibiting the ability of the model to accurately reproduce aquifer recession responses with the necessary resolution. Indeed, the length of period 2 was only 4 days, representing by far the shortest defined stress period, and during which the model generally produced the best simulation match to the well data for all of the instrumented wells. The effective annual equivalent precipitation rate during this period for the middle/upper canyon area was over 284 inches/year! Thus, it appears that the model responded most accurately when the most severe stresses were most closely defined.

LAO-0.3

In Figure 42, the observed water level data for well LAO-0.3 consist of only 7 measurements, so as with the LAO-B data, there are significant gaps in the record where changes in the water level are undocumented. There is good agreement with the modeled heads at 7/10/94-7/27/94, encompassing the first part of period 1. At 7/27/94-8/24/94 (through about the middle of period 1), the measured data indicate a water level drop of approximately one foot whereas the model showed a continuous head rise. At 8/24/94-10/11/94 near the end of period 1, the measured data indicate a water level rise of over 3 feet giving a discrepancy with the modeled head of about 2 feet. The model's response to the increased recharge in period 2 shortly thereafter decreased the difference to about one foot, however. Following period 2, the next water level measurement was not until about

the middle of period 5 when declines in both the measured data and the modeled heads resulted in a difference of less than one foot. The next measurement in the middle of period 6 shows excellent agreement with the model, with a discrepancy of only 0.15 foot. Following this, the final measurement taken at 11/15/95 indicates a divergence from the modeled head of about one foot. Thus overall, the modeled head responses provided a reasonable to excellent fit with the observed data, and the few deviations which did occur were not very large.

LAO-0.6

In Figure 43, the water level observations for LAO-0.6 consist of the same 7 dates as for LAO-0.3, and thus there are substantial gaps in the record. It can be seen that the modeled head variations generally produced an excellent fit with the measured data throughout the entire modeled period. The most significant apparent deviations occurred at times between well observations and thus, the simulated aquifer responses cannot be confirmed by the well data. The greatest differences were for the periods 10/14/94-2/13/95 (stress periods 2-5) and 8/4/95-11/2/95 (stress periods 8-9), with the largest apparent deviations only slightly exceeding one foot, but with actual deviations of less than one-half foot when determined at the actual control points.

LAO-0.8

In Figure 44, the water level observations for LAO-0.8 were made on the same 7 dates as for LAO-0.3 and LAO-0.6, so there are again substantial gaps in the record. The well data pattern of minor water level fluctuations is highly similar to that for LAO-0.6, as is the pattern of head variations determined by the model. The modeled head variations again produced a generally excellent fit with the measured data throughout most of the modeled period, with the most significant apparent deviations occurring at times between well observations. Except for the interval 7/10/94-10/14/94 (stress period 1), the

deviations never exceeded one-half foot. During period 1, the model calculated heads showed a steady rise, while the measured water levels were relatively constant, but the maximum discrepancy was only about 0.9 foot.

LAO-0.91

In Figure 45, the modeled head results show what appears at first glance to be a fairly poor match with the observed well data. However, the magnitude of the total rise in head from the beginning of the simulation to the 4/28/95 measurement date in the middle of stress period 6 (approximately 6.5 feet) was reasonably well approximated. The next measurement date was not until 11/29/95 (assumed datum for the end of period 9), which was nearly a month later than the end of the simulation at 11/2/95. During the interval between measurements, nearly 8 feet of head loss occurred, and even though the comparison between the final simulation date and the observation date is somewhat tenuous, the simulated head loss trend at the end of the modeled time is clearly not steep enough to approach the final observed water level within the required time frame.

LAO-3

In Figure 46, the plot of measured well data represents one of the only two wells in the canyon for which daily water levels were available through the entire 480-day simulation period, and these data provided the basis for determining the divisions of the stress periods used in the transient modeling. As such, comparison of these data with the simulated head variations was expected to show a high degree of similarity. Inspection of the plot of modeled heads shows that this is partly the case, at least with respect to the timing of the major shifts between climbing heads and recessions. However, except during periods 1 and 2, the level of agreement with respect to the magnitude of head variations is weak, especially with respect to the recessionary periods.

At 7/10/94-10/14/94 (period 1), the model calculated heads show a steady rise of about one foot while the well data fluctuated within a range of about one foot. At 10/14/94-10/18/94 (period 2), the recorded sharp rise in the water level was simulated by the model as well, though not by enough magnitude. However, the combined modeled head increases from both periods 1 and 2 almost completely matched the 2.51 feet increase recorded in period 2, only falling short by 0.15 foot. This indicates that the average stresses applied to the model during the combined interval did cause the model to respond accurately on an average basis with regard to the initial head increase.

However, the rapid recessions of 2.19 feet recorded at 10/18/94-11/11/94 (period 3) and 7.26 feet at 12/8/94-2/13/95 (period 5) were poorly reproduced by the model which calculated head drops of only 0.29 and 0.71 foot respectively during these intervals. Whereas the period 5 recession was due to the winter freeze-up of the system, the drop in period 3 was caused by drought conditions. Period 3 was only 24 days long and was the second shortest stress period in the model after period 2. As such, the applied stresses were among the most closely defined in the transient simulations. The rates for precipitation and ET determined in the hydrologic budget analysis for this period reflected the dry conditions which caused the recession, with combined precipitation and ET resulting in negative effective annual equivalent surface infiltration rates of -42.23 inches/year in the upper basin and -6.31 inches/year in the middle/upper canyon areas. With essentially negative recharge rates applied to the model, it clearly was unable to effectively simulate the rapid head drops. This suggests that the simulated infiltration rates from the system are too low, and thus the modeled system does not drain rapidly enough.

It is instructive to note that the modeled heads did eventually closely match the measured level on 9/12/95 at the end of period 8. This again indicates that the averaged stresses over combined periods in the simulation did generate the correct magnitude of head rise in the model, but only over the length of most of the simulation. However, the model was clearly deficient in simulating the intervening dynamic recessions.

LAO-4

In Figure 47, the degree of correlation between modeled head variations and the daily water level data from LAO-4 is generally similar to that observed in LAO-3, with the main exception being that the major aquifer responses to recharge generally showed a time lag of a few days from the water level behavior observed in LAO-3. During period 1, the well data showed a recession of slightly over 2 feet while the modeled heads rose by just under 2 feet. The well response in period 2 is muted relative to the response observed in LAO-3, and both the well data and modeled heads rose by about one foot. Both profiles show a slight recession in period 3, while in period 4, the measured water levels finally rose in a lagged response to the high period 2 recharge, and the measured and modeled water levels nearly coincide. Following this, the pattern is similar to LAO-3 in that the model failed to simulate the magnitude of the winter recession in period 5, and was deficient in producing the abrupt ~7 foot water level rise in period 6 which lagged the LAO-3 response by several days. The well data show a steep recession of ~4 feet in period 7 during which the model showed a head loss of only 0.11 feet. Both profiles then show about a one foot rise in period 8 followed by about a one foot drop in the well data but only about a half foot drop in the modeled heads in period 9. At the end of the simulation, the modeled head exceeded the measured water level by about 3.5 feet. Thus, the model was again most deficient in simulating the dynamic water level recessions, and with the exception of the match in period 4, performed even more poorly than for LAO-3 in producing the correct magnitude of overall head rise throughout the simulation period.

LAO-6

Figure 48 shows the last of the available daily water level data which were from LAO-6 and which covered the same limited 110-day interval at the beginning of the total simulation period as did the LAO-C data. This well is located farthest downgradient in the system and as is seen, exhibited the poorest correlation to the model results of any of the

data analyzed. The model shows a rise in head of about a half foot in period 1, followed by about a 1.5 foot rise in period 2 and a slight drop in the early part of period 3. However, from the beginning of period 1, the well data showed a decline of about one foot through about 8/9/94, followed by a steep drop of nearly 4 feet which occurred within a period of 7 days, after which the well was dry for the remainder of the record. Thus the model failed to simulate the observed water level behavior for this part of the system with any reasonable accuracy. This is likely due to some of the same reasons as noted previously, such as the deficiency in producing dynamic recession responses which is probably a result of underestimated infiltration losses from the system. Also, the fact that no data from this well were available for the calibration of the steady-state model left the lower part of the model largely uncontrolled.

Transient Error Analysis

An initial analysis of the model errors was performed by determining the differences between the observed heads and the model calculated heads for the corresponding well control points at the end of each stress period. The total mean errors, mean absolute errors, and root mean squared errors were then calculated for each period's results. The calculated and observed heads were also converted to saturated thicknesses for relative comparison. These calculations are detailed in Appendix AA.

The mean errors are simple arithmetic averages of the errors determined at each well for which data were available in each stress period. These figures can be somewhat misleading however, since combining positive and negative head differences can cancel each other out, yielding a low mean error which does not truly represent the degree of the model's deviation from the observed data. The mean absolute errors are determined as the average of the absolute values of the errors from each well. These numbers are more representative of the magnitude of total average model error for each transient simulation. The root mean squared (RMS) errors are determined as the square root of the average of

the squared errors from each well. This statistic is similar to the standard error and accentuates the larger magnitude errors while minimizing the contributions of smaller errors from each well.

The observed saturated thicknesses were plotted against the model calculated saturated thicknesses at the end of each stress period. These plots are included as Figures 49-57 which show the data points' deviation from a straight line correspondence and also summarize the results of the mean error calculations. They are useful as a visual conveyance of the degree of accuracy of the model calculated heads at the end of each stress period, while the mean error results quantify the degree of correlation. Data points that lie above the line indicate that the observed saturation levels exceeded the calculated heads, and the points which plot below the line show that the observed levels fell below the calculated heads, while the vertical (or horizontal) distances from the points to the line indicate the degree of discrepancy.

Inspection of these plots confirms the trends that were qualitatively observed in the calculated and observed water level graphs (Figures 40-48), mainly being that the best correlations of model results with the well data were most consistently at wells LAO-0.3, LAO-0.6, LAO-0.8, and LAO-C (where available), while there were occasionally good matches for LAO-B (at the end of period 6), LAO-0.91 (at the ends of periods 5 and 6), LAO-3 (at the ends of periods 1, 2, 4, 6, and 8), and LAO-4 (at the ends of periods 4 and 6). Mean errors ranged from a low of -0.44 feet for period 6 to a high of 3.12 feet for period 3, which also had the highest mean absolute error and root mean squared error (3.12 feet and 3.64 feet respectively). The lowest mean absolute error was 0.48 feet at the end of period 4, but the only data available for that time were from LAO-3 and LAO-4. The best overall correlation was seen at the end of period 6 with a mean absolute error of 0.72 feet.

The preceding analysis evaluated only the errors determined for the final head distributions from each stress period. As such, it was indicative of model performance at

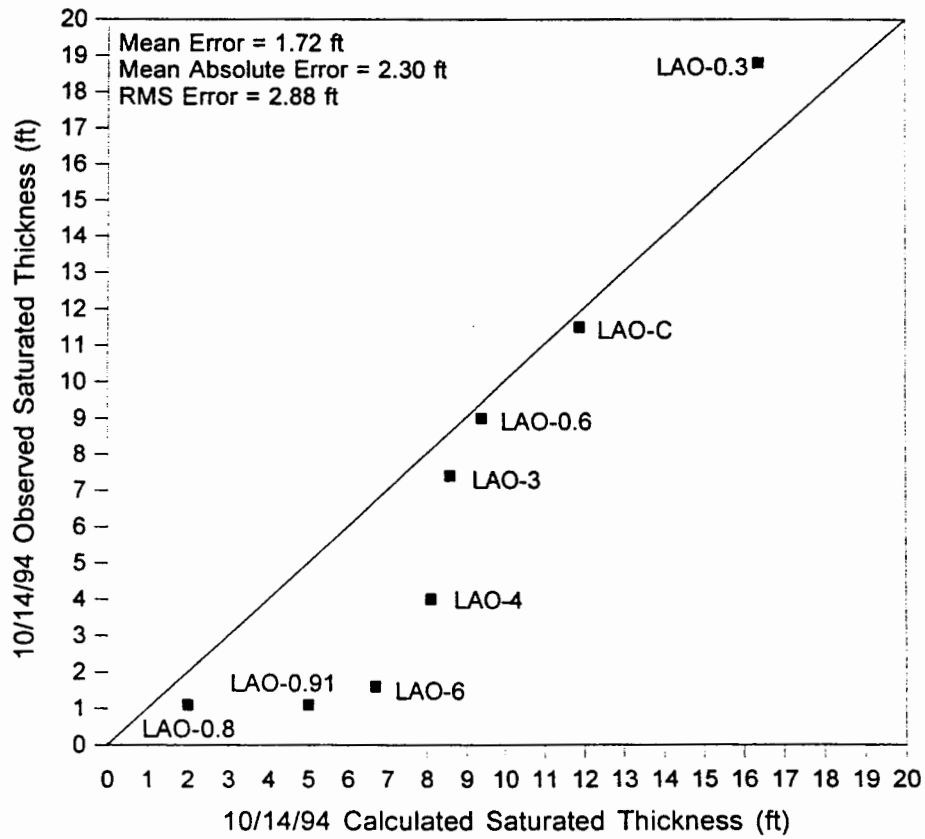


Figure 49: Model AL1296T1 (Transient) Observed vs Calculated Saturated Thickness at 10/14/94 (End Period 1)

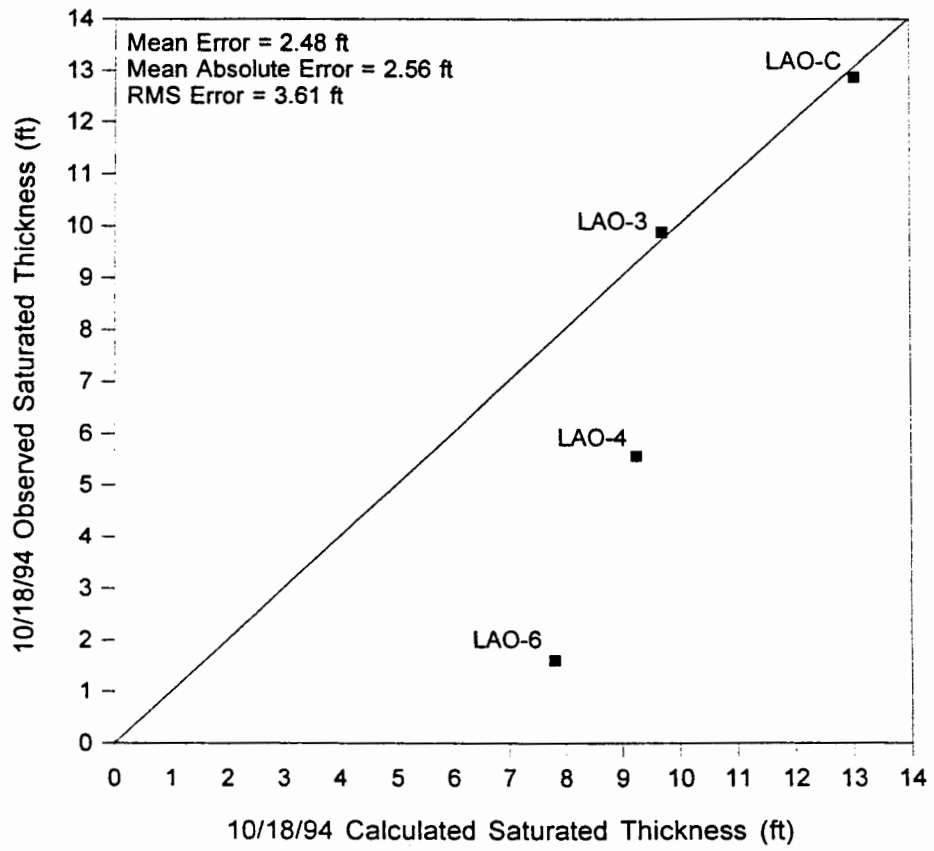


Figure 50: Model AL1296T2 (Transient) Observed vs Calculated Saturated Thickness at 10/18/94 (End Period 2)

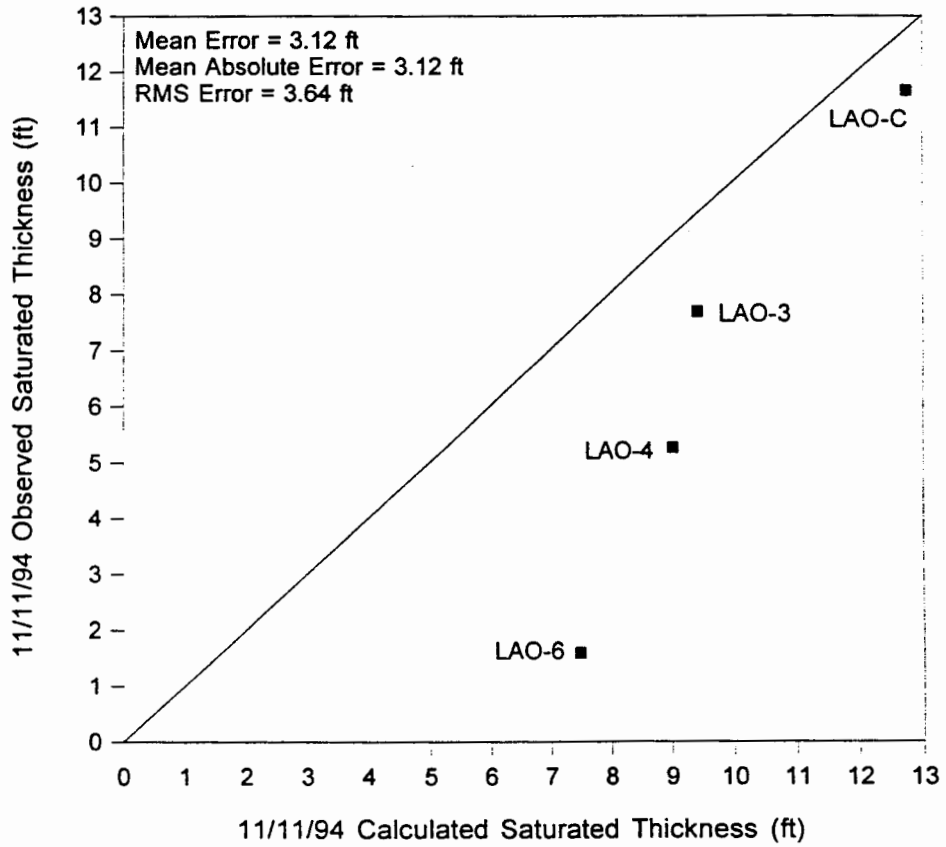


Figure 51: Model AL1296T3 (Transient) Observed vs Calculated Saturated Thickness at 11/11/94 (End Period 3)

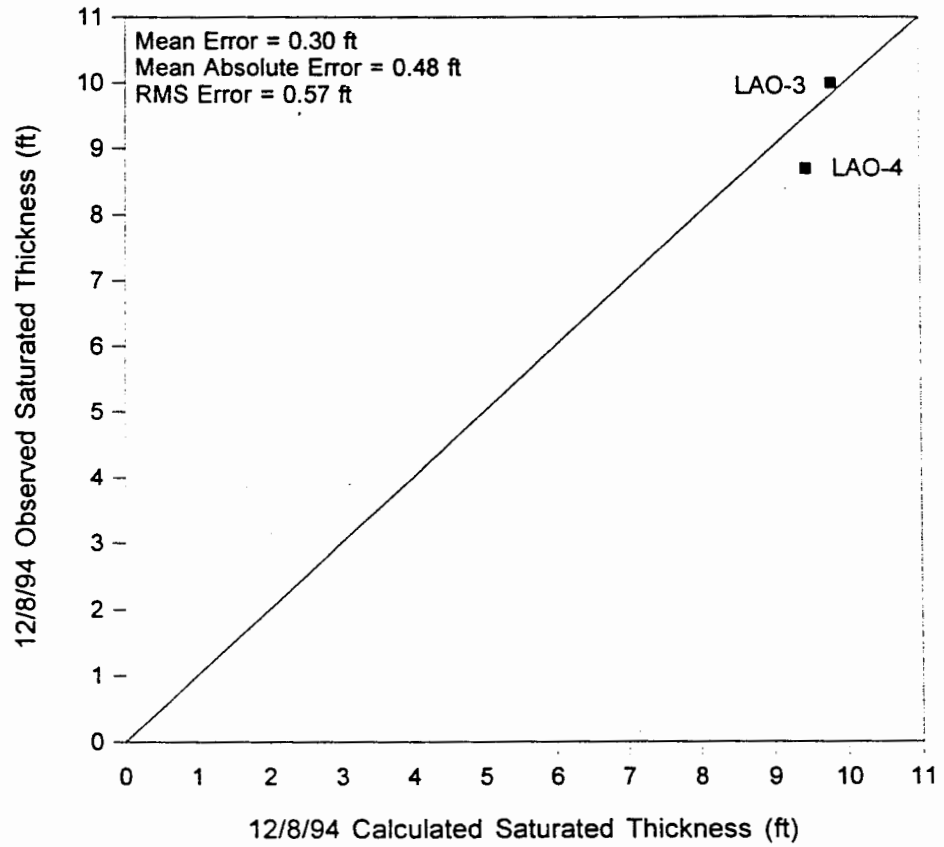


Figure 52: Model AL1296T4 (Transient) Observed vs Calculated Saturated Thickness at 12/8/94 (End Period 4)

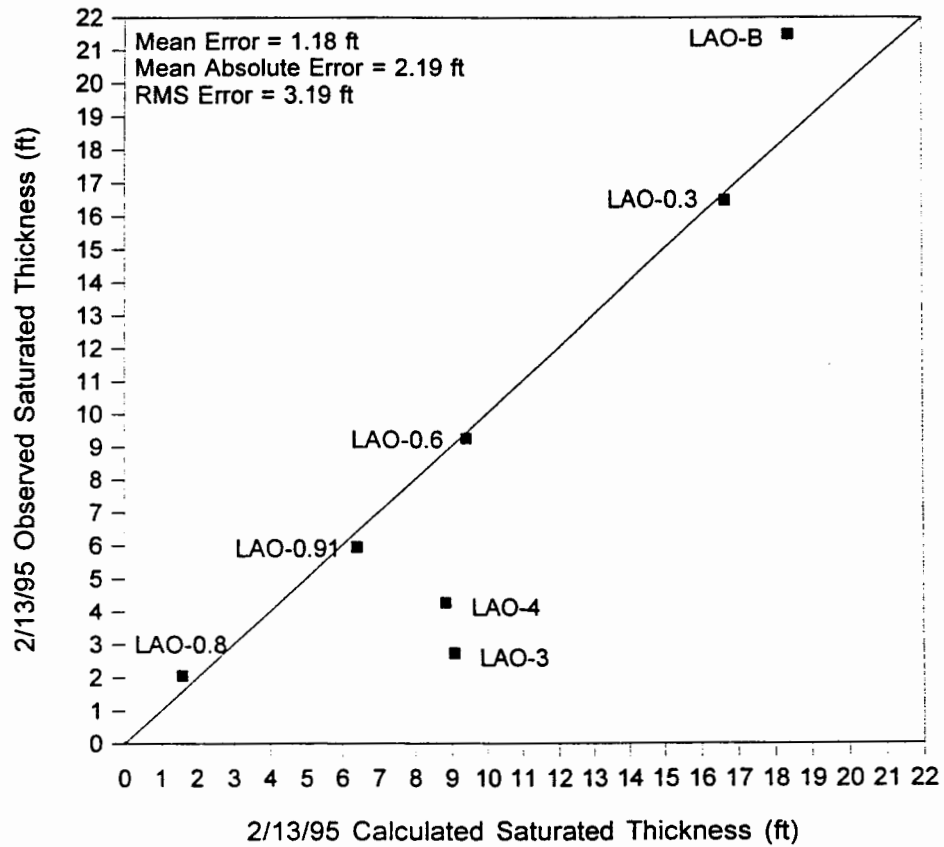


Figure 53: Model AL1296T5 (Transient) Observed vs Calculated Saturated Thickness at 2/13/95 (End Period 5)

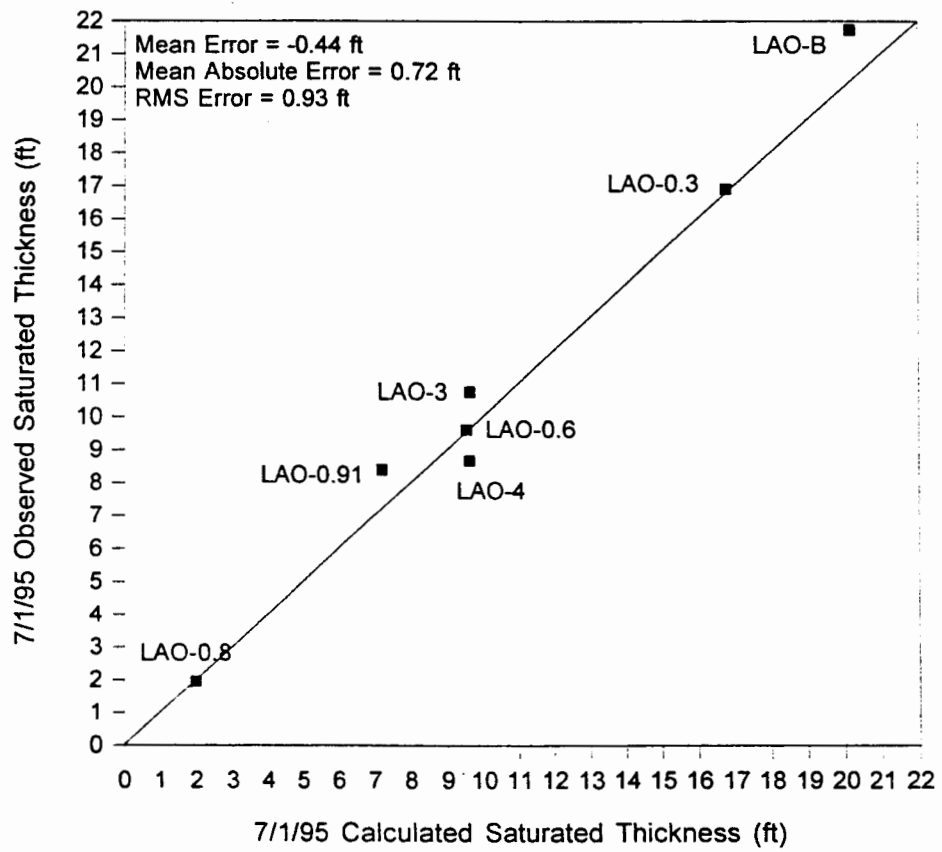


Figure 54: Model AL1296T6 (Transient) Observed vs Calculated Saturated Thickness at 7/1/95 (End Period 6)

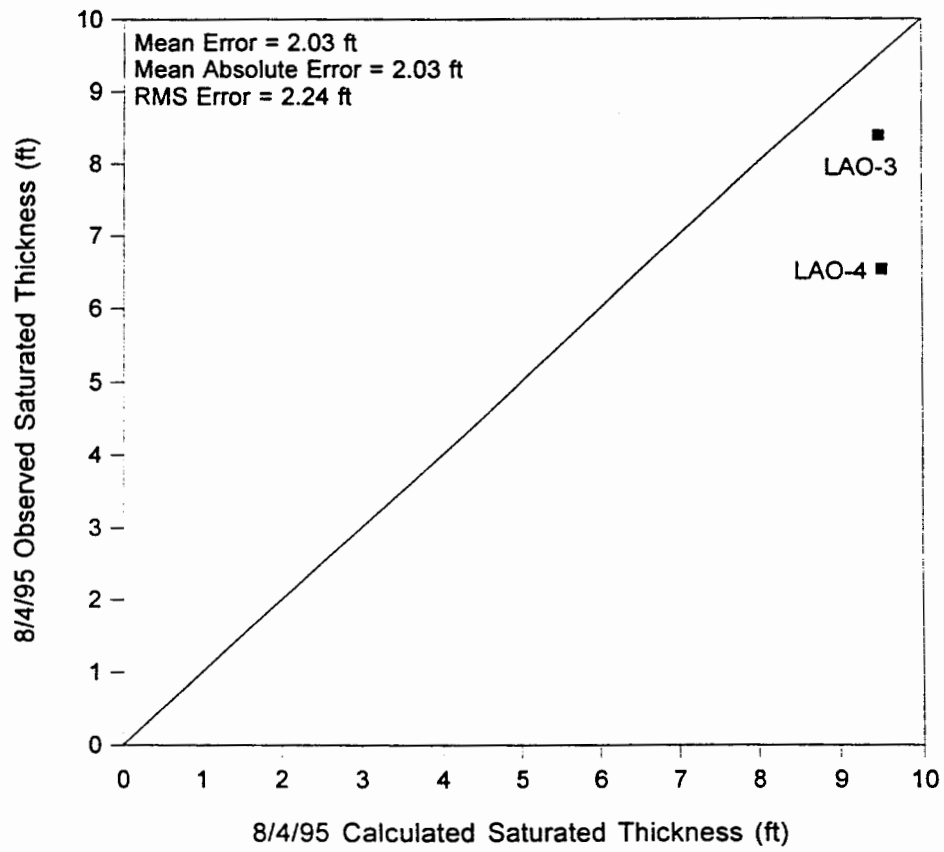


Figure 55: Model AL1296T7 (Transient) Observed vs Calculated Saturated Thickness at 8/4/95 (End Period 7)

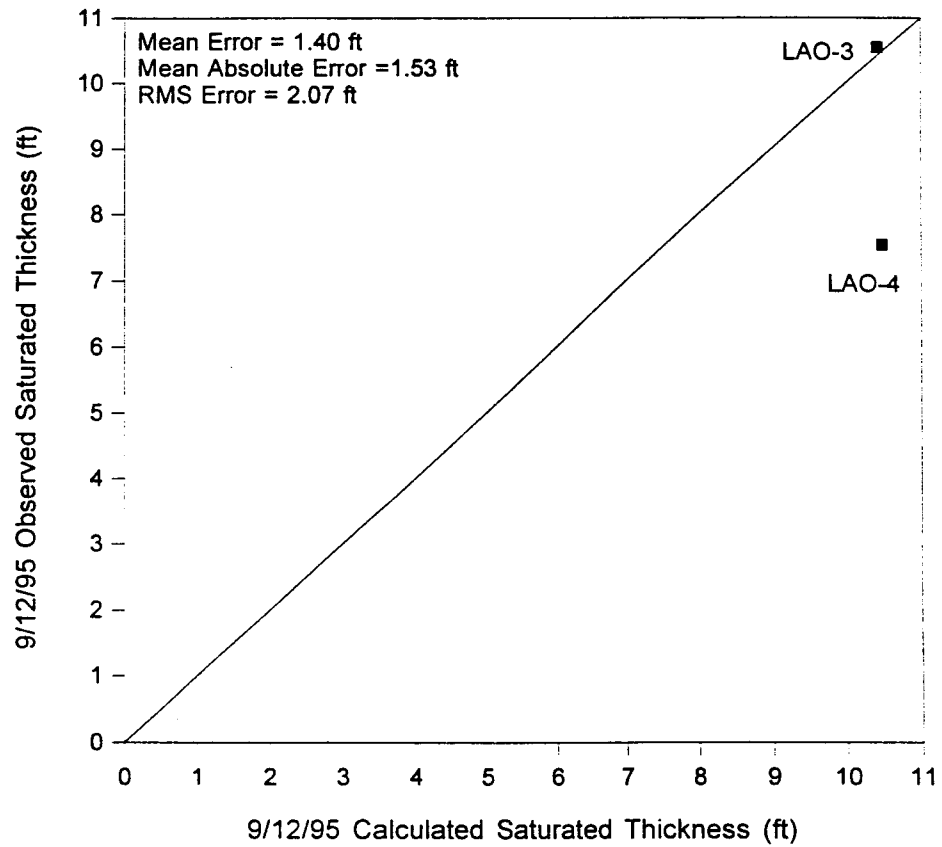


Figure 56: Model AL1296T8 (Transient) Observed vs Calculated Saturated Thickness at 9/12/95 (End Period 8)

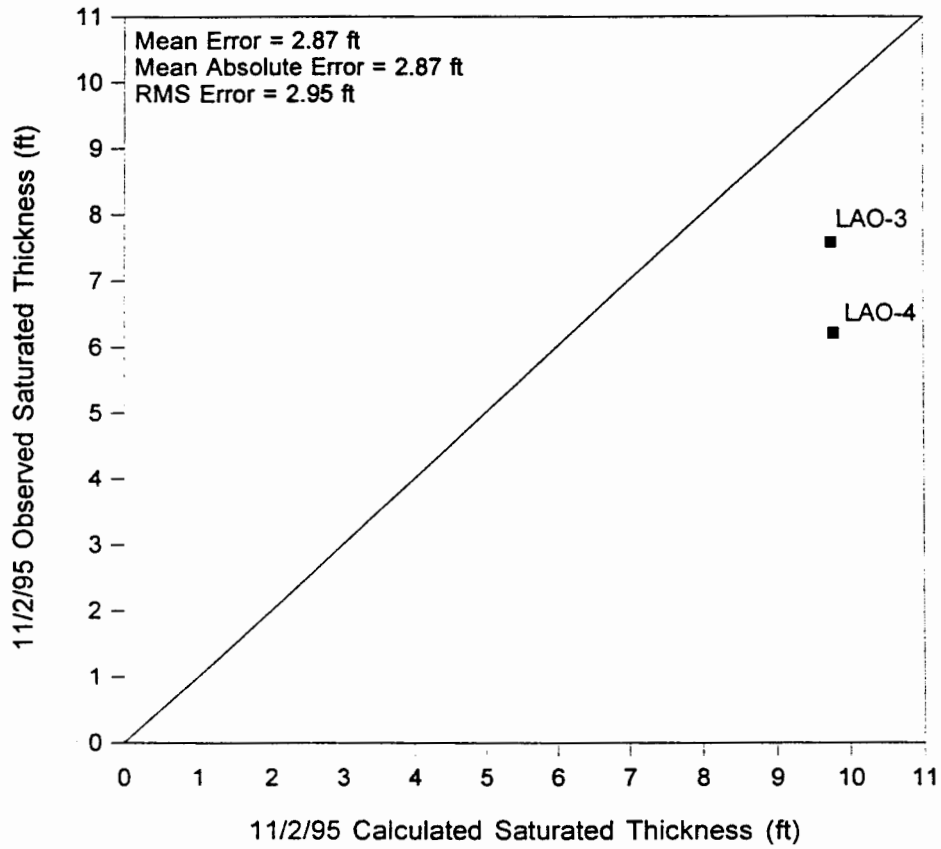


Figure 57: Model AL1296T9 (Transient) Observed vs Calculated Saturated Thickness at 11/2/95 (End Period 9)

only 9 discrete points in time. A more comprehensive error analysis was also conducted which gives a more complete picture of the level of overall model accuracy and specifies mean error variations for each well site incorporating all of the model calculated head data within each stress period. These calculations were performed in the calculated head vs. time results spreadsheets included as Appendices R-Z which include determinations of model errors (modeled head minus observed head) for each well at each model time interval, plus the calculation of mean errors, mean absolute errors, and root mean squared errors for each stress period and each well. In these calculations, the mean errors are the arithmetic averages of all the model errors in each stress period, while the mean absolute errors are determined as the average of the absolute values of all the model errors in each stress period, and the root mean squared errors are determined as the square root of the average of the squared errors in each stress period. The results of these calculations are summarized in Table 10.

This summary also includes the results of determinations of the RMS error to total head loss ratio, for which the calculations were also performed in the calculated head vs. time results spreadsheets (Appendices R-Z). This parameter is useful in evaluating the impact of the magnitudes of the average errors on the model's performance since if the ratio of the RMS error to the total head loss in the system is small, the errors are only a small part of the overall model response (Anderson and Woessner, 1992).

The magnitudes of the maximum head changes in the system at each well were also determined in the calculated head vs. time results spreadsheets (Appendices R-Z) by simply subtracting the minimum observed head from the maximum observed head in each wells' data. An areally weighted average total head loss for the system was then calculated, and this determination is shown in Table 11. For the 552 model cells which comprise the study area of interest west of State Road 4, the weighted average total head loss determined from the available well data was 4.75 feet. This number was then used for the RMS error to total head loss ratio determinations.

Table 10: Transient Models Mean Calculated Head Errors Summary

Well	Stress Period:	1	2	3	4	5	6	7	8	9	Totals
	From:	7/10/94	10/14/94	10/18/94	11/11/94	12/8/94	2/13/95	7/1/95	8/4/95	9/12/95	7/10/94
	To:	10/14/94	10/18/94	11/11/94	12/8/94	2/13/95	7/1/95	8/4/95	9/12/95	11/2/95	11/2/95
Well	No. of Days:	96	4	24	27	67	138	34	39	51	480
LAO-B	Mean Error (ft):	0.15				-2.36	-2.12			-1.66	-0.95
	Mean Abs. Error:	0.32				2.36	2.12			1.66	1.18
	RMS Error:	0.43				2.36	2.12			1.66	1.49
	RMS Error:Total Head Loss Ratio:	0.34				1.87	1.68			1.32	1.30
LAO-C	Mean Error (ft):	0.10	0.03	1.00							0.27
	Mean Abs. Error:	0.11	0.32	1.00							0.32
	RMS Error:	0.17	0.36	1.07							0.53
	RMS Error:Total Head Loss Ratio:	0.11	0.23	0.68							0.34
LAO-0.3	Mean Error (ft):	-0.40				0.62	-0.15			1.28	0.02
	Mean Abs. Error:	0.89				0.62	0.15			1.28	0.93
	RMS Error:	1.27				0.62	0.15			1.28	1.19
	RMS Error:Total Head Loss Ratio:	0.35				0.17	0.04			0.35	0.23
LAO-0.6	Mean Error (ft):	0.19				0.52	-0.10			0.01	0.17
	Mean Abs. Error:	0.19				0.52	0.10			0.01	0.23
	RMS Error:	0.26				0.52	0.10			0.01	0.30
	RMS Error:Total Head Loss Ratio:	0.43				0.86	0.17			0.01	0.37
LAO-0.8	Mean Error (ft):	0.39				-0.23	-0.03			0.43	0.25
	Mean Abs. Error:	0.42				0.23	0.03			0.43	0.39
	RMS Error:	0.53				0.23	0.03			0.43	0.48
	RMS Error:Total Head Loss Ratio:	0.58				0.25	0.03			0.47	0.33
LAO-0.91	Mean Error (ft):	2.05				0.69	-1.48			6.55	2.00
	Mean Abs. Error:	2.05				0.69	1.48			6.55	2.82
	RMS Error:	2.47				0.69	1.48			6.55	3.41
	RMS Error:Total Head Loss Ratio:	0.33				0.09	0.20			0.87	0.37
LAO-3	Mean Error (ft):	0.87	0.31	0.34	-0.21	1.90	0.55	-0.55	1.07	0.48	0.60
	Mean Abs. Error:	0.87	0.51	0.47	0.63	1.94	1.74	0.76	1.14	0.55	1.06
	RMS Error:	1.03	0.67	0.71	0.75	2.92	2.17	0.82	1.25	0.89	1.54
	RMS Error:Total Head Loss Ratio:	0.12	0.08	0.71	0.09	0.35	0.26	0.10	0.15	0.11	0.15
LAO-4	Mean Error (ft):	1.21	3.67	4.00	1.36	1.77	2.08	1.89	3.35	3.01	2.24
	Mean Abs. Error:	1.22	3.67	4.00	1.41	1.77	3.19	1.89	3.35	3.01	2.44
	RMS Error:	1.73	3.68	4.00	1.85	2.02	3.56	1.99	3.36	3.02	2.80
	RMS Error:Total Head Loss Ratio:	0.23	0.50	0.54	0.25	0.27	0.48	0.27	0.45	0.41	0.38
LAO-6	Mean Error (ft):	1.68	5.66	6.15							3.03
	Mean Abs. Error:	1.68	5.66	6.15							3.03
	RMS Error:	2.60	5.67	6.15							3.99
	RMS Error:Total Head Loss Ratio:	0.60	1.32	1.43							1.12
Totals	Mean Error (ft):	0.69	2.42	2.87	0.57	0.42	-0.18	0.67	2.21	1.44	0.85
	Mean Abs. Error:	0.86	2.54	2.91	1.02	1.16	1.26	1.32	2.24	1.93	1.38
	RMS Error:	1.16	2.60	2.98	1.30	1.34	1.37	1.40	2.31	1.98	1.75
	RMS Error:Total Head Loss Ratio:	0.34	0.53	0.84	0.17	0.55	0.41	0.18	0.30	0.51	0.51

Table 11: Maximum Observed Head Losses

Well	Area of Influence Columns	Area of Influence No. of Cells	Maximum Total Head Loss (ft) *	No. of Cells x Head Loss
LAO-B	1-40	96	1.26	120.96
LAO-C	41-60	42	1.57	65.94
LAO-0.3	61-69	28	3.62	101.36
LAO-0.6	70-75	15	0.60	9.00
LAO-0.8	76-78	11	0.92	10.12
LAO-0.91	79-100	67	7.51	503.17
LAO-3	101-125	104	8.23	855.92
LAO-4	126-135	46	7.42	341.32
LAO-6	136-160	143	4.31	616.33
			Weighted	
			Average Total	
	Area of Interest Total:	552	Head Loss (ft):	4.75
Outside Model				
Area of Interest	161-200	263		
	Model Total:	815		
* From observation period 7/10/94-11/2/95				

As is seen in Table 10, the inclusion of all of the transient model calculated head data in the error analysis showed the same trends as was seen in the period end results analysis, namely that model accuracy was best for the upper part of the system, and it became generally poorer downgradient from well LAO-0.91. These results also show that including the additional data in the mean error calculations generally determined slightly to substantially lower mean absolute errors for most of the stress periods than were determined by the period end results, with a few exceptions where the values increased from those initially determined.

For period 1, the mean absolute error (MAE) from the initial analysis was 2.30 feet, but totaled only 0.86 feet in the more comprehensive analysis. The period 2 MAE of 2.54 feet from the detailed analysis was virtually unchanged from the 2.56 feet initially determined. The period 3 MAE differed only slightly, from 3.12 feet in the initial analysis to 2.91 feet in the detailed analysis, while the MAE values for periods 5, 7, and 9 all showed significant decreases from the initial analysis: from 2.19 to 1.16 feet; from 2.03 to 1.32 feet; and from 2.87 to 1.93 feet respectively.

Only in periods 4, 6, and 8 did the comprehensive analysis result in higher MAE values than determined by the period end results: from 0.48 to 1.02 feet; from 0.72 to 1.26 feet; and from 1.53 to 2.24 feet respectively. It is interesting to note that with the exception of periods 1 and 2, these were the periods of active recharge interspersed between the bounding dry periods. Nevertheless, the more comprehensive error analysis results should give a better overall estimate of the model's accuracy in simulating the physical data.

Of particular interest in these results are the values determined for the RMS error to total head loss ratios for each well during each period. Thirty-one of the 44 total determinations of this parameter (70%) were less than 0.5. Since a small ratio is indicative that the errors comprise only a small portion of the overall model response, this suggests that while certainly it is a less than perfect simulation, the model generally does reasonably

well in simulating major portions of the actual physical system (excluding the lower part of the system).

The summary results in Table 10 were grouped by well and by stress period, for which total mean errors for the complete model and entire simulation period were determined. Figure 58 displays these data in graphical form. The upper graph shows mean error variations by well and indicates that the areas of best model performance were at wells LAO-C, LAO-0.3, LAO-0.6, LAO-0.8, and LAO-3 in which MAE values were slightly to substantially less than one foot, except for LAO-3 where it was just slightly over one foot. The worst overall model performance was at wells LAO-0.91, LAO-4, and LAO-6 where MAE values were approximately 3 feet. The plot of the total RMS error to total head loss ratios for each well shows that this parameter ranged between 0.15 and 0.38 throughout the main, central portion of the model, only exceeding 1.0 in LAO-B and LAO-6, the uppermost and lowermost data points. This indicates that the model results should be reasonably representative of the actual physical system with the most accurate performance throughout most of its primary, middle region, while the results from the model's extremities are more questionable.

The lower graph shows mean error variations by stress period and indicates that the best model performance occurred in periods 1, 4, 5, 6, and 7 which all exhibited total MAE values of about one foot, more or less. The worst model performance occurred in periods 2, 3, 8, and 9 when the mean absolute errors were on the order of 2 to 3 feet. Inspection of the plot of total RMS error to total head loss ratio shows it was less than 0.5 in periods 1, 4, 6, 7, and 8 and substantially exceeded 0.5 only in period 3 while it was close to 0.5 in periods 2, 3, and 9. Thus, except for the extreme deviation in period 3, most of the modeled stress periods should define generally reasonable model behaviors.

In summary, the error analysis of the model performance under transient stresses indicated certain areas of weakness, primarily in the model extremities, and when simulating the system's dynamic recessions. However, because the average total head loss

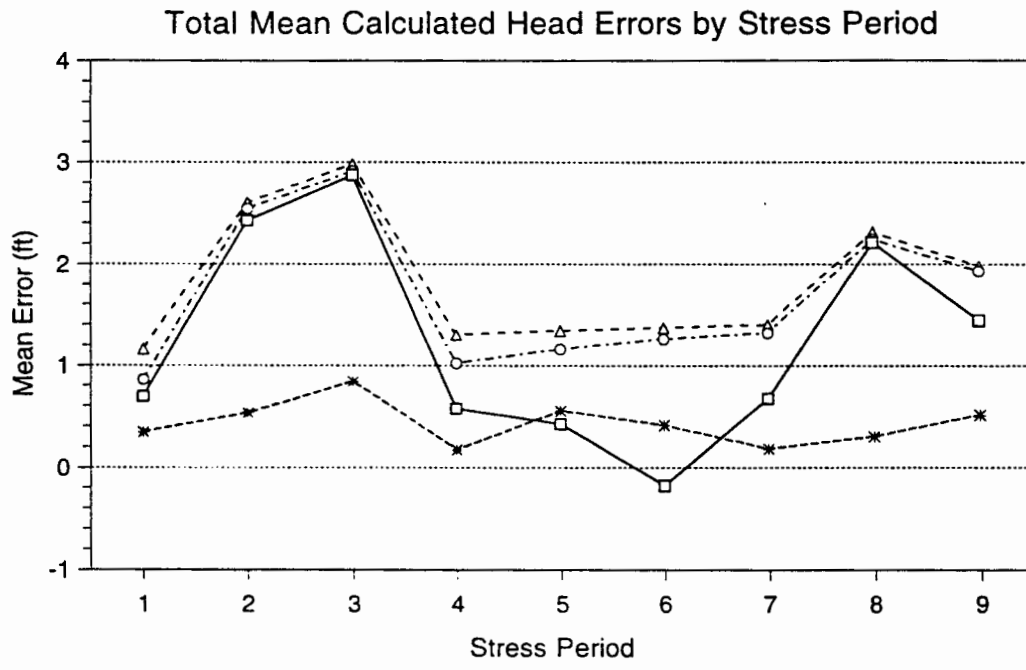
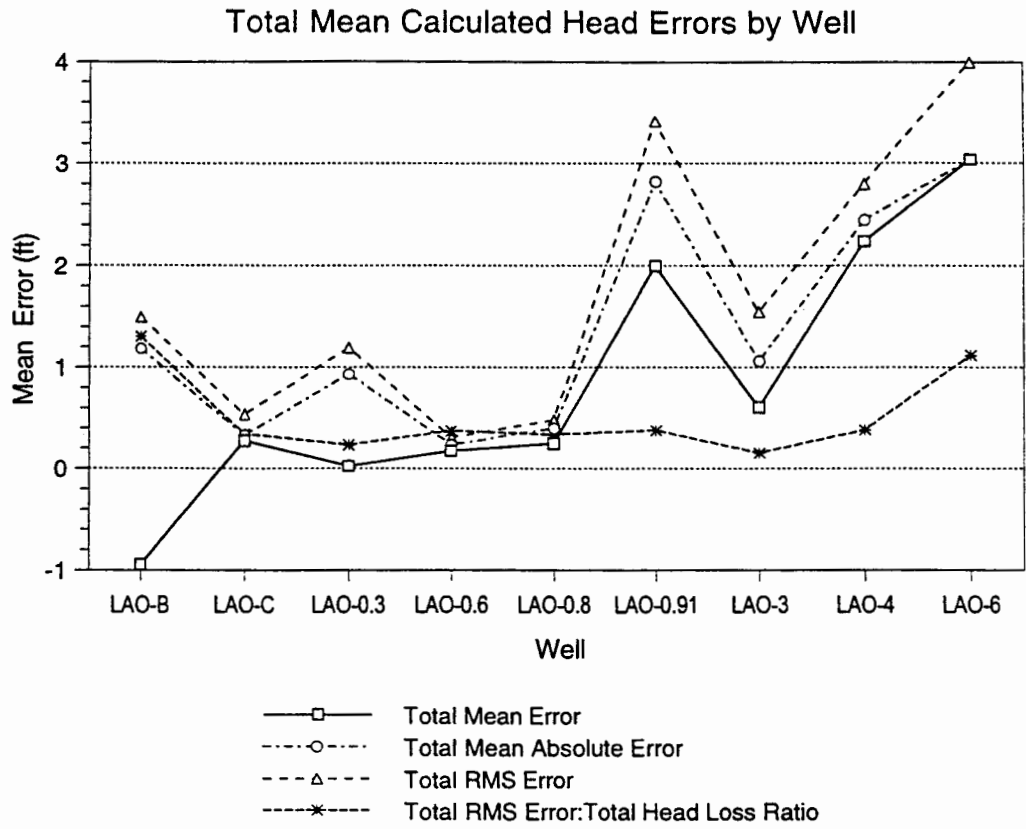


Figure 58: Total Mean Calculated Head Errors

in the system is rather large, the relative magnitude of the model errors was generally small. Considering the number of parameter assumptions required and the degree of simplification of system heterogeneities entailed in the model's design, its performance was reasonably good. As such, the model was judged to represent a reasonable simulation of the alluvial system for the most part, and the validity of the ZONEBUDGET quantifications of the system's hydrologic budget components is thus fairly corroborated.

The hydrologic budget's loss component of most interest in this investigation is the amount of infiltration seepage from the alluvial system into the underlying strata because of its attendant ramifications for disseminating contamination. The error analysis suggests that for the most part, the model results are likely to underestimate this quantity.

Transient ZONEBUDGET Analysis

As was done with the steady-state simulation, the ZONEBUDGET code was run for each of the 9 transient simulations with the same zone specifications used as before. The results of the ZONEBUDGET computations are given in Tables 12-20 which include the computed daily volumetric loss rates for infiltration, ET, downgradient flow loss, and storage within each zone and for the total study area west of State Road 4. Each table contains the results determined from the final modeled head distributions at the end of each of the 9 defined stress periods. The percentages of the total losses comprised by each budget component are also shown, along with the average loss rates in inches/day determined for each component within each zone and for the total study area.

The zonal variations in volumetric loss rates and average loss rates for each stress period are graphically displayed in Figures 59-67. The computed volumetric loss rates quantify these variations over the different regions of the alluvial system. However, since the zones differ considerably in size, it is more appropriate to use the average loss rates in making comparisons between the separate zones and stress periods. It is seen in comparing Figure 59 (transient simulation results for stress period 1) to Figure 33 (which

Table 12: Transient Model AL1296T1 Zonebudget Results (End Period 1)

Volumetric Losses:			Zone Budget Results						
Zone #	Area/Wells	Columns		Infiltration	ET Loss	Downgradient	Loss to	Constant	Total Loss
		From	To	(ft ³ /day)	(ft ³ /day)	Flow Loss	Storage	Head Loss	
				(ft ³ /day)	(ft ³ /day)				
1	LA Reservoir to 1100 ft east of Bridge/LAO-B	1	47	18624.0	11238.0	1961.0	0.0		31823.0
2	LAO-C, LAO-0.3	48	69	2882.6	2707.0	2531.8	1104.2		9225.6
3	LAO-0.6	70	75	1859.0	652.3	1855.2	158.1		4524.6
4	LAO-0.8	76	78	2728.4	0.0	396.1	182.8		3307.4
5	LAO-0.91, LAO-1	79	100	1561.6	548.6	445.6	6627.9		9183.7
6	LAO-2, LAO-3a	101	125	6999.4	81.7	2005.2	5059.6		14145.9
7	LAO-4, LAO-4.5, LAO-6	126	160	13846.0	3283.2	2028.0	7757.3		26914.5
West of St. Rd. 4 Totals:				48501.0	18510.8	2028.0	20890.0		89929.7
8	St. Rd. 4 to Lab boundary	161	192	17691.0	8149.4	962.03	7798.7		34601.1
9	East of Lab boundary	193	200	987.2	439.4		495.86	884.4	2806.8
Loss Percentages:			Loss to		Downgradient	Loss to		Total (%)	
Zone #	Area/Wells	Columns		Infiltration %	ET %	Flow %	Storage %		Const. Head %
		From	To	of Total Loss					
1	LA Reservoir to 1100 ft east of Bridge/LAO-B	1	47	58.52	35.31	6.16	0.00	100.00	
2	LAO-C, LAO-0.3	48	69	31.25	29.34	27.44	11.97	100.00	
3	LAO-0.6	70	75	41.09	14.42	41.00	3.49	100.00	
4	LAO-0.8	76	78	82.49	0.00	11.98	5.53	100.00	
5	LAO-0.91, LAO-1	79	100	17.00	5.97	4.85	72.17	100.00	
6	LAO-2, LAO-3a	101	125	49.48	0.58	14.18	35.77	100.00	
7	LAO-4, LAO-4.5, LAO-6	126	160	51.44	12.20	7.53	28.82	100.00	
West of St. Rd. 4 Totals:				53.93	20.58	2.26	23.23	100.00	
8	St. Rd. 4 to Lab boundary	161	192	51.13	23.55	2.78	22.54	100.00	
9	East of Lab boundary	193	200	35.17	15.65	0.00	17.67	31.51	
Average Losses:			Avg. Loss to		Avg. Loss to	Avg. Loss to		Average	
Zone #	Area/Wells	Columns		Infiltration	ET	Downgrad. Flow	Storage	Constant Head	Total Losses
		From	To	(inches/day)	(inches/day)	(inches/day)	(inches/day)	(inches/day)	(inches/day)
1	LA Reservoir to 1100 ft east of Bridge/LAO-B	1	47	0.079	0.048	0.008	0.000		0.135
2	LAO-C, LAO-0.3	48	69	0.026	0.025	0.023	0.010		0.084
3	LAO-0.6	70	75	0.059	0.021	0.059	0.005		0.145
4	LAO-0.8	76	78	0.119	0.000	0.017	0.008		0.144
5	LAO-0.91, LAO-1	79	100	0.011	0.004	0.003	0.047		0.066
6	LAO-2, LAO-3a	101	125	0.032	0.000	0.009	0.023		0.065
7	LAO-4, LAO-4.5, LAO-6	126	160	0.035	0.008	0.005	0.020		0.068
West of St. Rd. 4 Total Averages:				0.042	0.016	0.002	0.018		0.078
8	St. Rd. 4 to Lab boundary	161	192	0.034	0.016	0.002	0.015		0.067
9	East of Lab boundary	193	200	0.030	0.013	0.000	0.015	0.027	0.084
* Number of cells/zone (utilized in average loss calculations):								Cell Length (ft):	250
#1=113, #2=53, #3=15, #4=11, #5=67, #6=104, #7=189, #8=247, #9=16, 1-7=552.								Cell Width (ft):	100
								Cell Area (ft ²):	25000

Table 13: Transient Model AL1296T2 Zonebudget Results (End Period 2)

								-----Zone Budget Results-----			
Volumetric Losses:				Infiltration	ET Loss	Downgradient	Loss to	Constant			
		Columns		(Drain Loss)	(ft ³ /day)	Flow Loss	Storage	Head Loss	Total Loss		
Zone #	Area/Wells	From	To	(ft ³ /day)	(ft ³ /day)						
1	LA Reservoir to 1100 ft east of Bridge/LAO-B	1	47	19403.0	4751.0	2492.7	77938.0			104584.7	
2	LAO-C, LAO-0.3	48	69	3016.9	2765.6	2633.5	78793.0			87209.0	
3	LAO-0.6	70	75	2020.2	788.8	2173.1	21634.0			26616.1	
4	LAO-0.8	76	78	3098.6	0.0	542.0	16105.0			19745.6	
5	LAO-0.91, LAO-1	79	100	1305.5	164.1	326.2	105770.0			107565.8	
6	LAO-2, LAO-3a	101	125	7224.2	69.9	2088.8	157110.0			166492.9	
7	LAO-4, LAO-4.5, LAO-6	126	160	14536.0	3801.4	2274.2	283580.0			304191.6	
West of St. Rd. 4 Totals:				50604.4	12340.8	2274.2	740930.0			806149.4	
8	St. Rd. 4 to Lab boundary	161	192	19105.0	9105.1	1111.9	367610			396932.0	
9	East of Lab boundary	193	200	1060.9	491.1		21041	883.0		23476.0	
Loss Percentages:				Loss to	Loss to	Downgradient	Loss to	Const. Head %			
		Columns		Infiltration %	ET %	Flow %	Storage %	of Total Loss	Total (%)		
Zone #	Area/Wells	From	To	of Total Loss							
1	LA Reservoir to 1100 ft east of Bridge/LAO-B	1	47	18.55	4.54	2.38	74.52		100.00		
2	LAO-C, LAO-0.3	48	69	3.46	3.17	3.02	90.35		100.00		
3	LAO-0.6	70	75	7.59	2.96	8.16	81.28		100.00		
4	LAO-0.8	76	78	15.69	0.00	2.75	81.56		100.00		
5	LAO-0.91, LAO-1	79	100	1.21	0.15	0.30	98.33		100.00		
6	LAO-2, LAO-3a	101	125	4.34	0.04	1.25	94.36		100.00		
7	LAO-4, LAO-4.5, LAO-6	126	160	4.78	1.25	0.75	93.22		100.00		
West of St. Rd. 4 Totals:				6.28	1.53	0.28	91.91		100.00		
8	St. Rd. 4 to Lab boundary	161	192	4.81	2.29	0.28	92.61		100.00		
9	East of Lab boundary	193	200	4.52	2.09	0.00	89.63	3.76	100.00		
Average Losses:				Avg. Loss to	Average						
		Columns		Infiltration	ET	Downgrad. Flow	Storage	Constant Head	Total Losses		
Zone #	Area/Wells	From	To	(inches/day)	(inches/day)	(inches/day)	(inches/day)	(inches/day)	(inches/day)		
1	LA Reservoir to 1100 ft east of Bridge/LAO-B	1	47	0.082	0.020	0.011	0.331			0.444	
2	LAO-C, LAO-0.3	48	69	0.027	0.025	0.024	0.714			0.790	
3	LAO-0.6	70	75	0.065	0.025	0.070	0.692			0.852	
4	LAO-0.8	76	78	0.135	0.000	0.024	0.703			0.862	
5	LAO-0.91, LAO-1	79	100	0.009	0.001	0.002	0.758			0.771	
6	LAO-2, LAO-3a	101	125	0.033	0.000	0.010	0.725			0.768	
7	LAO-4, LAO-4.5, LAO-6	126	160	0.037	0.010	0.006	0.720			0.773	
West of St. Rd. 4 Total Averages:				0.044	0.011	0.002	0.644			0.701	
8	St. Rd. 4 to Lab boundary	161	192	0.037	0.018	0.002	0.714			0.771	
9	East of Lab boundary	193	200	0.032	0.015	0.000	0.631	0.026		0.704	
									Cell Length (ft):	250	
									Cell Width (ft):	100	
									Cell Area (ft ²):	25000	
* Number of cells/zone (utilized in average loss calculations)											
#1=113, #2=53, #3=15, #4=11, #5=6, #6=104, #7=189, #8=247, #9=16, 1-7=552											

Table 14: Transient Model AL1296T3 Zonebudget Results (End Period 3)

Volumetric Losses:			Zone Budget Results						
Zone #	Area/Wells	Columns		Infiltration	ET Loss	Downgradient	Loss to	Constant	Total Loss
		From	To	(ft ³ /day)	(ft ³ /day)	(ft ³ /day)	Storage	Head Loss	
				(ft ³ /day)	(ft ³ /day)				
1	LA Reservoir to 1100 ft east of Bridge/LAO-B	1	47	18683.0	15989.0	2255.9	0.0		36927.9
2	LAO-C, LAO-0.3	48	69	2958.5	1729.5	2578.4	0.0		7266.4
3	LAO-0.6	70	75	1936.4	454.2	1984.9	0.0		4375.5
4	LAO-0.8	76	78	2623.5	0.0	395.8	0.0		3019.3
5	LAO-0.91, LAO-1	79	100	1307.2	134.7	355.7	1057.5		2855.1
6	LAO-2, LAO-3a	101	125	6862.7	28.6	1991.3	0.0		8882.6
7	LAO-4, LAO-4.5, LAO-6	126	160	13823.0	2113.5	2099.0	0.0		18035.5
West of St. Rd. 4 Totals:				48194.3	20449.5	2099.0	1057.5		71800.3
8	St. Rd. 4 to Lab boundary	161	192	18096.0	5276.4	1009.1	0		24381.5
9	East of Lab boundary	193	200	1011.8	285.6		15.046	887.7	2200.1
Loss Percentages:			Loss to		Downgradient	Loss to		Total (%)	
Zone #	Area/Wells	Columns		Infiltration %	ET %	Flow %	Storage %		Const. Head %
		From	To	of Total Loss					
1	LA Reservoir to 1100 ft east of Bridge/LAO-B	1	47	50.59	43.30	6.11	0.00	100.00	
2	LAO-C, LAO-0.3	48	69	40.71	23.80	35.48	0.00	100.00	
3	LAO-0.6	70	75	44.26	10.38	45.36	0.00	100.00	
4	LAO-0.8	76	78	86.89	0.00	13.11	0.00	100.00	
5	LAO-0.91, LAO-1	79	100	45.79	4.72	12.46	37.04	100.00	
6	LAO-2, LAO-3a	101	125	77.26	0.32	22.42	0.00	100.00	
7	LAO-4, LAO-4.5, LAO-6	126	160	76.64	11.72	11.64	0.00	100.00	
West of St. Rd. 4 Totals:				67.12	28.48	2.92	1.47	100.00	
8	St. Rd. 4 to Lab boundary	161	192	74.22	21.64	4.14	0.00	100.00	
9	East of Lab boundary	193	200	45.99	12.98	0.00	0.68	40.35	100.00
Average Losses:			Avg. Loss to		Avg. Loss to	Avg. Loss to		Average	
Zone #	Area/Wells	Columns		Infiltration	ET	Downgrad. Flow	Storage	Constant Head	Total Losses
		From	To	(inches/day)	(inches/day)	(inches/day)	(inches/day)	(inches/day)	(inches/day)
1	LA Reservoir to 1100 ft east of Bridge/LAO-B	1	47	0.079	0.068	0.010	0.000		0.157
2	LAO-C, LAO-0.3	48	69	0.027	0.016	0.023	0.000		0.066
3	LAO-0.6	70	75	0.062	0.015	0.064	0.000		0.140
4	LAO-0.8	76	78	0.114	0.000	0.017	0.000		0.132
5	LAO-0.91, LAO-1	79	100	0.009	0.001	0.003	0.008		0.020
6	LAO-2, LAO-3a	101	125	0.032	0.000	0.009	0.000		0.041
7	LAO-4, LAO-4.5, LAO-6	126	160	0.035	0.005	0.005	0.000		0.046
West of St. Rd. 4 Total Averages:				0.042	0.018	0.002	0.001		0.062
8	St. Rd. 4 to Lab boundary	161	192	0.035	0.010	0.002	0.000		0.047
9	East of Lab boundary	193	200	0.030	0.009	0.000	0.000	0.027	0.066
								Cell Length (ft):	250
								Cell Width (ft):	100
								Cell Area (ft ²):	25000
* Number of cells/zone (utilized in average loss calculations):									
#1=113, #2=53, #3=15, #4=11, #5=67, #6=104, #7=189, #8=247, #9=16, 1-7=552									

Table 15: Transient Model AL1296T4 Zonebudget Results (End Period 4)

				-----Zone Budget Results-----					
Volumetric Losses:				Infiltration	ET Loss	Downgradient	Loss to	Constant	
Zone #	Area/Wells	Columns From	To	(ft^3/day)	(ft^3/day)	(ft^3/day)	(ft^3/day)	(ft^3/day)	Total Loss (ft^3/day)
1	LA Reservoir to 1100 ft east of Bridge/LAO-B	1	47	18608.0	3560.3	2157.2	1595.4		25920.9
2	LAO-C, LAO-0.3	48	69	3020.0	1519.6	2641.0	3501.7		10682.3
3	LAO-0.6	70	75	1975.2	407.3	2045.5	633.4		5061.3
4	LAO-0.8	76	78	2932.9	0.0	438.3	452.8		3824.0
5	LAO-0.91, LAO-1	79	100	1548.6	260.3	431.1	8916.4		11156.4
6	LAO-2, LAO-3a	101	125	7351.1	62.0	2119.5	7616.3		17148.9
7	LAO-4, LAO-4.5, LAO-6	126	160	14717.0	2095.5	2215.3	13523.0		32550.8
West of St. Rd. 4 Totals:				50152.8	7904.9	2215.3	36239.0		96512.0
8	St. Rd. 4 to Lab boundary	161	192	19205.0	5028.9	1061.5	16709		42004.4
9	East of Lab boundary	193	200	1080.4	267.7		1041.8	923.5	3313.5
Loss Percentages:				Loss to	Loss to	Downgradient	Loss to	Constant	
Zone #	Area/Wells	Columns From	To	Infiltration % of Total Loss	ET % of Total Loss	Flow % of Total Loss	Storage % of Total Loss	Const. Head % of Total Loss	Total (%)
1	LA Reservoir to 1100 ft east of Bridge/LAO-B	1	47	71.79	13.74	8.32	6.15		100.00
2	LAO-C, LAO-0.3	48	69	28.27	14.23	24.72	32.78		100.00
3	LAO-0.6	70	75	39.03	8.05	40.41	12.51		100.00
4	LAO-0.8	76	78	76.70	0.00	11.46	11.84		100.00
5	LAO-0.91, LAO-1	79	100	13.88	2.33	3.86	79.92		100.00
6	LAO-2, LAO-3a	101	125	42.87	0.36	12.36	44.41		100.00
7	LAO-4, LAO-4.5, LAO-6	126	160	45.21	6.44	6.81	41.54		100.00
West of St. Rd. 4 Totals:				51.97	8.19	2.30	37.55		100.00
8	St. Rd. 4 to Lab boundary	161	192	45.72	11.97	2.53	39.78		100.00
9	East of Lab boundary	193	200	32.61	8.08	0.00	31.44	27.87	100.00
Average Losses:				Avg. Loss to	Avg. Loss to	Avg. Loss to	Avg. Loss to	Avg. Loss to	Average
Zone #	Area/Wells	Columns From	To	Infiltration (inches/day)	ET (inches/day)	Downgrad. Flow (inches/day)	Storage (inches/day)	Constant Head (inches/day)	Total Losses (inches/day)
1	LA Reservoir to 1100 ft east of Bridge/LAO-B	1	47	0.079	0.015	0.009	0.007		0.110
2	LAO-C, LAO-0.3	48	69	0.027	0.014	0.024	0.032		0.097
3	LAO-0.6	70	75	0.063	0.013	0.065	0.020		0.162
4	LAO-0.8	76	78	0.128	0.000	0.019	0.020		0.167
5	LAO-0.91, LAO-1	79	100	0.011	0.002	0.003	0.064		0.080
6	LAO-2, LAO-3a	101	125	0.034	0.000	0.010	0.035		0.079
7	LAO-4, LAO-4.5, LAO-6	126	160	0.037	0.005	0.006	0.034		0.083
West of St. Rd. 4 Total Averages:				0.044	0.007	0.002	0.032		0.084
8	St. Rd. 4 to Lab boundary	161	192	0.037	0.010	0.002	0.032		0.082
9	East of Lab boundary	193	200	0.032	0.008	0.000	0.031	0.028	0.099
								Cell Length (ft):	250
								Cell Width (ft):	100
								Cell Area (ft^2):	25000
* Number of cells/zone (utilized in average loss calculations):									
#1=113, #2=53, #3=15, #4=11, #5=67, #6=104, #7=189, #8=247, #9=16, 1-7=552.									

Table 16: Transient Model AL1296T5 Zonebudget Results (End Period 5)

Volumetric Losses:			Zone Budget Results						
Zone #	Area/Wells	Columns		Infiltration	ET Loss	Downgradient	Loss to	Constant	Total Loss
		From	To	(Drain Loss) (ft ³ /day)	(ft ³ /day)	Flow Loss (ft ³ /day)	Storage (ft ³ /day)	Head Loss (ft ³ /day)	
1	LA Reservoir to 1100 ft east of Bridge/LAO-B	1	47	17507.0	2957.5	1933.3	0.0		22397.8
2	LAO-C, LAO-0.3	48	69	2891.6	698.6	2529.7	0.0		6119.9
3	LAO-0.6	70	75	1828.0	159.2	1718.5	0.0		3705.7
4	LAO-0.8	76	78	2098.6	0.0	227.4	0.0		2326.0
5	LAO-0.91, LAO-1	79	100	1526.3	152.8	451.4	699.8		2830.3
6	LAO-2, LAO-3a	101	125	6420.2	11.1	1837.9	0.0		8269.2
7	LAO-4, LAO-4.5, LAO-6	126	160	13060.0	718.8	1818.0	0.0		15596.8
West of St. Rd. 4 Totals:				45331.7	4698.0	1818.0	699.8		52547.5
8	St. Rd. 4 to Lab boundary	161	192	17053.0	1945.2	802.8	0		19801.0
9	East of Lab boundary	193	200	949.6	97.8		0	923.6	1970.9
Loss Percentages:			Loss to	Loss to	Downgradient	Loss to	Constant	Total (%)	
Zone #	Area/Wells	Columns		Infiltration %	ET %	Flow %	Storage %		Const. Head %
		From	To	of Total Loss	of Total Loss	of Total Loss	of Total Loss	of Total Loss	
1	LA Reservoir to 1100 ft east of Bridge/LAO-B	1	47	78.16	13.20	8.63	0.00	100.00	
2	LAO-C, LAO-0.3	48	69	47.25	11.41	41.34	0.00	100.00	
3	LAO-0.6	70	75	49.33	4.30	46.37	0.00	100.00	
4	LAO-0.8	76	78	90.22	0.00	9.78	0.00	100.00	
5	LAO-0.91, LAO-1	79	100	53.93	5.40	15.95	24.73	100.00	
6	LAO-2, LAO-3a	101	125	77.64	0.13	22.23	0.00	100.00	
7	LAO-4, LAO-4.5, LAO-6	126	160	83.74	4.61	11.66	0.00	100.00	
West of St. Rd. 4 Totals:				86.27	8.94	3.46	1.33	100.00	
8	St. Rd. 4 to Lab boundary	161	192	86.12	9.82	4.05	0.00	100.00	
9	East of Lab boundary	193	200	48.18	4.96	0.00	0.00	46.86	100.00
Average Losses:			Avg. Loss to	Avg. Loss to	Avg. Loss to	Avg. Loss to	Avg. Loss to	Average	
Zone #	Area/Wells	Columns		Infiltration	ET	Downgrad. Flow	Storage	Constant Head	Total Losses
		From	To	(inches/day)	(inches/day)	(inches/day)	(inches/day)	(inches/day)	(inches/day)
1	LA Reservoir to 1100 ft east of Bndg/LAO-B	1	47	0.074	0.013	0.008	0.000		0.095
2	LAO-C, LAO-0.3	48	69	0.026	0.006	0.023	0.000		0.055
3	LAO-0.6	70	75	0.058	0.005	0.055	0.000		0.119
4	LAO-0.8	76	78	0.092	0.000	0.010	0.000		0.101
5	LAO-0.91, LAO-1	79	100	0.011	0.001	0.003	0.005		0.020
6	LAO-2, LAO-3a	101	125	0.030	0.000	0.008	0.000		0.038
7	LAO-4, LAO-4.5, LAO-6	126	160	0.033	0.002	0.005	0.000		0.040
West of St. Rd. 4 Total Averages:				0.039	0.004	0.002	0.001		0.046
8	St. Rd. 4 to Lab boundary	161	192	0.033	0.004	0.002	0.000		0.038
9	East of Lab boundary	193	200	0.028	0.003	0.000	0.000	0.028	0.059
								Cell Length (ft):	250
								Cell Width (ft):	100
								Cell Area (ft ²):	25000

* Number of cells/zone (utilized in average loss calculations):

#1=113, #2=53, #3=15, #4=11, #5=67, #6=104, #7=189, #8=247, #9=16, 1-7=552.

Table 17: Transient Model AL1296T6 Zonebudget Results (End Period 6)

Volumetric Losses:				Zone Budget Results					
Zone #	Area/Wells	Columns		Infiltration	ET Loss	Downgradient	Loss to	Constant	
		From	To	(ft ³ /day)	(ft ³ /day)	Flow Loss	Storage	Head Loss	Total Loss
				(ft ³ /day)	(ft ³ /day)				
1	LA Reservoir to 1100 ft east of Bridge/LAO-B	1	47	17883.0	10404.0	1726.7	2832.8		32846.5
2	LAO-C, LAO-0.3	48	69	2891.1	2165.0	2552.8	346.8		7955.7
3	LAO-0.6	70	75	1851.3	501.9	1775.8	54.6		4183.6
4	LAO-0.8	76	78	2572.6	0.0	365.6	32.5		2970.7
5	LAO-0.91, LAO-1	79	100	2100.8	1258.6	644.1	3606.9		7610.4
6	LAO-2, LAO-3a	101	125	7322.0	156.2	2033.1	2419.2		11930.5
7	LAO-4, LAO-4.5, LAO-6	126	160	14426.0	2747.8	1971.2	3392.8		22537.8
West of St. Rd. 4 Totals:				49046.8	17233.5	1971.2	12685.7		80937.1
8	St. Rd. 4 to Lab boundary	161	192	18256.0	6749.2	953.33	2829.7		28788.2
9	East of Lab boundary	193	200	1009.3	336.5		189.23	938.0	2473.0
Loss Percentages:				Loss to	Loss to	Downgradient	Loss to	Const. Head %	Total (%)
Zone #	Area/Wells	Columns		Infiltration %	ET %	Flow %	Storage %	Const. Head %	Total (%)
		From	To	of Total Loss	Total (%)				
				of Total Loss	Total (%)				
1	LA Reservoir to 1100 ft east of Bridge/LAO-B	1	47	54.44	31.67	5.26	8.62		100.00
2	LAO-C, LAO-0.3	48	69	36.34	27.21	32.09	4.36		100.00
3	LAO-0.6	70	75	44.25	12.00	42.45	1.31		100.00
4	LAO-0.8	76	78	86.60	0.00	12.31	1.09		100.00
5	LAO-0.91, LAO-1	79	100	27.60	16.54	8.46	47.39		100.00
6	LAO-2, LAO-3a	101	125	61.37	1.31	17.04	20.28		100.00
7	LAO-4, LAO-4.5, LAO-6	126	160	64.01	12.19	8.75	15.05		100.00
West of St. Rd. 4 Totals:				60.60	21.29	2.44	15.67		100.00
8	St. Rd. 4 to Lab boundary	161	192	63.41	23.44	3.31	9.83		100.00
9	East of Lab boundary	193	200	40.81	13.61	0.00	7.65	37.93	100.00
Average Losses:				Avg. Loss to	Average				
Zone #	Area/Wells	Columns		Infiltration	ET	Downgrad. Flow	Storage	Constant Head	Total Losses
		From	To	(inches/day)	(inches/day)	(inches/day)	(inches/day)	(inches/day)	(inches/day)
				(inches/day)	(inches/day)	(inches/day)	(inches/day)	(inches/day)	(inches/day)
1	LA Reservoir to 1100 ft east of Bridge/LAO-B	1	47	0.076	0.044	0.007	0.012		0.140
2	LAO-C, LAO-0.3	48	69	0.026	0.020	0.023	0.003		0.072
3	LAO-0.6	70	75	0.059	0.016	0.057	0.002		0.134
4	LAO-0.8	76	78	0.112	0.000	0.016	0.001		0.130
5	LAO-0.91, LAO-1	79	100	0.015	0.009	0.005	0.026		0.055
6	LAO-2, LAO-3a	101	125	0.034	0.001	0.009	0.011		0.055
7	LAO-4, LAO-4.5, LAO-6	126	160	0.037	0.007	0.005	0.009		0.057
West of St. Rd. 4 Total Averages:				0.043	0.015	0.002	0.011		0.070
8	St. Rd. 4 to Lab boundary	161	192	0.035	0.013	0.002	0.005		0.056
9	East of Lab boundary	193	200	0.030	0.010	0.000	0.006	0.028	0.074
								Cell Length (ft):	250
								Cell Width (ft):	100
								Cell Area (ft ²):	25000
* Number of cells/zone (utilized in average loss calculations):									
#1=113, #2=53, #3=15, #4=11, #5=67, #6=104, #7=189, #8=247, #9=16, 1-7=552.									

Table 18: Transient Model AL1296T7 Zonebudget Results (End Period 7)

			Zone Budget Results						
Volumetric Losses:			Infiltration	ET Loss	Downgradient	Loss to	Constant		
Zone #	Area/Wells	Columns From To	(Drain Loss) (ft ³ /day)	(ft ³ /day)	Flow Loss (ft ³ /day)	Storage (ft ³ /day)	Head Loss (ft ³ /day)	Total Loss (ft ³ /day)	
1	LA Reservoir to 1100 ft east of Bridge/LAO-B	1 47	16976.0	14224.0	1793.2	0.0		32993.2	
2	LAO-C, LAO-0.3	48 69	2816.0	3793.5	2467.0	0.0		9076.5	
3	LAO-0.6	70 75	1773.8	811.0	1661.3	0.0		4246.1	
4	LAO-0.8	76 78	2235.2	0.0	272.4	1.3		2508.9	
5	LAO-0.91, LAO-1	79 100	1673.7	1196.5	499.4	1586.7		4956.3	
6	LAO-2, LAO-3a	101 125	6511.8	88.0	1837.9	78.3		8516.0	
7	LAO-4, LAO-4.5, LAO-6	126 160	12985.0	3787.1	1775.5	138.3		18685.9	
West of St. Rd. 4 Totals:			44971.5	23900.2	1775.5	1804.6		72451.7	
8	St. Rd. 4 to Lab boundary	161 192	16531.0	10226.0	811.93	0		27568.9	
9	East of Lab boundary	193 200	910.8	514.9		0	897.5	2323.2	
Loss Percentages:			Loss to	Loss to	Downgradient	Loss to	Const. Head %		
Zone #	Area/Wells	Columns From To	Infiltration % of Total Loss	ET % of Total Loss	Flow % of Total Loss	Storage % of Total Loss	of Total Loss	of Total Loss	Total (%)
1	LA Reservoir to 1100 ft east of Bridge/LAO-B	1 47	51.45	43.11	5.44	0.00			100.00
2	LAO-C, LAO-0.3	48 69	31.03	41.79	27.18	0.00			100.00
3	LAO-0.6	70 75	41.77	19.10	39.12	0.00			100.00
4	LAO-0.8	76 78	89.09	0.00	10.86	0.05			100.00
5	LAO-0.91, LAO-1	79 100	33.77	24.14	10.08	32.01			100.00
6	LAO-2, LAO-3a	101 125	76.47	1.03	21.58	0.92			100.00
7	LAO-4, LAO-4.5, LAO-6	126 160	69.49	20.27	9.50	0.74			100.00
West of St. Rd. 4 Totals:			62.07	32.99	2.45	2.49			100.00
8	St. Rd. 4 to Lab boundary	161 192	59.96	37.09	2.95	0.00			100.00
9	East of Lab boundary	193 200	39.21	22.16	0.00	0.00	38.63		100.00
Average Losses:			Avg. Loss to	Avg. Loss to	Avg. Loss to	Avg. Loss to	Avg. Loss to	Average	
Zone #	Area/Wells	Columns From To	Infiltration (inches/day)	ET (inches/day)	Downgrad. Flow (inches/day)	Storage (inches/day)	Constant Head (inches/day)	Total Losses (inches/day)	
1	LA Reservoir to 1100 ft east of Bridge/LAO-B	1 47	0.072	0.060	0.008	0.000		0.140	
2	LAO-C, LAO-0.3	48 69	0.026	0.034	0.022	0.000		0.082	
3	LAO-0.6	70 75	0.057	0.026	0.053	0.000		0.136	
4	LAO-0.8	76 78	0.098	0.000	0.012	0.000		0.109	
5	LAO-0.91, LAO-1	79 100	0.012	0.009	0.004	0.011		0.036	
6	LAO-2, LAO-3a	101 125	0.030	0.000	0.008	0.000		0.039	
7	LAO-4, LAO-4.5, LAO-6	126 160	0.033	0.010	0.005	0.000		0.047	
West of St. Rd. 4 Total Averages:			0.039	0.021	0.002	0.002		0.063	
8	St. Rd. 4 to Lab boundary	161 192	0.032	0.020	0.002	0.000		0.054	
9	East of Lab boundary	193 200	0.027	0.015	0.000	0.000	0.027	0.070	
								Cell Length (ft):	250
								Cell Width (ft):	100
								Cell Area (ft ²):	25000
* Number of cells/zone (utilized in average loss calculations):									
#1=113, #2=53, #3=15, #4=11, #5=67, #6=104, #7=189, #8=247, #9=16, 1-7=552.									

Table 19: Transient Model AL1296T8 Zonebudget Results (End Period 8)

				Zone Budget Results					
Volumetric Losses:				Infiltration	ET Loss	Downgradient	Loss to	Constant	
Zone #	Area/Wells	Columns From	To	(Drain Loss) (ft ³ /day)	(ft ³ /day)	Flow Loss (ft ³ /day)	Storage (ft ³ /day)	Head Loss (ft ³ /day)	Total Loss (ft ³ /day)
1	LA Reservoir to 1100 ft east of Bridge/LAO-B	1	47	17881.0	13454.0	1772.1	15748.0		48855.1
2	LAO-C, LAO-0.3	48	69	2944.1	3585.6	2603.2	4945.4		14078.3
3	LAO-0.6	70	75	1907.9	887.5	1916.3	1373.3		6085.0
4	LAO-0.8	76	78	3155.7	0.0	496.5	822.0		4474.2
5	LAO-0.91, LAO-1	79	100	2128.8	2026.1	630.2	11234.0		16019.1
6	LAO-2, LAO-3a	101	125	7872.9	341.5	2192.4	14329.0		24735.8
7	LAO-4, LAO-4.5, LAO-6	126	160	15319.0	5260.0	2176.7	23309.0		46064.7
West of St. Rd. 4 Totals:				51209.4	25554.6	2176.7	71760.7		150701.5
8	St. Rd. 4 to Lab boundary	161	192	19272.0	12136.0	1070.3	27056		59534.3
9	East of Lab boundary	193	200	1072.3	624.0		1683.9	936.1	4316.3
Loss Percentages:				Loss to	Loss to	Downgradient	Loss to	Constant	Total
Zone #	Area/Wells	Columns From	To	Infiltration % of Total Loss	ET % of Total Loss	Flow % of Total Loss	Storage % of Total Loss	Const. Head % of Total Loss	Total (%)
1	LA Reservoir to 1100 ft east of Bridge/LAO-B	1	47	36.60	27.54	3.63	32.23		100.00
2	LAO-C, LAO-0.3	48	69	20.91	25.47	18.49	35.13		100.00
3	LAO-0.6	70	75	31.35	14.58	31.49	22.57		100.00
4	LAO-0.8	76	78	70.53	0.00	11.10	18.37		100.00
5	LAO-0.91, LAO-1	79	100	13.29	12.65	3.93	70.13		100.00
6	LAO-2, LAO-3a	101	125	31.83	1.38	8.86	57.93		100.00
7	LAO-4, LAO-4.5, LAO-6	126	160	33.26	11.42	4.73	50.60		100.00
West of St. Rd. 4 Totals:				33.98	16.96	1.44	47.62		100.00
8	St. Rd. 4 to Lab boundary	161	192	32.37	20.38	1.80	45.45		100.00
9	East of Lab boundary	193	200	24.84	14.46	0.00	39.01	21.69	100.00
Average Losses:				Avg. Loss to	Avg. Loss to	Avg. Loss to	Avg. Loss to	Avg. Loss to	Average
Zone #	Area/Wells	Columns From	To	Infiltration (inches/day)	ET (inches/day)	Downgrad. Flow (inches/day)	Storage (inches/day)	Constant Head (inches/day)	Total Losses (inches/day)
1	LA Reservoir to 1100 ft east of Bridge/LAO-B	1	47	0.076	0.057	0.008	0.067		0.208
2	LAO-C, LAO-0.3	48	69	0.027	0.032	0.024	0.045		0.128
3	LAO-0.6	70	75	0.061	0.028	0.061	0.044		0.195
4	LAO-0.8	76	78	0.138	0.000	0.022	0.036		0.195
5	LAO-0.91, LAO-1	79	100	0.015	0.015	0.005	0.080		0.115
6	LAO-2, LAO-3a	101	125	0.036	0.002	0.010	0.066		0.114
7	LAO-4, LAO-4.5, LAO-6	126	160	0.039	0.013	0.006	0.059		0.117
West of St. Rd. 4 Total Averages:				0.045	0.022	0.002	0.062		0.131
8	St. Rd. 4 to Lab boundary	161	192	0.037	0.024	0.002	0.053		0.116
9	East of Lab boundary	193	200	0.032	0.019	0.000	0.051	0.028	0.129
								Cell Length (ft):	250
								Cell Width (ft):	100
								Cell Area (ft ²):	25000
* Number of cells/zone (unused in average loss calculations):									
#1=113, #2=53, #3=15, #4=11, #5=67, #6=104, #7=189, #8=247, #9=16, 1-7=552.									

Table 20: Transient Model AL1296T9 Zonebudget Results (End Period 9)

Volumetric Losses:			Zone Budget Results						
Zone #	Area/Wells	Columns		Infiltration	ET Loss	Downgradient	Loss to	Constant	Total Loss
		From	To	(ft ³ /day)	(ft ³ /day)	Flow Loss	Storage	Head Loss	
				(ft ³ /day)	(ft ³ /day)				
1	LA Reservoir to 1100 ft east of Bridge/LAO-B	1	47	16785.0	5011.8	1662.8	0.0		23459.6
2	LAO-C, LAO-0.3	48	69	2794.6	1900.6	2483.5	0.0		7178.7
3	LAO-0.6	70	75	1772.3	402.4	1635.3	0.0		3810.0
4	LAO-0.8	76	78	2172.3	0.0	279.7	0.0		2452.0
5	LAO-0.91, LAO-1	79	100	2019.7	1052.9	619.3	5.4		3697.2
6	LAO-2, LAO-3a	101	125	7047.7	110.5	1965.4	0.0		9123.6
7	LAO-4, LAO-4.5, LAO-6	126	160	13714.0	2125.7	1837.0	0.0		17676.7
West of St. Rd. 4 Totals:				46305.6	10603.9	1837.0	5.4		58751.9
8	St. Rd. 4 to Lab boundary	161	192	17046.0	5424.2	866.37	0		23336.6
9	East of Lab boundary	193	200	948.7	277.0		0	913.6	2139.3
Loss Percentages:			Loss to		Loss to	Downgradient	Loss to		
Zone #	Area/Wells	Columns		Infiltration %	ET %	Flow %	Storage %	Const. Head %	Total (%)
		From	To	of Total Loss					
				(%)	(%)	(%)	(%)	(%)	(%)
1	LA Reservoir to 1100 ft east of Bridge/LAO-B	1	47	71.55	21.36	7.09	0.00		100.00
2	LAO-C, LAO-0.3	48	69	38.93	26.48	34.60	0.00		100.00
3	LAO-0.6	70	75	46.52	10.56	42.92	0.00		100.00
4	LAO-0.8	76	78	88.59	0.00	11.41	0.00		100.00
5	LAO-0.91, LAO-1	79	100	54.63	28.48	16.75	0.14		100.00
6	LAO-2, LAO-3a	101	125	77.25	1.21	21.54	0.00		100.00
7	LAO-4, LAO-4.5, LAO-6	126	160	77.58	12.03	10.39	0.00		100.00
West of St. Rd. 4 Totals:				78.82	18.05	3.13	0.01		100.00
8	St. Rd. 4 to Lab boundary	161	192	73.04	23.24	3.71	0.00		100.00
9	East of Lab boundary	193	200	44.35	12.95	0.00	0.00	42.71	100.00
Average Losses:			Avg. Loss to		Avg. Loss to	Avg. Loss to	Avg. Loss to	Avg. Loss to	Average
Zone #	Area/Wells	Columns		Infiltration	ET	Downgrad. Flow	Storage	Constant Head	Total Losses
		From	To	(inches/day)	(inches/day)	(inches/day)	(inches/day)	(inches/day)	(inches/day)
1	LA Reservoir to 1100 ft east of Bridge/LAO-B	1	47	0.071	0.021	0.007	0.000		0.100
2	LAO-C, LAO-0.3	48	69	0.025	0.017	0.022	0.000		0.065
3	LAO-0.6	70	75	0.057	0.013	0.052	0.000		0.122
4	LAO-0.8	76	78	0.095	0.000	0.012	0.000		0.107
5	LAO-0.91, LAO-1	79	100	0.014	0.008	0.004	0.000		0.026
6	LAO-2, LAO-3a	101	125	0.033	0.001	0.009	0.000		0.042
7	LAO-4, LAO-4.5, LAO-6	126	160	0.035	0.005	0.005	0.000		0.045
West of St. Rd. 4 Total Averages:				0.040	0.009	0.002	0.000		0.051
8	St. Rd. 4 to Lab boundary	161	192	0.033	0.011	0.002	0.000		0.045
9	East of Lab boundary	193	200	0.028	0.008	0.000	0.000	0.027	0.064
								Cell Length (ft):	250
* Number of cells/zone (utilized in average loss calculations):								Cell Width (ft):	100
#1=113, #2=53, #3=15, #4=11, #5=67, #6=104, #7=189, #8=247, #9=16, 1-7=552.								Cell Area (ft ²):	25000

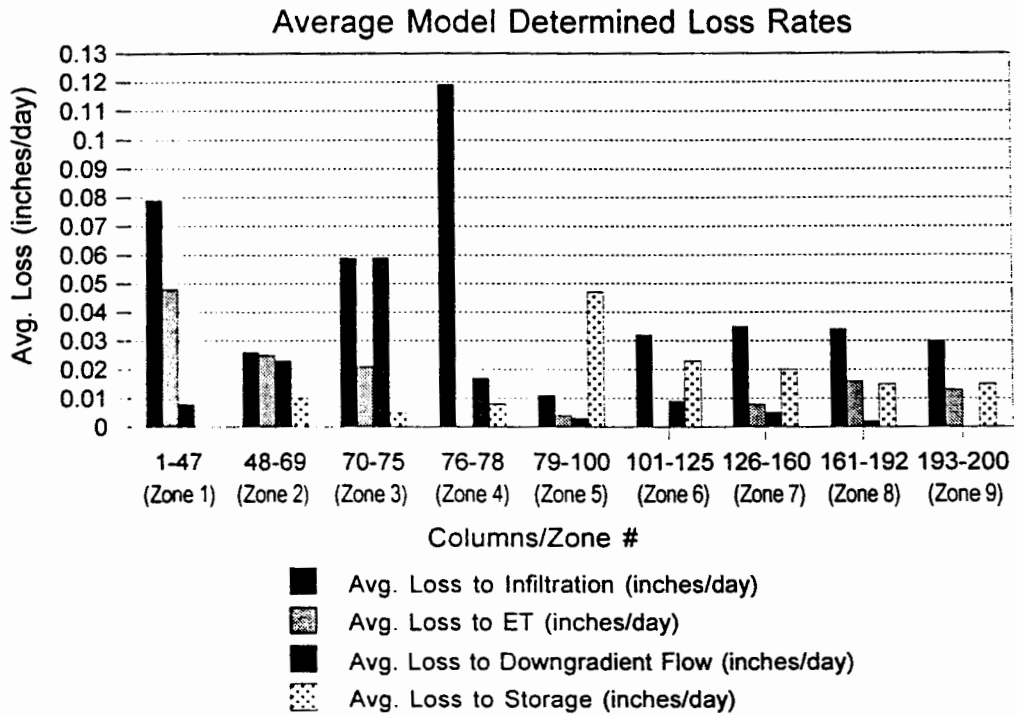
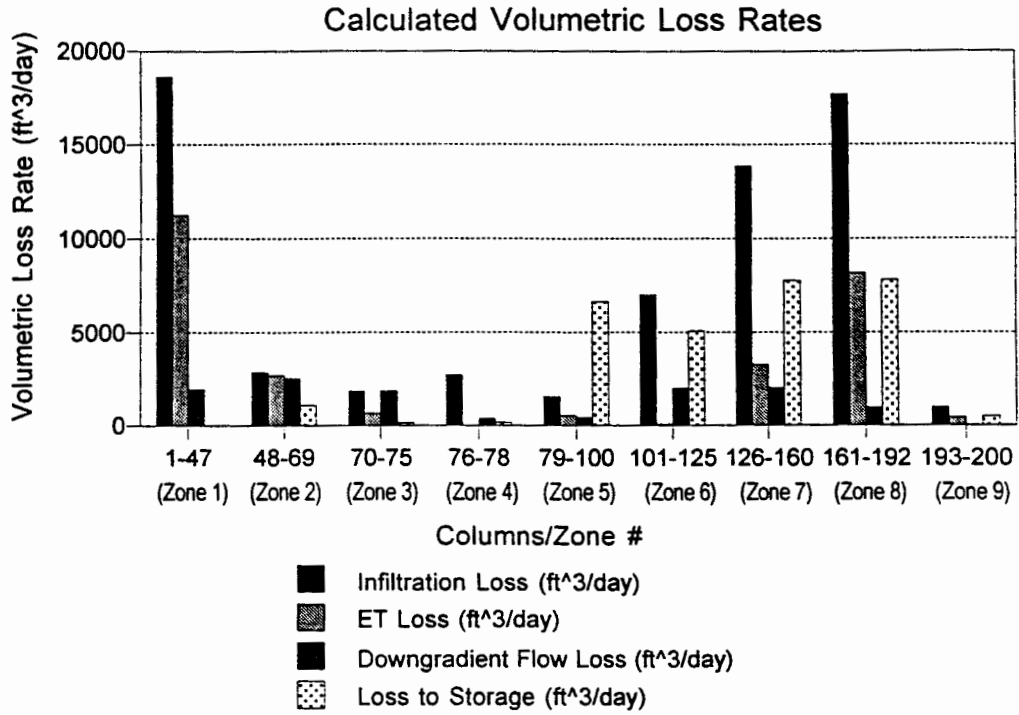


Figure 59: Model AL1296T1 (Transient-Period 1) Zonebudget Results

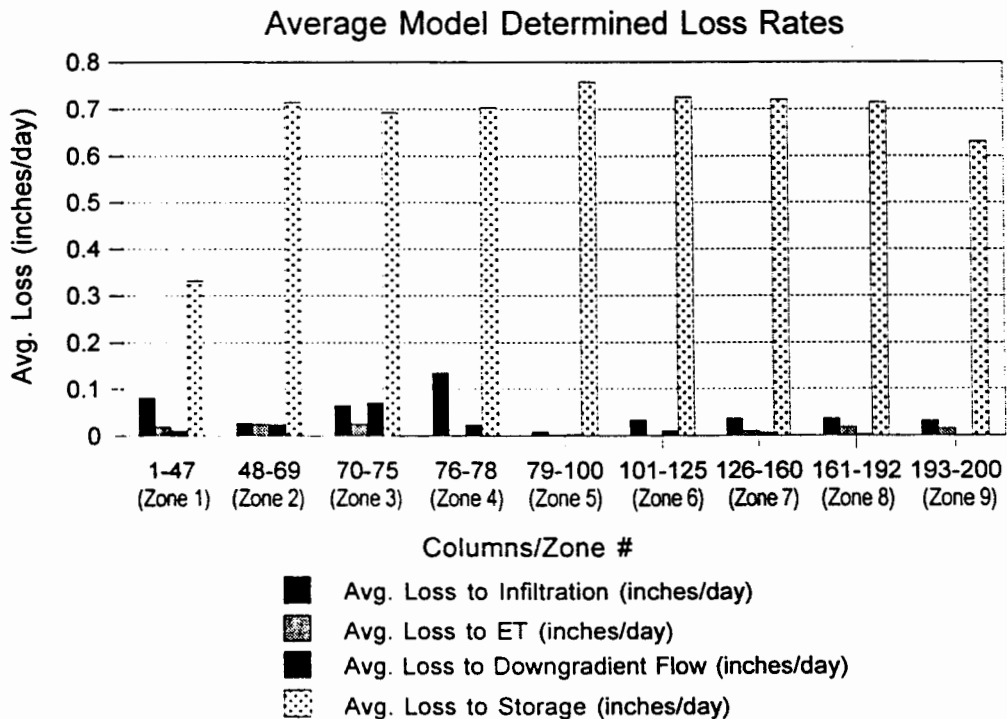
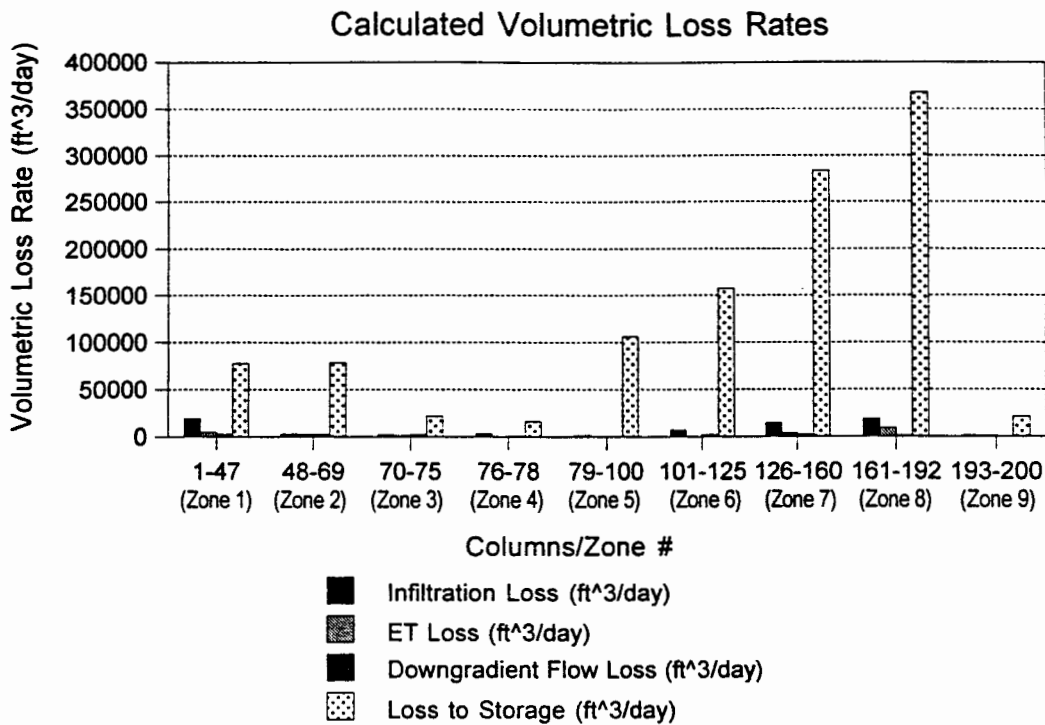


Figure 60: Model AL1296T2 (Transient-Period 2) Zonebudget Results

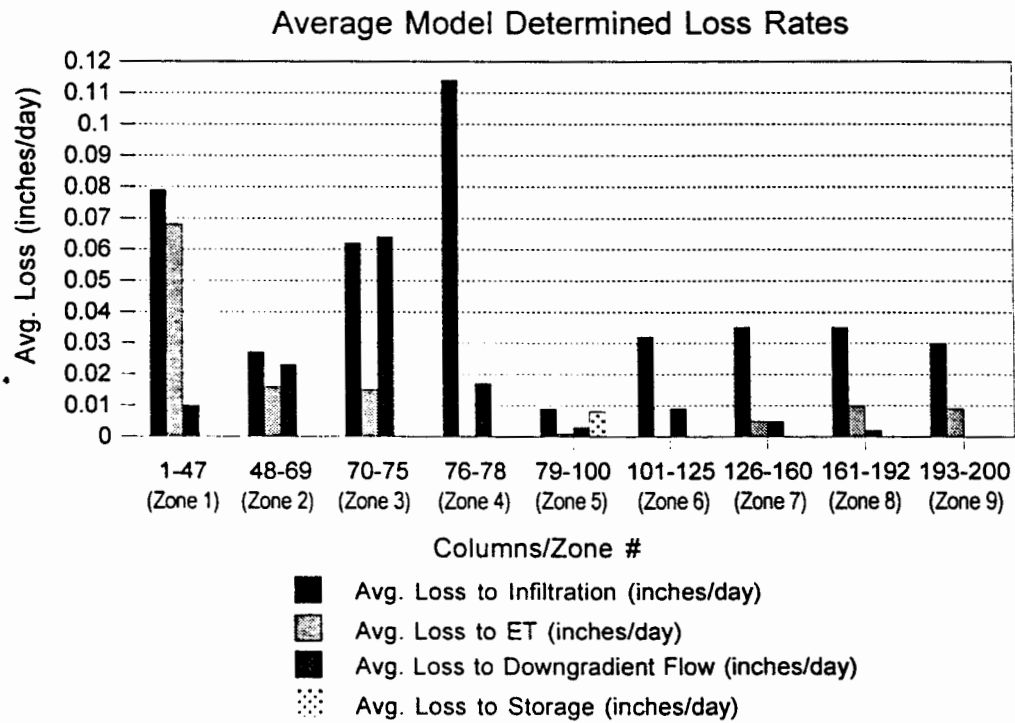
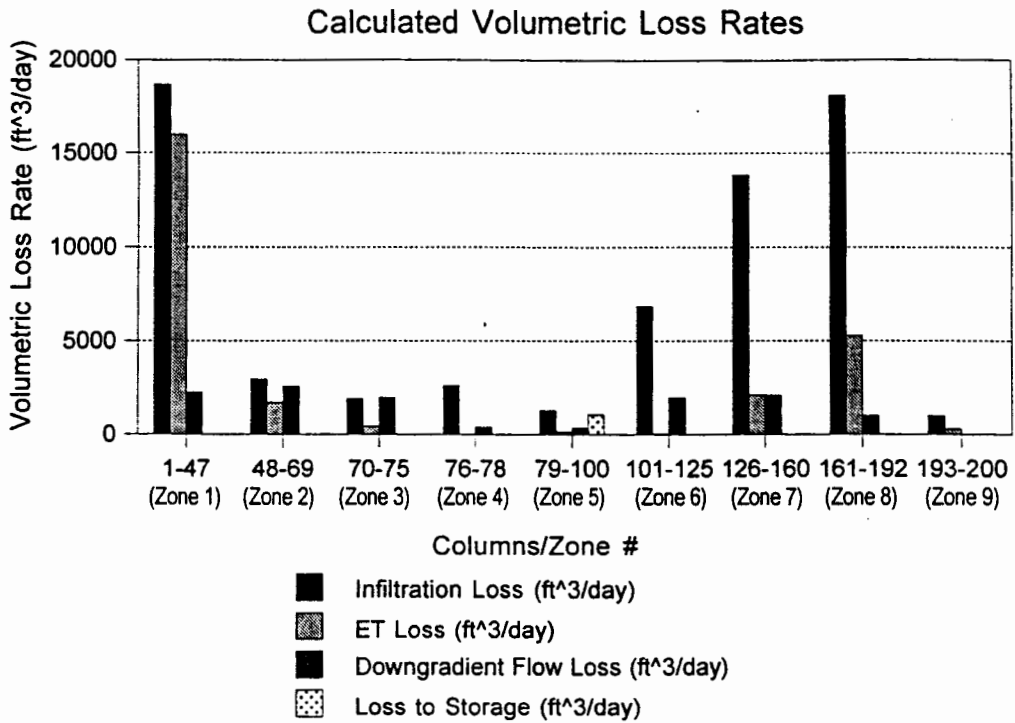


Figure 61: Model AL1296T3 (Transient-Period 3) Zonebudget Results

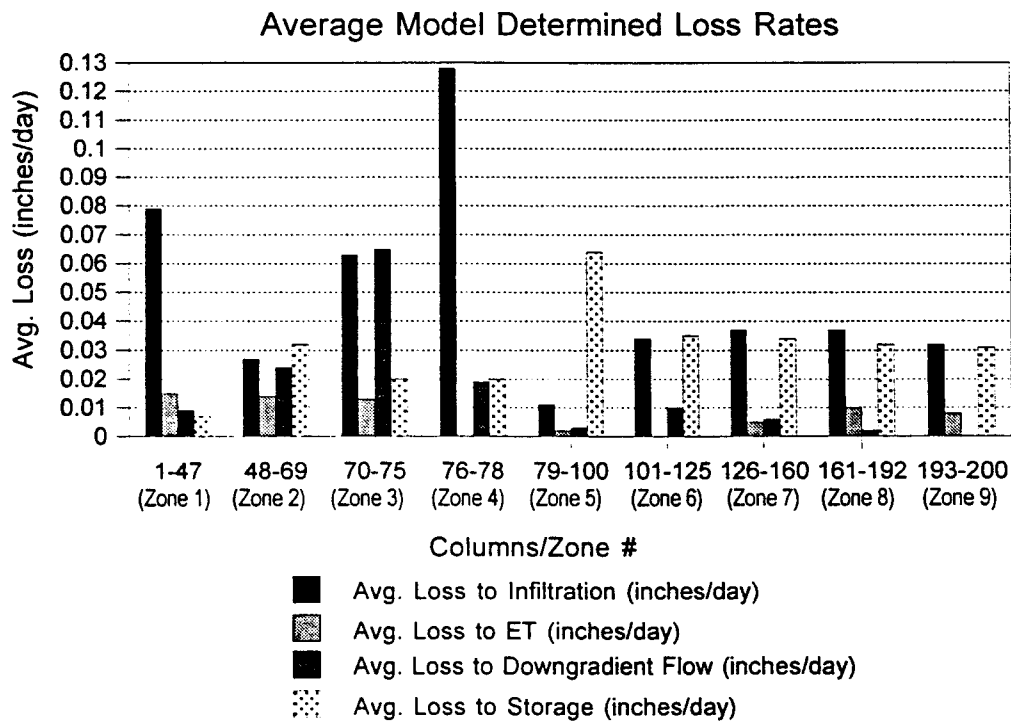
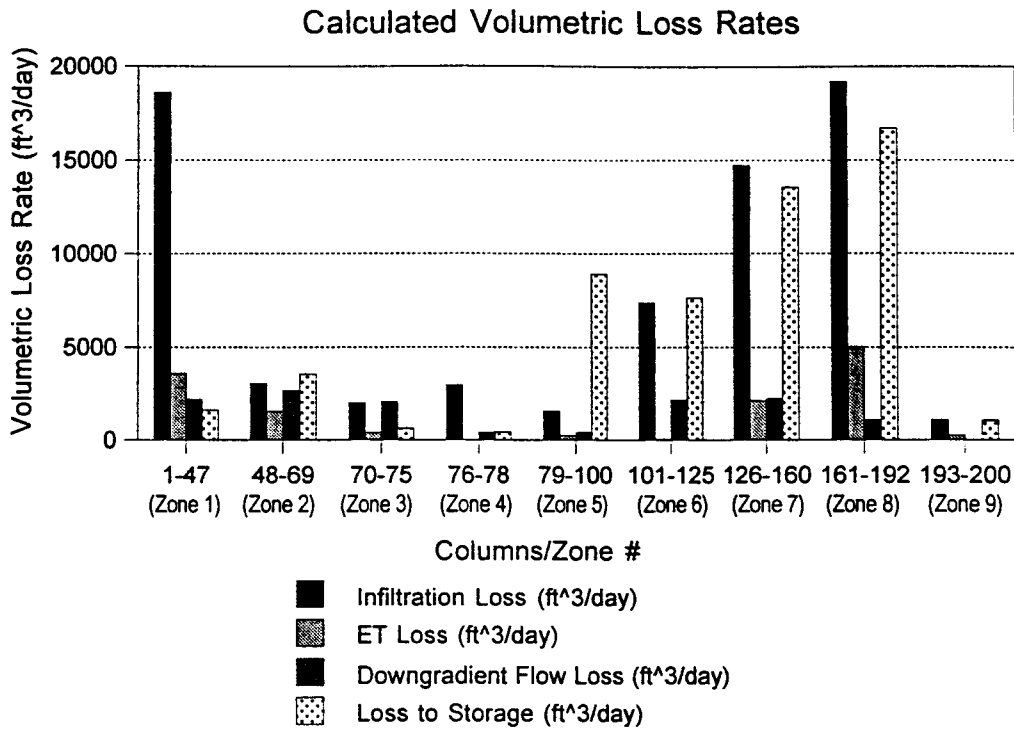


Figure 62: Model AL1296T4 (Transient-Period 4) Zonebudget Results

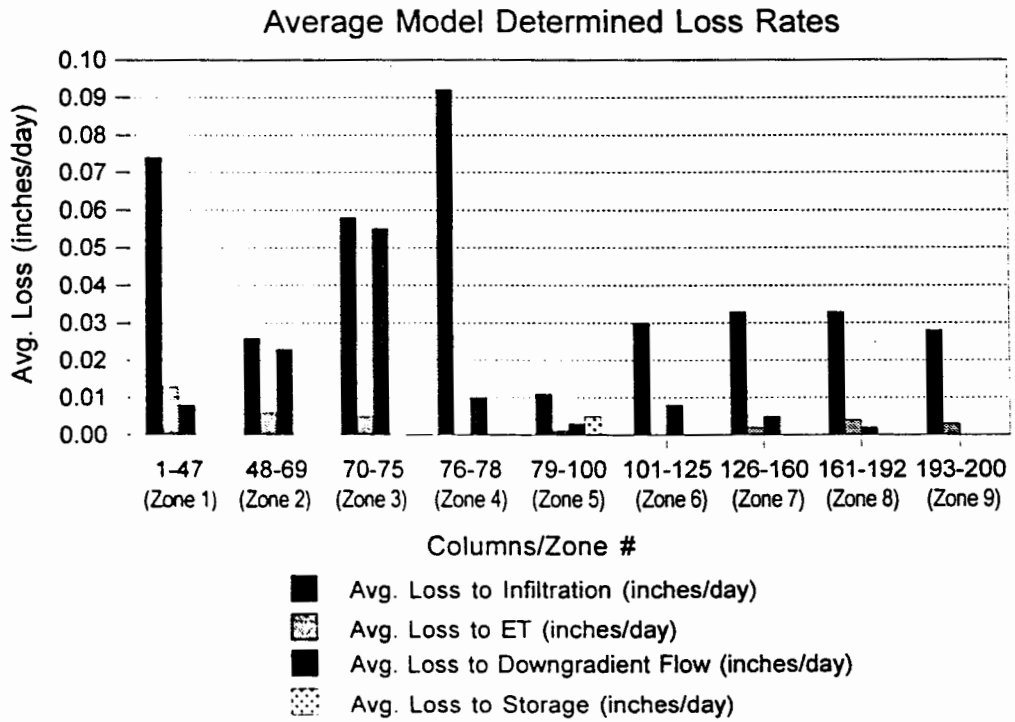
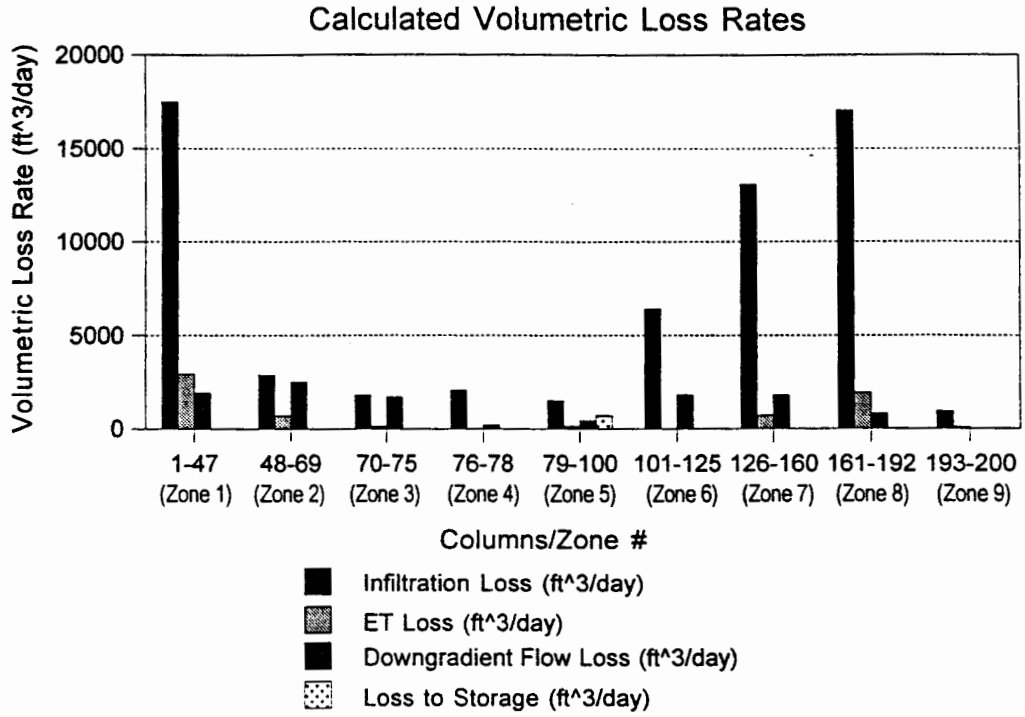


Figure 63: Model AL1296T55 (Transient-Period 5) Zonebudget Results

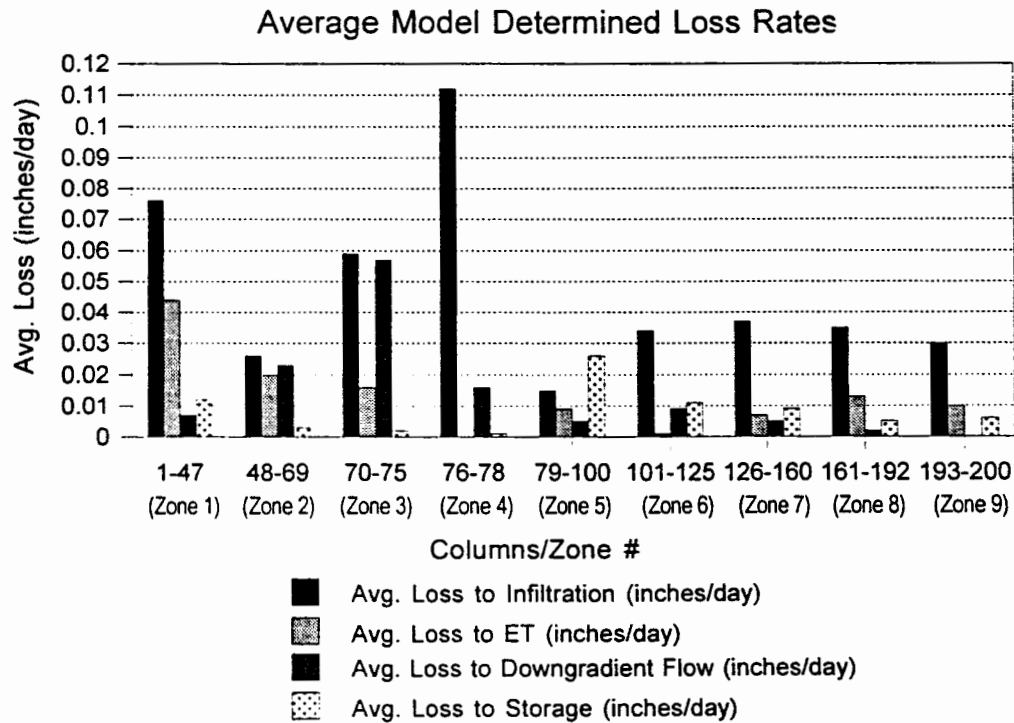
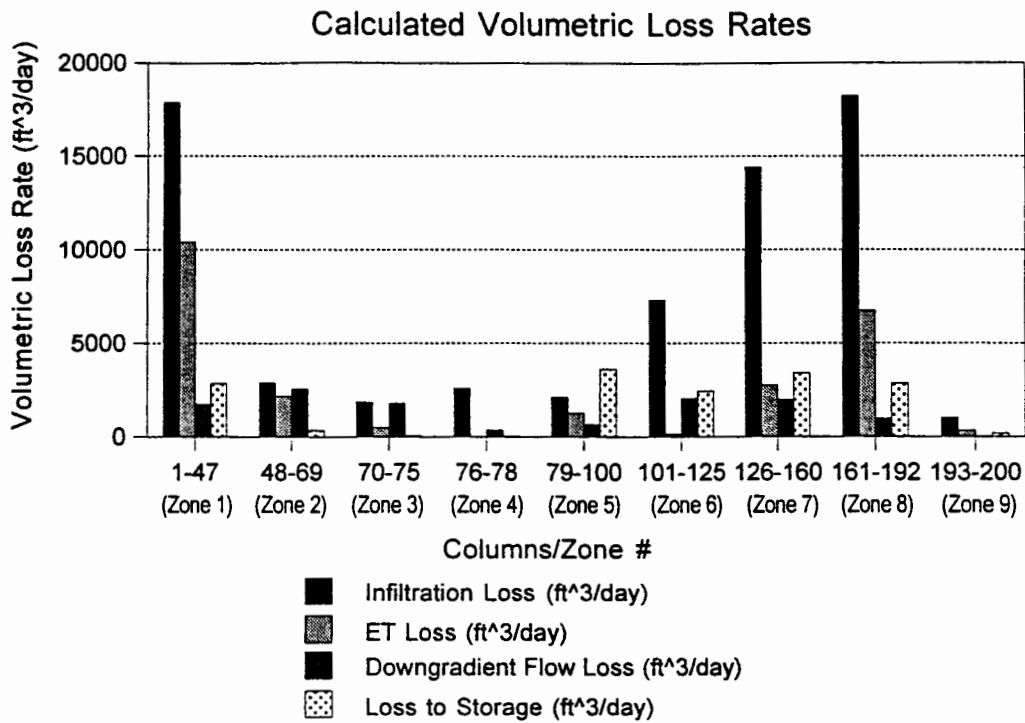


Figure 64: Model AL1296T6 (Transient-Period 6) Zonebudget Results

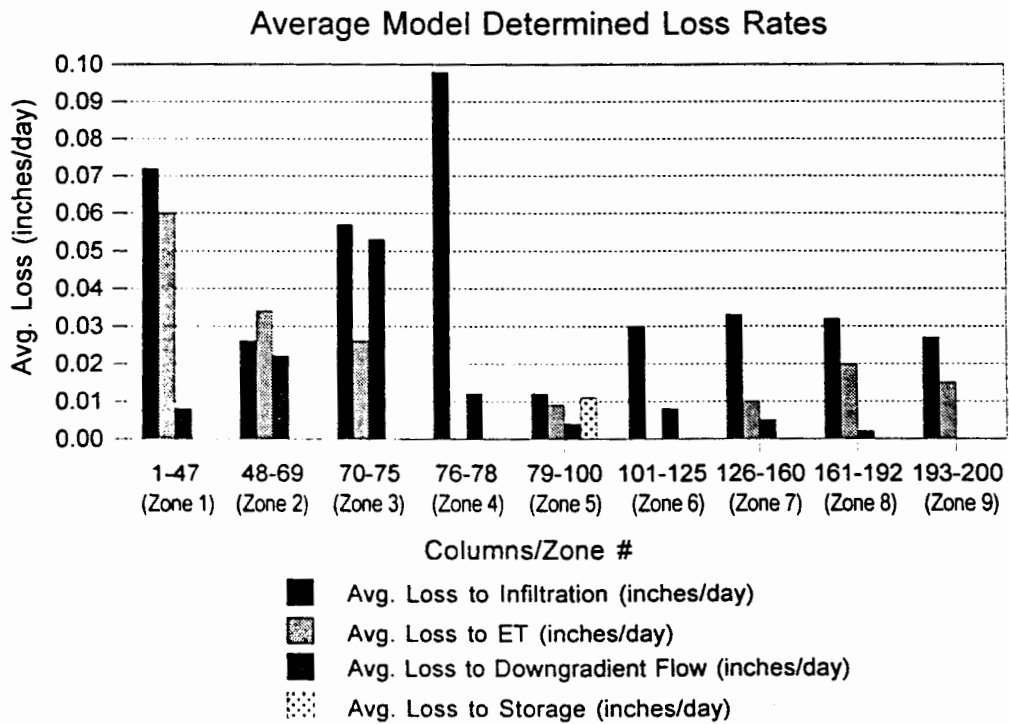
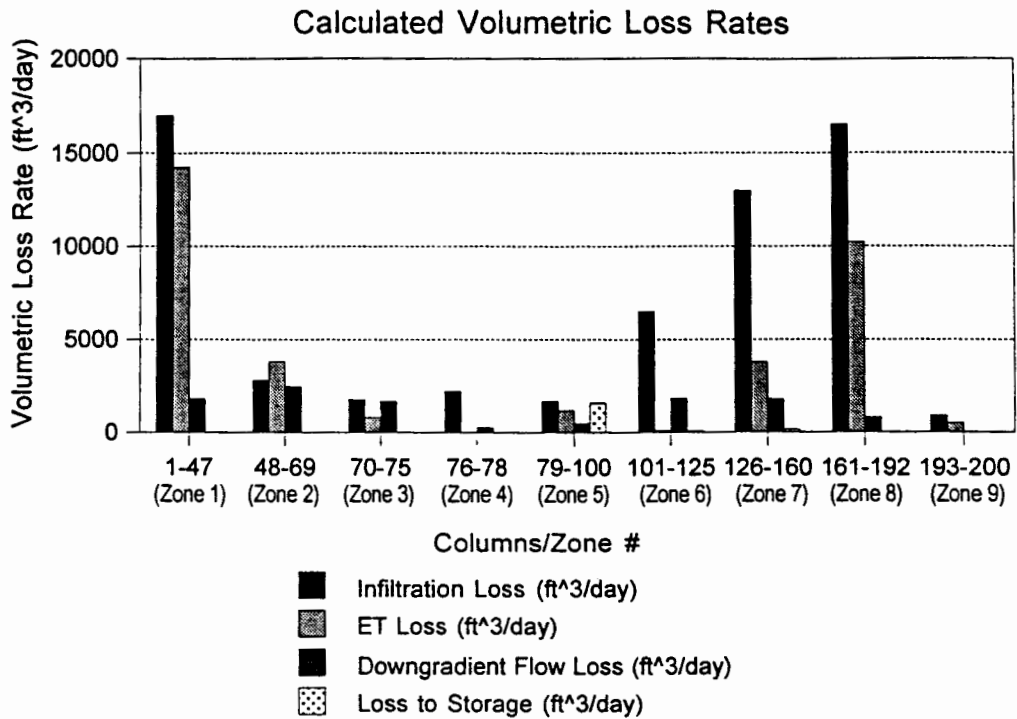


Figure 65: Model AL1296T7 (Transient-Period 7) Zonebudget Results

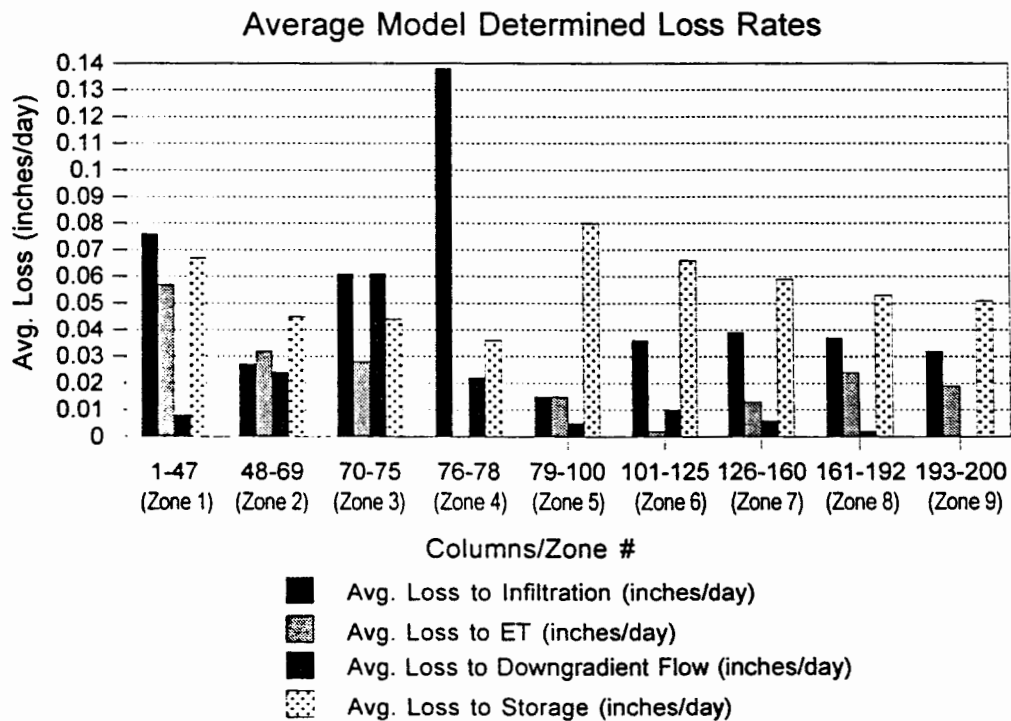
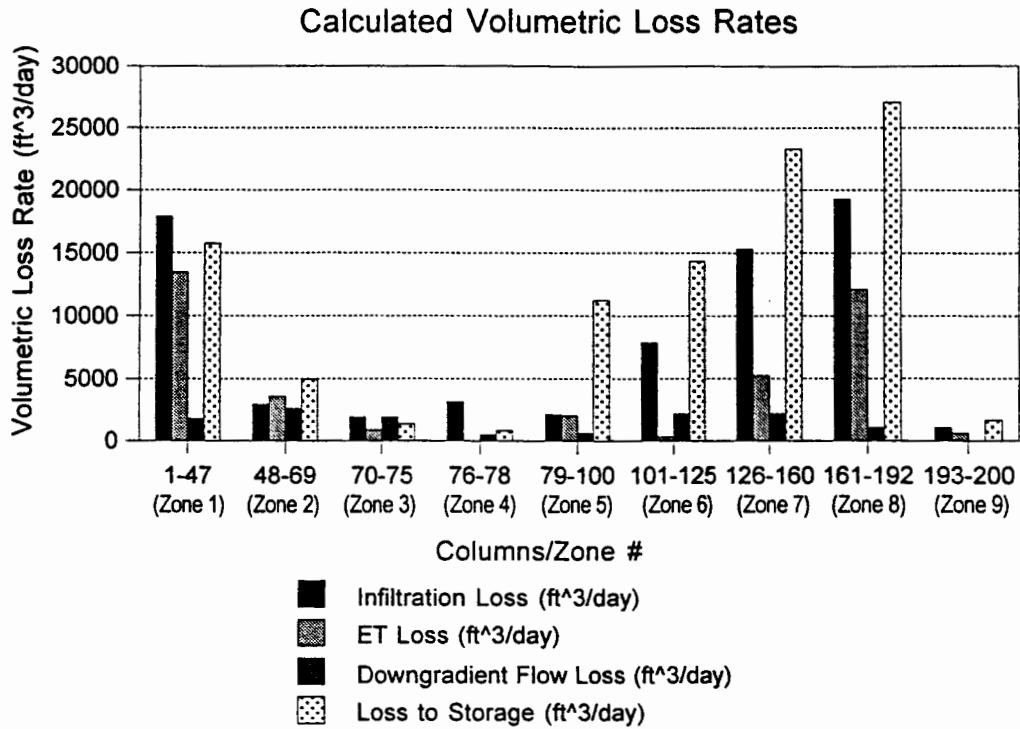


Figure 66: Model AL1296T8 (Transient-Period 8) Zonebudget Results

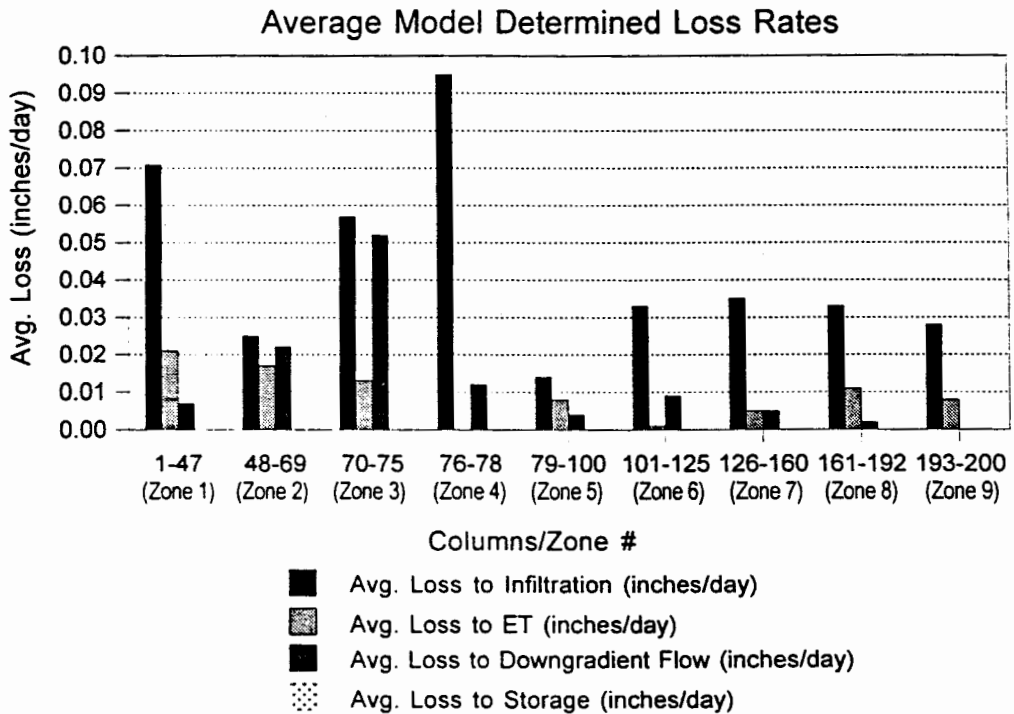
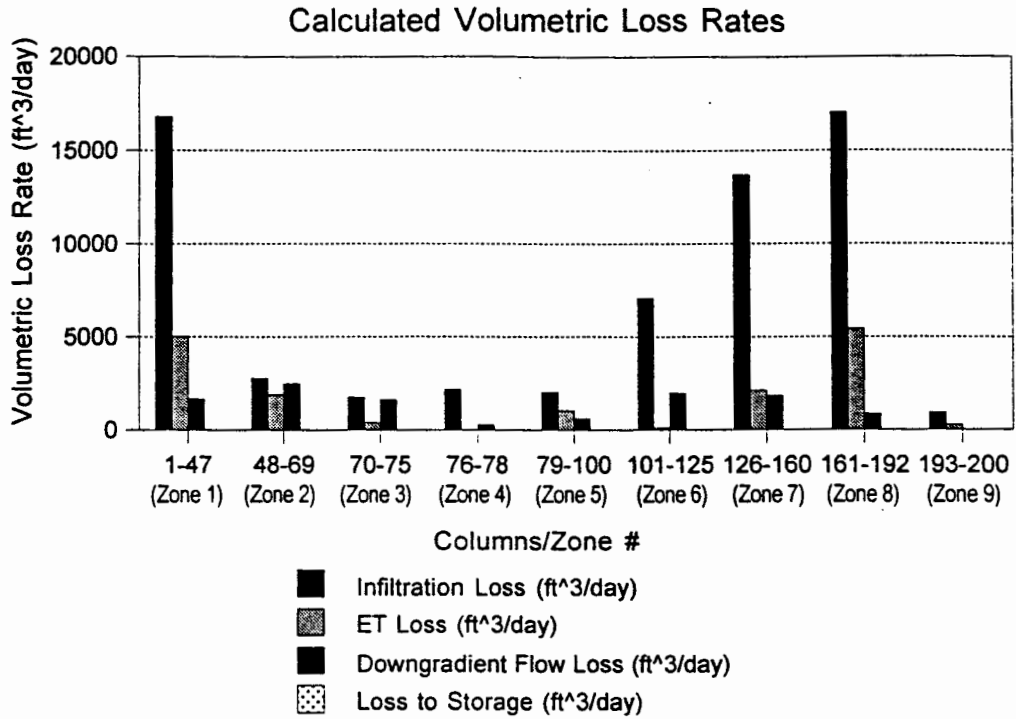


Figure 67: Model AL1296T9 (Transient-Period 9) Zonebudget Results

shows the steady-state model ZONEBUDGET results) that where the amounts of loss to storage are minimal to absent, the loss rates for the other budget components are (not surprisingly) quite similar to those determined in the steady-state simulation. However, where storage effects are present, the other budget components showed fairly substantial reductions in loss rates from the steady-state results.

For example, in zones 1-4 during period 1 where storage losses are minimal, the daily rates of infiltration, ET, and downgradient flow are nearly identical to the steady-state results, with the greatest infiltration totaling nearly 0.12 inches in zone 4, and ranging between about 0.025 inches and 0.08 inches in zones 1-3. The daily rates for ET and downgradient flow in zones 1-4 during period 1 are also nearly identical to the steady-state results, with downgradient flow increasing from less than 0.01 inches in zone 1 to about 0.06 inches in zone 3 while ET varied between about 0.02 inches and 0.05 inches in zones 1-3. As in the steady-state model, there is no ET loss in zone 4, and the daily downgradient flow loss there is less than 0.02 inches.

In zone 5 however, the daily loss to storage dominates the budget and totals nearly 0.05 inches. The daily infiltration loss at about 0.01 inches is less than one-half the steady-state daily loss of 0.024 inches in this zone, while daily ET and downgradient flow losses at about 0.003 inches are significantly reduced from the steady-state daily losses of about 0.02 inches and 0.01 inches respectively. In zones 6-9, the daily storage losses are not as great, averaging about 0.02 inches. Daily infiltration, which was about 0.04 inches for these zones in the steady-state model, dropped by about 25% in the transient model, while the ET and downgradient flow losses which were relatively low in the steady-state model, dropped by much smaller amounts.

For the entire study area west of State Road 4, infiltration still dominated the budget in the transient simulation for period 1, representing ~51% of the total losses, while storage losses were ~23%, followed by ET at ~21% and downgradient flow at ~3% of the total losses. In comparison, the total study area results from the steady-state

simulation indicated that infiltration was ~69%, ET was ~28%, and downgradient flow was ~3% of the total budget losses. It thus appears that under conditions with moderate storage effects, the loss component most effected is infiltration which undergoes a fairly substantial reduction in both magnitude and relative proportion.

Figure 60 (transient simulation results for stress period 2) illustrates the response of the system to a significant recharge event after generally dry conditions. It shows that storage losses dominated the system's budget in period 2, which is a logical result since the period was defined to encompass the dynamic head increase observed in the LAO-3 hydrograph at that time. The storage component provides the mechanism for the head increase as the response to the undercapacity of the system's other losses to maintain equilibrium in the system. The model results quantify these relations.

As is seen in the upper graph, whereas significant daily storage volumes are accommodated in the upper part of the system relative to the other losses (totaling ~190,000 ft³ in zones 1-4 compared to ~28,000 ft³ for infiltration, ~8,000 ft³ for ET and only 542 ft³ for downgradient flow), the lower part of the system accumulated huge daily volumes of storage relative to the other losses (totaling ~550,000 ft³ in zones 5-7 compared to ~23,000 ft³ for infiltration, ~4,000 ft³ for ET, and ~2,000 ft³ for downgradient flow). The lower graph shows that the average storage rate was generally consistent throughout the model however at ~0.7 inches/day except in zone 1 where it was ~0.3 inches/day. The total study area average infiltration rate showed only a 5% increase over period 1 with most of the increases occurring in zones 1, 3, and 4, while it actually decreased in zone 5. The ET rate in zone 1 decreased by 58% from period 1, and by 75% in zone 5. Elsewhere the ET losses were relatively unchanged, as were the losses to downgradient flow except in zones 1, 3, and 4 which saw increases of 38%, 19%, and 41% respectively.

Figure 61 shows that following the massive accumulation of storage in period 2, the effects of storage disappeared almost completely in period 3, which is again a logical

situation since period 3 was defined for a receding water table. As such, the pattern of losses in the system is quite similar to that for the steady-state simulation with somewhat greater ET in zone 1 and slightly reduced infiltration in zones 6-9. In zone 5 where a small amount of storage loss continued (almost 0.01 inches/day), infiltration dropped by 80%, ET by 95%, and downgradient flow by 70% from the steady-state rates.

Figure 62 shows the return of storage effects in period 4, with daily rates of about 0.01-0.02 inches in zones 1, 3, and 4 and about 0.03 inches in zones 2 and 6-9, while its highest rate was in zone 5 at just over 0.06 inches/day. However, infiltration losses and downgradient flow losses were virtually unchanged from period 3, while ET dropped by 61% for the total study area, mostly in zone 1. This was due to the fact that freezing conditions accompanied by initial snowpack accumulation were mainly prevalent in only the upper basin portion of the watershed during this time.

Figure 63 shows the disappearance of storage effects again in period 5, with a pattern of losses that is highly similar to that determined for period 3, with the exception that ET in zone 1, which was nearly 0.07 inches/day in period 3, dropped to about 0.01 inches/day in period 5, about the same as was determined for period 4. This was due to the fact that period 5 was during the winter freeze-up, and ET rates are known to decline then (see Figure 14). ET declines in the other zones were not as dramatic, with reductions of about 50% or less from those determined in period 4.

Figure 64 shows the return of storage effects again during period 6, which represented the spring/summer snowmelt runoff period accompanied by a significant rise in water levels followed by a relatively prolonged period of more or less steady state conditions in the alluvial system. However, the graphs do not illustrate this as dramatically as was seen in period 2 because the increase was averaged over a time of 138 days, the longest defined stress period in the simulation, compared to only 4 days for period 2, the shortest stress period. In retrospect, this is seen as a major cause of model performance deficiency in that the overly lengthy stress period averaged out the dynamics of the initial

recharge stresses and adversely affected the model's ability to produce the head response (and thus storage increase) with the necessary resolution. As such, apart from the inclusion of moderate rates of storage, the pattern and magnitudes of losses are nearly identical to those determined for period 5 as well as in the steady-state simulation, with the exception of ET increases averaging 275% for the entire study area over period 5.

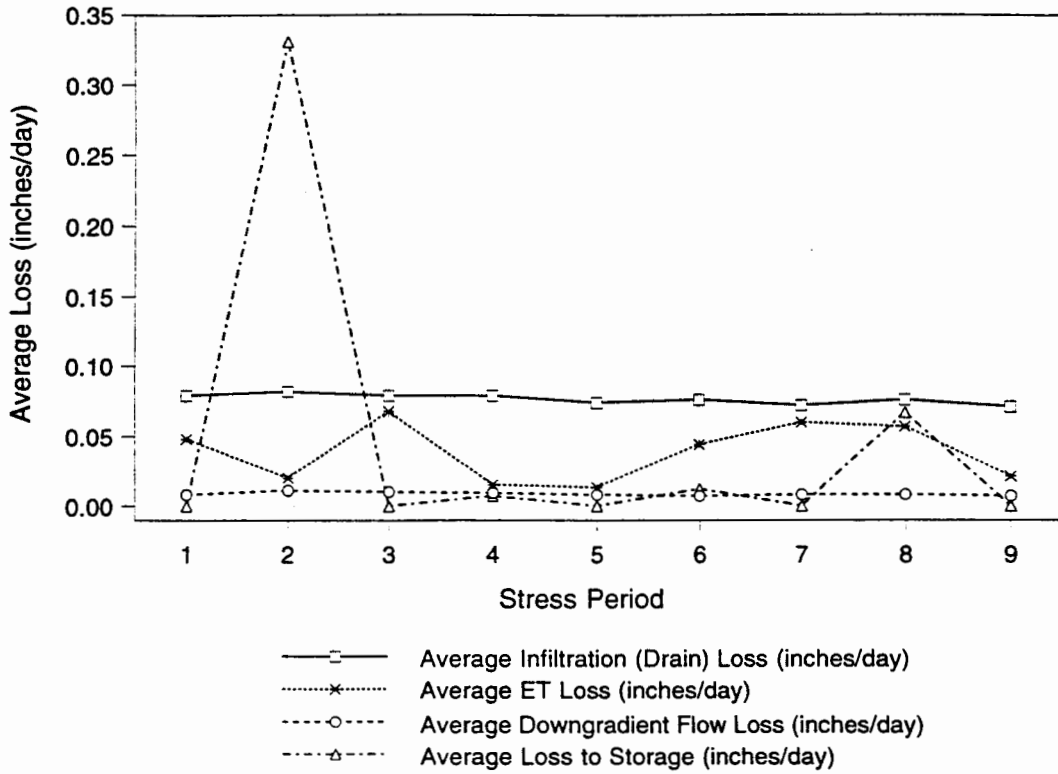
Figure 65 shows the subsequent disappearance of storage effects under the recessionary conditions of period 7. As such, the pattern and magnitudes of losses are quite similar to those determined for period 3, which represented similarly dry climatic conditions. Infiltration rates are only slightly decreased (average -9%) from those determined in period 6. The biggest difference from the preceding period was the 40% average increase in ET, which occurred mostly in zones 1-3.

Figure 66 shows the return of significant storage effects in period 8, which was due to the water level rise in the system in response to the summer monsoons, and is particularly evident because the stress period was only 39 days long and thus did not average out the initial recharge stress so much as was done for period 6. Storage dominated the budget losses and represented ~48% of the total study area losses for the period, while infiltration, ET, and downgradient flow represented ~34%, ~17%, and ~1% of the total losses respectively. Total infiltration increased by 15% over period 7, while the rates for ET and downgradient flow were essentially unchanged.

Figure 67 shows the results for the final recessionary conditions in period 9. The total study area losses to infiltration dropped by 11% from period 8, and ET decreased by 59%, accompanied by the complete disappearance of storage effects in the system.

These graphs illustrate that not only are there substantial variations among the loss components of the hydrologic budget within the different zones of the model, but also that the loss rates can vary significantly over time. The variations in average loss rates over time (by stress period) for each zone in the study area are shown in Figures 68-74. The most apparent feature in each of these figures (seen in the upper graphs) is the huge

Zone #1 Average Losses



Zone #1 Average Losses (Expanded Scale)

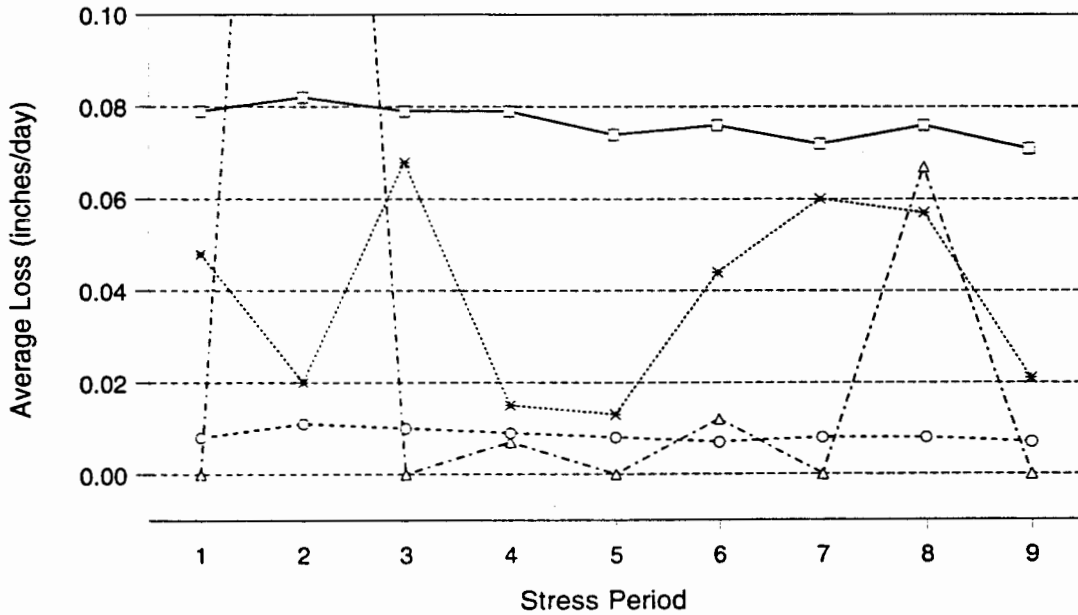


Figure 68: Transient Models Zone #1 Zonebudget Results Variation Over Time (Model Columns 1-47)

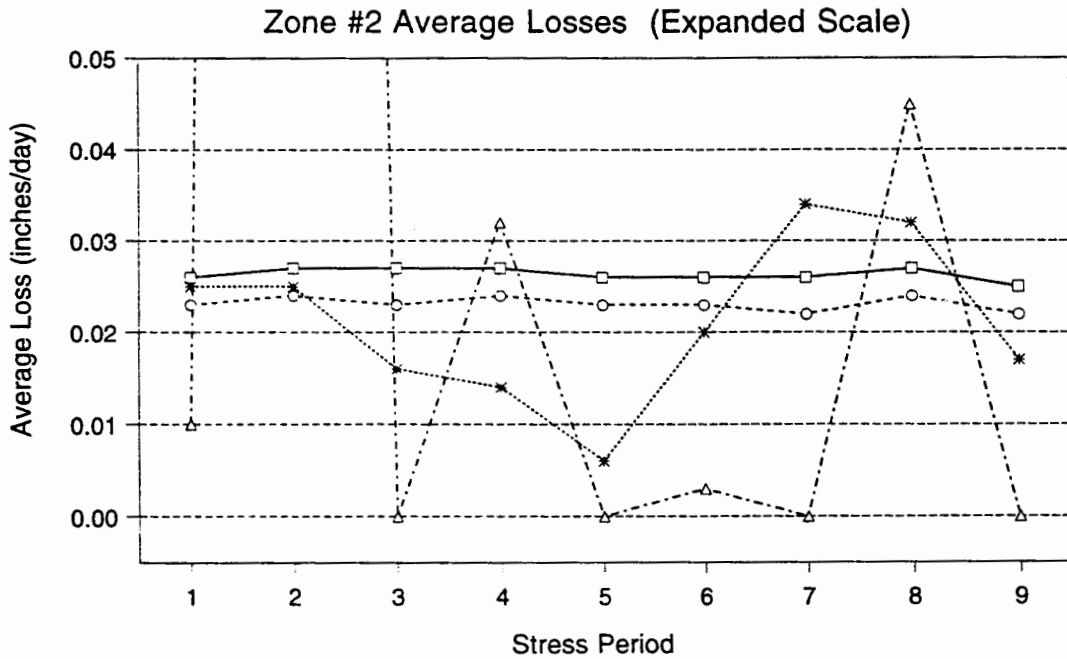
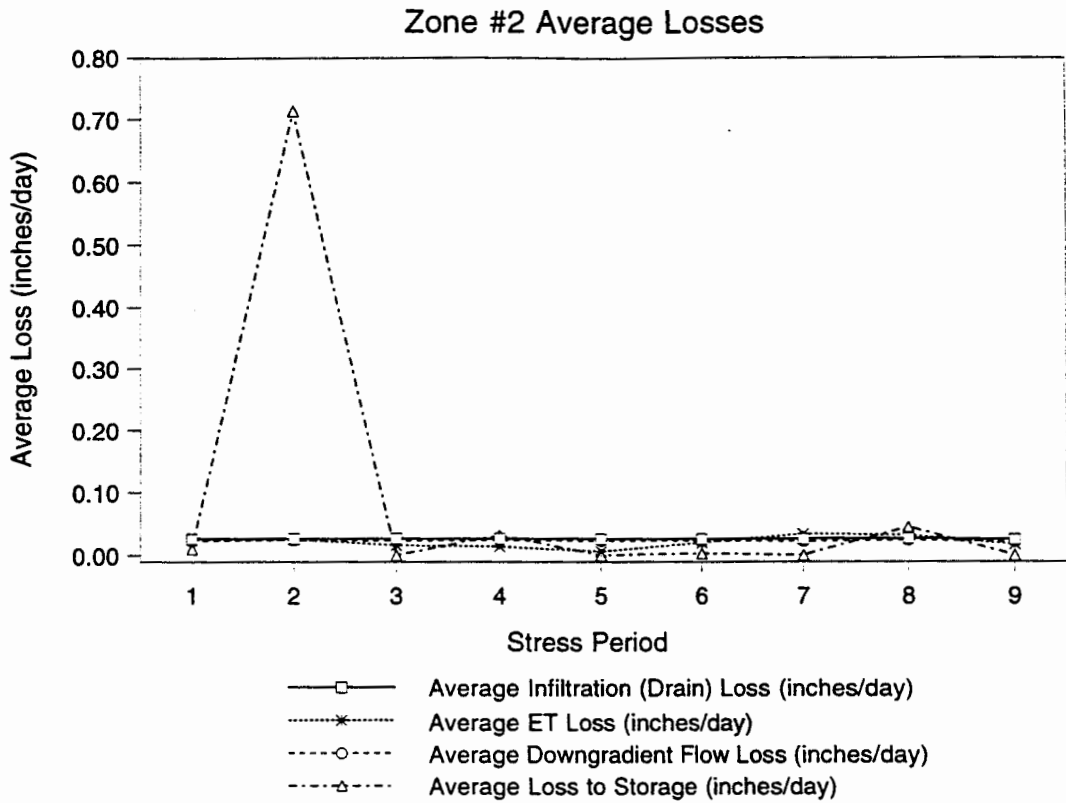


Figure 69: Transient Models Zone #2 Zonebudget Results Variation Over Time (Model Columns 48-69)

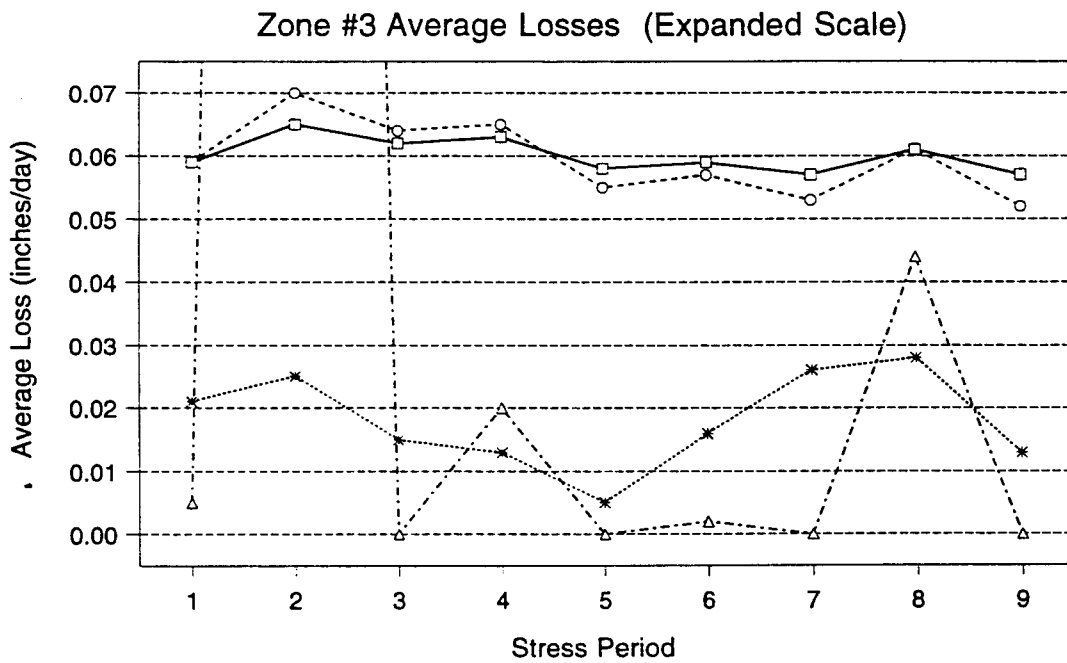
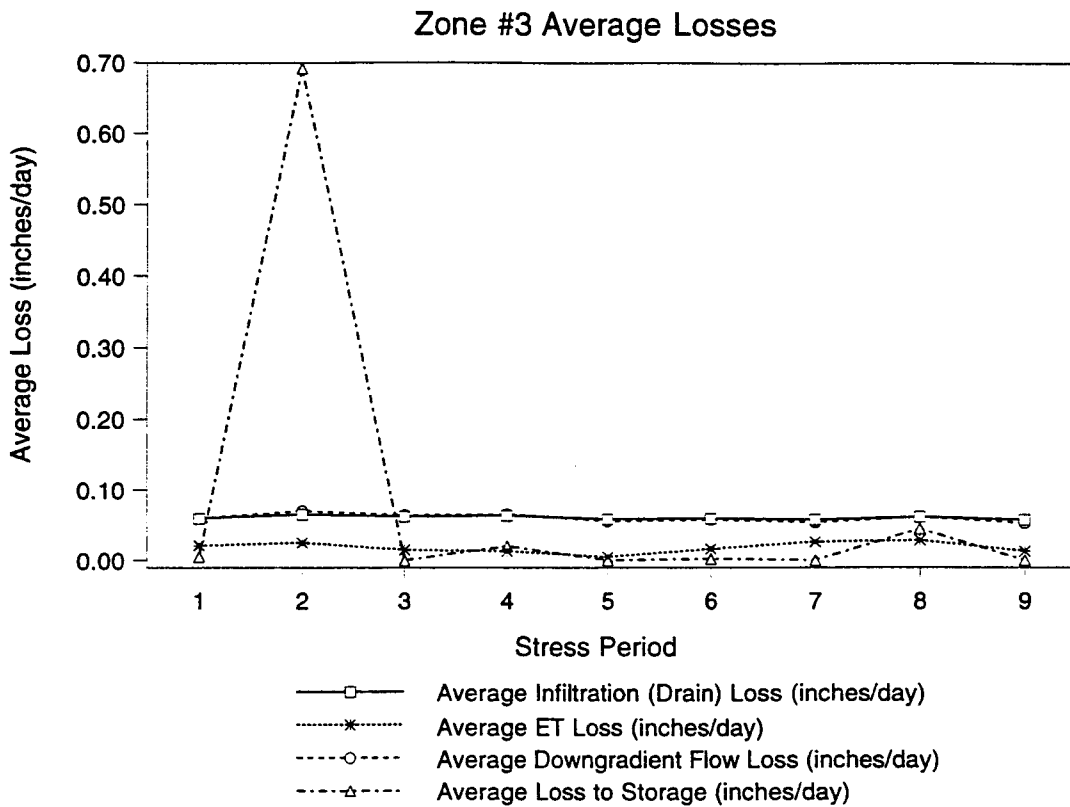
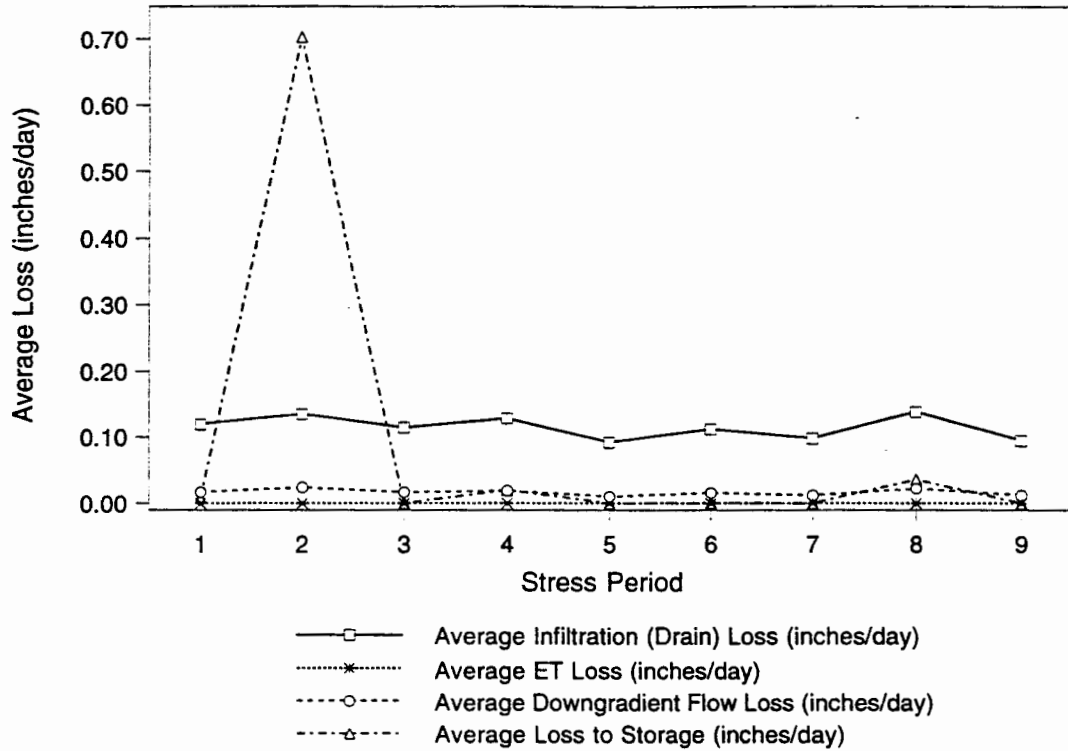


Figure 70: Transient Models Zone #3 Zonebudget Results Variation Over Time (Model Columns 70-75)

Zone #4 Average Losses



Zone #4 Average Losses (Expanded Scale)

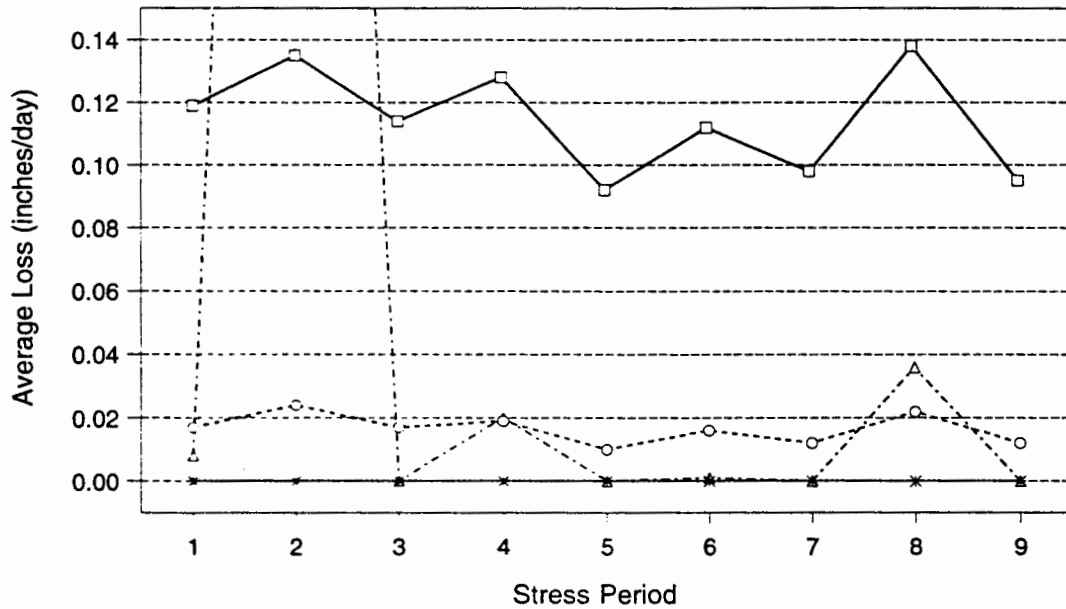


Figure 71: Transient Models Zone #4 Zonebudget Results Variation Over Time (Model Columns 76-78)

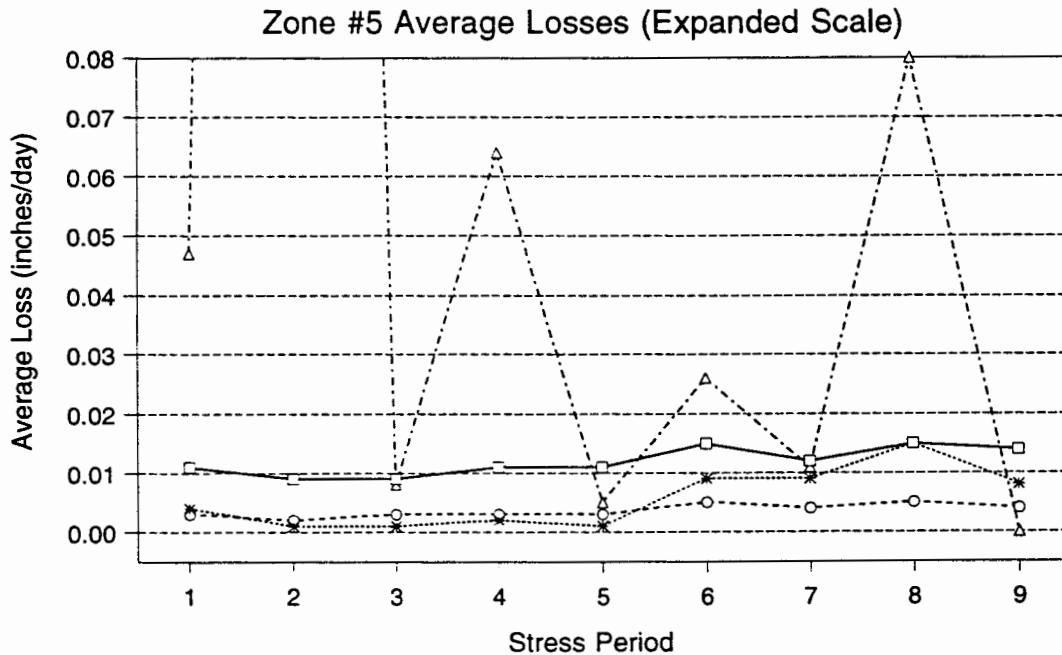
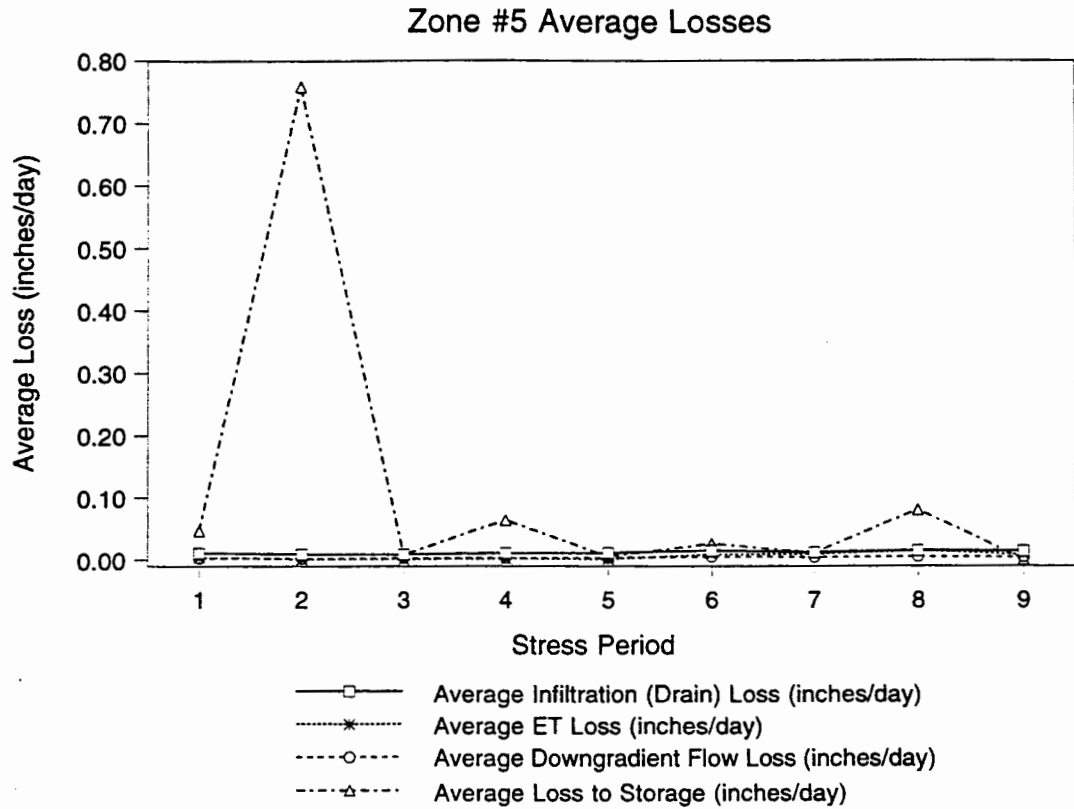


Figure 72: Transient Models Zone #5 Zonebudget Results Variation Over Time (Model Columns 79-100)

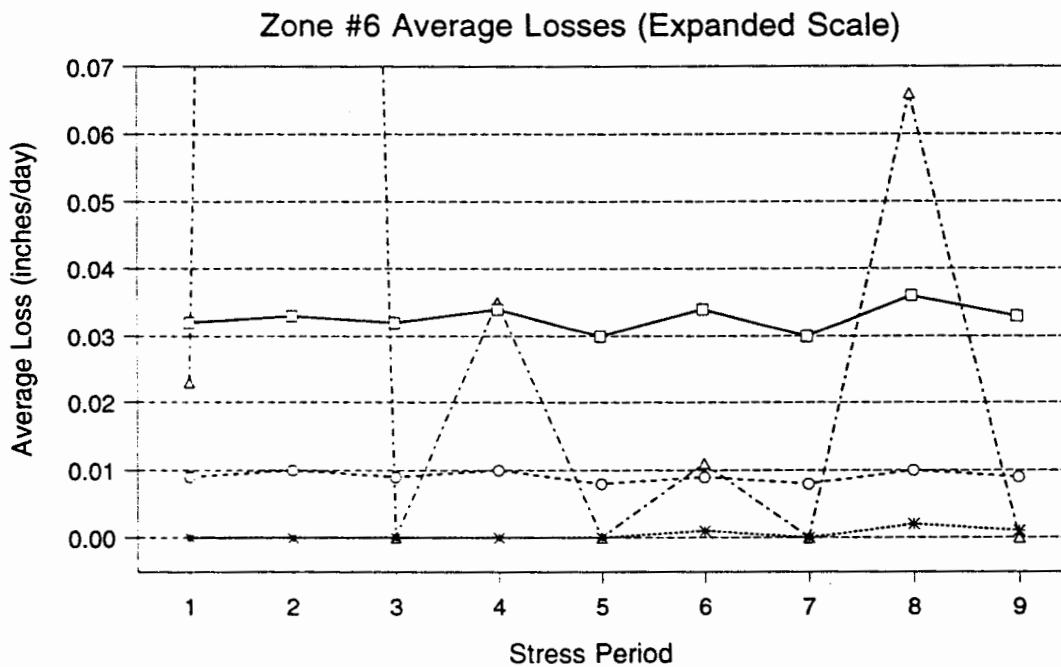
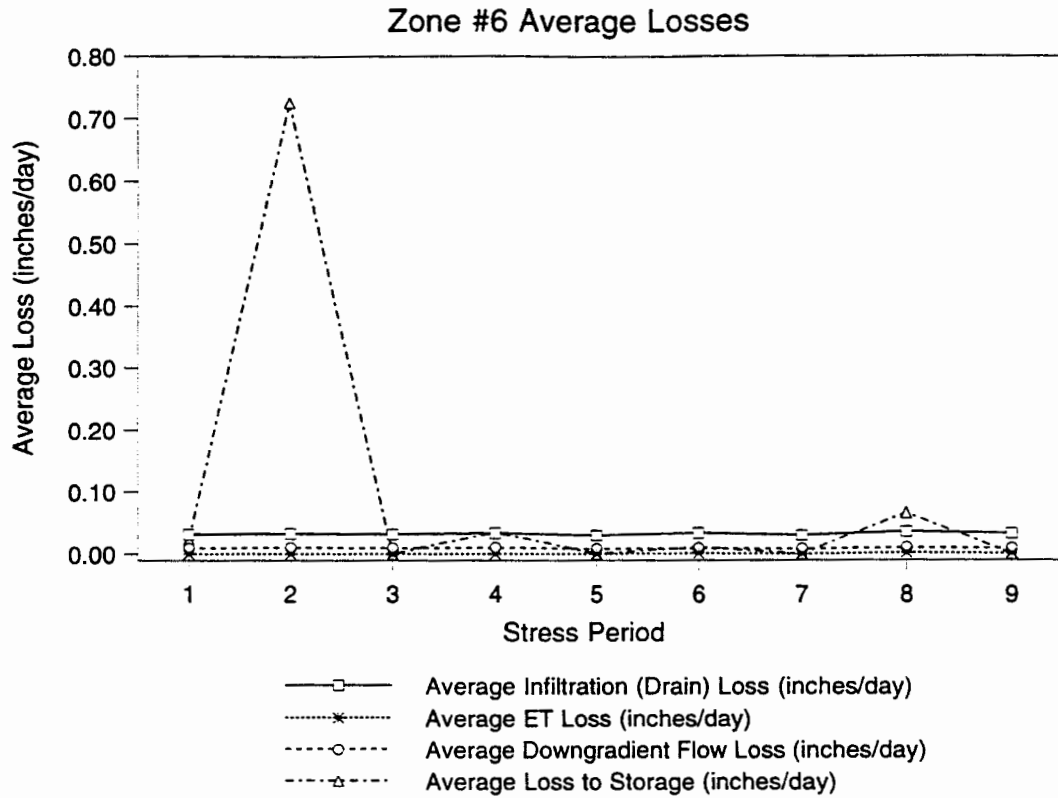


Figure 73: Transient Models Zone #6 Zonebudget Results Variation Over Time (Model Columns 101-125)

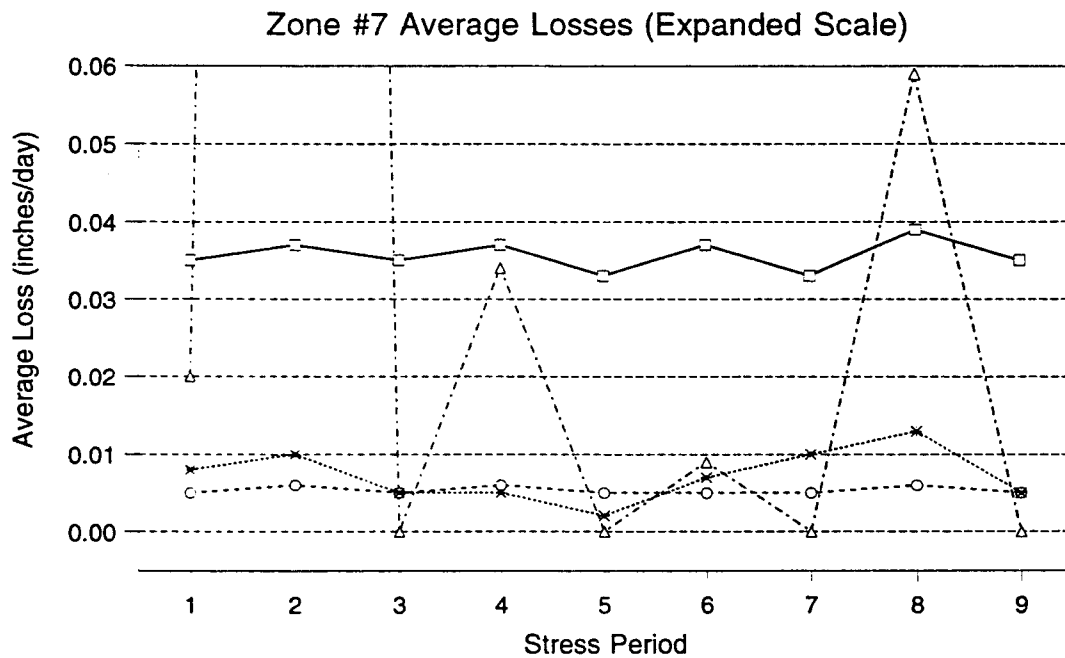
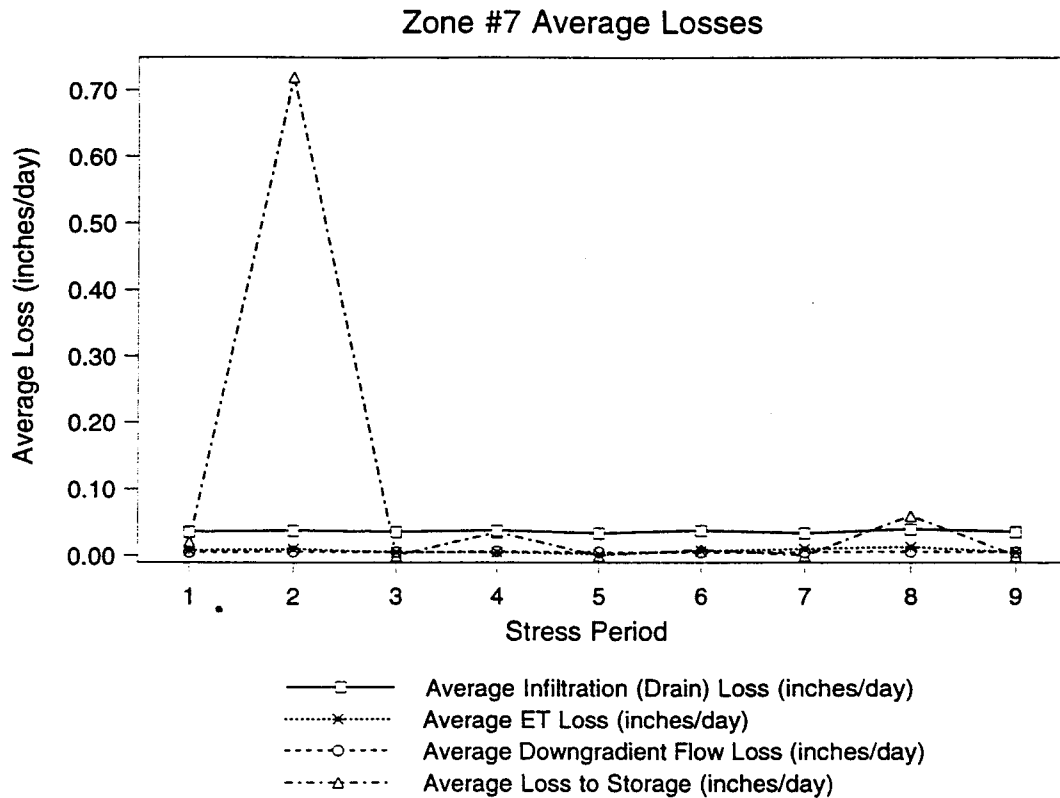


Figure 74: Transient Models Zone #7 Zonebudget Results Variation Over Time (Model Columns 126-160)

increase in storage which was determined for period 2. The size of this anomaly is due to the short length (only 4 days) of period 2 which defined a significant precipitation event and produced a level of resolution in model response that was not achieved at any other times during the simulation since the lengths of all the other stress periods were between 24 and 138 days. Because of the discrepancy in response magnitudes between period 2 and the other stress periods, the graphs were replotted at an expanded scale to adequately depict the variations in the budget loss components over the remaining stress periods (seen in the lower graphs). The variations in average losses for each loss component for the entire study area west of State Road 4 (zones 1-7) are shown in Figure 75.

These graphs show that while there were substantial differences in infiltration from zone to zone, the variations between stress periods were fairly minor with total daily loss differences of generally less than 0.005 inches throughout the simulation, with the one exception of zone 4. In this zone, daily infiltration losses varied between 0.09 and 0.14 inches and the temporal fluctuations were accentuated by the high drain conductances required there to simulate the enhanced infiltration seepage into the Guaje Mountain fault zone. Aside from the storage losses, the component that showed the most variation was ET. However, the biggest differences in the daily ET loss rates were only seen in zones 1 (about 0.02-0.06 inches), and zones 2 and 3 (about 0.01-0.03 inches). In zones 4-7, ET hardly ever exceeded 0.01 inches/day. Downgradient flow, while varying somewhat from zone to zone, was the most stable component with total variations of generally less than 0.005 inches/day during the entire simulation except in zone 3 where it fluctuated between 0.05 and 0.07 inches/day. Even excluding period 2 however, storage losses showed the greatest variability over time, with the largest deviations seen in zone 5 where it varied between 0.005 and 0.08 inches/day outside of period 2. For the entire study area (Figure 75), average daily losses were about 0.04-0.045 inches for infiltration, about 0.005-0.02 inches for ET, and 0.0 to about 0.06 inches for storage outside of period 2 when it exceeded 0.6 inches, while downgradient flow consistently averaged 0.002 inches/day.

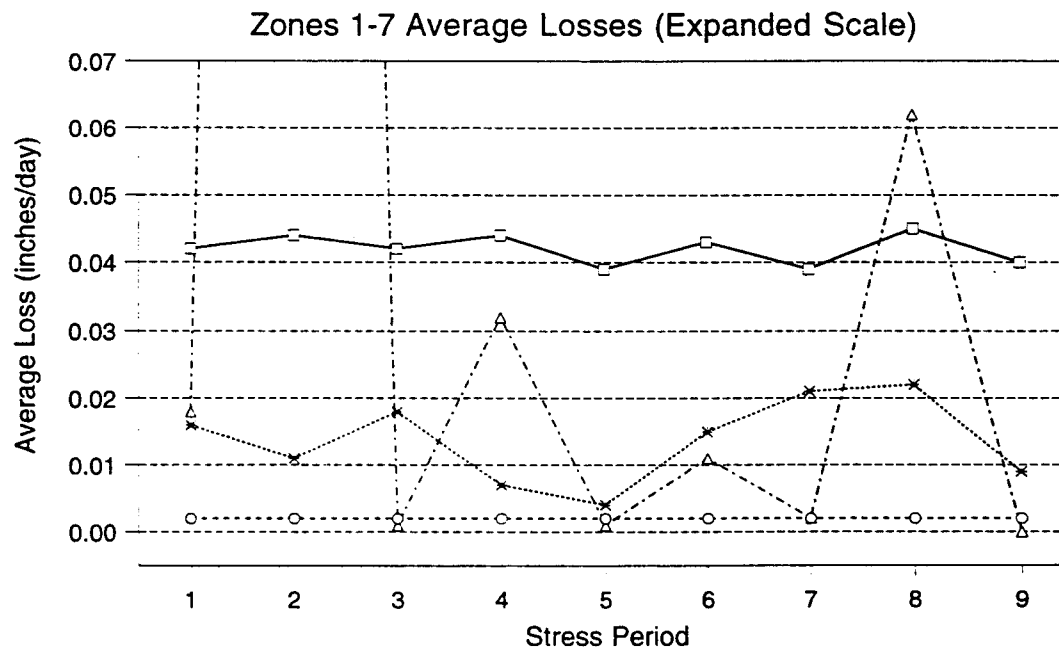
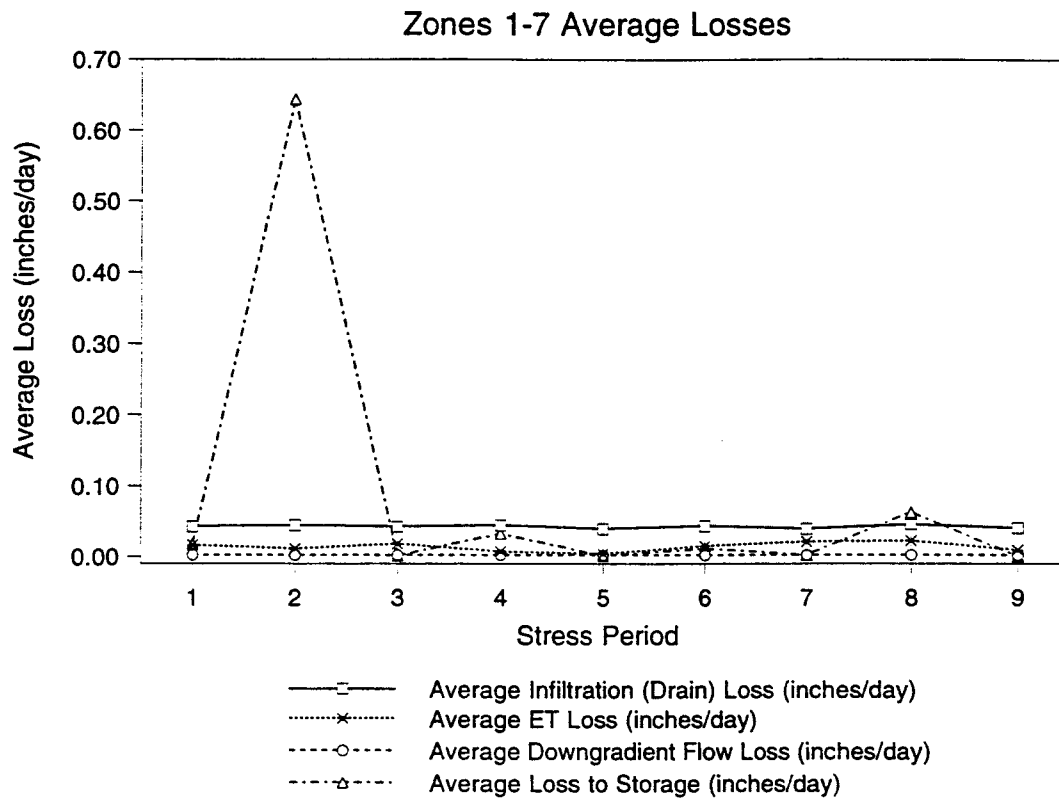


Figure 75: Transient Models Zones 1-7 Zonebudget Results Variation Over Time (Model Columns 1-160)

Sensitivity Analysis

A sensitivity analysis was performed in order to quantify the levels of uncertainty in the model that may be attributed to errors introduced by uncertainties within the assumed hydrologic parameters and stresses that were applied to the calibrated model. This was accomplished by incrementally varying the parameters and stresses up and down within their plausible range and evaluating the impact of these variations on the model results in terms of the magnitude of head changes from the head distribution produced by the calibrated steady-state model.

For the steady-state model, the varied parameters and stresses were hydraulic conductivity (K), recharge, ET, and the ET extinction depth. These parameters were varied by negative and positive 25% increments from the assumed values used in the steady-state simulation (see Table 7) within the expected minimum and maximum values, with the exception of vertical hydraulic conductivity (K_v) which was only varied by the negative increments as it was apparent that adjustments of this parameter had no effect on the simulation results. This process entailed running a total of 32 additional simulations with the steady-state model, for which the model determined heads at the locations of each of 9 alluvial wells were compared to the calibrated steady-state heads (each of which were matched to the actual 4/28/95 well data except for wells LAO-C and LAO-6). For each simulation, the mean head change, mean absolute head change, and root mean squared head change were determined from the deviations for each well. The results from each of these simulations along with the various applied stresses and parameter values are included in Appendix BB.

A similar analysis was also conducted on one of the transient simulations in order to assess the impact of hydrologic parameter and model stress uncertainties under transient conditions. The same procedure as outlined above was applied to the model for stress period 6, except for the additional inclusion of the S_y storage parameter, and the exclusion of K_v since the previous analysis showed that this parameter was not relevant to the model.

A total of 36 additional simulations were run with the transient model. The values of the various applied stresses and hydrologic parameters and the simulation results are included in Appendix CC.

The head changes at each well for each hydrologic parameter or stress increment determined in the steady-state model analysis are shown in Figures 76-79. These graphs depict the spatial distribution of head residuals reflecting differences in sensitivity to the parameter and stress variations within different portions of the model.

Figure 76 illustrates the various head changes resulting from the adjustments to hydraulic conductivity. This parameter was varied within the minimum and maximum values determined from the slug test results (see Table 7). The range of variability tested was from -87.5% to +151% of the 9.6×10^{-3} cm/s value used in the calibrated steady-state model. It is seen that with the exception of one well, most portions of the model were not overly sensitive to changes in this parameter. The maximum value applied resulted in less than one foot of head change for wells LAO-B, LAO-0.6, LAO-3, and LAO-4. Head changes totaled less than 2 feet for wells LAO-0.3, LAO-0.8, LAO-0.91, and LAO-6 at the maximum value. The one well which showed heightened sensitivity to hydraulic conductivity variations was LAO-C, for which the head change was nearly 8 feet at the maximum value. Reductions in the parameter had somewhat different effects for some wells. LAO-0.3 and LAO-0.91 exhibited total head changes of about 3.5 feet whereas LAO-B showed about a 2 foot change at the minimum applied value.

The behavior of model responses to adjustments in hydraulic conductivity was more complex than was seen for any of the other varied parameters or stresses. Different areas of the model reacted differently with respect to either increases or decreases in the parameter, and no discernible overall pattern was evident. For LAO-B, LAO-0.3, and LAO-0.91, increases in K resulted in lowered heads while decreases in K produced increased heads. At LAO-0.6, LAO-0.8, LAO-4, and LAO-6, increases in K caused increased heads and decreases in K led to lowered heads. In LAO-3, K increases had a

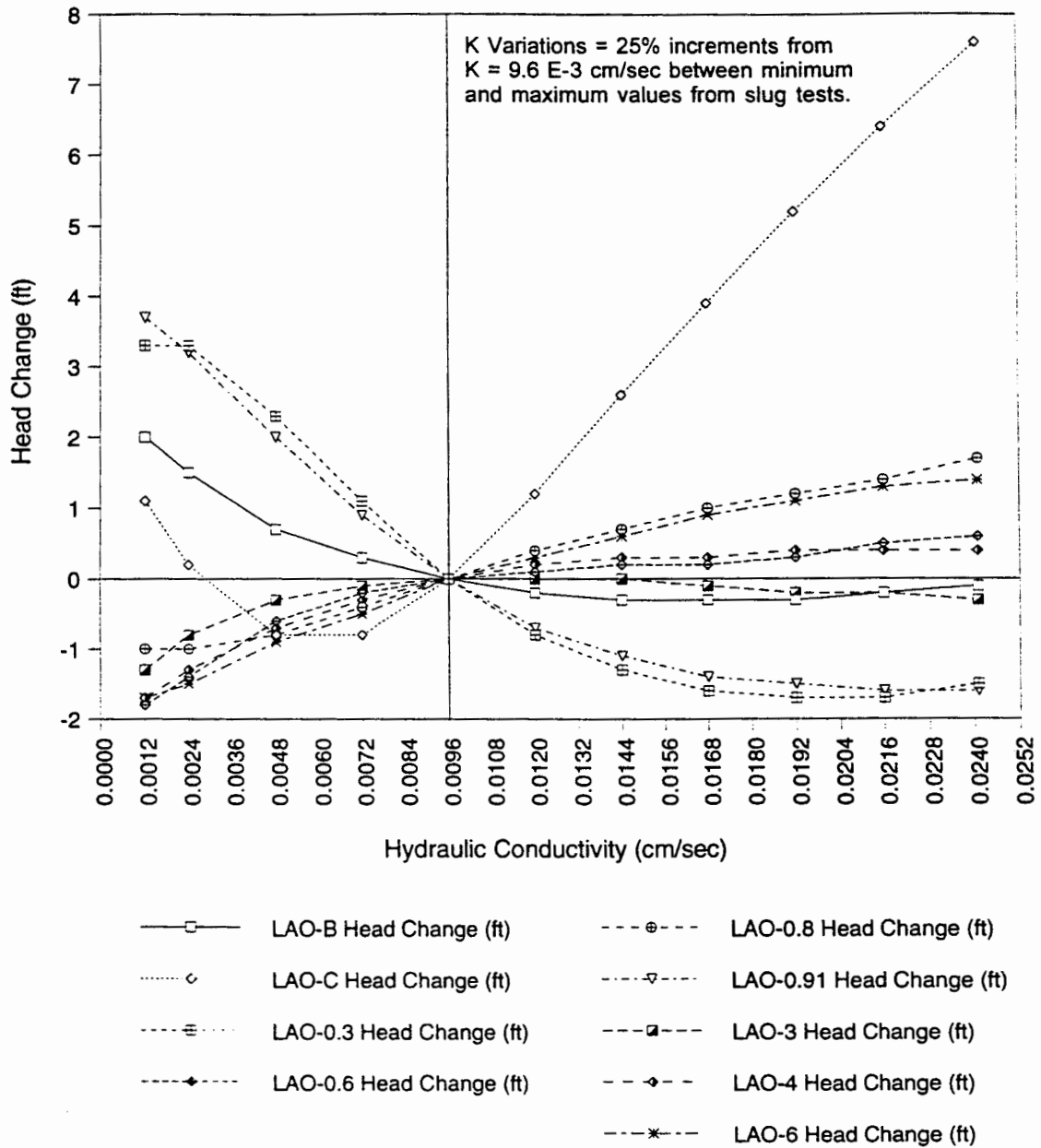


Figure 76: Model ALUV1196 (Steady-State) Sensitivity Results Head Change with Varying Hydraulic Conductivity

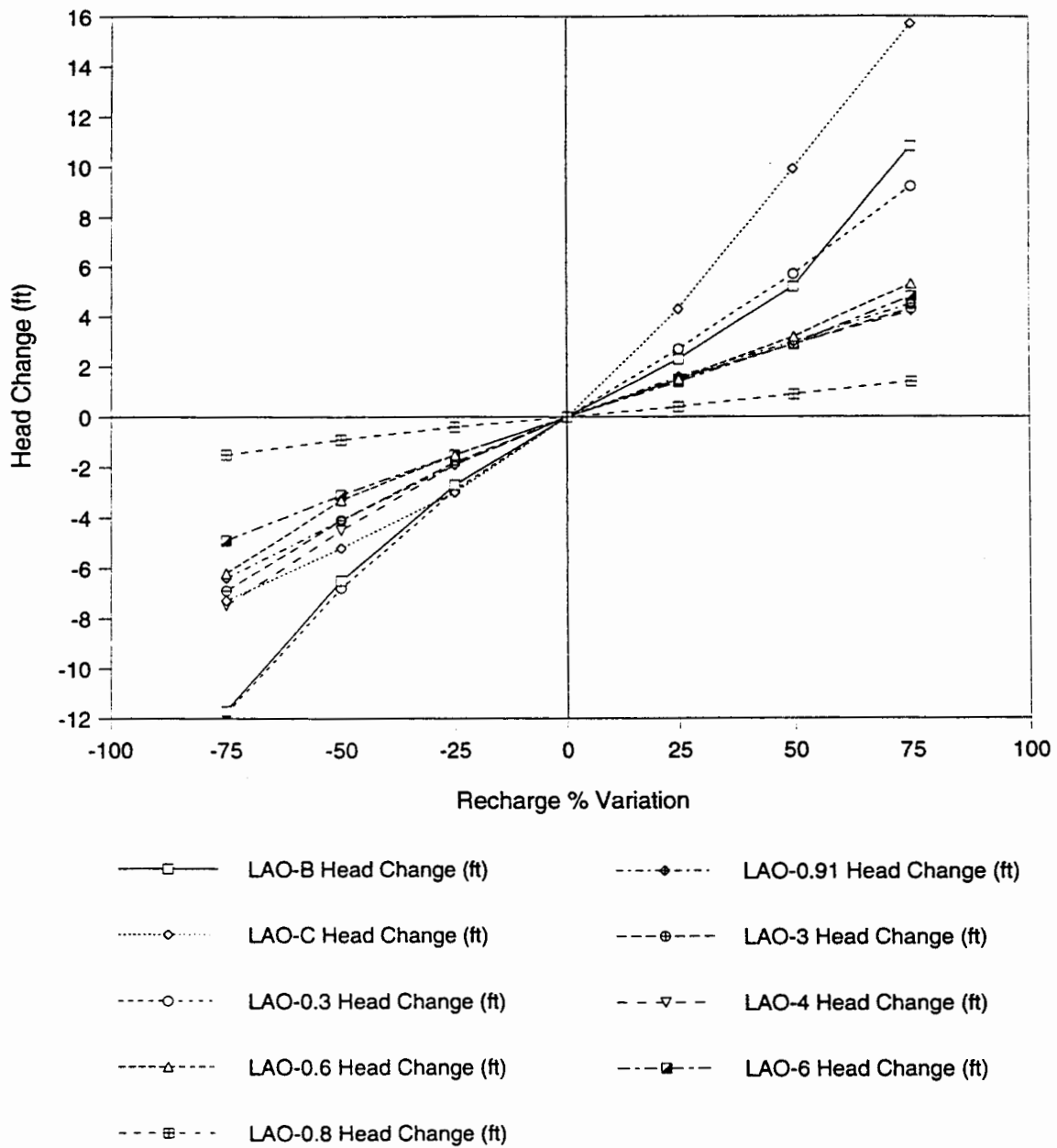


Figure 77: Model ALUV1196 (Steady-State) Sensitivity Results Head Change with Varying Recharge

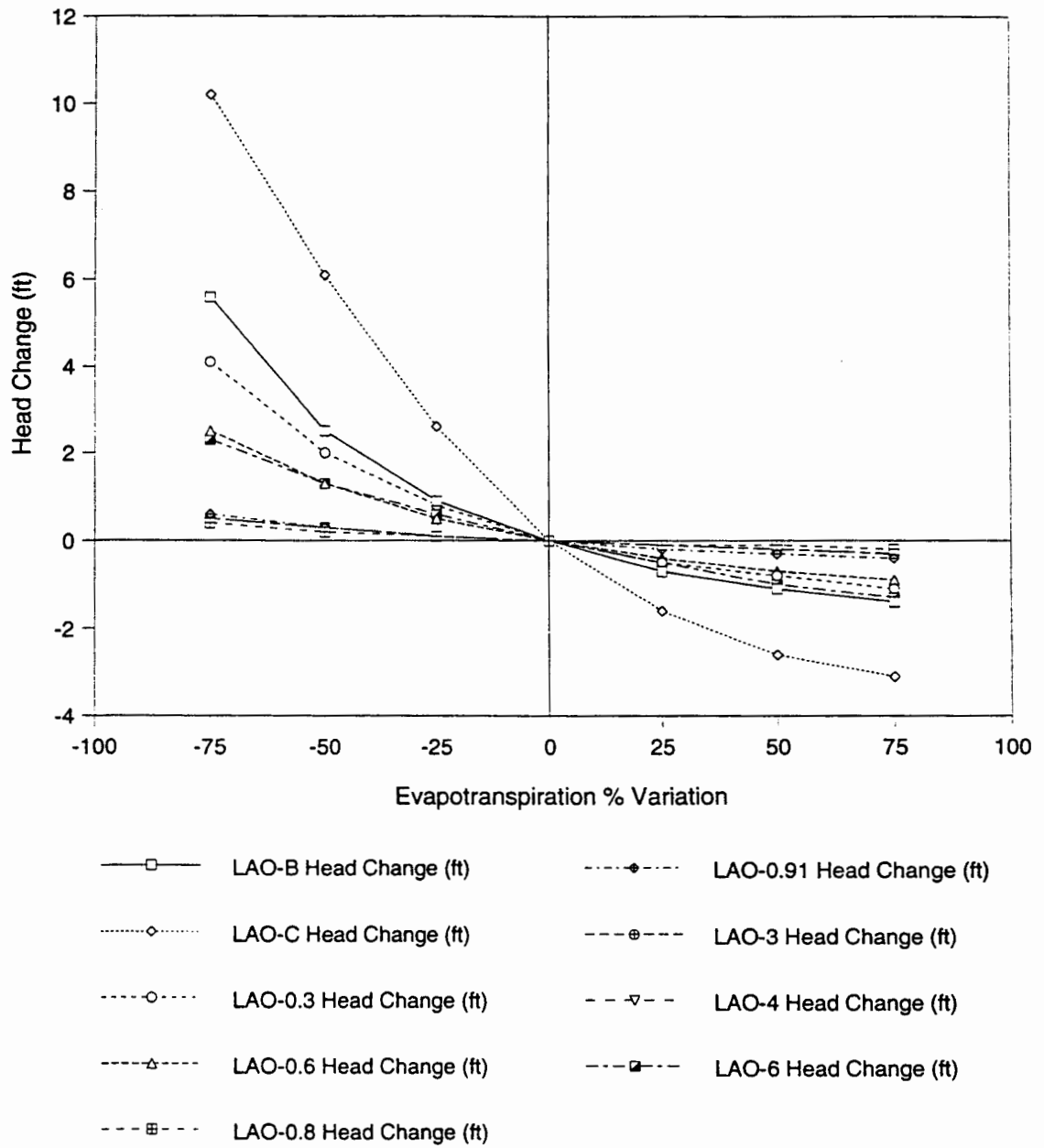


Figure 78: Model ALUV1196 (Steady-State) Sensitivity Results Head Change with Varying Evapotranspiration

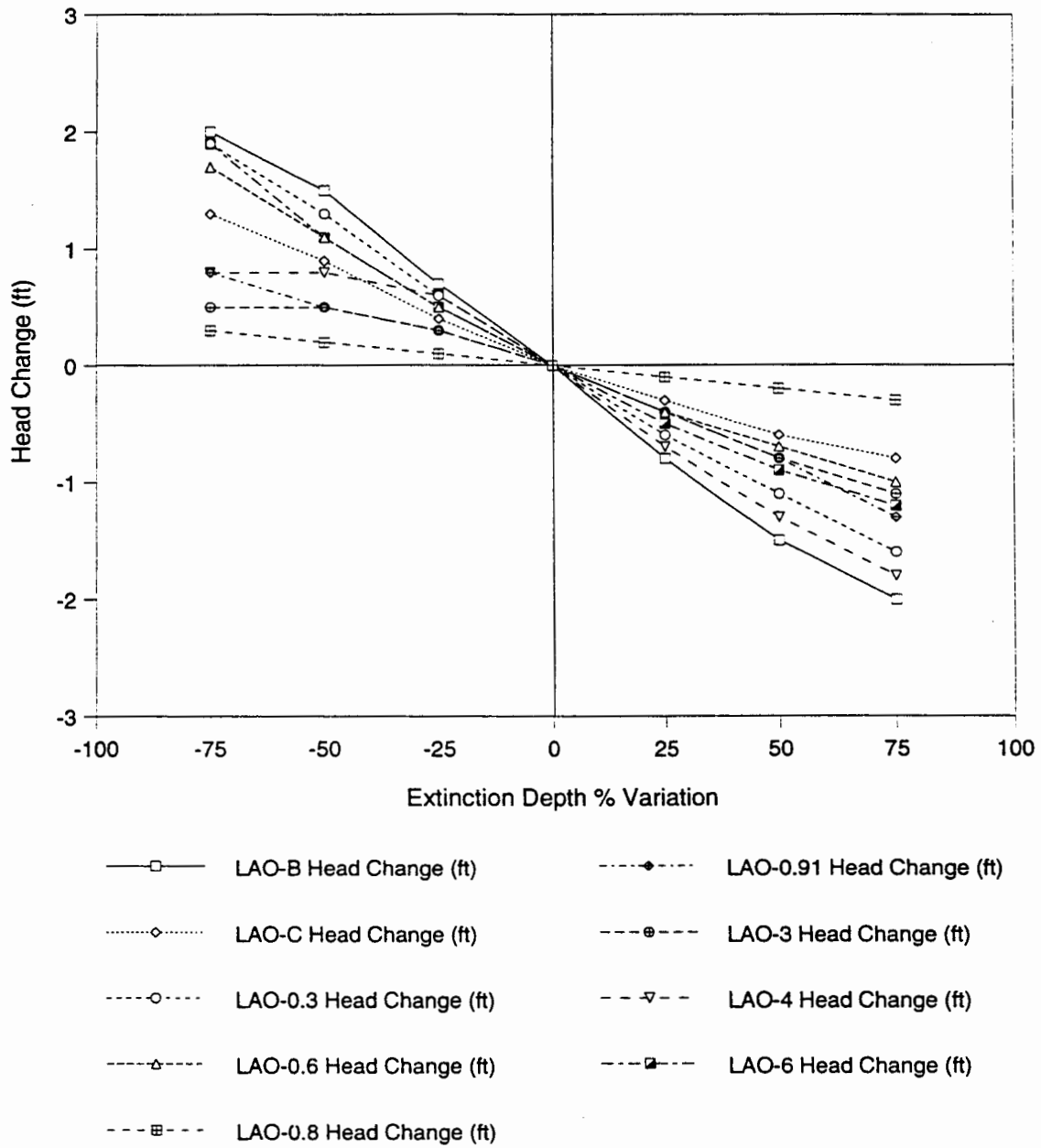


Figure 79: Model ALUV1196 (Steady-State) Sensitivity Results Head Change with Varying ET Extinction Depth

minimal head lowering effect, with a total decrease of only 0.3 feet at the maximum applied value, while decreases in K also caused lowered heads. LAO-C exhibited the most peculiar behavior, with increases in K producing anomalously large head increases. However, decreased K values resulted in lowered heads for the -25% and -50% increments, while increased heads were obtained for the -75% and -87.5% increments. Though it is not clear why, it is apparent that this portion of the model exhibits a particular degree of sensitivity to variations in the K parameter.

Figure 77 shows the results from adjustments to recharge. These results indicate that the model exhibited the greatest amount of sensitivity to changes in this parameter, with a maximum head increase of nearly 16 feet observed in LAO-C at the maximum applied value, and a maximum decrease of nearly 12 feet in LAO-C and LAO-0.3 at the minimum value. Elsewhere in the model, the degree of model responses varied substantially, with the minimum head changes occurring in LAO-0.8. The pattern of changes is logical with increased recharge causing raised heads, and vice versa. As with the K variations, the results for LAO-C indicate that this part of the model exhibits heightened sensitivity compared to the rest of the system.

Figure 78 displays the results from modifications in ET, and reveals that this parameter elicited the second highest degree of sensitivity in the model. Again, the largest responses were seen in LAO-C, with a maximum head increase of over 10 feet at the minimum applied value, and a maximum decrease of about 3 feet at the maximum value. The model was less sensitive to increases in ET than to decreases, as all the other wells showed maximum decreases of about one foot or less at the maximum applied ET, but showed substantially variant results for ET decreases, with maximum head rises ranging from less than one foot in LAO-0.8 and LAO-0.91 to nearly 6 feet in LAO-B. As was the case for recharge, the response pattern was rational, with ET increases resulting in lowered heads and ET decreases causing increased heads. As was determined in the K and recharge analyses, the distribution of responses also indicates that LAO-C represents an

area of elevated sensitivity in the model.

Figure 79 depicts the results from varying the ET extinction depth. Overall, the model was least sensitive to the changes in this parameter, as head decreases of less than one foot were produced in LAO-0.8, LAO-C, LAO-0.6, and LAO-3, while decreases between 1.0 and 2.0 feet occurred in LAO-6, LAO-0.91, LAO-0.3, LAO-4, and LAO-B at the maximum applied value. The minimum applied value resulted in head increases of less than one foot in LAO-0.8, LAO-3, LAO-0.91, and LAO-4, while increases between 1.0 and 2.0 feet were seen in LAO-C, LAO-0.6, LAO-0.3, LAO-6, and LAO-B. The portion of the model least sensitive to this parameter was at LAO-0.8, since the water table there is below all but the 2 greatest extinction depth values tested. The most sensitive area was at LAO-B, which has the highest water table. The model was more sensitive to decreases than increases in extinction depth at LAO-C, LAO-0.3, LAO-0.6, and LAO-6. It was more sensitive to increases than decreases at LAO-3 and LAO-4, while it was roughly equally sensitive to increases and decreases at LAO-B, LAO-0.8, and LAO-0.91.

Table 21 summarizes the values for the mean head change, mean absolute head change, and root mean squared head change determined from each simulation. The results for the mean absolute head change determinations by hydrologic parameter or stress are displayed graphically in Figures 80 and 81 for the steady-state model analysis and the transient model analysis, respectively.

Figure 80 shows the relations between the average model sensitivities to varying K, recharge, ET, and ET extinction depth for the steady-state model. By far the parameter that elicited the greatest sensitivity was recharge, followed in decreasing order by ET, then K and extinction depth. Negative and positive variations produced about the same average responses for recharge, K, and extinction depth, but responses to negative adjustments in ET were greater than for the positive changes in this parameter. Interestingly, the average model responses to increased K, ET, and extinction depth were all about the same with increases of 75% resulting in just slightly over one foot of mean absolute head change.

Table 21: Sensitivity Results Summary

		% Variation From Calibrated											
Steady-State Model ALUV1196:		-87.5	-75	-50	-25	25	50	75	100	125	151		
Parameter													
Hydraulic Conductivity	Mean Head Change (ft):	0.289	0.244	0.100	0.000	0.056	0.189	0.322	0.500	0.700	0.911		
	Mean Abs. Head Change:	1.956	1.578	1.011	0.511	0.433	0.789	1.078	1.322	1.522	1.689		
	RMS Head Change:	2.147	1.855	1.193	0.606	0.569	1.092	1.555	1.978	2.370	2.750		
Recharge	Mean Head Change (ft):		-7.133	-4.278	-1.956	1.911	4.067	6.689					
	Mean Abs. Head Change:		7.133	4.278	1.956	1.911	4.067	6.689					
	RMS Head Change:		7.738	4.603	2.103	2.173	4.747	7.869					
Evapotranspiration	Mean Head Change (ft):		2.967	1.589	0.644	-0.467	-0.778	-1.000					
	Mean Abs. Head Change:		2.967	1.589	0.644	0.467	0.778	1.000					
	RMS Head Change:		4.279	2.384	0.992	0.648	1.069	1.319					
Extinction Depth	Mean Head Change (ft):		1.244	0.878	0.444	-0.467	-0.878	-1.233					
	Mean Abs. Head Change:		1.244	0.878	0.444	0.467	0.878	1.233					
	RMS Head Change:		1.391	0.963	0.478	0.508	0.950	1.328					
		% Variation From											
Transient Model AL1296T6:		-90.5	-87.5	-75	-50	-25	25	50	75	100	109.5	125	151
Parameter													
Specific Yield	Mean Head Change (ft):	0.338		0.393	0.227	0.104	-0.062	-0.118	-0.173		-0.218		
	Mean Abs. Head Change:	0.962		0.640	0.296	0.129	0.091	0.140	0.196		0.238		
	RMS Head Change:	1.266		0.775	0.371	0.157	0.123	0.177	0.262		0.328		
Hydraulic Conductivity	Mean Head Change (ft):		-0.140	-0.118	-0.073	-0.051	0.071	0.082	0.149	0.182		0.204	0.249
	Mean Abs. Head Change:		0.700	0.611	0.411	0.211	0.200	0.389	0.567	0.711		0.844	0.978
	RMS Head Change:		0.753	0.658	0.442	0.225	0.210	0.423	0.608	0.757		0.910	1.047
Recharge	Mean Head Change (ft):			-1.740	-1.073	-0.429	0.871	1.471	2.093				
	Mean Abs. Head Change:			1.969	1.347	0.956	1.116	1.491	2.093				
	RMS Head Change:			2.427	1.803	1.282	1.225	1.662	2.216				
Evapotranspiration	Mean Head Change (ft):			0.682	0.516	0.382	0.082	-0.029	-0.162				
	Mean Abs. Head Change:			1.167	1.111	1.044	0.878	0.880	0.902				
	RMS Head Change:			1.325	1.206	1.108	0.987	1.007	1.030				
Extinction Depth	Mean Head Change (ft):			0.582	0.482	0.371	0.093	-0.062	-0.184				
	Mean Abs. Head Change:			1.111	1.033	1.011	0.933	0.956	0.967				
	RMS Head Change:			1.247	1.131	1.084	1.030	1.101	1.177				

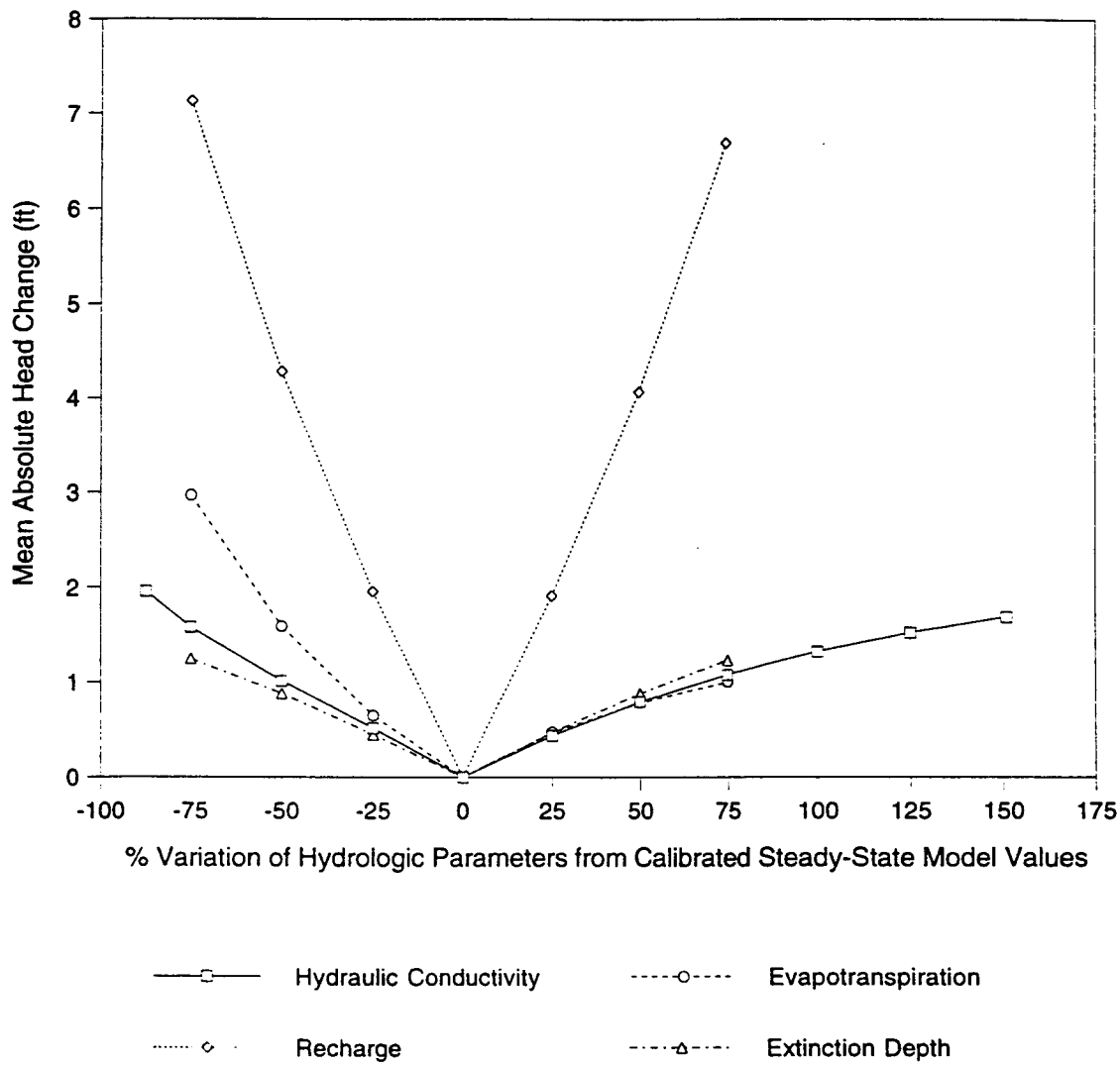
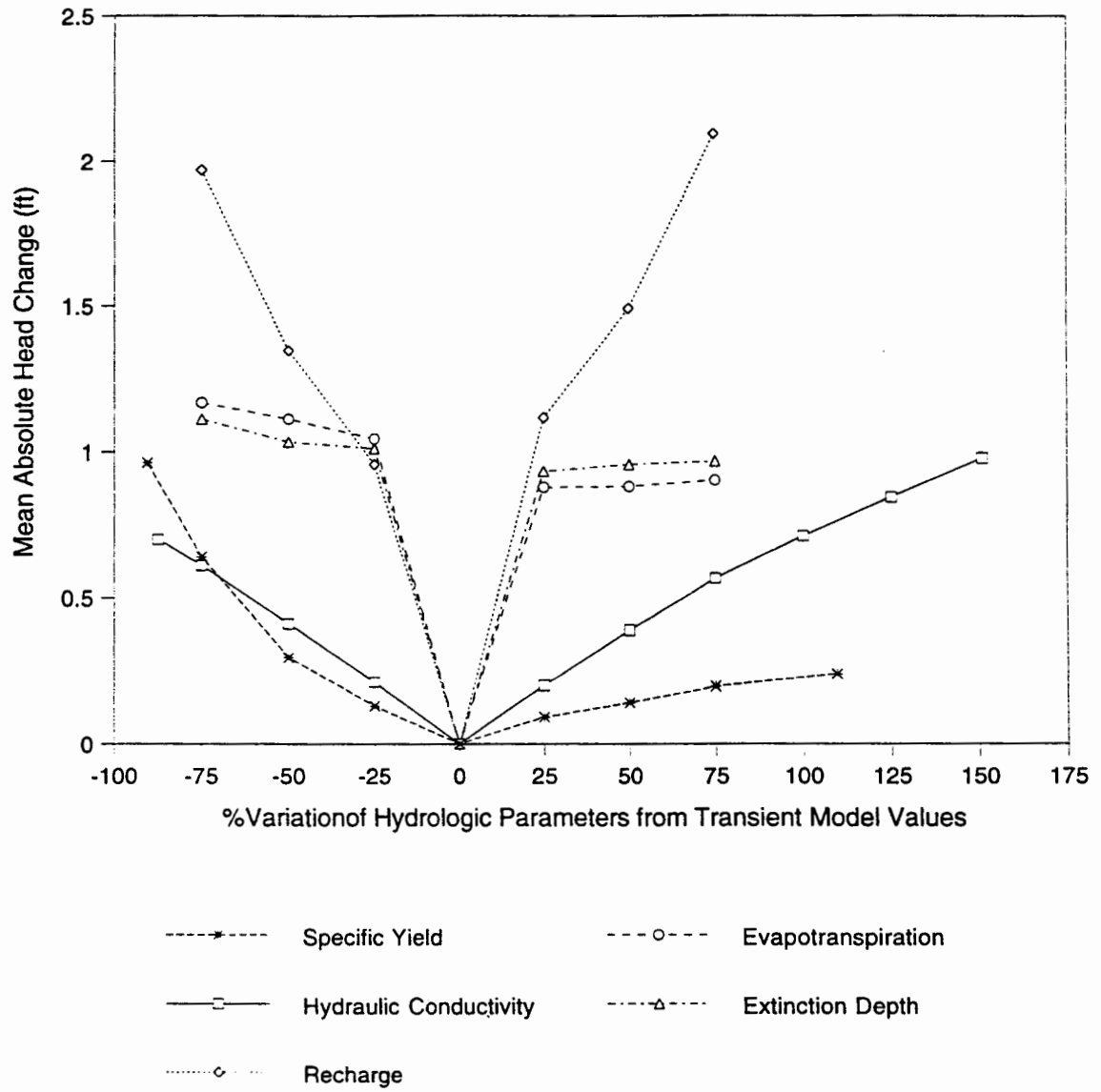


Figure 80: Model ALUV1196 (Steady-State) Sensitivity Results Mean Absolute Head Change Variation by Hydrologic Parameter



**Figure 81: Model AL1296T6 (Transient) Sensitivity Results
Mean Absolute Head Change Variation by Hydrologic Parameter**

The maximum mean absolute head change was less than 2 feet for K and extinction depth, while it was about 3 feet for ET and about 7 feet for recharge.

Figure 81 shows the relations between the average model sensitivities to the varied parameters and stresses for the transient model for period 6. The relationship between the model sensitivities is basically similar to that for the steady-state model, with the notable exception that the magnitude of head change responses was greatly reduced for recharge, ET, and K. The maximum mean absolute head change for recharge in the transient model analysis was about 2.0 feet, only ~29% of the maximum value for the steady-state model, while it was about 1.1 feet for ET and about one foot for K, only ~37% and ~50% respectively of those values determined for the steady-state model. The magnitude of responses for variations in extinction depth were basically unchanged from the steady-state model, however.

This graph also includes the results of testing the S_y storage parameter, which show that the model was generally least sensitive to this parameter relative to all the others, with responses only slightly exceeding those for K at the -75% and -90.5% increments. The model was far more sensitive to decreases in S_y than increases, with a mean absolute head change of almost one foot at the -90.5% increment, but only about 0.3 foot at the maximum +109.5% increment. The maximum mean absolute head change produced by varying K was less than one foot at the +151% increment, and the maximum values for ET and extinction depth were about the same at about 1.1 feet.

An unusual characteristic that is revealed in this graph is the pattern of responses for ET and extinction depth, for which practically all of the maximum amount of deviation in mean absolute head change was produced at the -25% and +25% increments, while the -50%, -75%, +50%, and +75% adjustments had practically no effect on the model responses. This is apparently due to the fact that the time dependence of the ET stress limits its impact regardless of its magnitude in the finite transient period, whereas no such limit is imposed on the steady-state solution. This limitation is also thought to be

responsible for the decreased responses to the recharge and K variations. Whereas recharge is also a time dependent variable, K is not, at least not directly. However, its relation as a component of the time dependent governing flow equation of the model (equation 5) provides the basis for the time limited head change reductions.

The impact of extinction depth, though associated with the time dependent ET stress, is apparently more dependent on its relation to the water table, as the magnitude of model responses produced by its variation was not significantly changed from the steady-state simulation.

In summary, the model is most sensitive to variations in recharge, and less so to ET, while varying K, extinction depth, and S_y had the least impact. The area of the model that generally exhibited the greatest sensitivity was the zone representing well LAO-C (columns 42-47) which elicited the largest responses to variations in K, recharge, and ET. It is not clear why this is the case, except perhaps for the fact that this was one of the two wells for which data were available, but which did not include the time at which the steady-state model was calibrated. The other well for which calibration data were lacking (LAO-6) did not produce any particularly evident heightened sensitivity though, except perhaps for decreased extinction depth where it gave the second highest response. However, this was the one parameter for which LAO-C exhibited only intermediate responses relative to the other wells.

Since the model is most sensitive to recharge and ET, possible errors in the magnitudes of these stresses are most likely to cause errors in the model's performance. The utilized values were determined by the hydrologic budget analysis, and great pains were taken to determine them as accurately as possible. However, there is undoubtedly some level of error in the hydrologic budget analysis results, with inaccuracies up to 10% probable for some of the utilized data and the necessary extrapolation of limited, point-source data utilized in the budget calculation procedure. It appears likely that much, if not most of the errors in model performance can be attributed to these uncertainties.

SUMMARY AND CONCLUSIONS

Overview

At its inception, the goal of this study was to enhance the state of knowledge of the hydrology of Los Alamos Canyon, which at first seemed like a well delimited topic suitable for concentrated research. It soon became apparent that a tighter focus would be required to allow the type of detailed investigation required to adequately analyze the complex relations within the canyon's hydrologic systems.

The research initially emphasized analysis of the Los Alamos Canyon watershed's surface hydrologic budget components, since aside from the inherent controls imposed by the geologic framework, the subsurface hydrologic conditions ultimately depend on the water inputs from and outputs to the meteorological and surface components of the hydrologic cycle. As far as is known, this study represents the most comprehensive hydrologic budget investigation ever attempted for the Los Alamos area. As such, the results should prove to be useful to future investigators who are engaged in the significant effort to characterize the complex hydrogeologic systems in the region, a task that has taken on a heightened level of urgency because of the possibility of LANL produced contamination impacting the regional groundwater supply.

The focus of the investigation then shifted to the groundwater system beneath the canyon, specifically focusing on the alluvial system. The hydrologic budget analysis results were used to constrain the water input and output stresses applied to a series of numerical groundwater flow simulations which provided the means of interpreting the dynamic relations between the shallow perched aquifer that occurs in the canyon bottom alluvium and the surface and deeper subsurface hydrologic regimes. Since there is ample documentation of significant levels of radionuclide contaminants in the alluvial system, a better understanding of the fate of the alluvial groundwater and the levels of partitioning that it undergoes in its journey through the hydrologic cycle is important knowledge.

The following sections summarize the principal findings of these investigations. A discussion of model limitations and deficiencies is included, and recommendations for future work in the area are reviewed. Finally, the major conclusions that were drawn from the study's results relevant to the characterization of the hydrologic systems in Los Alamos Canyon and their dynamic behavior are discussed.

Hydrologic Budget Analysis Summary

A significant result of the hydrologic budget analysis was the quantification of the relation between precipitation and elevation in the watershed (see Figure 13). It was previously known that this relationship existed, but establishing the strong correlation statistically allowed a high level of confidence to be placed on the determination of precipitation volumes which provide the input of water to the canyon's hydrologic systems. Over the 3-year period analyzed in the annual water budget calculations, average precipitation for the Los Alamos Canyon watershed was found to range between ~23 and ~29 inches/year. Within the 480-day period encompassed by the detailed water budget calculations, average precipitation for the entire watershed was determined as 31.5 inches/year.

These levels are significantly higher than most previously determined average precipitation rates for the Los Alamos area since those were ordinarily focused on estimates within the general boundaries of LANL, and did not account for the increased rates in the higher elevations of the Sierra de los Valles west of the LANL boundary. However, even though located outside the immediate LANL area, the contributions of the higher elevations to the hydrologic budget of the canyon are significant since so much of the runoff is generated by snowmelt. The inclusion of the SNOTEL data from the USDABNRC's Quemazon station in the upper basin area of the watershed in the detailed budget calculations allowed this contribution to be quantified, and also permitted the timing of the snowmelt releases to be accurately defined.

One of the most important results of the water budget study was the quantification of the evapotranspiration component, which was seen to substantially dominate the allocation of water in the surface and meteorological systems. Over the 3-year period analyzed, ET was found to represent between ~71% and ~83% of the total hydrologic budget for the Los Alamos Canyon watershed. In terms of magnitude, this amounts to between 18 and 21.5 inches of average annual ET within the analyzed period.

It is recognized that the assumptions applied to these determinations are not insignificant, namely the extrapolation of the single point-source latent heat flux data throughout the entire watershed on a constant percentage basis. It is thought to be highly likely that the ET quantities may vary significantly throughout the study area by elevation because of the differences in precipitation, temperature, and vegetation that are observed within the substantial elevation range of the watershed. This is an area ripe for further research, and could easily provide the material for an entire dissertation on its own.

Lacking specific data on soil moisture storage, it was thus assumed that the change in storage was approximately zero. By then factoring in the streamflow discharge data, the amount of infiltration recharge to the subsurface could then be estimated as the residual to the basic hydrologic mass balance equation. In the annual water budget calculations, this was determined to represent between about 17% and 26% of the total water budget averaged over the entire watershed, or in terms of magnitude, from about 4 inches/year to 7.3 inches/year within the 3 year analyzed period. For the 480 day period analyzed in the detailed budget calculations, it was determined that surface infiltration averaged 5.6 inches/year in the middle/upper canyon area but was only 3.8 inches/year in the upper basin area of the watershed.

Analysis of streamflow discharge data showed that the stream-aquifer relations are complex and variant over time. The seepage run analysis determined that significant portions of the upper part of the stream system exhibited gaining behavior during the conditions of peak snowmelt runoff, by as much as an average vertical depth of ~10

feet/day within the approximated streambed area (see Figure 25). This behavior is not consistent however, as the middle station discharge infrequently exceeded the upper station discharge outside of the peak snowmelt runoff period (see Figure 24). The lower reaches of the stream displayed losing behavior during the peak runoff conditions with average infiltration rates of generally between 2 and 2.5 feet/day of vertical depth within the estimated active flow area of the streambed (see Figure 25). For the entire 1995 water year, the stream reach between the upper and middle gages showed an average net gain of 9.5 vertical feet, while the reach between the middle and lower gages showed a net infiltration loss of 91.4 vertical feet within the estimated streambed area.

Groundwater Flow Simulations Summary

The groundwater flow model constructed for the simulations that were run in this study is a simplified representation of the complex heterogeneities present in the actual physical system. However, the error analysis conducted on the transient simulations indicated that its performance was reasonably close enough to the observed transient conditions in the alluvial aquifer to generally corroborate the ZONEBUDGET computations made with the model. Thus, these computations quantify the partitioning of the groundwater in the alluvial system among the various loss components of the hydrologic budget for the alluvial aquifer under both steady-state and transient conditions. Both magnitudes of losses and relative variations in losses within the system and over time were determined in the ZONEBUDGET analysis.

A significant result from the simulations was the confirmation of enhanced infiltration seepage from the alluvial system into the underlying strata in the area of the Guaje Mountain fault zone (zone 4). This preferential pathway for groundwater recharge to the underlying hydrologic systems had been previously inferred from the examination of head profile variations over time (see Figure 10). The modeling results permitted quantification of the magnitude of this water movement, both in absolute terms and relative

to other losses elsewhere in the system.

Volumetrically, the amount of groundwater flow into the fault zone appears insignificant relative to infiltration losses in other parts of the canyon. Under steady-state conditions, the infiltration to zone 4 was determined at about 2,650 ft³/day. Total steady-state infiltration losses upgradient from there were over 22,000 ft³/day while infiltration losses downgradient from there within the study area totaled nearly 30,000 ft³/day. However, when measured on an areally averaged basis, the steady-state infiltration rate in zone 4 was nearly 0.12 inches/day, compared to an average of about 0.06 inches/day in the upgradient areas and about 0.04 inches/day in the downgradient section of the study area. It thus appears that the fault zone likely represents the most efficient pathway in the canyon for concentrated groundwater movement into the lower hydrologic systems.

The MODPATH results showed that the downgradient advective velocities varied substantially throughout the alluvial system, and averaged 727 feet/year overall. However, this result appears to be less relevant to the fate of the groundwater in the alluvial system than the infiltration losses based on the partitions determined by the ZONEBUDGET results. For the entire study area, it was determined that fully 69% of the alluvial system's losses were accountable to infiltration losses, compared to less than 3% to downgradient flow, with the remaining 28% lost to ET under steady-state conditions.

Under transient conditions, the infiltration rates appeared to be relatively consistent within each zone, with the exception of zone 4 where it varied between 0.09 and 0.14 inches/day. The rates of storage loss fluctuated most dramatically, ranging from zero in recessionary periods to a maximum of 0.75 inches/day during period 2. Overall average ET losses ranged between about 0.005 and 0.02 inches/day during the 480-day length of the simulations.

The sensitivity analysis determined that the model is most sensitive to variations in the applied recharge rate, and second most sensitive to varying ET, while the other tested parameters elicited comparatively minor model responses. Thus, the errors inherent in the

hydrologic budget analysis probably represent the major contribution to errors in the model's performance.

Model Limitations and Deficiencies

Several aspects of the model's design incorporated significant simplifications of the actual alluvial system, and certain assumptions were necessary in view of the lack of more detailed data. Among these was the assumption of a homogeneous and isotropic medium for the alluvial material, certainly a major simplification, but the necessary data to assume otherwise were simply not available. The assumed value for K was based on a limited number of slug tests, which are not the most desirable means of determining this parameter. Also, the values for S_y and n were assumed from limited data or literature sources.

The bottom of the aquifer was assumed to occur at the base of the alluvium, the configuration of which was determined from a limited number of well logs. Thus, significant extrapolations were assumed in areas without data. Furthermore, it is not really clear that the base of the zone of saturation consistently occurs at the base of the alluvium. Indeed, several of the older wells from which data were utilized had screened intervals that extended beneath the alluvium according to their drill logs. The intent of this procedure in developing the wells was not clear, and it is felt that this was done because of the uncertainty about the actual depths of saturation. Records from the newer wells are more detailed and they were drilled during times of actual saturated conditions. Their logs indicate that the bottom of the saturated zone was defined by a perching layer of clay which occurred at the contact between the alluvium and the underlying tuff. However, the assumption that this is the case throughout the alluvial system may be incorrect.

The constant head boundary assumed at the upgradient end of the system simulated baseflow recharge from the upper basin portion of the watershed. This boundary was placed at the location of Los Alamos Reservoir since that is the most likely situation.

However, the closest well control point (LAO-B) was ~6,000 feet downgradient from the reservoir, so the constant head boundary was based on its data and thus represents a somewhat tenuous assumption. As such, the modeling results from zone 1 are fairly suspect, and indeed the error analysis indicated that this was the case.

The assumption of an arbitrarily chosen constant head boundary representing a one foot saturated thickness at a point approximately 10,000 feet downgradient from the study area of interest west of State Road 4 was even more tenuous since there were no well data for calibrating a large part of the downgradient portions of the model. The limited data from LAO-6 indicated that the lower part of the study area likely had significant saturation under the steady-state conditions of maximum snowmelt runoff, but that at other times it was completely dried up. The model failed to dry out in the downgradient portions during the transient simulations, indicating a major deficiency in its performance. As such, the modeling results for the downgradient portions of the system have a higher degree of uncertainty, and this was again borne out in the error analysis.

One of the biggest simplifications was the assumption of areal recharge as the primary mechanism for water input to the system. As was seen in the analysis of the streamflow discharge data, rather substantial depths of infiltration seepage can occur within the limited area of active flow in the streambed (which has an average width of only about 5.5 feet) under both maximum runoff conditions and when averaged over an entire water year. The incorporation of the snowpack data in the hydrologic budget analysis did allow this component to be included in the areally averaged precipitation amounts which provided the basis for assigning areal recharge to the model. However, these effects were likely averaged out over too great an area (the entire watershed), whereas the streamflow contributions to recharge were much more concentrated in certain portions. Also, the streamflow characteristics were seen to vary over both space and time, with gaining conditions occurring in parts of the upgradient portions of the system, but only during peak runoff conditions. Therefore, it appears that most of the streamflow contributions to

recharge were rather highly focused in the downgradient portions of the system.

The calibration of the steady-state model did not take this situation into account, and thus the calibrated drain conductances were too low to allow enough infiltration seepage from the bottom of the alluvial system into the underlying strata to allow the system to dry out during the dry periods simulated, as was seen in the model's inability to simulate the rapid water table recessions indicated by the well data. The effects of this deficiency on the model results differed according to the actual physical conditions. During the times when the system was saturated, the estimates of infiltration seepage from the system were underestimated. However, during the times when the system had dried out, the infiltration was overestimated. Thus, lacking the data necessary for calibration in the down-gradient portions of the study area, and by not incorporating the more focused streamflow recharge source, the model failed to adequately simulate these complex and dynamic aquifer behaviors.

Recommendations for Future Work

The recommendations to improve on the hydrologic budget analysis include having better control on the ET determinations by installing additional instrumentation to better represent the variable conditions of temperatures and vegetation types and density that exist at the varying elevations throughout the watershed. Indeed, two additional sites instrumented to measure latent heat flux have been recently installed in Mortandad Canyon, and their limited data sets were examined to see if any substantial difference was seen or correlation could be made between the data from the canyon bottom sites and the data from the mesa-top site of TA-6 utilized in this study. It was thought that the greater density of vegetation in the canyon bottom would lead to higher rates of ET.

The Mortandad Canyon data showed generally close agreement with the TA-6 data during the winter period when ET was low. However, during the spring warm-up when increased ET was measured at TA-6, the Mortandad Canyon data showed significantly

lower ET, exactly opposite from the expected results. It was determined that the instruments were mounted on a tower at 12 meters above ground level at TA-6, but were mounted at a height of only 2 meters in the canyon. As such, the canyon instruments were not high enough to measure the transpiration coming off of the trees, whereas the TA-6 instruments were high enough to detect this major component of ET. Thus, it was felt that the Mortandad Canyon data was deficient, and the data from TA-6 was utilized exclusively. It would therefore seem prudent to mount any additional heat flux instrumentation on towers high enough to get above the tree-tops. Unfortunately, this would entail significant additional expense and perhaps environmental objections.

Additional future work that would improve the hydrologic budget analysis would be the incorporation of a study on soil moisture variation throughout the watershed in order to quantify the component of change in storage in the hydrologic mass balance equation. This would entail the installation of a number of access tubes throughout the watershed from which neutron probe data could be systematically collected over time. This would be a fairly intensive effort though, and could be the subject of another entire dissertation.

Future work recommendations to improve on the modeling efforts would include more detailed determination of the hydrologic parameters used as model inputs. Pump tests of the alluvial wells would give better determinations of hydraulic conductivity and would also quantify the S_y storage parameter. This may prove difficult with many of the wells however, since they typically have only 2-inch casing and previous water sampling efforts have indicated that they are not very productive.

The model performance in producing more accurate responses under transient stresses would likely be improved by a more explicit division of the simulation time into smaller stress periods which more closely define observed variations in aquifer behavior. The detailed hydrologic budget would then have to be recalculated to reflect these divisions. This would result in a more refined definition of the magnitudes of the transient

stress variations and would allow a greater level of resolution in producing the highly dynamic aquifer responses observed in the well data.

Installation of additional pressure transducers in the alluvial wells is highly recommended in order to generate a more substantial database for model calibration and error analysis. Drilling of additional wells in the data poor downgradient section of the study area and the upgradient section between Los Alamos Reservoir and well LAO-B is recommended as well.

Future work recommended to improve the model itself would be the inclusion of a stream routing package that would account for the additional concentrated recharge source that the stream provides. Accurate representation of the complex streamflow dynamics will likely require more detailed streamflow investigations however, a project that could easily become quite involved in itself.

A more easily constructed variation of the existing model could simply include a series of narrow cells representing the streambed in which enhanced recharge could be applied, based on the results of the seepage run analysis. These data would be appropriate for a steady-state simulation. Running the model under transient conditions would be quite a bit more complicated however, as the necessary detailed data on varying gaining and losing behaviors and magnitudes are not currently available. More detailed analysis of the data from the 3 permanently installed streamflow gages could allow determination of generalized gross variations for the upper and lower sections however.

Finally, the model results for infiltration seepage from the alluvial system could be applied as the water input data for simulations of unsaturated flow in the underlying tuff. Incorporation of preferential flow along fracture zones associated with the Guaje Mountain Fault would be desirable. These modeling efforts would require the application of a computer code that is more sophisticated than MODFLOW however, with capabilities of simulating unsaturated flow as well as the saturated conditions that exist in the clay-filled fractures during active recharge into the fault zone.

Major Conclusions

The surface hydrologic budget results indicate that ET represents the dominant component, which was found to comprise between ~71% and ~83% of the total water budget for the watershed in the annual budget calculations. In the detailed budget calculations, it was found to represent ~84% of the total water budget for the entire watershed during the 480 day period analyzed. This amount was found to vary within the watershed however, as it was determined to represent ~87% of the total water budget in the upper basin area, but ~75% in the middle/upper canyon area.

The runoff component was found to represent a fairly insignificant portion of the water budget, totaling only 1.5% of the entire budget in the detailed budget calculations. The surface infiltration determined as the residual of the hydrologic mass balance equation was between 17.4% and 25.7% of the total water budget in the annual budget calculations, and was found to represent 13.9% of the total water budget in the detailed budget calculations. Average infiltration rates varied between 3.8 inches/year in the upper basin area and 5.6 inches/year in the middle/upper canyon area in the detailed budget analysis, and were determined to average between 4.0 and 7.3 inches/year for the entire watershed during the 3-year period analyzed in the annual budget calculations. The average infiltration rate of 4.4 inches/year for the total watershed determined in the detailed budget calculations was about 1/6 of the magnitude of the average determined ET rate of 26.6 inches/year, while runoff losses were less than 2% of the total ET losses.

Thus, the determination of the magnitude of ET losses in the watershed represents a critical result relevant to the partitioning of the hydrologic budget components and establishing the magnitudes of water inputs and outputs for the groundwater flow simulations.

The groundwater flow modeling results show that the major loss component of the hydrologic budget for the alluvial aquifer is infiltration seepage from the bottom of the alluvial system into the underlying strata, representing ~69% of the total system losses

compared to ~28% for ET and ~3% for downgradient flow within the study area west of State Road 4 under steady-state conditions. For the total study area, this amounted to ~55,000 ft³/day of infiltration seepage during the peak runoff period of spring snowmelt. During 1995, the system was in approximately steady-state conditions from about March 9 through June 30 for a total of 114 days (based on the hydrograph for well LAO-3; Figure 16). Thus an estimated 6,260,000 ft³ or 143.7 acre-feet of infiltrated groundwater left the alluvial system and entered into the lower hydrologic systems during this single time interval. This is a fairly sizable amount of groundwater movement within the relatively confined area of the canyon, and it thus carries considerable implications for attendant migration of the mobile radionuclide contaminants (e.g. tritium) present in the alluvial system.

The transient simulations give an idea of the variability in the alluvial system's water budget loss components, in which the storage parameter plays an important role. Thus, an enhanced level of understanding of the dynamics of the alluvial system was achieved. The model's confirmation that the Guaje Mountain Fault zone represents a preferred pathway for infiltration seepage from the alluvial system by a proportion of 2:1 over the average rate in the upgradient portion and by 3:1 over the downgradient section indicates that this is an area of elevated concern with regard to the likelihood of possible contamination of the lower hydrologic systems, including the regional aquifer water supply.

Thus overall, the various results of the intensive efforts employed in this study indicate that the implications for surface water and groundwater contaminant migration into the lower hydrologic systems are significant. These results should then provide an impetus and basis for further, more detailed investigations of the hydrologic processes within and beneath Los Alamos Canyon and the other canyons of the Pajarito Plateau.

REFERENCES

- Abrahams, J.H., Baltz, E.H., and Purtyman, W.D., 1962, Movement of perched groundwater in alluvium near Los Alamos, New Mexico, *in* Short papers in geology, hydrology, and topography-articles 1-59, Geological Survey research 1962: U.S. Geological Survey Professional Paper 450-B, p. 93-94.
- Abrahams, J.H., and Purtyman, W.D., 1966, The hydrology and chemical and radio-chemical quality of surface and ground water at Los Alamos, New Mexico, July 1957 through June 1961: Albuquerque, NM, U.S. Geological Survey Administrative Release.
- Aldrich, M.J. Jr., 1986, Tectonics of the Jemez lineament in the Jemez Mountains and Rio Grande rift: *Journal of Geophysical Research*, v. 91, p. 1753-1762.
- Anderson, M.P. and Woessner, W.W., 1992, Applied groundwater modeling: San Diego, Academic Press, 381 p.
- Bailey, R.A., Smith, R.L., and Ross, C.S., 1969, Stratigraphic nomenclature of volcanic rocks in the Jemez Mountains, New Mexico, *in* Contributions to stratigraphy, 1968: U.S. Geological Survey Bulletin 1274-P, 19 p.
- Baldrige, W.S., and Olsen, K.H., 1989, The Rio Grande rift: *American Scientist*, v. 77, p. 240-247.
- Birdsell, K.H., Soll, W.E., Rosenberg, N.D., and Robinson, B.A., 1995, Numerical modeling of unsaturated groundwater flow and radionuclide transport at MDA G: Los Alamos, New Mexico, Los Alamos National Laboratory report LA-UR-95-2735, 49 p.
- Blake, W.D., Goff, F., Adams, A.I., and Counce, D., 1995, Environmental geochemistry for surface and subsurface waters in the Pajarito Plateau and outlying areas, New Mexico: Los Alamos, New Mexico, Los Alamos National Laboratory report LA-12912-MS, 43 p.
- Bowen, B.R., 1990, Los Alamos climatology: Los Alamos, New Mexico, Los Alamos National Laboratory report LA-11735-MS, 254 p.
- Broxton, D.E., Heiken, G.H., Chipera, S.J., and Byers, F.M., Jr., 1995a, Stratigraphy, petrography, and mineralogy of Bandelier Tuff and Cerro Toledo deposits, *in* Broxton, D.E., and Eller, P.G., eds., Earth science investigations for environmental restoration-Los Alamos National Laboratory Technical Area 21: Los Alamos, New Mexico, Los Alamos National Laboratory report LA-12934-MS, p. 33-63.
- Broxton, D.E., Longmire, P.A., Eller, P.G., and Flores, D., 1995b, Preliminary drilling results for boreholes LADP-3 and LADP-4, *in* Broxton, D.E., and Eller, P.G., eds., Earth science investigations for environmental restoration-Los Alamos National Laboratory Technical Area 21: Los Alamos, New Mexico, Los Alamos National Laboratory report LA-12934-MS, p. 93-109.

- Cushman, R.L., 1965, An evaluation of aquifer and well characteristics of municipal wells in Los Alamos and Guaje Canyons near Los Alamos, New Mexico *in* Contributions to the hydrology of the United States, 1964: U.S. Geological Survey Water-Supply Paper 1809-D, 50 p.
- Daniel B. Stephens & Associates, Inc., 1995, Laboratory analysis of soil hydraulic properties of TA-2 soil samples, prepared for ERM/Golder, Los Alamos, New Mexico: Albuquerque, New Mexico, 88 p.
- Davis, L.A., and Neuman, S.P., 1983, Documentation and user's guide: UNSAT2 variably saturated flow model: Washington D.C., U.S. Nuclear Regulatory Commission, 198 p.
- Domenico, P.A., and Schwartz, F.W., 1990, Physical and chemical hydrogeology: New York City, John Wiley and Sons, 824 p.
- Dransfield, B.J., and Gardner, J.N., 1985, Subsurface geology of the Pajarito Plateau, Española basin, New Mexico: Los Alamos, New Mexico, Los Alamos National Laboratory report LA-10455-MS, 15 p.
- Environmental Assessments and Resource Evaluations Group, 1996, Environmental surveillance at Los Alamos during 1994: Los Alamos, New Mexico, Los Alamos National Laboratory report LA-13047-ENV, 370 p.
- Environmental Protection Group, 1995, Environmental surveillance at Los Alamos during 1993: Los Alamos, New Mexico, Los Alamos National Laboratory report LA-12973-ENV, 10 ch.
- Evolution Computing, 1992, FastCad® reference manual, 218 p.
- FIMAD (Facility for Information Analysis and Display), 1994, Wells-Los Alamos and Pueblo Canyons, 1":1,000' scale topographic map: Los Alamos, New Mexico, Los Alamos National Laboratory Earth and Environmental Sciences Division, FIMAD plot id. no. 102767.
- Frenzel, P.F., 1995, Geohydrology and simulation of ground-water flow near Los Alamos, North-Central New Mexico: U.S. Geological Survey Water-Resources Investigations Report 95-4091, 92 p.
- Gallaher, B., 1995, Groundwater velocities in Los Alamos Canyon: Los Alamos, New Mexico, Los Alamos National Laboratory memorandum ESH-18/WQ&H-95-409.
- Gardner, J.N., Goff, F., Garcia, S., and Hagan, R.C., 1986, Stratigraphic relations and lithologic variations in the Jemez volcanic field, New Mexico: Journal of Geophysical Research, v. 91, no. B2, p. 1763-1778.
- Gardner, J.N., Baldrige, W.S., Gribble, R., Manley, K., Tanaka, K., Geissman, J.W., Gonzales, M., and Baron, G., 1990, Results from seismic hazards trench #1 (SHT-1). Los Alamos seismic hazards investigations: Los Alamos, New Mexico, Los Alamos National Laboratory report EES1-SH90-19, 57 p.

- Gardner, J.N., and House, L., 1987, Seismic hazards investigations at Los Alamos National Laboratory, 1984 to 1985: Los Alamos, New Mexico, Los Alamos National Laboratory report LA-11072-MS, 76 p.
- Geddis, A.M., 1992, Preliminary modeling of moisture movement in the tuff beneath Mortandad Canyon, Los Alamos National Laboratory: Los Alamos, New Mexico, Los Alamos National Laboratory report LA-UR-92-2577, 68 p.
- Goff, F.E., and Sayer, S., 1980, Geothermal investigation of springs and well water in the Los Alamos region, New Mexico: Los Alamos, New Mexico, Los Alamos National Laboratory report LA-8326-MS, 25 p.
- Goff, F.E., and Adams, A., 1993, Tritium and trace elements in the main aquifer and other waters within the Pajarito Plateau region: Los Alamos, New Mexico, Los Alamos National Laboratory memorandum, (September 15, 1993).
- Golden Software, Inc., 1991, SURFER[®] version 4 reference manual, 8 ch.
- Golombek, M.P., 1983, Geology, structure, and tectonics of the Pajarito fault zone in the Española basin of the Rio Grande rift, New Mexico: Geological Society of America Bulletin, v. 94, p. 192-205.
- Griggs, R.L., 1964, Geology and ground-water resources of the Los Alamos area, New Mexico: U.S. Geological Survey Water-Supply Paper 1753, 107 p.
- Harbaugh, Arlen W., 1990, A computer program for calculating subregional water budgets using results from the U.S. Geological Survey modular three-dimensional finite-difference ground-water flow model: U.S. Geological Survey Open-File Report 90-0392, 46 p.
- In-Situ Inc., 1992, Well Sentinel Model LTM 3000 operator's manual, 50 p.
- Knisel, W.G., Jr., Ed., 1980, CREAMS: A field-scale model for chemicals, runoff, and erosion from agricultural management systems: U.S. Dept. of Agriculture Conservation Research report no. 26, 653 p.
- Koenig, E.D., and McLin, S.G., 1992, Application of a lumped-parameter model toward understanding the behavior of the Mortandad Canyon perched alluvial system, Los Alamos, New Mexico: unpublished independent graduate study, New Mexico Tech. Univ., 45 p.
- Longmire, P.A., Kung, S., Boak, J.M., Adams, A.I., Caporuscio, F., and Gray, R.N., 1996, Aqueous geochemistry of upper Los Alamos Canyon, Los Alamos, New Mexico. *in* Goff, F., Kues, B.S., Rogers, M.A., McFadden, L.D., and Gardner, J.N., eds., The Jemez Mountains region: New Mexico Geological Society, Forty-Seventh Annual Field Conference guidebook, p. 473-480.
- Los Alamos National Laboratory, 1996, Detailed station description for TA-6: Los Alamos, New Mexico, Los Alamos National Laboratory Meteorology Group World Wide Web home page (www@weather.lanl.gov), document http://weather.lanl.gov/html/monplan/sites/stn_ta6.html.

- Los Alamos National Laboratory, 1995, Work Plan for Operable Unit 1049: Los Alamos, New Mexico, Los Alamos National Laboratory report LA-UR-95-2053, 7 ch.
- Los Alamos National Laboratory, 1993, Installation work plan for environmental restoration, Los Alamos, New Mexico, Los Alamos National Laboratory report LA-UR-93-3987, 4 ch.
- Los Alamos National Laboratory, 1992, RFI Work Plan for Operable Unit 1098, Los Alamos, New Mexico, Los Alamos National Laboratory report LA-UR-92-3825, 8 ch.
- Los Alamos National Laboratory, 1990, Los Alamos National Laboratory site development plan-technical site information: Los Alamos, New Mexico, Facilities Engineering Division Planning Group, ENG-2 and ICF Kaiser Engineers, Inc., Los Alamos National Laboratory report LA-CP-90-405, 283 p.
- Los Alamos National Laboratory Environmental Restoration Program, 1994a, Core sample log, Borehole ID LAOI(a)-1.1: Los Alamos, New Mexico, unpublished document dated 9/1/94-9/8/94, prepared by Dennis Newell, 11 p.
- Los Alamos National Laboratory Environmental Restoration Program, 1994b, Core sample log, Borehole ID LAO-B: Los Alamos, New Mexico, unpublished document dated 4/25/94-4/26/94, prepared by Dennis Newell, 2 p.
- McAda, D.P., and Wasiolek, M., 1988, Simulation of the regional geohydrology of the Tesuque aquifer system near Santa Fe, New Mexico: U.S. Geological Survey Water-Resources Investigations Report 87-4056, 71 p.
- McAda, D.P., 1990, Simulation of the effects of ground-water withdrawal from a well field adjacent to the Rio Grande, Santa Fe County, New Mexico: U.S. Geological Survey Water-Resources Investigations Report 89-4184, 27 p.
- McLin, S.G., 1992, Determination of 100-year flood plain elevations at Los Alamos National Laboratory: Los Alamos, New Mexico, Los Alamos National Laboratory report LA-12195-MS, 83 p.
- McDonald, M.G. and Harbaugh, A.W., 1988, A modular three-dimensional finite-difference ground-water flow model *in* Techniques of water-resources investigations of the United States Geologic Survey, Book 6, Chapter A1: U.S. Geological Survey, 512 p.
- Morris, D.A., and Johnson, A.I., 1967, Summary of hydrologic and physical properties of rock and soil materials as analyzed by the Hydrologic Laboratory of the U.S. Geological Survey 1948-1960 *in* Contributions to the hydrology of the United States, 1966: U.S. Geological Survey Water-Supply Paper 1839-D, 42 p.
- Nyhan, J.W., 1989, A hydrologic modeling study of water balance relationships at the Area P landfill in Los Alamos, New Mexico: Los Alamos, New Mexico, Los Alamos National Laboratory report LA-11521-MS, 28 p.

- Nyhan, J.W., Beckman, R., and Bowen, B., 1989, An analysis of precipitation occurrences in Los Alamos, New Mexico for long-term predictions of waste repository behavior: Los Alamos, New Mexico, Los Alamos National Laboratory report LA-11459-MS, 27 p.
- Pollock, David W., 1989, Documentation of computer programs to compute and display pathlines using results from the U.S. Geological Survey modular three-dimensional finite-difference ground-water flow model: U.S. Geological Survey Open-File Report 89-381, 81 p.
- Pope, M., 1993, Evapotranspiration at TA-59 and Area G: Los Alamos, New Mexico, unpublished draft report, 20 p.
- Priestly, C.H.B., 1959, Turbulent transfer in the lower atmosphere: Chicago, The University of Chicago Press, 130 p.
- Purtyman, W. D., 1995, Geologic and hydrologic records of observation wells, test holes, test wells, supply wells, springs, and surface water stations in the Los Alamos area: Los Alamos, New Mexico, Los Alamos National Laboratory report LA-12883-MS, 339 p.
- Purtyman, W.D., Stoker, A.K., and Maes, M.N., 1987, Water supply at Los Alamos during 1986: Los Alamos, New Mexico, Los Alamos National Laboratory report LA-11046-PR, 38 p.
- Purtyman, W.D., 1984, Hydrologic characteristics of the main aquifer in the Los Alamos area: Development of ground water supplies: Los Alamos, New Mexico, Los Alamos National Laboratory report LA-9957-MS, 44 p.
- Purtyman, W.D., Hansen, W.R., and Peters, R.J., 1983, Radiochemical quality of water in the shallow aquifer in Mortandad Canyon, 1967-1978: Los Alamos, New Mexico, Los Alamos National Laboratory report LA-9675-MS, 18 p.
- Purtyman, W.D., 1977, Hydrologic characteristics of the Los Alamos well field with reference to the occurrence of arsenic in well LA-6: Los Alamos, New Mexico, Los Alamos National Laboratory report LA-7012-MS, 37 p.
- Purtyman, W.D., 1975, Geohydrology of the Pajarito Plateau with reference to quality of water, 1949-1972: Los Alamos, New Mexico, Los Alamos National Laboratory informal report, 344 p.
- Purtyman, W.D., 1974, Dispersion and movement of tritium in a shallow aquifer in Mortandad Canyon at the Los Alamos Scientific Laboratory: Los Alamos, New Mexico, Los Alamos National Laboratory report LA-5716-MS, 10 p.
- Purtyman, W.D., 1967, The disposal of industrial effluents in Mortandad Canyon, Los Alamos County, New Mexico: U.S. Geologic Survey Open-File Report, 74 p.
- Rogers, D.B., and Gallaher, B.M., 1995, Unsaturated hydraulic characteristics of the Bandelier Tuff: Los Alamos, New Mexico, Los Alamos National Laboratory report LA-12968-MS, 76 p.

- Shaul, D.A., Alexander, M.R., and Reynolds, R.P., 1996a, Surface water data at Los Alamos National Laboratory: 1995 water year: Los Alamos, New Mexico, Los Alamos National Laboratory report LA-13177-PR, 42 p.
- Shaul, D.A., Alexander, M.R., Reynolds, R.P., and McLean, C.T., 1996b, Surface water data at Los Alamos National Laboratory: 1996 water year: Los Alamos, New Mexico, Los Alamos National Laboratory report LA-13234-PR, 53 p.
- Smith, R.L., Bailey, R.A., and Ross, C.S., 1970, Geologic map of the Jemez Mountains, New Mexico: U.S. Geological Survey Misc. Investigations Map I-571, scale 1:250,000.
- Spell, T.L., Harrison, T.M., and Wolf, J.A., 1990, $^{40}\text{Ar}/^{39}\text{Ar}$ dating of the Bandelier Tuff and San Diego Canyon ignimbrites, Jemez Mountains, New Mexico: Temporal constraints on magmatic evolution: *Journal of Volcanology and Geothermal Research*, v. 43, p. 175-193.
- Stoker, A.K., Goff, F., and Spangler, R., 1993, Age of water in the Los Alamos main aquifer: Albuquerque, New Mexico, Abstract *in* Proceedings of the Rocky Mountain Ground Water Conference, New Mexico Section.
- Stoker, A.K., McLin, S.G., Purtyman, W.D., Maes, M.N., and Hammock, B.G., 1992, Water supply at Los Alamos during 1989: Los Alamos, New Mexico, Los Alamos National Laboratory report LA-12276-PR, 51 p.
- Stoker, A.K., Purtyman, W.D., McLin, S.G., and Maes, M.N., 1991, Extent of saturation in Mortandad Canyon: Los Alamos, New Mexico, Los Alamos National Laboratory report LA-UR-91-1660, 137p.
- Stone, W.J., 1995. Preliminary results of modeling the shallow aquifer, Mortandad Canyon. Los Alamos National Laboratory, New Mexico: Santa Fe, New Mexico, DOE Oversight Program, Remediation Section, Ground Water Protection and Remediation Bureau. New Mexico Environment Department, 32 p.
- Stull, R.B., 1988. An introduction to boundary layer meteorology: Boston, Kluwer Academic Publishers, 666 p.
- Theis, C.V., 1950. Geologic background of waste and water supply problems at Los Alamos: Los Alamos, New Mexico, U.S. Atomic Energy Commission, Meeting of AEC Waste Processing Committee, TID-460.
- Theis, C.V., and Conover, C.S., 1962, Pumping tests in the Los Alamos Canyon well field near Los Alamos, New Mexico: U.S. Geological Survey Water-Supply Paper 1619-I, 24 p.
- Tierney, G.D., and Foxx, T.S., 1987, Root lengths of plants on Los Alamos Laboratory lands: Los Alamos, New Mexico, Los Alamos National Laboratory report LA-10865-MS, 59 p.
- U.S. Department of Energy, 1979, Final environmental impact statement, Los Alamos Scientific Laboratory site, Los Alamos, New Mexico: Washington D.C., U.S. Department of Energy DOE/EIS-0018, 502 p.

- U.S. Geological Survey, 1962, Rio Grande Basin low-flow investigation, *in* Surface water supply of the United States 1960, Part 8, Western Gulf of Mexico basins: U.S. Geological Survey Water-Supply Paper 1712, p. 481.
- U.S. Geological Survey, 1961, Rio Grande Basin low-flow investigation, *in* Surface water supply of the United States-1959, Part 8, Western Gulf of Mexico basins: U.S. Geological Survey Water-Supply Paper 1632, p. 508-509.
- Vaniman, D., and Wohletz, K., 1990, Geology of North-Central Los Alamos National Laboratory: Los Alamos, New Mexico, Earth and Environmental Sciences Division geologic map, FIMAD plot id. no. G101089.
- Viessman, W., Lewis, G.L. and Knapp, J.W., 1989, Introduction to hydrology, 3rd ed.: New York City, Harper Collins, 779 p.
- Wang, H.F., and Anderson, M.P., 1982, Introduction to groundwater modeling: San Francisco, W.H. Freeman and Company, 237 p.
- Waterloo Hydrogeologic Software, 1996, Visual MODFLOW[®] user's manual, 196 p.
- Weir, J.H., Abrahams, J.H., Waldon, J.R., and Purtyman, W.D., 1963, Chemical and radiochemical quality of surface and ground water, 1949-1955: Los Alamos, New Mexico, U.S. Geological Survey Administrative Report.
- Wilcox, B.P., Davenport, D.W., Smith, S., and Ferris, J., 1996, Investigations of surface hydrology in Los Alamos Canyon: Los Alamos, New Mexico, unpublished draft report, 12 p.
- Winter, Thomas, C., 1981, Uncertainties in estimating the water balance of lakes: American Water Resources Association Bulletin, v. 17, no. 1, p. 82-115.
- Young, H.D., 1992, University physics, eighth edition: Reading, Mass., Addison-Wesley Publishing Co., 1,356 p.
- Zyvoloski, G.A., Robinson, B.A., Dash, Z.V., and Trease, L.L., 1995, Models and methods summary for the FEHMN application: Los Alamos, New Mexico, Los Alamos National Laboratory report LA-UR-94-3787, 70 p.